Redox and metallomic profiling in human coronary artery smooth muscle cells under physiological normoxia and hypoxia-reoxygenation injury: crosstalk between Nrf2 signalling and zinc

Yang, Fan

Awarding institution:
King's College London

Redox and metallomic profiling in human coronary artery smooth muscle cells under physiological normoxia and hypoxia-reoxygenation injury: crosstalk between Nrf2 signalling and zinc

Thesis submitted by Fan YANG

For the degree of Doctor of Philosophy in the Faculty of Life Sciences and Medicine

King's College London

King's BHF Centre of Research Excellence
School of Cardiovascular and Metabolic Medicine & Sciences
Faculty of Life Sciences and Medicine
King's College London

01 September 2023

Table of Contents

Abstract **6**

Acknowledgements **9**

Publications **10**

List of Figures **11**

List of Tables **14**

List of Abbreviations **15**

Chapter 1 – Introduction **19**

1.1 Heart and coronary circulation 19

1.1.1 General overview of the heart 19

1.1.2 General overview of coronary circulation 20

1.1.3 O_2 distribution in coronary arteries *in vivo* 24

1.2 Human coronary smooth muscle cells 25

1.2.1 Histologic features of the normal coronary arteries 25

1.2.2 Characteristics and function of coronary artery smooth muscle cell 26

1.2.3 Interactions between vascular endothelial and smooth muscle cells 28

1.3 Coronary ischaemia-reperfusion injury (IR) 30

1.3.1 General overview of coronary ischaemia-reperfusion injury 30

1.3.2 Underlying mechanisms and consequences of coronary ischaemia - reperfusion injury 31

1.4 Keap1-Nrf2 cellular antioxidant signalling pathway 35

1.4.1 Nrf2-Keap1 interactions 37

1.4.2 Alternative mechanisms of Nrf2 regulation 39

1.4.3 Activation Nrf2 by sulforaphane 41

1.4.4 Nrf2-regulted antioxidant enzymes 43

1.4.5 Nrf2 affords protection in vascular and coronary ischaemia-reperfusion injury 46

1.5 Metal profiling in coronary ischaemia-reperfusion injury 48

1.5.1 General overview of cellular metal homeostasis 48

1.5.2 Antioxidant properties of zinc 49

1.5.4 Iron and Copper function in ischaemia-reperfusion injury 52

1.5.5 Crosstalk between metals and Nrf2 redox signalling pathway 53

1.6 Physiological oxygen levels 55

1.6.1 Importance of physiological oxygen levels 55

1.6.2 Hypoxia-inducible factor-1 57

1.7 Aims of the project 61

Chapter 2 - Methods 62

2.1 Culture of human coronary artery smooth muscle cells 62

2.1.1 Thawing and culturing of HCASMCs 63

2.1.2 Subculture of HCASMCs 63

2.1.3 Cryopreservation of HCASMCs 64

2.2 Cell counting using a haemocytometer 65

2.3 Bicinchoninic acid protein assay for immunoblotting 66

2.4 Measurement of cell proliferation 67

2.4.1 Measurement of cell proliferation using cell counting 68

2.4.2 Measurement of cell proliferation by comparing protein content 68

2.4.3 Measurement of cell proliferation using an iCELLigence™ platform 68

2.5 MTT assay 69

2.6 Firefly lantern extract chemiluminescence-based ATP assay 71

2.7 Measurement of intracellular reduced glutathione by fluorometric assay 73

2.8 Immunostaining 75

2.9 Nuclear translocation of Nrf2 76

2.10 Quantification of mRNA expression using quantitative reverse transcription polymerase chain reaction (qRT-PCR) 77

2.10.1 Extraction of ribonucleic acid (RNA) using RNeasy® Mini Kit 77

2.10.2 Complementary DNA (cDNA) synthesis 79

2.10.3 Primer design and qRT-PCR 79

2.11 Immunoblotting 81

2.12 siRNA Nrf2 silencing of Nrf2 83

2.13 Nrf2 overexpression 84

2.14 Phosphorescence lifetime measurements of O_2 levels in HCASMCs cytosol and medium 84

2.15 Measurement of intracellular free radical generation by L-012 chemiluminescence 85

2.16 Metallomic profiling in HCASMCs using inductively coupled plasma mass spectrometry (ICP-MS) 86

2.17 Statistical analysis 88

Chapter 3 – Results 89

Redox phenotype of HCASMCs under 18, 5 and 1kPa O_2 89

3.1 Characterisation of HCASMCs under 18, 5 and 1kPa O_2 89

3.1.1 Morphology of HCASMCs under 18, 5 and 1kPa O_2 89

3.1.2 Characterization of HCASMCs by immunostaining and immunoblotting 91

3.1.3 Proliferation of HCASMCs 93

3.2 Real-time measurement of O_2 levels in HCASMCs cytosol and medium 94

3.3 Stabilization of HIF-1α in HCASMCs adapted to 1kPa O_2 95

3.4 Basal ATP levels in HCASMCs cultured under 18, 5 and 1kPa O_2 96

3.5 Effects of different ambient O_2 levels on intracellular GSH and antioxidant enzyme levels in HCASMCs 97

3.6 Sulforaphane induces Nrf2 nuclear translocation 100

3.7 Nrf2-regulated target protein and mRNA expression under 18, 5 and 1kPa O_2 101

3.8 Effects of silencing Nrf2 on antioxidant protein expression 105

Chapter 3 – Discussion 107

Chapter 4 – Results 118

Metal profiles of HCASMCs under 18, 5 and 1kPa O_2 and crosstalk between Nrf2 signaling and Zn 118

4.1 Metal profiling under 18, 5 and 1kPa O_2 levels in HCASMCs using ICP-MS 118

4.2 Zn supplementation increases total Zn content in HCASMCs 120

4.3 Effects of Zn on Nrf2 signalling in HCASMCs under 18, 5 and 1kPa O_2 123

4.4 Effects of Zn on MT1 and ZnT1 expression in HCASMCs 126

4.5 Effects of silencing Nrf2 on total Zn levels in HCASMCs under 18, 5 and 1kPa O_2 129

4.6 Effects of Nrf2 overexpression on Zn levels in HCASMCs under 18, 5 and 1kPa O_2 132

4.7 Effects of Nrf2 inducer sulforaphane on total Zn content in HCASMCs under 18, 5 and 1kPa O_2 135

Chapter 4 – Discussion 137

Chapter 5 – Results 145

Hypoxia-reoxygenation effect on HCASMCs under 18 or 5kPa O_2 145

5.1 Reoxygenation induced free radical generation in HCASMCs under 18 and 5kPa O_2 145

5.2 Effects of SFN, Zn or TPEN on superoxide production under hypoxia-reoxygenation 147

5.3 Effects of hypoxia-reoxygenation on total Zn concentration in HCASMCs 149

5.4 Intracellular reduced GSH levels in HCASMCs under hypoxia-reoxygenation 149

5.5 Effects of hypoxia-reoxygenation on Nrf2-regulated target protein expression 150

5.6 Effects of hypoxia-reoxygenation injury on ZnT1 protein expression in HCASMCs 151

Chapter 5 – Discussion 152

Chapter 6 – General Discussion 161

6.1 Summary and significance 161

6.2 Adaptation to physiological normoxia alters the redox phenotype and metal profile in a cell-type specific manner 161

6.3 Crosstalk between Zn and Nrf2 and Zn homeostasis regulation 163

6.4 Evidence of free radical generation under hypoxia- reoxygenation 173

6.5 Clinical significance of SFN and Zn 173

6.6 Limitations of the study 175

6.7 Statement about the impact of Covid restrictions on the research 176

6.8 Future directions 177

Appendices 180

References 183

Abstract

Background: Oxidative stress and activation of cellular antioxidant defence pathways play critical roles in coronary ischaemia-reperfusion (IR) injury. Nuclear factor-E2-related factor 2 (Nrf2), a well-known antioxidant transcription factor, participates in maintaining cellular redox homeostasis. Notably, dysregulation of Zn homeostasis is associated with IR injury and linked with Nrf2 signalling pathway. Furthermore, the concept of cell culture under defined ambient oxygen levels that recapitulate pO_2 experienced *in vivo* has recently acquired renewed research focus. The present study aims to characterise the redox state and metal profiles in coronary artery smooth muscle cells (HCASMCs) adapted long-term to hyperoxia (18kPa O_2), physiological normoxia (5kPa O_2) and hypoxia (1kPa O_2). Compared to standard cell culture under 18kPa O_2, which has mistakenly been defined as normoxia in the past, our study provides novel insights into the role of Nrf2 and Zn underlying hypoxia-reoxygenation (HR) in HCASMCs adapted to physiological normoxia (5kPa O_2) and the crosstalk between Nrf2 signalling and Zn level.

Methods: Redox signalling was examined in HCASMCs adapted long-term (5 days) to defined O_2 levels (18, 5 and 1kPa). Intracellular redox status under different O_2 levels was determined by assaying intracellular glutathione (GSH) levels and protein expression of antioxidant enzymes. Immunoblotting and qPCR were employed to determine protein and mRNA expression of select Nrf2 targets (e.g.HO-1 and GCLM) under basal different O_2 levels and following treatment with the Nrf2 inducer sulforaphane (SFN, 2.5μM). Generation of reactive oxygen species (ROS) under basal conditions, following treatments and HR (18kPa/5kPa to 1kPa to 18kPa/5kPa), was measured using the chemiluminescence probe L-012. Metal profiles in HCASMCs under basal or HR were obtained using inductively coupled plasma mass spectrometry (ICP-MS). Crosstalk between Nrf2 and Zn was determined by measuring total Zn levels and protein expression of ZnT1 (main exporter of Zn on the

membrane) and MT (main intracellular storage protein of Zn) under hyperoxia, normoxia and hypoxia and following pre-treatment (16h) with SFN, N,N,N′,N′-tetrakis (2-pyridylmethyl) ethylenediamine (TPEN, a scavenger of free Zn^{2+}, 1.25μM) or 2-mercaptopyridine N-oxide sodium salt (a Zn^{2+} ionophore, 0.5μM) with $ZnCl_2$ (10μM).

Results: HCASMCs were adapted for 5 days to 18, 5 or 1kPa O_2. Hypoxia inducible factor-1α (HIF-1α) stabilisation was only observed in cells under 1kPa O_2. Lower basal intracellular antioxidant levels (e.g., GSH, CAT and SOD) and Nrf2-regulated target proteins (e.g.NQO1 and GCLM) were detected in cells adapted to 1kPa compared to 18 and 5kPa O_2. Total intracellular Zn^{66} levels were 0.345±0.037ng/μg protein in HCASMCs under 18kPa and similar under 5 and 1kPa O_2. Zn supplementation significantly increased total Zn content in HCASMC under 18 but not 5kPa O_2. Zn supplementation increased Nrf2 nuclear accumulation in cells under 18 or 5kPa O_2, whilst Nrf2 targeted HO-1 mRNA and protein expression in response to Zn supplementation was upregulated significantly in cells under 18kPa O_2, which were attenuated in cells under 5kPa O_2. Nrf2 siRNA silencing, overexpression or activation of Nrf2 with SFN did not significantly alter total Zn^{66} content. When HCASMCs were loaded with probe L-012 and exposed to hypoxia (1h) and reoxygenation, superoxide generation (PEG-SOD inhibitable) was only detected on reoxygenation. Pre-treatment of cells with SFN or Zn attenuated reoxygenation-induced superoxide generation. Furthermore, total intracellular Zn^{66} levels were not significantly changed in cells under HR injury under 18 and 5kPa O_2.

Conclusions: The present findings indicate that compared to physiological normoxia (5kPa O_2),hyperoxia (18kPa O_2) had negligible effects on the redox phenotype (e.g. GSH, antioxidant enzymes and Nrf2-regulated proteins) of HCASMCs, unlike umbilical vein and coronary artery endothelial cells. Notably, Zn supplementation activated the Nrf2 signalling pathway in HCASMCs, however activation of Nrf2 had negligible effects on total Zn^{66} levels.

ROS generation, primarily superoxide, was detected in first 20min after reoxygenation in HCASMCs under 18kPa O_2 and was significantly attenuated by pre-treatment with SFN or Zn, highlighting protective actions of Nrf2 activation and Zn supplementation in HR injury.

Acknowledgements

I would like to express my sincere appreciation to my supervisor Prof. Giovanni Mann and second supervisor Prof. Luigi Gnudi at King's College London. They provided valuable and helpful scientific advice throughout whole project. They believed in me and gave me a lot of encouragement when I faced difficulties. Prof. Giovanni Mann even helped me with rental issues. He is most trustworthy mentor, optimistic about life and passionate about science. I have learned a lot from him. I also want to thank him for helping me build up my resume and guide my career development. I am truly grateful to be his student.

I would also like to thank Dr. Gabriela Warpsinski, Dr. Emily Boorman, especially Dr. Matthew Smith for their assistance. Matthew Smith trained me in cell culture and many other basic laboratory skills, and I am indebted to his support. It has been a pleasure and fun to work with these colleagues in the laboratory, particularly as we suffered the consequences of COVID-19 during these three years. I would also like to thank Dr Alex Griffiths and Dr Theodore Stewart working at the London Metallomics Facility, and it was a pleasure collaboration. I want to thank Dr. Sarah Chapple's group members (e.g. Jessica Morris), Dr. Richard Siow's group members (e.g. Dr. Melissa Barber), Prof. Susan Brain's group members (e.g. Dr. Fulye Argunhan, Dr. Dibesh Thapa and Dr. De Sousa Valente, Joao) and Prof. Albert Ferro group members (e.g. Vasco Claro). We cycled together, camped together and went to conferences together. We supported each other during COVID and after COVID. These friendships helped me get used to living in London and made life easier and colourful.

Finally, I wish to thank my parents for their funding support and encouragement throughout my study. They always trusted me, supported me and loved me no matter what difficulties I faced. I hope they will be proud of their daughter.

Publications

Abstracts

Yang F, Smith MJ, Morrell A, Stewart T, Maret W, Mann GE. Influence of zinc on human coronary artery smooth muscle cells under hypoxia-reoxygenation: implications for Nrf2 redox signaling. Free Radical Biology and Medicine (2022).

Yang F, Smith MJ, Morrell A, Stewart T, Maret W, Mann GE. Nrf2-regulated redox signaling in human coronary smooth artery smooth muscle cells under hyperoxia, physiological normoxia and hypoxia. Free Radical Biology and Medicine (2021) 177: S86.

Yang F, Smith MJ, Morrell A, Stewart T, Maret W, Mann GE. Metallomic and redox profiling in human coronary smooth muscle cells under hyperoxia, physiological normoxia and hypoxia: crosstalk between Nrf2 signalling and zinc. Free Radical Biology and Medicine (2023).

Yang F, Smith MJ, Morrell A, Stewart T, Maret W, Mann GE. Crosstalk between Nrf2 Signalling and Zinc in Human Coronary Artery Cells under Hyperoxia, Physiological Normoxia and Hypoxia. 1st FEBS Redox Medicine Workshop (2023).

Peer-reviewed papers

Yang F, Smith MJ, Griffiths A, Morrell A, Sarah J. Chapple, Siow RC, Stewart T, Maret W, Gundi L, Mann GE. Vascular protection afforded by zinc supplementation in human coronary artery smooth muscle cells mediated by NRF2 signaling under hypoxia/reoxygenation. Redox Biology (2023) 64: 102777.

Smith MJ*, **Yang F***, Griffiths A, Morrell A, Sarah J. Chapple, Siow RC, Stewart T, Maret W, Gundi L, Mann GE. Redox and metal profiles in human coronary endothelial and smooth muscle cells under hyperoxia, physiological normoxia and hypoxia: Effects of NRF2 signaling on intracellular zinc. Redox Biology (2023) 62:102712. [*Joint first author]

Yang F, Smith MJ. Metallomic profiling in coronary ischaemia reperfusion injury: implications for Keap1-Nrf2 regulated redox signaling. Free Radical Biology Medicine (2023). Review. Submitted

Sevimli G, Smith MJ, Caglar T, Bilir S, Secilmis M, Altun HY, Yigit EN, **Yang F**, Keeley TP, Malli R, Oztürk G, Mann GE, Eroglu E. Nitric oxide biosensor uncovers diminished ferrous iron-dependency of cultured cells adapted to physiological oxygen levels. Redox Biology (2022) 53: 102319.

List of Figures

Chapter 1

Figure 1.1 Structure of the heart and blood flow through the heart 20
Figure 1.2 Anterior and posterior view of the coronary arterial and venous anatomy 22
Figure 1.3 Oxygen distribution in adult heart. 24
Figure 1.4 The basic structure of the coronary arterial wall. 26
Figure 1.5 The two phenotypes of vascular SMCs *in vivo*. 28
Figure 1.6 Crosstalk between vascular ECs and SMCs. 29
Figure 1.7 ROS generation by the mitochondrial electron transfer chain (ETC) 34
Figure 1.8 Interaction of Keap1 and Nrf2 under basal conditions and during oxidative stress 38
Figure 1.9 Post-translational mechanisms of Nrf2 regulation 40
Figure 1.10 Sulforaphane activation of Nrf2 signalling 43
Figure 1.11 GSH synthesis 44
Figure 1.12 Antioxidant effects of zinc 52
Figure 1.13 Representation of the regional distribution of PO_2 from the airways to the cytosol 56

Chapter 2

Figure 2.1 HCASMCs were cultured under controlled environment in a dual Sci-tive workstation. 63
Figure 2.2 Cryopreservation HCASMCs culture. 65
Figure 2.3 Cell number determination using haemocytometer. 66
Figure 2.4 Reaction of BCA protein assay and representative standard curve. 67
Figure 2.5 Overview of cellular impedance apparatus. 69
Figure 2.6 Schematic of MTT assay 71
Figure 2.7 Bioluminescent reactions catalysed by firefly luciferase 72
Figure 2.8 The reaction of OPA with GSH 74
Figure 2.9 Representative images of HCASMCs immunostained for SM22-α. 76
Figure 2.10 Example of RNeasy® Mini Kit procedure 78
Figure 2.11 Immunoblotting 82

Chapter 3

Figure 3.1 Phase images of HCASMCs cultures 90
Figure 3.2 Characterization of HCASMCs by immunostaining and immunoblotting 92
Figure 3.3 Proliferation of HCASMCs under 18, 5 and 1 kPa O_2 93
Figure 3.4 Doubling time of HCASMCs under 18, 5 and 1kPa O_2 level 94
Figure 3.5 Cytosolic and medium O_2 level in HCASMCs under 5kPa O_2 95
Figure 3.6 Effect of different ambient O_2 levels on HIF-1α expression in HCASMCs 96

Figure 3.7 Intracellular ATP levels in HCASMCs cultured under 18, 5 and 1kPa O_2 97
Figure 3.8 Intracellular GSH levels in HCASMCs cultured under 18, 5 and 1kPa O_2 98
Figure 3.9 Effects of different ambient O_2 levels on CAT, CuZnSOD and MnSOD expression in HCASMCs .. 99
Figure 3.10 Sulforaphane induced Nrf2 nuclear translocation in HCASMCs under 18, 5 and 1kPa O_2 100
Figure 3.11 Nrf2-regulated target protein expression in HCASMCs under 18, 5 and 1kPa O_2 102
Figure 3.12 Nrf2-regulated target mRNA expression in HCASMCs under 18, 5 and 1kPa O_2 103
Figure 3.13 Protein and mRNA expression of Bach1 in HCASMCs under 18, 5 and 1kPa O_2 104
Figure 3.14 Preliminary experiment with scrambled (control) or Nrf2 siRNA to knockdown Nrf2 transcriptional activity 105
Figure 3.15 Nrf2 silencing downregulates SFN-induced HO-1 and NQO1 protein expression 106
Figure 3.16 The effect of reactive oxygen species on modulation of vascular smooth muscle cell phenotypes 109
Figure 3.17 Graphical abstract of Chapter 3 117

Chapter 4

Figure 4.1 Total content of different metals in HCASMCs or culture medium following long-term adaptation of cells to 18, 5 and 1kPa O_2 119
Figure 4.2 Viability of HCASMCs following supplemented with $ZnCl_2$ and pyrithione or treated with TPEN 121
Figure 4.3 Total Zn content in HCASMCs supplemented with Zn or treated with TPEN under 18, 5 and 1kPa O_2 122
Figure 4.4 HO-1 and NQO1 protein and mRNA expression in HCASMCs supplemented with Zn or treated with TPEN under 18, 5 and 1kPa O_2 124
Figure 4.5 Zn supplementation induces Nrf2 nuclear translocation in HCASMCs under 18, 5 and 1kPa O_2 125
Figure 4.6 MT protein and mRNA expression in HCASMCs supplemented with Zn or treated with TPEN under 18, 5 and 1kPa O_2 127
Figure 4.7 ZnT1 protein expression in HCASMCs supplemented with Zn or treated with TPEN under 18, 5 and 1kPa O_2 128
Figure 4.8 Silencing Nrf2 transcriptional activity has a negligible effect on total Zn levels in HCASMCs 130
Figure 4.9 Nrf2, HO-1 and NQO1 protein expression in HCASMCs with Nrf2 silencing 131
Figure 4.10 Silencing Nrf2 transcriptional activity does not affect MT and ZnT1 protein expression in HCASMCs 132
Figure 4.11 Preliminary experiment with control vector 3.1C and hNrf2 vector induce Nrf2 overexpression .. 133
Figure 4.12 Nrf2 overexpression does not alter total Zn content in HCASMCs 133
Figure 4.13 Nrf2 overexpression does not affect MT and ZnT1 protein expression in HCASMCs 134
Figure 4.14 The Nrf2 inducer sulforaphane does not alter total Zn content or MT and ZnT1 protein expression in HCASMCs 136
Figure 4.15 Graphical abstract of Chapter 4 144

Chapter 5

Figure 5.1 Reoxygenation induced ROS generation in HCASMCs under 18 and 5kPa O_2 146
Figure 5.2 SFN or Zn supplementation attenuate reoxygenation-induced ROS production in HCASMCs 148
Figure 5.3 Total Zn content in HCASMCs pre-adapted to 18 or 5kPa O_2 and exposed to hypoxia-reoxygenation 149
Figure 5.4 Intracellular reduced GSH levels in HCASMCs under hypoxia-reoxygenation 150
Figure 5.5 NQO1 and GCLM protein expression in HCASMCs under hypoxia-reoxygenation..... 151
Figure 5.6 ZnT1 protein expression in HCASMCs under hypoxia-reoxygenation 152
Figure 5.7 Effects of GSH on cellular antioxidant status and Zn buffering in neurons following brain ischaemia 158
Figure 5.8 Graphical abstract for Chapter 5 160

Chapter 6

Figure 6.1 Subcellular localisation of ZnTs and ZIPs 171

List of Tables

Chapter 1

Table 1.1 Enzymatic sources of reactive oxygen species in tissues in IR injury 32
Table 1.2 Cellular antioxidant responses in ischaemia-reperfusion injury 36
Table 1.3 Studies of Nrf2 pathway in vessel and heart ischaemia-reperfusion injury 47
Table 1.4 Effects of oxygen on the proliferation, migration and phenotype of cultured cells 59

Chapter 2

Table 2.1 List of primary antibodies for immunostaining 76
Table 2.2 List of secondary antibodies for immunostaining 76
Table 2.3 Nrf2 antibody for immunostaining 77
Table 2.4 List of qPCR primers 80
Table 2.5 List of primary antibodies for immunoblotting 83
Table 2.6 List of secondary antibodies for immunoblotting 83

Chapter 3

Table 3.1 Studies of intracellular GSH levels in vascular smooth muscle cells 113

Chapter 4

Table 4.1 The metal content in human heart tissue 138

Chapter 5

Table 5.1 Effect of hypoxia-reoxygenation or ischaemia-reperfusion on Zn content 156

Chapter 6

Table 6.1 Zinc regulating genes and relation to oxygen 165

List of Abbreviations

ACh	Acetylcholine
Akt	Protein kinase B
AhR	Aryl hydrocarbon receptor
AMP	Adenosine monophosphate
APS	Ammonium persulfate
ARE	Antioxidant response element
ARNT	AhR nuclear translocator
3-AT	3-Amino-1,2,4-triazole
ATP	Adenosine 5′-triphosphate
ATTM	Ammonium tetrathiomolybdate
Bach1	BTB and CNC homology 1
BCA protein assay	Bicinchoninic acid protein assay
BSA	Bovine serum albumin
Ca	Calcium
Cav-1	Caveolin-1
CAT	Catalase
CBP	CREB-binding protein
Cd	Cadmium
CK2	Casein kinase 2
CO_2	Carbon dioxide
CTGF	Connective tissue growth factor
Cu	Copper
Cul3	Cullin 3
CPT	Cold pressure stress test
CRBP-1	Cellular retinol-binding protein-1
ddH_2O	Double-distilled water
DC	Double glycine repeat and C-terminal
DMSO	Dimethyl-sulfoxide
DMEM	Dulbecco’s modified Eagle’s medium-low glucose
DNA	Deoxyribonucleic acid
cDNA	Complementary DNA
DNase	Nuclease
dsDNA	Double-stranded DNA
D3T	3H-1,2-dithiole-3-thione
ECL	Enhanced chemiluminescence
ECs	Endothelial cells
ECM	Extracellular matrix
EDTA	Ethylenediaminetetraacetic acid
EDHF	Endothelium derived hyperpolarizing factor
EpRE	Electrophilic response element
ER	Endoplasmic reticulum
eNOS	Endothelial nitric oxide synthase
EpRE	Electrophile response element
ERK	Extracellular signal-regulated kinase
FBS	Fetal bovine serum
Fe	Iron
FPN1	Ferroportin-1

FTH1	Ferritin heavy chain 1
GCLC	Glutamate-cysteine ligase catalytic subunit
GCLM	Glutamate-cysteine ligase modifier subunit
GITC	Guanidine isothiocyanate
GLS	Glucosinolates
GPx	Glutathione peroxidase
GR	Glutathione reductase
GSH	Reduced glutathione
GSH-Px	Glutathione peroxidase
GSK3β	Glycogen synthase kinase 3β
GSSH	Oxidized glutathione
GS	GSH synthase
HAMP	Hepcidin antimicrobial peptide
HCASMCs	Human coronary artery smooth muscle cells
HCAECs	Human coronary artery endothelial cells
HIF-1α	Hypoxia-inducible factor 1
HO-1	Heme oxygenase-1
HODE	Hydroxyoctadecadienoic acid
HPLC	High-performance liquid chromatography
HRP	Horseradish peroxidases
HUVECs	Human umbilical vein endothelial cells
H_2O_2	Hydrogen peroxide
iNOS	Inducible nitric oxide
ICP-MS	Inductively coupled plasma mass spectrometry
IL-1	Interleukin-1
IR	Ischaemia-reperfusion
IS	Interventricular septum
ITC	Isothiocyanate
JNK	Jun N-terminal kinase
Keap1	Kelch-like ECH-associated protein 1
KH_2PO_4	Monopotassium phosphate
LAD	Left anterior descending
LA	Left atrium
L-NMMA	N^G-monomethyl-L-arginine
LV	Left ventricle
MAPK	Mitogen-activated protein kinase
MDA	Malondialdehyde
Mg	Magnesium
MI	Myocardial infarction
MiR	MicroRNA
Mn	Manganese
MPO	Myeloperoxidase
MRE	Metal response elements
MS	Mental stress
MsrA	Methionine sulfoxide reductase A
MTT	3-(4,5-dimethylthiazol-2-yl)-2,5-diphenyltetrazolium bromide
MTs	Metallothioneins
MT1	Metallothionein-1
MT2A	Metallothionein 2A
MT3	Metallothionein 3

MT4	Metallothionein 4
MTF-1	Metal responsive transcription factor 1
MVO_2	Myocardial volume oxygen
NaOH	Sodium hydroxide
$NaHCO_3$	Sodium bicarbonate
Na_2CO_3	Sodium carbonate
NAD	Nicotinamide adenine dinucleotide
$NADPH^+$	Nicotinamide adenine dinucleotide phosphate
NADPH	Reduced nicotinamide adenine dinucleotide phosphate
NDA	Naphthalene dicarboxaldehyde
NF-κB	Nuclear factor kappa B
NFκB1	Nuclear factor-κB subunit 1
Ni	Nickel
NO	Nitric oxide
NQO1	NAD(P)H quinone dehydrogenase 1
Nrf2	Nuclear factor erythroid 2-related factor 2
dNTP	Deoxy-ribonucleoside triphosphate
O_2^-	Superoxide anions
OD	Optical density
OGD	Oxygen-glucose deprivation
OH^-	Hydroxyl radicals
OPA	o-Phthalaldehyde
P	Phosphorylation
$p27^{kip1}$	Cyclin-dependent kinase inhibitor 1B
PBS	Ca^{2+}/Mg^{2+}-free phosphate buffered saline
PBS-T	Phosphate buffered saline + 0.1% Tween
PC	Phosphatidylcholine
pCAT	Polyethylene glycol catalase
PCR	Polymerase chain reaction
pSOD	Polyethylene glycol superoxide dismutase
PEA	Palmitoylethanolamide
PGF	Placental growth factor
PGI	Prostacyclin
PHD	Prolyl hydroxylase domain
PI3K	Phosphatidylinositol-3-kinase
PKCs	Protein kinase C family
PP_i	Pyrophosphate
P/S	Penicillin/streptomycin
PVDF	Polyvinylidene difluoride
RA	Right atrium
RNase	Ribonuclease
RPLP0	Ribosomal protein lateral stalk subunit P0
ROS	Reactive oxygen species
RT	Reverse transcription
RTKs	Receptor tyrosine kinases
RT-PCR	Reverse transcription PCR
qRT-PCR	Quantitative RT-PCR
Runx2	Runt-related transcription factor 2
RV	Right ventricle
Ry	Pyrithione

S.D.	Standard deviation
SDHA	Succinate dehydrogenase complex, subunit A
SDS	Sodium dodecyl sulfate
SDS-PAGE	Sodium dodecyl sulfate-polyacrylamide
SFN	Sulforaphane
SFR	Serum response factor
sGC	Soluble guanylyl cyclase
siRNA	Small interfering RNA
SMMHC	Smooth muscle myosin heavy chain
Sirt1	Silent information regulator 1
SLC30A	Solute carrier family 30A
SLC39A	Solute carrier family 39A
SM22-α	Smooth muscle protein 22-alpha
SMαA	Smooth muscle α-actin
sMaf	Maf proteins
SMCs	Smooth muscle cells
SMemb	Nonmuscle myosin heavy chain B
SMMHC	Smooth muscle myosin heavy chain
SOD	Superoxide dismutase
SOD1	Superoxide dismutase [Cu-Zn]
SOD2	Superoxide dismutase [Mn]
Sepw1	Selenoprotein1
TBP	TATA-binding protein
TCA	Trichloroacetic acid
Temed	N,N,N’,N’- Tetramethylethylenediamine
TLR4	Toll-like receptor 4
T_O	Oxidized thionein
T_R	Reduced thionein
βTrCP	β transducin repeats-containing proteins
TRPML1	Transient receptor potential mucolipin 1
TRPM2	Transient receptor potential melastatin 2
t-PA	Tissue-type plasminogen activator
TPEN	N,N,N′,N′-tetrakis(2-pyridinylmethyl)-1,2-ethanediamine
α-TOH	alpha-tocopherol
V	Voltage
VCAM-1	Vascular cell adhesion molecule 1
VSMCs	Vascular smooth muscle cells
vWF	Von Willebrand factor
XO	Xanthine oxidase
Xpo1	Exportin 1
XRE	Xenobiotic-responsive element
ZIPs	Zrt- and Irt-like proteins
Zn	Zinc
Zn^{2+}	Free zinc ions
ZNF658	Zinc finger protein 658
$ZnCl_2$	Zinc chloride
ZnTs	Zinc transporter proteins

Chapter 1 – Introduction

1.1 Heart and coronary circulation

1.1.1 General overview of the heart

The heart is a muscular organ located in the thoracic cavity medial to the lungs and posterior to the sternum and acts as a pump to provide the force for the blood circulation through the tissues of body. As shown in **Figure 1.1**, in humans, the heart is divided into four chambers: right atrium and ventricle and left atrium and ventricle (Akhter, 2011). Blood in the right ventricle is delivered to the pulmonary trunk and is then divided into the right and left lung by pulmonary arteries. Blood oxygenated in the lungs is returned to the left atrium by four pulmonary veins. Blood in left ventricle is pumped into the aorta, distributed to tissues of the entire body, and ultimately, deoxygenated blood is brought back to right atrium via the superior and inferior vena cava (Huber et al., 2018; Santini et al., 2016). Although blood is not directly contact with the tissues, oxygen, nutrients and waste products are exchanged through the walls of capillaries.

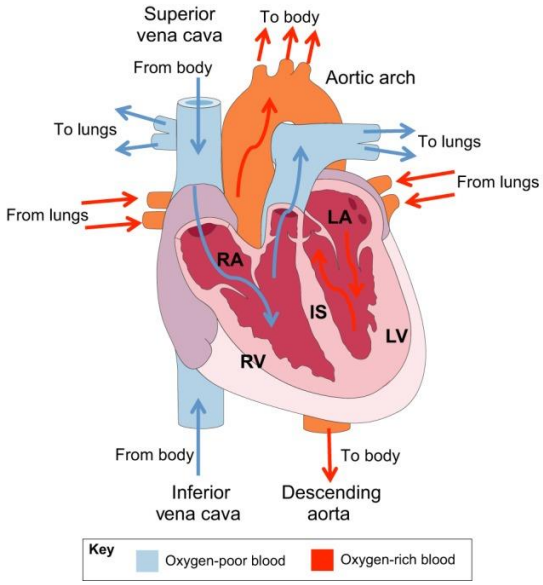

Figure 1.1 Structure of the heart and blood flow through the heart
The adult mammalian heart is made up of four chambers: right atrium and ventricle and left atrium and ventricle. Oxygen-poor blood (blue arrows) from tissues is collected into the right atrium via the superior and inferior vena cava and flows to the right ventricle via the tricuspid valve. Oxygen-rich blood (red arrows) from the lungs flows into the left atrium and is pumped into the left ventricle. Taken from (Santini et al., 2016).
Abbreviation: RA, right atrium; LA, left atrium; RV, right ventricle; LV, left ventricle; IS, interventricular septum.

1.1.2 General overview of coronary circulation

The term "coronary" is derived from the Latin *coronarius* (of a crown), which was first used in the 1670's to describe the blood vessels that lie within the subepicardial connective tissue and course over the surface of the heart (Goodwill et al., 2017). Coronary arteries are branches of the ascending aorta, which are responsible for suppling blood to the myocardium and other structures of the heart (Goodwill et al., 2017).

As illustrated in **Figure 1.2**, the main stem of left coronary artery originates in the left posterior sinus and then divides into two arteries of nearly equal diameter (3.7±0.4mm) (Dodge et al., 1992), namely left anterior descending (LAD) and the circumflex coronary arteries (Kato et al., 2018). The main stem of left coronary has variable length and can be

absent in ~1% of humans, with separate orifices for two primary branches. The LAD runs down the anterior interventricular groove to the apex of the heart and gives rise to the diagonals, the septal perforators, and the right ventricular branches. The circumflex coronary artery courses at roughly a right angle to the LAD and runs down the left atrioventricular groove and give rises to obtuse marginal branches. The circumflex coronary ends where the plane of the interventricular septum crosses the plane of the atrioventricular groove in nearly 90% of humans, whilst in around 10% of humans, it continues to the crux of the heart to give rise to the posterior descending artery (left dominance). The dominance of the coronary circulation depends on the artery from which the posterior descending artery originates (Allwork, 1987). The right coronary artery originates from anterior aortic sinus and runs anteriorly between the right atrium and the pulmonary trunk before reaching descending in the right atrioventricular groove and giving rise to acute marginal branches. In approximately 90% of humans, the right coronary artery runs down the posterior interventricular groove and bifurcates into the posterior descending coronary artery after reaching the plane of the posterior interventricular septum (right dominance) (Waller et al., 1992)

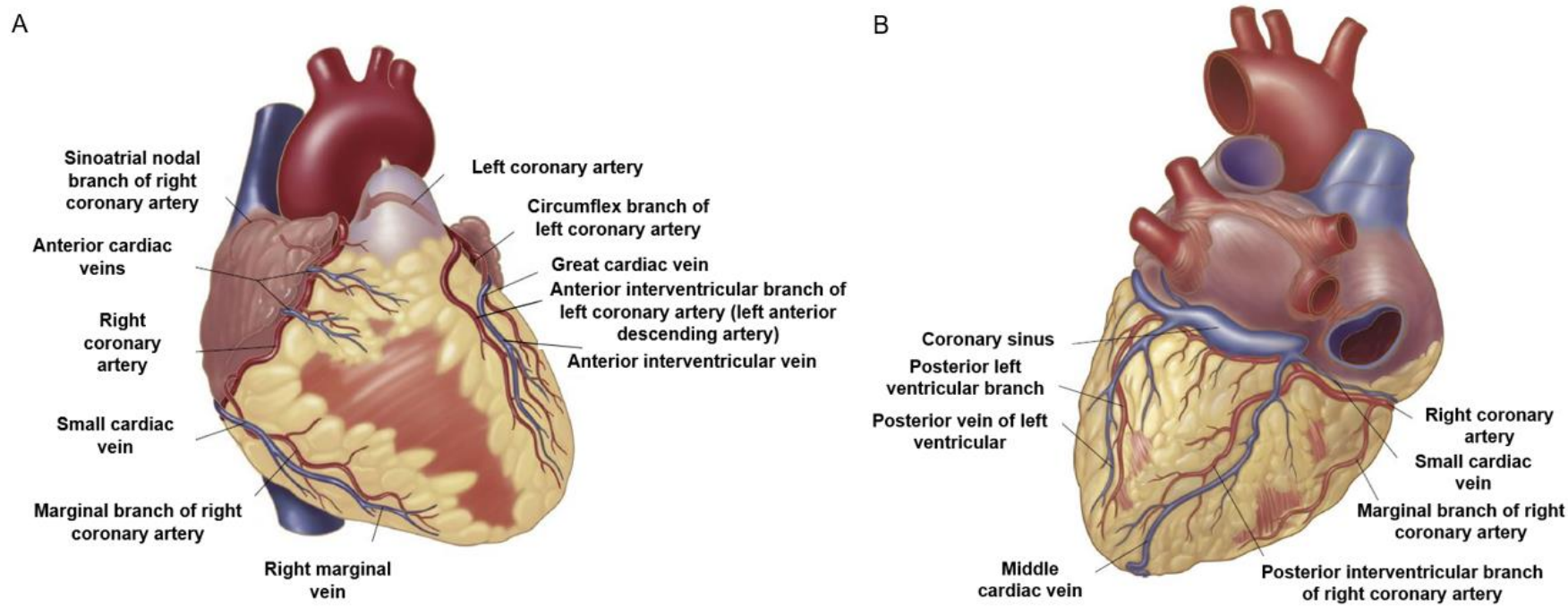

Figure 1.2 Anterior and posterior view of the coronary arterial and venous anatomy
The main stem of left coronary artery originates in the left posterior sinus and then divides into left anterior descending and the circumflex coronary arteries. The right coronary artery originates from anterior aortic sinus and reaches descending in the right atrioventricular groove, giving rise to acute marginal branches. Taken from (Akhter, 2011).

In the normal adult human heart in the awake state, resting left coronary blood flow ranges between ~0.5-1.0 ml/min/g (Duncker and Bache, 2008; Feigl, 1983), whilst right ventricular blood flow typically ranges between 0.3-0.6 ml/min/g (Hart et al., 2001; Murakami et al., 1989). This results from underlying differences in the rate of myocardial volume oxygen (MVO_2) between the left ventricle (~50-100µl O_2/min/g) and right ventricle (~30-50µl O_2/min/g) (Duncker and Bache, 2008; Goodwill et al., 2017).

Coronary veinscan be divided into the coronary sinus, the anterior right ventricular veins and thebesian veins. The veins of the heart predominantly drain into the coronary sinus, which lies in the posterior atrioventricular groove. It receives almost 55% of coronary venous blood flow primarily from left ventricle. The anterior right ventricular veins drain the right ventricle and receives approximately 35% of the coronary venous blood, which passes along the right atrioventricular groove and directly enter right atrium. The thebesian veins are small venous tributaries that drain around 10% of left ventricular venous blood into left ventricular cavity. Anterior and posterior view of the coronary arterial and venous anatomy in **Figure 1.2** (Akhter, 2011).

The heart has a high capillary density of 3000-4000/mm^2 (Laughlin and Tomanek, 1987), compared with 500-2000 capillaries/mm^2 in skeletal muscle (Gute et al., 1996). This facilitates a high level of oxygen extraction, noting that the heart extracts 70%-80% of arterially delivered oxygen under resting conditions (Goodwill et al., 2017), which is higher than the 30-40% in skeletal muscle (Duncker and Bache, 2008; Feigl, 1983).

1.1.3 O_2 distribution in coronary arteries *in vivo*

The heart is second only to the lungs in terms of exposure to O_2. Compared to the lungs, the heart requires more oxygen for pumping blood throughout the body. Previous studies have reported that O_2 levels in the ascending aorta of rats are ~12.5kPa (Keeley and Mann, 2019). Gundry and colleagues measured blood pO_2 from different coronary artery branches in patients undergoing coronary artery bypass grafting or aortic valve replacement surgery and reported levels of around 5kPa. Moreover, O_2 content is lower in the right and anterior/septal regions of the heart, resulting from more O_2 uptake (Gundry et al., 1996; Keeley and Mann, 2019). In addition, previous studies investigated blood pO_2 within the coronary sinus in humans, reporting values ranging from 2.7-4.5kPa (Keeley and Mann, 2019; McNulty et al., 2005; Vretzakis et al., 2004; White et al., 1991) (**Figure 1.3**). In surveying the literature, there appear to be no reports for O_2 content in the coronary artery of healthy humans or experimental animal models (Keeley and Mann, 2019).

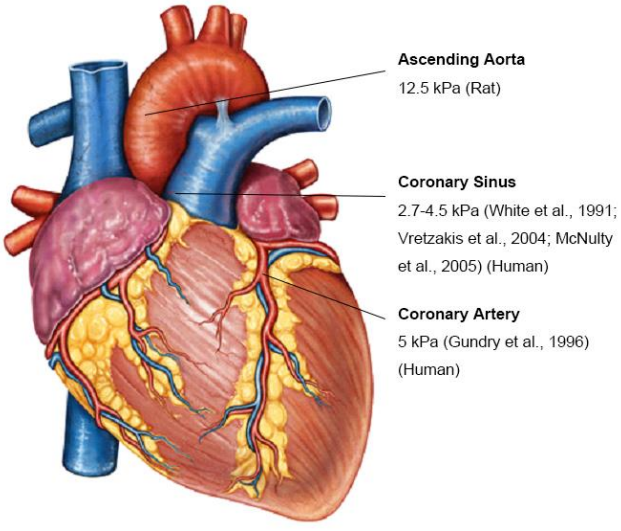

Figure 1.3 Oxygen distribution in adult heart.
A summary figure of published studies of artery O_2 content in the heart. Blood O_2 levels in different coronary artery branches in patients undergoing coronary artery bypass grafting or aortic valve replacement surgery has been reported to be ~5 kPa. Taken from (Gundry et al., 1996; Keeley and Mann, 2019).

1.2 Human coronary smooth muscle cells

1.2.1 Histologic features of the normal coronary arteries

The basic structure of the coronary arterial wall consists of tunica intima, tunica media and tunica adventitia from within to outward (see **Figure 1.4**). The confluent monolayer of endothelium is comprised endothelial cells (ECs), which provides a selective diffusion barrier between the blood and the other blood vessel wall layers. Previous studies have shown that ECs have unique metabolic and endocrine functions that play an important role in diseases (Adams et al., 1989; Pober et al., 2009). ECs can detect mechanical shear signals from blood flow and convert a sequence of biological responses such as changing endothelial transport junctions, altering ion channels and modulating gene expressions (Davies, 1995; Davies et al., 1984; Kaushal et al., 2001; Nagel et al., 1999; Tarbell, 2010). Moreover, ECs can produce an antithrombotic agent (prostacyclin, PGI_2), a prothrombotic agent (von Willebrand factor, vWF), a fibrinolytic agent (tissue-type plasminogen activator, t-PA), an inflammatory mediator (interleukin-1, IL-1) and growth factors (fibroblast growth factor, platelet-derived growth factor) (Niu et al., 2014; Waller et al., 1992). The media consists of up to 40 layers of helically or circumferentially oriented smooth muscle cells (SMCs), elastic fibers and collagen fibers (Waller et al., 1992). The thickness of normal tunica media is on average 200μm (125-350 μm) (Waller, 1989). The media layer is separated from the intimal layer and adventitial layer by a fenestrated sheet of elastic tissue called the internal elastic membrane and the external elastic membrane. The outermost layer is the tunica adventitia, which contains fibrous tissue.

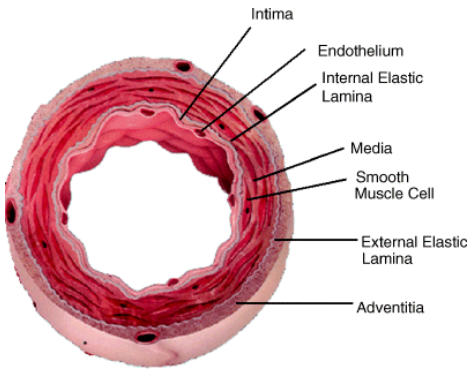

Figure 1.4 The basic structure of the coronary arterial wall.
The coronary arterial wall consists of tunica intima, tunica media and tunica adventitia. The media layer is separated from the intimal layer by an internal elastic membrane. Taken from (Davis et al., 2003).

1.2.2 Characteristics and function of coronary artery smooth muscle cell

Vascular SMCs, located in the tunica media layer of vessel walls, exhibit contractile function and regulate vascular tone and vessel diameter to maintain blood pressure and tissue perfusion (Owens et al., 2004). In humans, SMCs retain the characteristics of phenotypic modulation *in vivo*: a quiescent one with differentiated SMCs (contractile state) and a proliferating one with dedifferentiated SMCs (synthetic state). Morphologically, contractile SMCs are elongated and spindle-shaped, whilst synthetic SMCs have a rhomboid and cobblestone-like morphology (see **Figure 1.5**) (Rensen et al., 2007). Under normal homeostatic conditions, vascular SMCs display a contractile phenotype, whose main function is the maintenance of vascular tone. They exhibit a characteristic "muscle-like" appearance, with up to 75% of their cytoplasm containing contractile filaments (Thyberg et al., 1990; Wang et al., 2015). During vessel remodelling in physiological conditions, such as pregnancy and exercise, de-differentiated SMCs decrease the expression of contractile proteins and dramatically increase their rate of cell proliferation, migration and synthetic capacity (Owens et al., 2004; Yoshida et al., 2008). Due to these properties, SMCs are suited not only for short-term regulation of the vessel diameter but also for longer-term adaptation, via structural

remodelling by changing cell number and connective tissue composition (Rensen et al., 2007). Pathological conditions, such as hyperlipidaemia and hyperglycaemia and various disease states such as atherosclerosis and restenosis have been shown to modulate SMCs function from a contractile to a synthetic phenotype, implicating a critical role for SMCs in the development of vascular diseases (Jain, 2003; Madi et al., 2009; Rensen et al., 2007; Shen et al., 2013).

Meanwhile, *in vitro* cell culture is a process that involves loss of contractile markers and restoration of contractile markers after confluence. The degree of VSMCs differentiation can be detected by the expression level of VSMCs specific markers. Contractile phenotype markers of VSMCs are widely used in the literature, and are divided into early (smooth muscle α-actin (SMαA), myocardin and smooth muscle protein 22-alpha (SM22α)), mid-term (H-caldesmon and calponin 1) and late (smooth muscle myosin heavy chain (SMMHC)-1 and -2 and smoothelin) via their appearance during embryonic development or during differentiation of stem cells into VSMCs (Babij et al., 1992b; Han et al., 2008; Rashidi et al., 2018; Rodriguez et al., 2006). Previous studies have reported that late markers are the first to disappear during phenotype modulation (Babij et al., 1992a; van Eys et al., 2007; vanderLoop et al., 1996). For example, the cytoskeletal protein Smoothelin, is lost in primary or long-term SMCs cultures and is only found in fully differentiated contractile SMCs (van Eys et al., 2007; vanderLoop et al., 1996). SMαA is greatly decreased during the proliferative phase of cell growth in culture but post-confluence quiescent cells exhibit enhanced expression of SMMHC-1 and SMMHC-2 and SMαA (Fatigati and Murphy, 1984; Reusch et al., 1996; Rovner et al., 1986). There are several synthetic phenotype markers such as cellular retinol-binding protein-1 (CRBP-1) (Neuville et al., 1997; Rensen et al., 2007) and nonmuscle myosin heavy chain B (SMemb) (Aikawa et al., 1993; Kuroo et al., 1989). These

markers are utilized less widely due to their lower SMC specificity (Beamish et al., 2010). In addition, various factors affect the phenotype of VSMCs in culture such as the confluence of the culture, passage number and growth factors in medium.

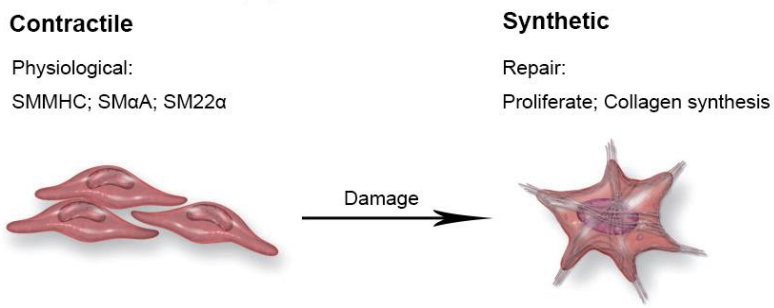

Figure 1.5 The two phenotypes of vascular SMCs *in vivo*.
A quiescent phenotype with differentiated SMCs (contractile states) and a proliferating one with de-differentiated SMCs (synthetic states). Taken from (Durham et al., 2018).

1.2.3 Interactions between vascular endothelial and smooth muscle cells

Interactions between vascular ECs and SMCs play an important role in maintaining vascular integrity, structure and function. Communication between endothelial cells (ECs) and SMCs occurs through direct cell-to-cell contact and through the secretion of paracrine signals. ECs regulate vascular tone through vasorelaxing molecules such as nitric oxide (NO), prostacyclin (PGI), and endothelium-derived hyperpolarising factor (EDHF) and vasoconstricting mediators such as endothelin-1 and thromboxane (Dora, 2001; Eelen et al., 2018; Erusalimsky and Moncada, 2007; Moncada and Higgs, 1993; Moncada et al., 1991; Pacher et al., 2007; Tousoulis et al., 2005; Triggle et al., 2012). NO is a key endothelium-derived relaxing factor that activates of soluble guanylate cyclase (sGC) and increases cGMP production, following metabolism of L-arginine to NO via endothelial NO synthase (eNOS) (Durante et al., 2007; Palmer et al., 1988; Seki et al., 1997). Stimuli (such as acetylcholine) normally lead to vasorelaxation in the presence of an intact vascular endothelium via receptor

mediated stimulation of endothelial NO production, however acetylcholine (ACh) causes vasoconstriction when acting directly on underlying SMCs in vascular areas with an injured endothelium (Tousoulis and Davies, 1998; Widlansky et al., 2003). Except for vasoconstricting factors released by ECs, SMCs regulate vascular tone via stretch-sensitive ion channels (Davis et al., 1992), phospholipase C (Segal, 1994; Triggle et al., 2012). These responses increase intracellular calcium in SMCs, thereby triggering contraction (Segal, 1994) (see **Figure 1.6**).

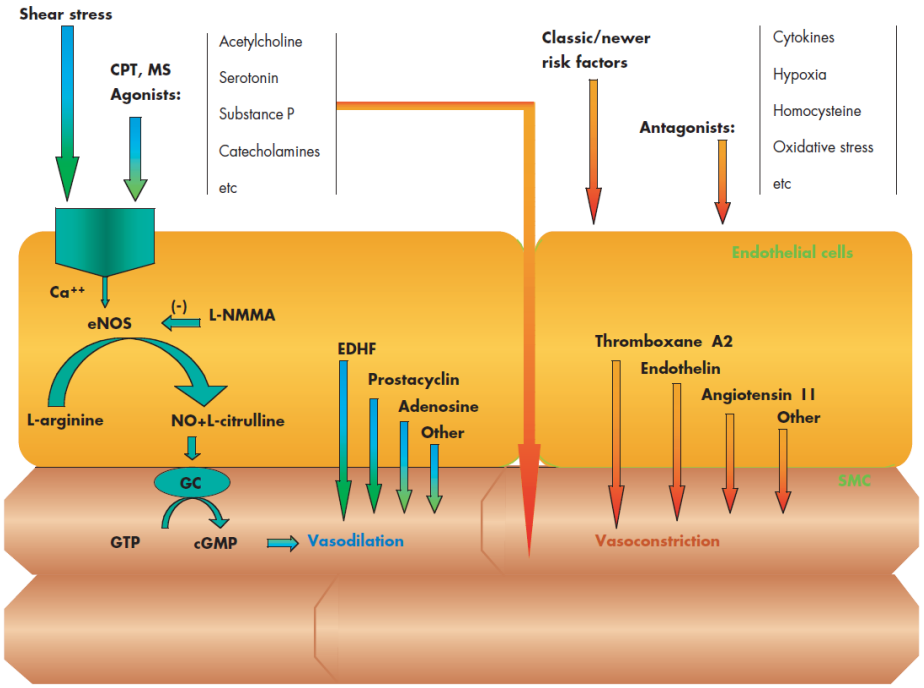

Figure 1.6 Crosstalk between vascular ECs and SMCs.
Factors leading to vasodilatation, include NO, PGI_2, EDHF and other agents, whilst factors leading to vasoconstriction include endothelin 1, thromboxane A2, Angiotensin II and other factors. Taken from (Tousoulis et al., 2005).
Abbreviations: ECs, endothelial cells; SMCs, smooth muscle cells; NO, nitric oxide; PGI, prostacyclin; EDHF, endothelium derived hyperpolarizing factor; CPT, cold pressure stress test; eNOS, endothelial nitric oxide synthase; GC, guanylyl cyclase; L-NMMA, N^G-monomethyl-L-arginine; MS, mental stress.

1.3 Coronary ischaemia-reperfusion injury (IR)

1.3.1 General overview of coronary ischaemia-reperfusion injury

Ischaemia-reperfusion (IR) is a pathological condition characterised by an interruption of blood supply to an organ followed by the restoration of perfusion. Coronary IR injury has high morbidity and mortality rate, leading to a variety of types of heart diseases such as myocardial infarction, heart failure and arrhythmias (Braunwald and Kloner, 1982; Granger and Kvietys, 2015). Occlusion of coronary artery blood supply is mainly caused by an atherosclerotic plaque rupture/erosion with superimposed thrombosis and results in a severe imbalance of oxygen and nutritious supply and demand (Altamirano et al., 2015; Heusch, 2016). IR injury also occurs in various clinical settings such as anti-platelet and anti-thrombotic therapy, coronary angioplasty, coronary artery bypass graft surgery and organ transplantation (Eltzschig and Collard, 2004; Turer and Hill, 2010). Whilst reperfusion and reoxygenation is essential for survival, it also initiates an exacerbation of tissue injury (Eltzschig and Collard, 2004; Hearse et al., 1993). For example, previous studies have reported that the reactive oxygen species (ROS) are produced on reperfusion of the ischaemic heart (Downey, 1990; Granger and Kvietys, 2015), noting that surgical revascularisation may actually induce periprocedural myocardial infarction (Heusch, 2016). Parker et al. reported that the coronary vascular resistance increases progressively during the first 3h of reperfusion after 2h of ischaemia in dog hearts (Parker et al., 1975). Coronary IR injury affects not only cardiomyocytes but also the coronary vasculature. Hence, it is important to understand the molecular mechanisms underlying coronary IR progression and to investigate the changes in cells lining the coronary arteries *in vivo*.

1.3.2 Underlying mechanisms and consequences of coronary ischaemia - reperfusion injury

In the previous decades, the understanding of the pathophysiology of IR injury has significantly advanced. The pathogenesis of IR is complex and involves oxidant production (Eltzschig and Collard, 2004), formation of inflammatory mediators (Collard et al., 1999), altered membrane ATP-dependent ionic pump function (Eltzschig and Collard, 2004), leukocyte adhesion (Toyokuni, 1999), transendothelial leukocyte migration (Carden and Granger, 2000), increased microvascular permeability and oedema formation (Hausenloy et al., 2019; Heusch, 2016), platelet-leukocyte aggregation and decreased endothelium-dependent relaxation (Maxwell and Lip, 1997; Reffelmann et al., 2003). Whilst a variety of mechanisms have been proposed, oxidative stress continues to receive much attention as a critical factor in the pathological process.

There are various sources of reactive oxygen species (ROS) generated in tissues following IR injury. The most likely processes involved in oxidative stress are xanthine oxidase (XO), NADPH oxidase (NOX), the mitochondrial electron transport chain (ETC), and uncoupled nitric oxide synthase (NOS) (Granger and Kvietys, 2015; Tejero et al., 2019). These sources are present in many tissues, whilst some sources of ROS production are especially enriched in certain tissues, like XO in intestinal tract and liver (Auscher et al., 1979; Della Corte et al., 1969) and mitochondria in the metabolically active brain and heart (Harrison, 2002; Parks and Granger, 1986). As recently reviewed, the enzymatic sources of ROS have been reported in IR injury in different tissues (see **Table 1.1**) (Granger and Kvietys, 2015; Risbano and Gladwin, 2013).

Table 1.1 Enzymatic sources of reactive oxygen species in tissues in IR injury

ROS source	Tissue	References
Xanthine oxidase	Intestine, heart, lung, liver, skin, brain, skeletal muscle, eye, pancreas, stomach, kidney, testes, joints, spinal cord	(Adkison et al., 1986; Akgur et al., 1994; Allison et al., 1990; Chambers et al., 1985; Granger et al., 1981; Hotter et al., 1995; Im et al., 1984; Korthuis et al., 1985; Paller et al., 1984; Patt et al., 1988; Perry et al., 1986; Qayumi et al., 1994; Rieger et al., 2002; Woodruff et al., 1986)
NADPH oxidase	Intestine, heart, eye, lung, brain, stomach, liver, kidney, testes	(Fisher et al., 1999; Ikeda et al., 2001; Jang et al., 2012; Korthuis et al., 1999; Lehnert et al., 2003; Nakagiri et al., 2007; Sener et al., 2015; Walder et al., 1997; Yokota et al., 2011)
Mitochondrial electron transport chain	Heart, brain, intestine, lung, skeletal muscle, liver, kidney, stomach, testes, spinal cord	(Gonzalez-Flecha and Boveris, 1995; Gonzalez-Flecha et al., 1993; Ichikawa et al., 2004; Lysiak et al., 2007; Muthuraman et al., 2011; Paradies et al., 2004; Piantadosi and Zhang, 1996; Powell and Jackson, 2003; Roseborough et al., 2006; Tran et al., 2012)
Nitric oxide synthase	Liver, heart	(De Pascali et al., 2014; Elrod et al., 2006; Moens et al., 2008; Perkins et al., 2012)

Abbreviations: NADPH, reduced nicotinamide adenine dinucleotide phosphate. Taken from (Granger and Kvietys, 2015).

NOX family enzymes and the mitochondrial respiratory chain appear to be main sources of ROS in vascular system (Cadenas, 2018; Tejero et al., 2019). NOXs, multiprotein enzyme complexes, catalyse the electron transport from NADPH to O_2, forming mainly superoxide (O_2^-) and hydrogen peroxide (H_2O_2). The mammalian NOX family comprises seven isoforms, namely NOX1-NOX5 and dual oxidases (DUOX) 1 and 2 (Bedard and Krause, 2007; Drummond et al., 2011). The most relevant isoforms expressed in human vasculature are NOX1, 2, 4 and 5 (Drummond and Sobey, 2014; Lassegue et al., 2012) and the isoforms NOX1 and 4 are abundant in VSMCs (Ellmark et al., 2005; Lassegue et al., 2001). Many studies have reported that high NOX1 levels are involved in IR injury (Kahles et al., 2010), coronary artery disease (Guzik et al., 2006) and hypertension (Wind et al., 2010). The ETC has been considered as the physiological significant generator of ROS in vascular cells (see **Figure 1.7**) (Tejero et al., 2019). Under normal conditions, the transfer of electrons from ETC complex I and complex II release energy to pump H^+ from the matrix to the inner membrane space, which generates a proton-motive force used to move H^+ through adenosine triphosphate (ATP) synthase and phosphorylation of adenosine diphosphate (ADP) to ATP at complex V (Chen and Zweier, 2014; Krauss et al., 2005). The majority of electrons reduce oxygen to water at complex IV, whilst around 2-11% electrons escape from the chain mainly at complex I and complex III to form $O_2^{\cdot-}$ (Boveris and Chance, 1973; Granger and Kvietys, 2015). The ETC and NADH pool become reduced and succinate increases in IR injury, which promotes reverse electron (e^-) transfer upon reperfusion, resulting in increased O_2^- production (Chouchani et al., 2014; Zorov et al., 2014). In addition, early studies reported XO is a main source of ROS after IR injury (Berry and Hare, 2004). Xanthine dehydrogenase (XDH) is converted to XO during ischaemia using O_2 as the electron acceptor, leading to the formation of ROS such as O_2^-, H_2O_2 and hydroxyl radicals (OH^-) (Li and Jackson, 2002; McCord, 1985; Nishino, 1994). Several studies showed a beneficial effect of XO during reperfusion of the

dog heart (Chambers et al., 1985), whilst human and rabbit hearts did not show protection after XO inhibition (Downey et al., 1987; Eddy et al., 1987). Animal studies have shown that XO leaks from enzyme-rich tissues into plasma and binds to vascular endothelial cells in tissues (e.g. lung vasculature) distant from the liver or intestinal tract and is involved in ROS production in IR injury (Adachi et al., 1993; Terada et al., 1992; Vickers et al., 1998; Yokoyama et al., 1990). Although most studies of the role of oxidative stress in IR damage have focused on a single source of ROS, it is the most likely that there are interactions between ROS producing enzymes. ROS are produced by one source such as NOX and then activate a second source such as mitochondria to increase further ROS production, which is supported by H_2O_2, a relatively stable primary or secondary product of all sources with a cellular half-life of around 10^{-3} s, that mediates ROS induced ROS production (Cai, 2005; D'Autreaux and Toledano, 2007; Granger and Kvietys, 2015; Sies and Jones, 2020) .

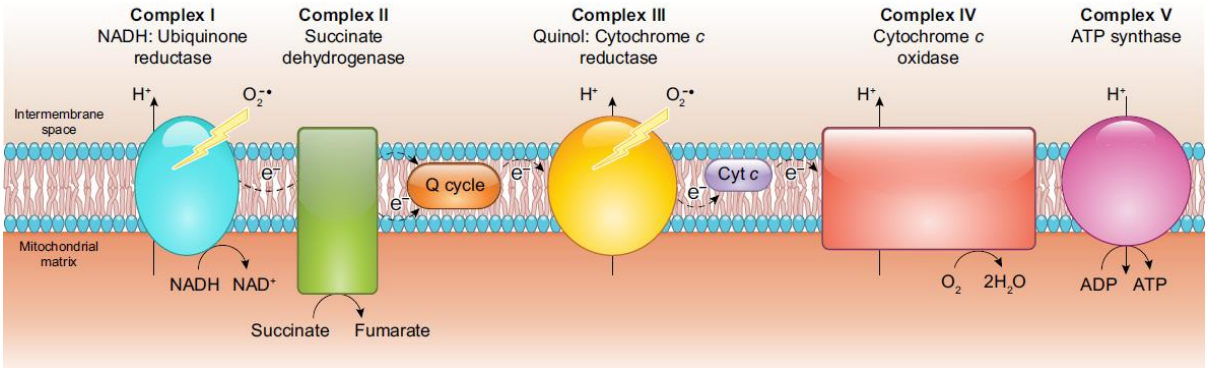

Figure 1.7 ROS generation by the mitochondrial electron transfer chain (ETC)
The ETC consists of complexes I-IV coupled by mobile carriers (coenzyme Q and cytochrome c). Mitochondria generate ATP at complex V through proton-motive force generated by the transferation of electrons from ETC complex I and complex II. Most electrons reduce oxygen to water at complex IV, whilst the leakage of electrons mainly at complex I or complex III form O_2^- via reduction of O_2. Taken from (Tejero et al., 2019).
Abbreviations: ETC, mitochondrial electron transfer chain; ADP, adenosine diphosphate; ATP, adenosine triphosphate; O_2^-, superoxide; Q, Coenzyme Q; Cyt c, cytochrome c; NADH, nicotinamide adenine dinucleotide; e^-, electrons.

1.4 Keap1-Nrf2 cellular antioxidant signalling pathway

Notably, many studies have reported an imbalance between ROS generation and the ability of tissues to detoxify ROS during IR damage (Granger and Kvietys, 2015; Granger et al., 1981; Guarnieri et al., 1980). The oxidative stress induced by overproduction of ROS in cells is counteracted by the upregulation of cellular antioxidant defences. As summarized in **Table 1.2,** numerous studies have reported antioxidant responses in IR injury such as GSH, antioxidant enzymes and antioxidant transcription factors, all of which have the potential for therapeutic interventions to ameliorate IR injury *in vivo*.

Table 1.2 Cellular antioxidant responses in ischaemia-reperfusion injury

Species	Tissue or cell	Ischaemia duration	Reperfusion duration	Antioxidant responses	Reference
Human	Cardiomyocytes; blood	-	-	Allopurinol- ROS↓ in cardiomyocytes, SOD↑ in blood of patients during tetralogy of Fallot surgical correction	(Rachmat et al., 2013)
Human	Human renal proximal tubule cell line HK-2	4-6h	4-6h	Necrostatin-1- HIF-1α↓, MDA↓ and $NADP^+$/NADPH ratio↓	(Shen et al., 2019a)
Human	Human intestinal epithelial cell line Caco-2	2h	4h	Glutamine- intracellular GSH↑ and DNA synthesis	(Wasa et al., 2005)
Mice	Cardiac tissue	1h	+	α-TOH (the strongest antioxidant form of vitamin E) - MPO expression and activity↓, ROS↓ within the infarcted tissue	(Wallert et al., 2019)
Rat	Cardiomyocyte	-	-	HO-1 gene expression 5-fold↑ 1 week after myocardial infarction; return to basal levels after a further 4 weeks	(Lakkisto et al., 2002)
Rat	Cardiac tissue; Plasma	30min	1h	SFN mediated cardioprotection by transient Nrf2 activation↑ (observed after 15min reperfusion), followed by phase I enzymes↑ at end of reperfusion (via AhR/XRE binding), long-term protective mechanism	(Silva-Palacios et al., 2019)
Rat	Cardiomyocyte	2h	4h	Activation of Sirt1 signalling - SOD activity↑, myocardium superoxide generation↓, NOX2 expression↓, MDA level↓	(Yu et al., 2016)
Rat	Cardiac tissue	30min	2h	PEA and Baicalein (9:1 in mass) at a dose of 10 mg/kg - MDA↓, SOD activity↑, GSH levels↑ and CAT activities ↑ in myocardial tissue	(D'Amico et al., 2019)
Rat	Lung tissue	1h	2h	Ozone oxidative preconditioning - Nrf2 pathway↑	(Wang et al., 2018)

Abbreviations: ROS, reactive oxygen species; SOD, superoxide dismutase; HIF-1α, hypoxia-inducible factor 1-alpha; $NADP^+$, nicotinamide adenine dinucleotide phosphate; NADPH, reduced nicotinamide adenine dinucleotide phosphate; α-TOH, alpha-tocopherol; PC, phosphatidylcholine; HODE, hydroxyoctadecadienoic acid; Sirt1, silent information regulator 1; I/R, ischaemia/reperfusion; MDA, malondialdehyde; SOD, superoxide dismutase; NOX2, NADPH oxidase 2; PEA, palmitoylethanolamide; AhR, ary hydrocarbon recepter; XRE, xenobiotic response elements; SFN, sulforaphane; CAT, catalase; MPO, myeloperoxidase; GSH, glutathione.

1.4.1 Nrf2-Keap1 interactions

Nuclear factor erythroid 2- related factor 2 (Nrf2), a well-known antioxidant transcription factor, that belongs to the cap-n-collar subfamily of basic region leucine zipper-type transcription factors (Motohashi & Yamamoto, 2004), and which plays a critical role in the maintenance of cellular redox homeostasis involving in a variety of diseases, such as neurodegeneration (Johnson et al., 2008), inflammation (Rangasamy et al., 2005), cancer (Kansanen et al., 2013) and cardiovascular disease (Jiang et al., 2016). Importantly, Nrf2 serves as a critical regulator to counteract oxidative stress (Cheng et al., 2013; Itoh et al., 1999; Maltese et al., 2017). The activation of Nrf2 can induce more than 200 different protective genes (Chorley et al., 2012), including antioxidant enzymes and detoxifying enzymes (Bellezza et al., 2018; Holmstrom et al., 2016; Shen et al., 2019b; Yamamoto et al., 2018).

As summarized in **Figure 1.8**, Nrf2 protein levels are maintained relatively low under physiological conditions due to rapid ubiquitination and proteasomal degradation mediated by Kelch-like ECH-associated protein 1 (Keap1) (Suzuki and Yamamoto, 2015). Keap1, an adaptor of Cullin 3 (CUL3)-E3 ubiquitin ligase (RBX1) complex, is not only an important negative regulator of Nrf2 but also a sensor of chemical Nrf2 inducers *in vivo* (Suzuki and Yamamoto, 2015). Upon exposure to Nrf2 inducers, Keap1 select cysteine residues (e.g., C151) are modified, resulting in repression of Nrf2 ubiquitination and stabilisation of Nrf2 (Bryan et al., 2013; Holland and Fishbein, 2010; Zhang and Hannink, 2003). Previous studies have reported that distinct chemicals that induce the Keap1-Nrf2 pathway are related to different patterns of Keap1 cysteine modification (Suzuki et al., 2019; Yamamoto et al., 2008; Zhang and Hannink, 2003). This process is referred to as the cysteine code. Subsequently,

newly synthesised Nrf2 translocates into the nucleus. Nrf2 heterodimerizes with small Maf proteins (sMaf) and binds to the antioxidant response element (ARE) or electrophilic response element (EpRE) in the promoter region of target genes (Ahn et al., 2010; Satoh et al., 2013), serving as a cytoprotective regulator to upregulate antioxidant gene expression such as NAD(P)H Quinone Dehydrogenase 1 (NQO1), heme oxygenase-1 (HO-1), and glutamate-cysteine ligase catalytic subunit (GCLC) (Chapple et al., 2012; Ishii et al., 2000; Maltese et al., 2017; Suzuki et al., 2019).

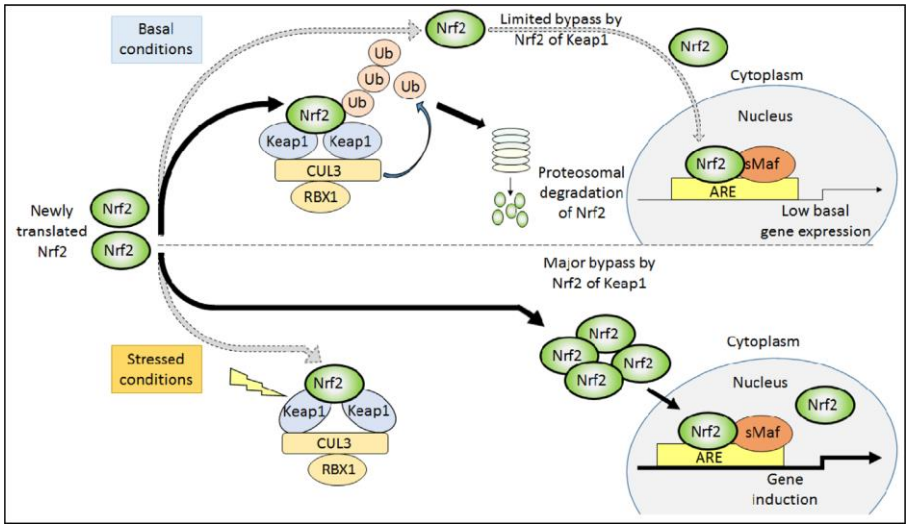

Figure 1.8 Interaction of Keap1 and Nrf2 under basal conditions and during oxidative stress
In the basal state, Keap1 is a key negative regulator of Nrf2, which results in proteasomal degradation and ubiquitination of Nrf2. Following oxidative or electrophilic stress, Nrf2 translocates into the nucleus and binds to the ARE in target genes, serving as a cytoprotective regulator. Taken from (Tebay et al., 2015).
Abbreviations: Nrf2, nuclear factor erythroid 2- related factor 2; Keap1, Kelch-like ECH-associated protein 1; ARE, antioxidant response element; sMaf, small Maf proteins; CUL3, Cullin 3; RBX1, E3 ubiquitin ligase; Ub, ubiquitination.

In addition to ubiquitination by Keap1, Nrf2 is targeted for proteasomal degradation by beta-transducin repeats-containing proteins (β-TrCP) as well binding to DSGIS or DSAPGS peptide sequences in the Neh6 domain of Nrf2 (Chowdhry et al., 2013; Tebay et al., 2015). Meanwhile, the phosphorylation of residues in DSGIS motif by glycogen synthase kinase-3 (GSK-3) contributes to β-TrCP-mediated degradation of Nrf2 (Chowdhry et al., 2013; Tebay

et al., 2015; Wu and He, 2006) (see **Figure 1.9**). The β-TrCP and GSK-3 axis plays a key role in the stability of Nrf2 in the nucleus (McMahon et al., 2018). GSK-3 was discovered over 40 years ago as an important regulator of glycogen metabolism that represses the last step in glycogen synthesis. Whilst GSK-3 is now well-known in the regulation of many cell functions, such as insulin signalling, cell fates specification during embryonic development, cell division, apoptosis and microtubule function (Cohen and Frame, 2001; Frame and Cohen, 2001). Chowdhry and his colleagues have reported that activation of GSK-3 in human lung A549 cells containing mutant Keap1 markedly decreased endogenous Nrf2 protein and reduced by 10-50% normal levels of mRNA of Nrf2-regulated enzymes, such as the GCLC, HO-1 and NQO1 (Chowdhry et al., 2013).

1.4.2 Alternative mechanisms of Nrf2 regulation

Despite the Nrf2-Keap1 defence pathway system, several studies have implicated alternative Keap1-independent regulation of Nrf2 (**Figure 1.9**). Post translationally, Nrf2 is regulated by 5' AMP-activated protein kinase (AMPK) and targets of rapamycin (mTOR) via feedback loops in response to cellular energy and nutrition (Fraenkel et al., 2008; Tebay et al., 2015). As illustrated in **Figure 1.9**, the binding of insulin and growth factors to receptors activates phosphoinositide 3-kinases (PI3K), which increases the activity of protein kinase B (Akt) and mTOR complex 2 (mTORC2) (O'Reilly et al., 2006; Sarbassov et al., 2005). The activation of PI3K-Akt-mTORC2 signalling pathway inhibits GSK-3 activity, resulting in inhibition of β-TrCP-mediated Nrf2 degradation. Meanwhile, GSK-3 phosphorylates Nrf2, leading to Fyn-mediated Nrf2 nuclear exclusion (Culbreth and Aschner, 2018). Under low nutrient conditions, the activity of mTOR complex 1 (mTORC1) is decreased by activation of AMPK, leading to the decrease phosphorylation by mTORC1 of the STGE motif in sequestosome-1

(p62/SQSTM1) and decreased elimination of Keap1 by autophagy (Frame and Cohen, 2001; Ichimura et al., 2013). Except for the autophagy signalling pathway, mitochondria and inflammatory signalling pathways decrease Keap1-mediated degradation of Nrf2 through competitively binding of phosphoglycerate mutase family member 5 (PGAM5) and inhibitor of κB kinase β (IKKβ) to keap1 (Tebay et al., 2015). Redox stressors cause a modification of Keap1, attenuating Keap1 mediated ubiquitination of Nrf2. Newly synthesized Nrf2 translocates to nucleus and binds to the ARE, inducing cytoprotective gene expression.

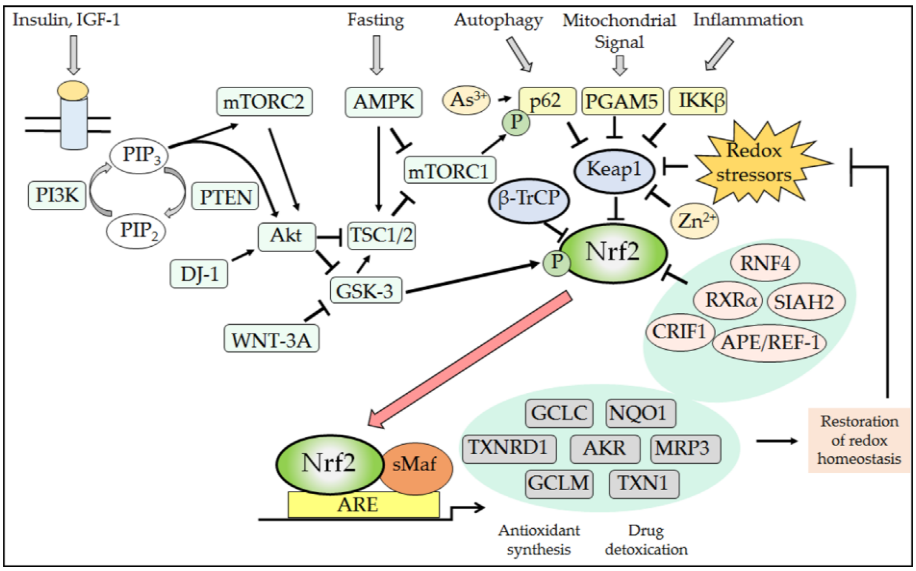

Figure 1.9 Post-translational mechanisms of Nrf2 regulation
Nrf2 is also targeted for proteasomal degradation and ubiquitination in a basal state via the dual actions of β-TrCP and Keap1. Phosphorylation of GSK-3 increases β-TrCP-mediated degradation of Nrf2. Post translationally, Nrf2 is regulated by AMPK and mTOR via feedback loops in response to cellular energy and nutrition. Taken from (Tebay et al., 2015).
Abbreviations: IGF-1, insulin-like growth factor 1; PI3K, phosphoinositide 3-kinases; PIP3, phosphatidylinositol (3,4,5)-trisphosphate; PIP2, phosphatidylinositol 4,5-bisphosphate; PTEN, phosphatase and tensin homolog; DJ-1, Parkinson disease protein 7; Akt, protein kinase B; AMPK, 5' AMP-activated protein kinase; mTOR, mechanistic target of rapamycin; mTORC1, mTOR complex 1; mTORC2, mTOR complex 2; GSK-3, glycogen synthase kinase-3; TSC1/2, tuberous sclerosis complex 1/2; PGAM5, phosphoglycerate mutase family member 5; IKKβ, inhibitor of κB kinase β; β-TrCP, beta-transducin repeats-containing proteins; Keap1, kelch-like ECH-associated protein 1; Nrf2, nuclear factor erythroid 2-related factor 2; ARE, antioxidant response element; sMaf, small Maf proteins; Zn^{2+}, free zinc ions; APE1/REF-1, apurinic/apyrimidinic endonuclease/redox factor-1; SIAH2, seven in absentia homolog 2; CRIF1, CR6-interacting factor 1; RXRα, retinoid X receptor alpha; RNF4, ring finger protein 4; GCLC, glutamate-cysteine ligase catalytic subunit; NQO1, NAD(P)H Quinone Dehydrogenase 1; AKR, aldo-keto reductase; MRP3, multidrug-resistant protein-3; GCLM, glutamate-cysteine ligase modifier subunit; TXN1, thioredoxin 1.

1.4.3 Activation Nrf2 by sulforaphane

Sulforaphane (SFN) is an isothiocyanate (ITC) broadly contained in cruciferous vegetables like broccoli, cauliflower and cabbage that is useful for promoting cardiovascular health and reducing related mortality due to its antioxidant property (Ahn et al., 2010; Robledinos-Anton et al., 2019; Zhang et al., 2011). Glucosinolates (GLS) are hydrolyzed by myrosinase enzyme into isothiocyanate sulforaphane (SFN) during chopping and chewing of these vegetables as GLS and myrosinase are localized to vacuoles and myrosin granules respectively (Kissen et al., 2009; Wu et al., 2021). The metabolic pathway of hydrolyzing GLS to ITC by gut microbiota has been published as well (Liou et al., 2020) (Lai et al., 2010). Myrosinase is unstable under heat and refrigerated storage, limiting its bioavailability (Li et al., 2013). Okunade et al. have reported that cooking broccoli for 2 and 6min led to 40% and 90% loss in myrosinase activity respectively (Okunade et al., 2018). In the mammalian cells, SFN is rapidly metabolized to mercapturic acid via a conjugation reaction with glutathione (GSH), of which 70%-90% is excreted in urine within 2h (Fahey et al., 2017; Ruhee and Suzuki, 2020).

SFN as a classic Nrf2 activator used in present study and as an electrophile can react with thiol groups of proteins to form thionoacyl adducts. Numerous studies have reported that SFN decreases endothelial activation in athero-susceptible sites of mouse aorta, reduces hypertension in rat models, improves coronary flow in IR injury in rat hearts and suppresses diabetic mediated fibrosis in mouse hearts (Piao et al., 2010a; Wu and Juurlink, 2001; Xue et al., 2008; Zakkar et al., 2009a; Zhang et al., 2014). SFN can affect cysteine 151 residues of Keap1 to modify its conformation, blocking Keap1-mediated ubiquitination and degradation of Nrf2 and activating the Nrf2 signalling pathway (Dinkova-Kostova et al., 2005; Satoh et al., 2013). Moreover, SFN can trigger the activity of Nrf2 upstream kinases including

mitogen-activated protein kinases (MAPK), phosphoinositide 3-kinases (PI3K) and protein kinase C (PKC) to phosphorylate Nrf2 (e.g. serine 40 residues) and thereby modulate its binding and stability (**Figure 1.10**) (Ahn et al., 2010; Bai et al., 2015; Huang et al., 2000; Kensler et al., 2013; Sun et al., 2009; Yu and Kensler, 2005). Leoncini et al. have demonstrated that SFN elicits cardioprotection through an indirect mechanism in cultured rat cardiomyocytes by activating PI3K/Akt and extracellular signal-regulated kinase 1 and 2 (ERK1/2) pathways (Leoncini et al., 2011).

Although SFN is excreted from body within few hours, *in vitro* cell culture models showed that SFN leads to a long-term protection against oxidative stress (Bai et al., 2015). For instance, Warpsinski et al. have demonstrated that 0.5-2.5μM SFN significantly upregulated Nrf2 regulated HO-1 protein levels for 24h, consistent with Bergstrom's findings in rat astrocytes (Bergstrom et al., 2011; Warpsinski et al., 2020). Bai et al. also reported that diabetic mice treated with SFN for 3 months showed a reduced incidence of cardiomyopathy at the end of the treatment, with protection even more significant after 6 months (Bai et al., 2013).

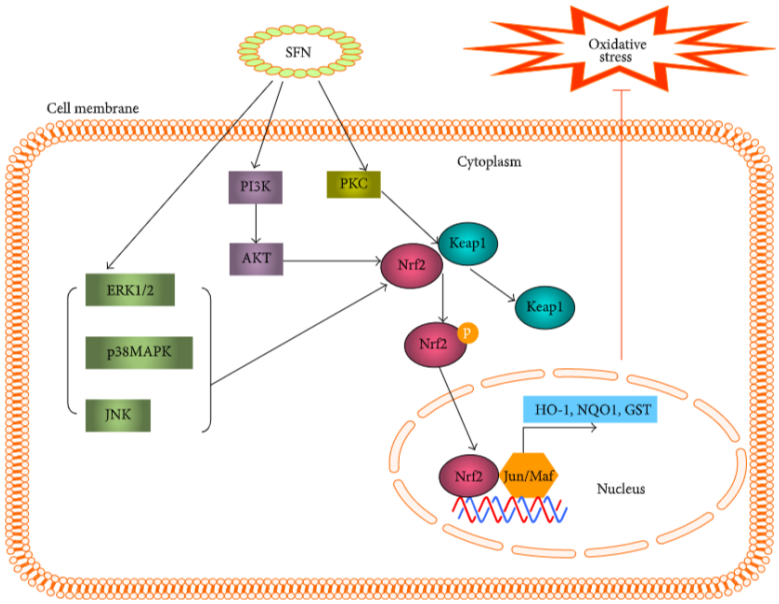

Figure 1.10 Sulforaphane activation of Nrf2 signalling
SFN can augment activity of MAPK (ERK, p38MAPK and JNK), PI3K/Akt and PKC to phosphorylate Nrf2, leading to Nrf2 nuclear translocation and antioxidant gene expression. Taken from (Bai et al., 2015).
Abbreviations: SFN, sulforaphane; MAPK, mitogen-activated protein kinases; ERK, extracellular signal-regulated protein kinase; JNK, c-Jun N-terminal kinase; PI3K, phosphatidylinositol 3-kinase; Akt, protein kinase B; PKC, protein kinase C; Nrf2, nuclear factor erythroid 2- related factor 2; Keap1, Kelch-like ECH-associated protein 1; Maf, small Maf proteins; P, phosphorylation; HO-1, heme oxygenase-1; NQO1, NAD(P)H Quinone Dehydrogenase 1; GST, glutathione S-transferase.

1.4.4 Nrf2-regulted antioxidant enzymes

Since it was first cloned in 1994 as a nuclear factor erythroid 2-like basic leucine zipper transcriptional activator for the transcriptional stimulation of β-globin genes, Nrf2 continues to emerge a critical mediator for antioxidant stress response and drug detoxification (Dodson et al., 2019; Moi et al., 1994). Many studies have detailed Nrf2-regulated antioxidant genes such as GSH, GCLC, GCLM, HO-1 and NQO1 involved in redox regulation, heme metabolism, iron homeostasis and phase II detoxification enzymes (Ma, 2013; Tonelli et al., 2018).

γ-glutamylcysteinylglycine, known as glutathione (GSH), is the most abundant non-protein thiol in all mammalian tissues that defends against oxidative stress and regulates redox signalling (Meister, 1993). It is a tripeptide that synthesized by sequentially adding cysteine to glutamic acid followed by glycine (see **Figure 1.11**) (Lu, 2013). The synthesis of GSH contains two ATP- requiring enzymatic steps. The first reaction is rate limiting and catalysed by GCLC, a catalytic subunit, and GCLM, a modifier subunit to form γ-glutamylcysteine, and GCLC can be feedback inhibited by GSH (Forman et al., 2009). The second step of GSH biosynthesis is catalysed by GSH synthase (GS) (Forman et al., 2009; Meister, 1974). GSH exists in the thiol-reduced form (GSH) and disulfide-oxidized (GSSG) form (Zitka et al., 2012). Reduced GSH form is predominant under physiological conditions, accounting for more than 98% of total GSH (Mari et al., 2013), whilst the GSH: GSSG ratio dropped to 10:1 or even 1:1 under oxidative stress (Chai et al., 1994). GSH undergoes a redox reaction to scavenger ROS like H_2O_2 into H_2O, which is mediated by glutathione peroxidase (GPx). GSH is oxidized to GSSG and is reduced back to GSH by the enzymatic reaction of glutathione reductase (GR), which requires NADPH to form a redox cycle (Lu, 2009).

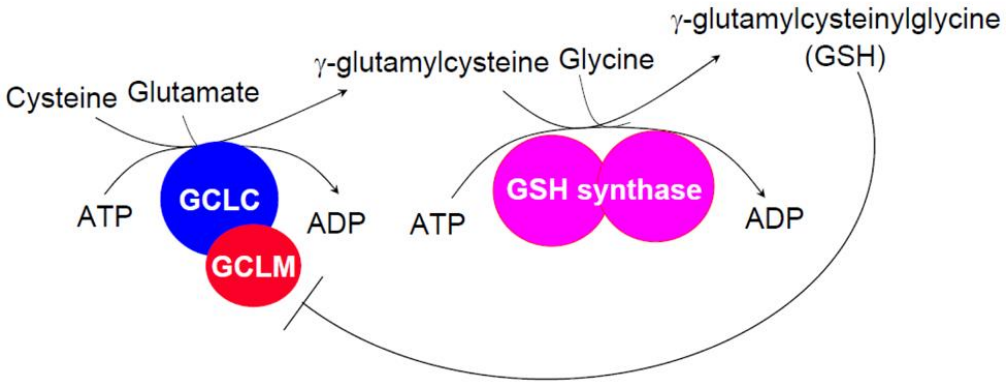

Figure 1.11 GSH synthesis
GSH biosynthesis occurs in two steps: i) Cysteine conjugates with glutamate to form γ-glutamylcysteine. The first step is catalysed by glutamate-cysteine ligase (GCL) (GCLC, catalytic subunits and GCLM, modifier subunits) and couple with ATP hydrolysis; ii) Glycine are added to γ-glutamylcysteine to form γ-glutamylcysteinylglycine (GSH), which can exert a negative feedback inhibition on GCL. The second step is catalysed by GSH synthase and also coupled with ATP hydrolysis. Taken from (Lu, 2013).
Abbreviations: ATP, adenosine triphosphate; ADP, adenosine diphosphate; GCLC, glutamate-cysteine ligase catalytic subunit; GCLM, glutamate-cysteine ligase modifier subunit; GSH, glutathione; GS, GSH synthase.

Heme oxygenase (HO) is originally identified catalysing the initial reaction of heme catabolism by Tenhunen et al. in 1968 (Tenhunen et al., 1968). Until 1989, Tyrrell et al. firstly showed that it is highly induced by many agents causing oxidative stress (Keyse and Tyrrell, 1989). HO catalyzes the first and rate-limiting step of heme degradation into biliverdin, CO, and free iron (Choi and Alam, 1996). Subsequently, biliverdin is converted to bilirubin via NADPH- dependent biliverdin reductase (Otterbein and Choi, 2000). There are three isoforms of HO, with HO-1 induced by numerous stimuli such as hypoxia, hyperoxia, shear stress and heavy metals, HO-2 is constitutively expressed, mainly in the brain and testes, and HO-3 had two heme regulatory motifs but no catalytic activity (Maines, 1988; McCoubrey et al., 1997). Moreover, Hayashi et al. has reported that there are no functional HO-3 genes in rat and two HO-3 related genes are processed pseudogenes derived from HO-2 genes (Hayashi et al., 2004).

NQO1 was firstly discovered by Ernster et al. in 1958 as detoxification enzyme, and as a flavoprotein catalyses two-electron reduction and reduces quinones and its derivatives to less toxic and less reactive hydroquinones (Ernster, 1958; Ernster and Navazio, 1958; Ross et al., 2000). Moreover, the two-electron reduction bypasses semiquinone generation and NQO1 can prevent semiquinone-induced ROS production (Siegel et al., 2004). Furthermore, after free radical attack NQO1 mediates the formation of ubiquinone and vitamin E to their antioxidant forms ubiquinol and vitamin E hydroquinone, respectively (Ross and Siegel, 2004). As Vitamin E forms Vitamin E quinone during free radical attack, but lacks of antioxidant activity, NQO1 may extend the antioxidant potential of vitamin E by production of vitamin E hydroquinone (Kohar et al., 1995; Landi et al., 1997).

1.4.5 Nrf2 affords protection in vascular and coronary ischaemia-reperfusion injury

Notably, GSH, GCLC, GCLM, HO-1 and NQO1 are highly inducible enzymes that is regulated by the Keap1-Nrf2 pathway (Suzuki and Yamamoto, 2015; Yamamoto et al., 2018). In the past two decades, accumulating evidence implicates the Keap1-Nrf2 antioxidant defence pathway as an important endogenous homeostatic mechanism associated with vessel and heart protection in atherosclerosis, diabetic vascular disease, cardiac hypertrophy, heart failure and IR injury (Itoh et al., 1999; Kerins and Ooi, 2018; Tebay et al., 2015) (see **Table 1.3**). As an antioxidant transcription factor, Nrf2 is considered important in suppressing atherosclerotic lesion formation by reducing foam cell formation and atherosclerosis progression (Chen et al., 2015; Ishii et al., 2004; Ishikawa et al., 2001; Zhu et al., 2008). It has been reported that HO-1, a downstream target gene of Nrf2, can suppress atherosclerotic lesion formation and promoting atherosclerotic plague stability (Bouche et al., 2002; Gough et al., 2006; Juan et al., 2001). Moreover, a few Nrf2 inducers have been shown to reduce infarct size, attenuate adverse ventricular remodelling and decrease adverse events such as arrhythmia in response to MI in mouse or rat models (Bubb et al., 2017; Chen and Maltagliati, 2018; Piao et al., 2010b; Wang et al., 2014; Xu et al., 2014a).

In addition, recent studies have focused on the association between trace metal micronutrients such as zinc and coronary artery/heart disease (Little et al., 2010; Viswanath et al., 2011; Xu and Zhou, 2013). Although dysregulation of Zn^{2+} homeostasis has been reported that is associated with IR injury (Bodiga et al., 2017; Bodiga et al., 2020), the role of Zn in IR injury and crosstalk between Zn and antioxidant signalling is still elusive and poorly understood.

Table 1.3 Studies of Nrf2 pathway in vessel and heart ischaemia-reperfusion injury

Species	Cells or tissue	Main Findings	Reference
Human	Coronary arterial EC	Adaptive activation of the Nrf2/ARE pathway confers endothelial protection under diabetic conditions	(Ungvari et al., 2011)
Mice	Aorta	HO-1, induced under hyperlipidaemia, functions as an intrinsic protective factor against atherosclerotic lesion formation by inhibiting lipid peroxidation and influencing the NO pathway	(Ishikawa et al., 2001)
Mice	Aortic EC	Nrf2 prevents ECs at atheroprotective site from exhibiting a proinflammatory state via suppression of p38-vascular cell adhesion molecule 1 (VCAM-1) signalling	(Zakkar et al., 2009b)
Mice	Cardiomyocyte	HO-1 activity stimulates genomic mitochondrial biogenesis mediated by Nrf2 highlighting HO-1 protection mechanisms	(Piantadosi et al., 2008)
Mice	Heart	Nrf2 knockout mice have increased infarct size following coronary ischemia-reperfusion injury and a reduced degree of cardiac protection by ischaemic preconditioning	(Xu et al., 2014a)
Mice	Heart Cardiomyocyte	Nrf2 -$p27^{kip1}$ pathway protects against angiotensin II-induced cardiac hypertrophy in mouse model	(Li et al., 2011)
Rat	Cardiomyocyte	Nrf2 activator DH404 attenuates adverse ventricular remodeling post-myocardial infarction by modifying redox signalling	(Bubb et al., 2017)
Mice Rat	Cardiomyocyte	Cardiac specific activation of Nrf2 suppresses cardiac maladaptive remodeling and dysfunction most likely by enhancing autophagic clearance of toxic protein aggregates	(Wang et al., 2014)
Rat	Heart	Diet-relevant phytochemical intake affects the cardiac aryl hydrocarbon receptor (AhR) and Nrf2 transcriptome and reduces heart failure in hypertensive rats	(Seymour et al., 2013)

Abbreviations: NO, nitric oxide; VCAM-1, vascular cell adhesion molecule 1; ECs, endothelial cells; Nrf2, nuclear factor erythroid 2-related factor 2; HO-1, heme oxygenase-1; IR, ischaemia reperfusion injury; $p27^{kip1}$, cyclin-dependent kinase inhibitor 1B; AhR, aryl hydrocarbon receptor.

1.5 Metal profiling in coronary ischaemia-reperfusion injury

1.5.1 General overview of cellular metal homeostasis

Metals, as new biomarkers in diagnosis and as therapy, have merged as a new research focus in recent years due to the close links with oxidative stress (Maret, 2018; Yin et al., 2017). Previous studies have shown that the plasma magnesium (Mg), calcium (Ca), potassium (K), zinc (Zn) and nickel (Ni) are significantly lower in acute coronary syndrome (ACS) patients (Ising et al., 1987; Solini et al., 2006; Yin et al., 2017). It is noteworthy that some metals (e.g., iron (Fe), cooper (Cu) and manganese (Mn)) are redox-active, which undergo redox cycling reactions and can react with oxygen to produce reactive free radicals such as $O_2^{\bullet-}$ and hydroxyl radicals ($OH^{\bullet}$) (Jomova and Valko, 2011; Mates et al., 2008; Rahman, 2007). Whilst some metals such as cadmium (Cd) and Mg are redox-inert. Notably, Zn, a redox-inactive metal, plays an important role against oxidative stress in an indirect way via stabilizing thiol groups against the free radical attack (Maret, 2003; Marreiro et al., 2017).

Notably, some studies have described a protective and promotor role of Zn in IR injury in cardiomyocytes *in vivo* and *in vitro*. Accumulating evidence suggests that exogenous Zn reduces $O_2^{\bullet-}$ generation, lowers apoptotic indices and restores ATP levels and left ventricular pressure by attenuating nicotinamide adenine dinucleotide phosphate (NADPH) oxidase mediated intracellular oxidative stress, thereby preserving protein kinase C isoforms and the mitochondrial permeability transition pore (Karagulova et al., 2007; Kasi et al., 2011; Viswanath et al., 2011; Zhang et al., 2018). In contrast, another study has shown that addition of zinc pyrithione at onset of reperfusion increases the severity of MI (Lien et al., 2018). Other studies report that addition of Zn^{2+} to cardiomyocytes induces generation of ROS, and

increased cytosolic Zn induces accumulation of Zn in mitochondria and results in mitochondrial ROS generation in rat aortic SMCs (Lin et al., 2011a; Salazar et al., 2017; Tuncay and Turan, 2016). Thus, based on these conflicting reports, further investigation of the relationship between oxidative stress and metals under IR injury is warranted. Notably, the link between the regulation of metals and other antioxidant enzymes or signalling pathways is still poorly understood. In my project, the complex interactions between metals, especially Zn, and coronary IR injury, are addressed in the context of Keap1-Nrf2 regulated redox signalling.

1.5.2 Antioxidant properties of zinc

Zinc is a critical element for life, which is associated with differentiation and regeneration of cardiac muscle, cardiac conduction and acute stress responses (Kown et al., 2000; Lin et al., 2011b). The human body contains 2-3g zinc, which nearly 90% is in muscle and bone (Plum et al., 2010a; Wastney et al., 1986). At a cellular level, around 50% of zinc exists in the cytosol, 30-40% in the nucleus and the remainder is associated with membranes (Vallee and Falchuk, 1993). Human blood plasma contains around 9.6-31.6μM zinc, which is less than 0.2% of total body zinc (Coverdale et al., 2019), whilst only a small fraction existing as free Zn^{2+} concentration is around 0.1-2μM (Mammadova-Bach and Braun, 2019). The intracellular concentration of free Zn^{2+} is extremely low in most cells (<1nM), and most of the intracellular zinc bounds to proteins or nucleic acids (Foster and Samman, 2010; Krezel and Maret, 2006). In resting cardiomyocytes, intracellular Zn^{2+} levels below 100 and 520pM have been reported (Auld, 2001) (Bodiga et al., 2017).

Zinc is involved in numerous biological processes. There are three key roles played by zinc, including as a structural, catalytic and signalling functions (Kambe et al., 2015). In addition, numerous studies have highlighted the relationship between Zn and oxidative stress. For example, zinc prevents mitochondrial oxidative stress in IR injury in rat heart and $ZnCl_2$ increases cardiac oxidative phosphorylation and suppresses mitochondrial ROS production during reperfusion (Bian et al., 2018).

Even though Zn is a redox-inactive metal, it is involved in protection against oxidative stress as summarized in **Figure 1.12** (Eide, 2011a). Firstly, zinc is a structural component of the enzyme superoxide dismutase [Cu-Zn] (SOD1), catalysing the conversion of two $O_2^{\bullet-}$ to hydrogen peroxide (H_2O_2) and molecular oxygen (O_2) to reduce the toxicity of ROS (Eleutherio et al., 2021). Nedd et al. reported that removal of Zn from SOD1 results in immediate enzyme inactivation and SOD1 misfolding is thought to involve mutations that cause Zn loss (Nedd et al., 2014). Secondly, zinc competes with redox-active metals like Fe and Cu for negative charges in the lipid bilayer or binding sites on proteins, thereby protecting the cell membrane from lipid oxidation or inhibiting the Fenton reaction (Zago and Oteiza, 2001). Moreover, previous studies have described that zinc plays an indirect antioxidant role via binding to and protecting free thiol groups in proteins, inhibiting NADPH oxidase, decreasing expression of misfolded protein in endoplasmic reticulum (ER) and as a component of many proteins in the mitochondrial transport chain (Choi et al., 2018; Eide, 2011a; Ye et al., 2001).

Meanwhile, Zn^{2+} participates in a redox cycle with metallothionein (MT), which a cysteine-rich low-molecular weight protein. Under oxidation, Zn^{2+} is released from MT and

MT forms a bisulfide bound (Andrews, 2000; Ruttkay-Nedecky et al., 2013). MT also have the ability to protect against excessive heavy metals such as Zn, Cu and Cd (Marreiro et al., 2017). It is worth noting that the Zn^{2+} can be sensed by histidine 225, cysteine 226 and 613 residues of Keap1, leading to alteration in the conformation of Keap1 (Jenkitkasemwong et al., 2012). This means that Zn^{2+} actives Nrf2 signalling indirectly through the loss of Keap1-mediated Nrf2 ubiquitination and degradation (McMahon et al., 2010; McMahon et al., 2018). Besides, free Zn^{2+} can also activate metal regulatory transcription factor 1 (MTF-1), which has an important role in regulating antioxidant responses and maintaining metal homeostasis (Grzywacz et al., 2015). The activation of MTF-1 upregulates expression of the MTs and selenoprotein1 (Sepw1) gene, which encodes an antioxidant glutathione-binding protein scavenging free radicals (Bonaventura et al., 2015). MTF-1 and Nrf2 transcription factors are linked through a pool of free Zn^{2+} provided by both MT and Keap1 (Grzywacz et al., 2015; Maret, 2006). Another mechanism is that zinc regulates the expression of glutamate-cysteine ligase (GCL), which is the rate-limiting enzyme of glutathione synthesis and a downstream target gene of Nrf2 (Eide, 2011b; Ha et al., 2006). The mechanisms by which Zn protects against oxidative stress are complex and overlapping, and have not been well discussed, and thus merit further investigation. In addition, there is a narrow range between safe and unsafe intake as both low (deficiency) and high (overload) zinc levels can induce oxidative stress (Maret, 2006).

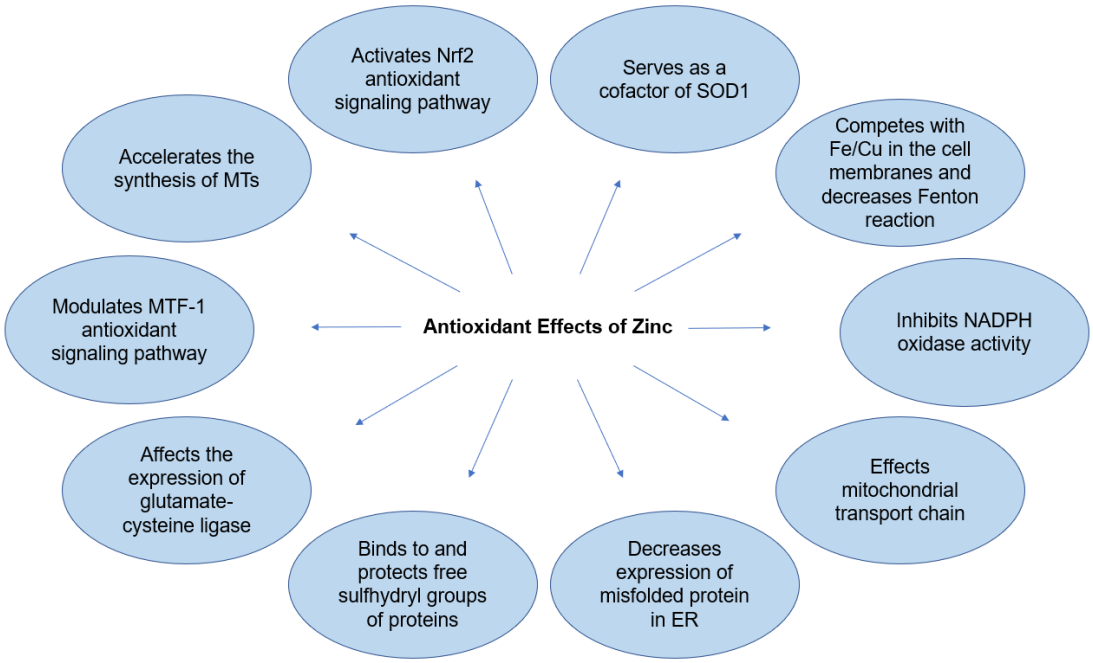

Figure 1.12 Antioxidant effects of zinc
Summary figures of zinc antioxidant effects. Zn stabilizes sulfhydryl groups of protein, serves as a cofactor of SOD1 and links with Nrf2 antioxidant signalling pathway against oxidative stress.
Abbreviations: Nrf2, nuclear factor erythroid 2-related factor 2; MTs, metallothionines; MTF-1, metal regulatory transcription factor 1; ER, Endoplasmic reticulum; NADPH, nicotinamide adenine dinucleotide phosphate; Fe, iron; Cu, copper; SOD1, superoxide dismutase [Cu-Zn]. Adapted from (Marreiro et al., 2017).

1.5.4 Iron and Copper function in ischaemia-reperfusion injury

Fe and Cu are redox-active metals, and act as both antioxidant and a pro-oxidant in biology due to their different charges and being cofactors of antioxidant enzymes (Jomova and Valko, 2011; Valko et al., 2016). Fe is the most abundant metal in the human body, with a content of 4-5g (Valko et al., 2005), and the human body contains around 100mg Cu, which is the 3rd rich metal (Bost et al., 2016). However, only a very small number of free ions are present in the form of a redox-active pool. As pro-oxidant, they catalyse the formation of ROS via the Fenton reaction (Fe(II)/Cu(I) + $H_2O_2 \rightarrow$ Fe(III)/Cu(II) + OH^- + $^{\cdot}OH$) (Jomova and Valko, 2011). Hydroxyl radicals are very reactive, inducing DNA damage. Chang et al. has described that mitochondrial Fe contributes to cardiac IR damage and the development of cardiomyopathy by reducing ROS generation (Chang et al., 2016). On the other hand, Fe and

Cu are cofactors of many antioxidant enzymes. For example, SOD1 contains Cu and Zn, which detoxifies $O_2^{\bullet-}$ to H_2O_2. Moreover, catalase contains Fe, which converts H_2O_2 to H_2O. A study reported that Cu deficiency may be a leading cause of ischaemic heart disease (DiNicolantonio et al., 2018). Taken together, Fe and Cu are closely related to oxidative and antioxidant processes.

1.5.5 Crosstalk between metals and Nrf2 redox signalling pathway

As shown in **Figure 1.9**, Nrf2 activity is also increased by some metal(loid)s by interaction with Keap1 (Dinkova-Kostova et al., 2005). For example, a study has reported that Cd^{2+}, As^{3+}, Se^{4+} and Zn^{2+} are sensed by histidine 225, cysteine 226 and cysteine 613 residues of Keap1 (McMahon et al., 2010). Subsequently, the altered conformation of Keap1 triggered by these free metal ions binding inhibits ubiquitination of Nrf2 via Keap1 (McMahon et al., 2018). Meanwhile, the increases of intracellular Zn^{2+} inactivates GSK3β as well, which is a Nrf2 inhibitor (Kambe et al., 2015; Maret, 2006). Zinc is considered as a component of antioxidant defence network except for the Nrf2-Keap1 signalling pathway.

Due to the fact that Zn cannot cross cell membranes by passive diffusion, cellular zinc homeostasis is mainly mediated by three mechanisms: zinc transporters, zinc-binding proteins such as metallothionein (MT) and metal regulatory transcription factor 1 (MTF-1), a zinc-sensing transcription factor (Maret, 2017a; Plum et al., 2010b). In humans, Zn transporters have at least 24 membrane transporters and play fundamental roles, including zinc transporters (ZnT1-10), also known as solute carrier family 30A (SLC30A) proteins and Zrt- and Irt-like proteins (ZIP1-14), also known as SLC39A (Takagishi et al., 2017). ZIPs take zinc into cells or out of subcellular compartments, whilst ZnTs efflux zinc out of cells or

into subcellular compartments (Karagulova et al., 2007). MTs play a role in detoxification against toxic heavy metals (e.g., Zn, Cu, Cd and Cr) and participate in protection against stress responses because of its cysteinyl thiolate groups (Ruttkay-Nedecky et al., 2013). There are four isoforms of MTs and 13 MT-like proteins discovered in human (Ghoshal and Jacob, 2001). MT-1 and MT-2 are widely expressed in various tissues, whilst MT-3 is brain specific and MT-4 is expressed mainly in skin and tongue (Palmiter, 1987; Palmiter et al., 1992; Quaife et al., 1994). MTs are reported to be induced by oxidative stress and Zn^{2+} increase, which is also transcriptionally regulated by Nrf2 (Dalton et al., 1996; Gu et al., 2017). In addition, previous studies have highlighted that ZnT1, 2, 4, 8 and ZIP 1, 2, 3, 6, 7, 9, 10, 11, 12, 13, 14 are regulated under IR (Aguilar-Alonso et al., 2008; Bodiga et al., 2017; Gerber et al., 2014; Malairaman et al., 2014; Zhao et al., 2015). Ishida and colleagues have described that mRNA levels of ZnT-1, 3 and 6 significantly increase and ZnT10 and ZIP3 mRNA levels significantly decreases after activation of Nrf2 signalling pathway (Ishida and Takechi, 2016a). Meanwhile, ZnT1 and ZnT2 are upregulated and ZIP10 is downregulated by redox-sensitive MTF-1 (Gunther et al., 2012).

In addition, several studies have reported that Zn^{2+} accumulates in cardiomyocytes after hypoxia, whilst reoxygenation downregulates intracellular Zn^{2+} concentration, resulting from cytosolic and mitochondrial Zn^{2+} release (Bodiga et al., 2017; Karagulova et al., 2007; Lin et al., 2011b). In addition, Zn supplementation promotes functional recovery after spinal cord injury, inhibits the high glucose-induced epithelial-mesenchymal transition of peritoneal mesothelial cells and induces HO-1 expression in cancer cells by activating Nrf2 antioxidant pathway (Gao et al., 2019; Li et al., 2020a; Xue et al., 2013). Thus, elevated intracellular Zn^{2+} activates Nrf2 signalling and in turn, Nrf2 signalling regulates intracellular Zn^{2+}

concentration. However, the effect of IR on Nrf2 signalling and Zn in human coronary artery SMCs (HCASMCs) is still unclear.

Numerous studies have reported that Cu^{2+} activates Nrf2 signalling pathway in mouse hepatocytes, human AREc32 reporter cell line and human breast cancer cells (Sirbu et al., 2017; Song et al., 2014; Wang et al., 2010). Moreover, overload of Fe^{2+} stimulates Nrf2 expression to prevent neurotoxicity in mouse brain astrocytes and hepatocytes (Cui et al., 2016; Silva-Gomes et al., 2014), noting that these metals also regulate each other as well. For example, Zn substitutes for Fe/Cu as a cofactor and decreases the Fenton reaction (Prasad and Bao, 2019). Santon et al. have shown that Zn treatment decreases Fe accumulation in rat hepatoma cells, whilst MTs induced by Zn increases intracellular Cu content. Notably, our understanding of the field of relationship between Nrf2 signalling and Zn^{2+}, Fe^{2+} and Cu^{2+} in coronary IR and how they tightly regulate each other requires investigation. Nevertheless, these findings demonstrate the critical role of these metals and Nrf2 signalling in IR, and thus may serve as therapeutic targets for improving prognosis and increasing survival rates.

1.6 Physiological oxygen levels

1.6.1 Importance of physiological oxygen levels

O_2 is the central for human physiology but can also act as a harmful molecule influencing biological aging, oxidative damage, mutagenesis and cancer (Bunn and Poyton, 1996; Droge, 2002). An O_2 content of 20.9 kPa refers to standard dry atmospheric air at sea level. Cellular O_2 consumption coupled with the limitation of diffusion through the tissues means that the O_2 levels *in vivo* range from ~10-13 kPa in the pulmonary circulation to ~3-5 kPa in most microvascular capillary beds (Keeley and Mann, 2019; Keeley et al., 2017) (**Figure 1.13**). In

many fields, most cell culture is conducted within an incubator gassed with 5 kPa CO_2 and ~18.5 kPa O_2 (Newby et al., 2005), which has been assumed to reflect normoxia. However, cells *in vivo* experience significantly lower O_2 levels, as recently reviewed by Keeley & Mann (Chen et al., 2018; Keeley and Mann, 2019; Sies et al., 2022). The concept of physiological normoxic cell culture has received increasing attention in recent years. In fact, cells are exposed to hyperoxia in a standard incubator, which reduces the lifespan of cells (Parrinello et al., 2003), alters adaptive antioxidant defenses (Atkuri et al., 2007; Chapple et al., 2016; El Alami et al., 2014; Kumar et al., 2016) thereby limiting translation from bench to bedside. Previous work in our laboratory has shown that long-term culture of human coronary artery endothelial cells (HCAECs) in an O_2-regulated Sci-tive workstation under 5 kPa O_2 results in a cytosolic O_2 level of 3.7 kPa (Chapple et al., 2016). Warpsinski et al. has reported that physiological normoxia alters the redox phenotype of mouse microvascular brain ECs (Warpsinski et al., 2020). The relationship between oxygen level with the proliferation, migration and phenotype of cultured cells is summarized in **Table 1.4**.

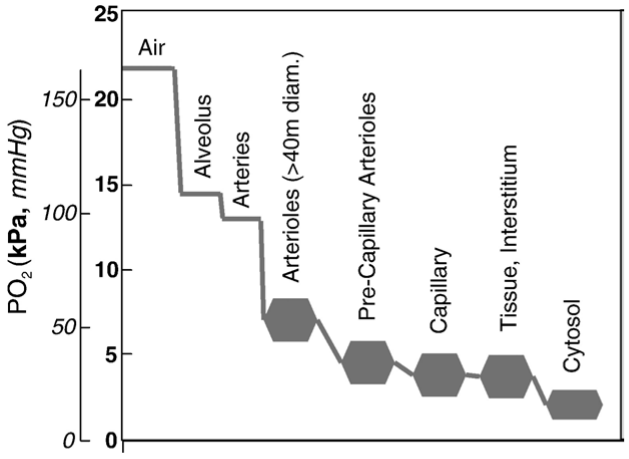

Figure 1.13 Representation of the regional distribution of PO_2 from the airways to the cytosol
The O_2 levels in the body *in vivo* change from the air we breathe (20.9 kPa O_2), through the lung, small arteries, arterioles, capillaries (~3-5 kPa), tissues and the cytosol of different cells. Taken from (Ward, 2008).

1.6.2 Hypoxia-inducible factor-1

Hypoxia-inducible factor-1 (HIF-1) has been reported as a primary transcriptional factor response to hypoxia, which consists of two subunits, α (the active oxygen-regulated subunit) and β (oxygen-independent subunit) (Bhattarai et al., 2018; Jatho et al., 2021; Kaelin, 2002; Salceda and Caro, 1997; Semenza, 2014). Hypoxia decreases the hydroxylation of HIF-1α, resulting in limitation of proteolytic degradation (Zimna and Kurpisz, 2015). Stable HIF-1α translocates to the nucleus and dimerizes with HIF-1β and binds to hypoxia response element (HRE), activating target gene transcription (Koyasu et al., 2018; Ratcliffe et al., 1998). Under physiological normoxia *in vivo*, HIF-1α is hydroxylated to suppress transcriptional activation (Chen et al., 2018; Srinivas et al., 1999). Liu and colleagues have found that HIF-1α mRNA appears within the first 4h and peaks at 8h and then significantly decreases by 24h in human aortic SMCs under hypoxia (1kPa O_2) (Liu et al., 2017). The average half-life of HIF-1α protein is around 46h (Keeley and Mann, 2019). We have described that HIF-1α protein stabilisation requires 5d in HUVECs when they are exposed to 5kPa from 18kPa (Keeley et al., 2017). Meanwhile, HIF-1 affects many factors and previous studies have reported that HIF-1 plays a role in proliferation, migration and phenotypes of VSMCs (Fu et al., 2010; Jain et al., 2018; Liu et al., 2017; Ratcliffe et al., 1998).

To more accurately replicate antioxidant defense mechanisms *in vivo*, in the present study HCASMCs were adapted long-term (5 days) to 5kPa O_2 levels, as encountered *in vivo*, and then subjected to hypoxia-reoxygenation. Metal profiling of HCASMCs was conducted in cells adapted to physiological normoxia, hypoxia and hyperoxia, with the latter reflecting a standard cell culture O_2 environment used in the majority of studies *in vitro*. The

understanding of Nrf2- regulated redox signalling and the role of metals in cardiac physiology and cellular redox signalling pathways may inform further development of novel treatments for IR injury.

Table 1.4 Effects of oxygen on the proliferation, migration and phenotype of cultured cells

Species	SMC cell type	Oxygen level	Signalling	Main findings	Reference
Human	aortic SMCs	1 kPa	HIF-1α↑, AEG-1↓, PI3K/Akt↑	Under hypoxia, SMαA and SM22α (contractile states markers) ↓, OPN expression (synthetic states markers) ↑ HIF-1α plasmids - ↓ proliferation and ↑ migration of aortic SMCs	(Liu et al., 2017)
Human	umbilical artery SMCs	3 kPa	HIF-1α↑, MIF↑	Under hypoxia for 24h - proliferation↑ (113.6%) and migration ↑	(Fu et al., 2010)
Human	umbilical vein ECs	18, 5 kPa	-	Human umbilical vein ECs proliferated more rapidly during culture under air (18 kPa O_2) compared to 5 kPa O_2 level 5 days adaptation to 5 kPa O_2 had negligible effects on cell morphology	(Chapple et al., 2016)
Human	umbilical vein ECs	20, 5 kPa	-	5 kPa O_2 promoted human umbilical vein ECs proliferation, ECM secretion, and intercellular adhesion	(Zhao et al., 2009)
Human	primary osteoblastic cells	18, 1 kPa	HIF-1α↑ under 1 kPa	Exposure to hypoxia (1 kPa O_2) for 48h, proliferative activity of primary osteoblastic cells ↓ compared to in air	(Lechler et al., 2011)
Human	primary lymphocytes	20, 5 kPa	intracellular NO↑, peak expression of CD69 is delayed and more sustained under 5 kPa	CD3/CD28-induced T cell proliferation higher under air (20 kPa) than under physiological (5 kPa) O_2 level.	(Atkuri et al., 2007)
Human	peripheral blood mononuclear cells	20, 10, 5 kPa	-	Antigen CD3/CD28 cross-linking or Con A → proliferation ↑ at 5%, whilst no phytohemagglutinin → proliferation ×	(Atkuri et al., 2005)
Human	chondrocytes	20, 5 kPa	-	Proliferation increased under more physiological levels of oxygen (5 kPa)	(Murphy and Polak, 2004)
Bovine	granulosa cells	21, 5 kPa	HIF-1↑ under 5 kPa	GCs proliferated more rapidly during culture under 5 kPa (low) O_2 level for 24h compared to under 21 kPa O_2 level	(Shiratsuki et al., 2016)
Bovine	chondrocytes	20, 5, 2 kPa	-	Exposure under 5 and 2 kPa O_2 levels reduced the proliferation compared to 20 kPa	(Heywood and Lee, 2010)

(Table **1.4** continued)

Species	SMC cell type	Oxygen level	Signalling	Main findings	Reference
Mouse	neural stem cells	20, 10, 4, 3, 2, 1 kPa	-	The highest proliferation was observed under 2 kPa O_2 level	(Horie et al., 2008)
Rat	satellite cells	21, 3 kPa	cell cycle progression factors (cyclin D1, E, A) ↑, phosphorylation of Akt, the cell cycle inhibitor $p27^{Kip1}$ ↓ under 3 kPa	Under 3 kPa O_2 conditions, the proliferation ability of satellite cells (considered the 'stem cells' of mature myofibers) ↑ compared to under 21 kPa	(Chakravarthy et al., 2001)
Rat	primary osteoblasts cells	20, 5, 2 kPa	-	Reduction of pO_2 from 20 kPa to 5 kPa and 2 kPa → formation of mineralized bone nodules↓ 1.7-fold and 11-fold respectively	(Utting et al., 2006)

Abbreviations: SMCs, smooth muscle cells; ECs, endothelial cells; HIF-1α, hypoxia inducible factor 1α; AEG-1, astrocyte elevated gene-1; PI3K/Akt, phosphatidylinositol 3-kinase/protein kinase B; SMαA, smooth muscle α-actin; SM22α, smooth muscle 22α; OPN, osteopontin; MIF, macrophage migration inhibitory factor; ECM, extracellular matrix; GCs, granulosa cells;

1.7 Aims of the project

The underlying hypothesis in the present study is that the redox state and metal profile in HCASMCs may be altered after long-term (5 days) adaptation to hyperoxia (18kPa O_2), physiological normoxia (5kPa O_2) or hypoxia (1kPa O_2). Compared to 18kPa O_2, normally defined as normoxia in the majority of previous cell culture studies, this study provides the first novel insights into the mechanisms underlying hypoxia-reoxygenation induced changes in vascular SMCs pre-adapted to physiological normoxia with implications for improved bench-to-bedside translation in cardiovascular medicine.

The aims of this thesis were to:

1. Characterize redox phenotype of HCASMCs under hypoxia, normoxia and hyperoxia
2. Obtain metal profiles of HCASMCs long-term adapted to hypoxia, normoxia and hyperoxia
3. Address crosstalk between Zn and Nrf2 signaling in HCASMCs under 18, 5 and 1kPa O_2
4. Determine ROS generation during hypoxia-reoxygenation in HCASMCs adapted to physiological normoxia (5kPa) and hyperoxia (18kPa)
5. Explore protective roles of Zn and SFN, Nrf2 inducer, against oxidative stress in HCASMCs under 18, 5 and 1kPa O_2

Chapter 2 - Methods

2.1 Culture of human coronary artery smooth muscle cells

All procedures were performed under sterile, aseptic techniques in either a Class 2 laminar flow hood safety cabinet or in a dual Sci-tive, oxygen-regulated workstation (Baker-Ruskinn Technologies, UK, see **Figure 2.1**). Primary human coronary artery smooth muscle cells (HCASMCs, C-12511) were obtained from PromoCell, Germany. Cell in passage 5^{th} to 8^{th} were cultured in smooth muscle cell basal medium 2 (SMC BM2) (PromoCell, C-22262), supplemented with growth medium 2 supplement pack (PromoCell, C-39262) and 1% penicillin (100 U/ml)/ streptomycin (100 µg/ml). **Appendix 1** provides a detailed listing of the composition of supplement pack smooth muscle cell growth medium 2. HCASMCs were initially cultured in a standard incubator gassed with 5% CO_2 in air and then in a dual Sci-tive, oxygen-regulated workstation (Baker-Ruskinn Technologies, UK) gassed with 5% CO_2 and either 18, 5, or 1kPa O_2 (75% humidity) with subculture and all treatments conducted within the Sci-tive workstation. All culture media were pre-adapted in 18, 5 or 1kPa O_2 in the Sci-tive workstation prior to experiments. **Figure 2.1** illustrates the experimental setup and the use of a small Etaluma microscope (Etaluma, USA) to view cells within the workstation.

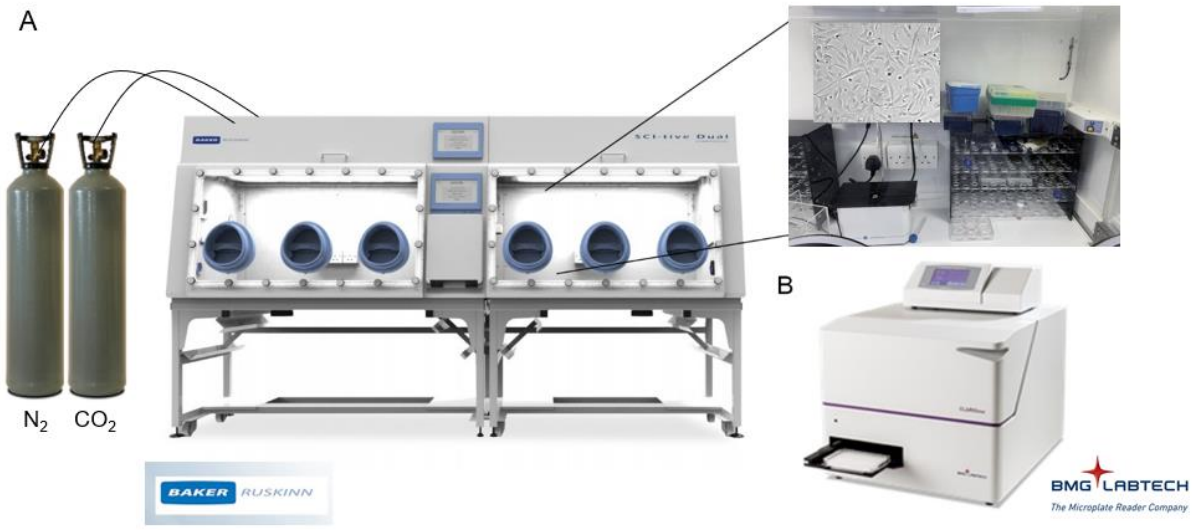

Figure 2.1 HCASMCs were cultured under controlled environment in a dual Sci-tive workstation.
(**A**) The sealed workstation allows for complete control of gaseous ambient conditions, which can be maintained at 18 kPa or 5 kPa, or 1 kPa O_2 under 5% CO_2, 75% humidity and 37ºC. Thus, long-term cell culture can be conducted under a controlled environment without the need for re-exposure of cells to ambient, room air oxygen levels. Cells can be transferred from one workstation unit to the adjacent workstation unit using an interlock between both sides of the Sci-tive (Baker-Ruskinn, UK), noting that each side can be maintained under different O_2 levels. (**B**) HCASMCs adapted for 5 days to either 18 kPa, 5 kPa or 1 kPa can then be transferred rapidly to an O_2-controlled CLARIOstar 96-well plate reader to monitor the effects of ischaemia-reoxygenation on the generation of reactive oxygen species and free intracellular zinc levels measured using fluorescent indicators.

2.1.1 Thawing and culturing of HCASMCs

Cells were thawed rapidly at 37°C and initially transferred to a T25 culture flask containing complete smooth muscle cell basal medium 2 and supplement pack smooth muscle cell growth medium 2. Cells were maintained in a humidified incubator gassed with 5% CO_2 at 37°C. Medium was replaced 8 h after seeding and changed regularly every 48 h.

2.1.2 Subculture of HCASMCs

When cells reached around 80% confluence, cultured HCASMCs were washed twice with warm sterile Ca^{2+}/Mg^{2+}-free phosphate buffered saline (PBS) to remove serum components that could interfere with the trypsinisation of cells. Cells in T25 or T75 flasks were

respectively incubated with 0.5 ml and 1.5 ml of trypsin/EDTA solution (0.1% trypsin and 0.02% EDTA, Sigma-Aldrich) for 5 min in an incubator to detach cells. Trypsin/ EDTA was deactivated by adding 1.0 ml and 3.0 ml complete medium and then centrifuged at 1000 rpm for 5 min. The supernatant was aspirated, and remaining cell pellets were re-suspended in complete medium. Cells were then seeded into T25 or T75 flasks for long-term culture (at least 5 days) in an O_2-controlled incubator (Sci-tive, Baker Ruskinn, **Figure 2.1**) adapted to 1kPa O_2, 5 kPa O_2 or air (18 kPa O_2). Confluent monolayers of HCASMCs were then again trypsinised and seeded into plates or onto coverslips for imaging experiments.

2.1.3 Cryopreservation of HCASMCs

Confluent monolayers of HCASMCs were detached with trypsin/EDTA (0.1% trypsin and 0.02% EDTA, Sigma-Aldrich) using the same method described in Section 2.1.2. Trypsin/ EDTA was deactivated by adding complete medium and then centrifuged at 1000 rpm for 5 min. The supernatant was aspirated, and remaining cell pellets were re-suspended in 5% dimethyl sulfoxide (DMSO) (Sigma-Aldrich, D8418) and 50% fetal bovine serum (FBS) (Sigma-Aldrich, F7524) in complete medium. Cells were transferred into cryo-vials (1ml/vial) and slowly frozen at -80℃ for 24 h before transfer to liquid nitrogen for long-term storage. The cryopreservation of HCASMCs culture is illustrated in **Figure 2.2**. By the time cells were defrosted they were at passage 4 (P_4).

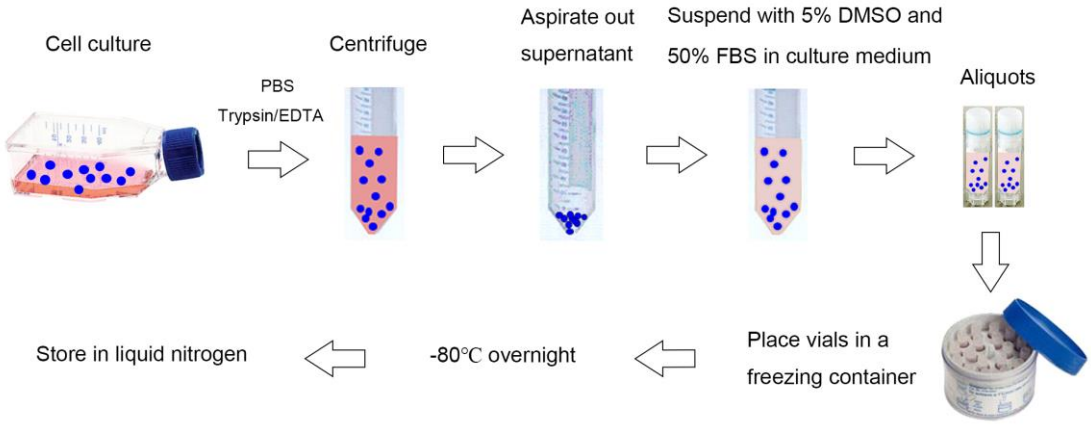

Figure 2.2 Cryopreservation HCASMCs culture.
To cryopreserve cells, a confluent monolayer of HCASMCs was detached using trypsin and re-suspended in medium containing serum and centrifuged at 1000 rpm for 5 min at room temperature. The supernatant was aspirated, and pellets were re-suspended in 5% DMSO and 50% FBS in complete medium. Aliquots were placed in a freezing container, which was then stored at -80℃ overnight before being transferred to liquid nitrogen for long-term storage.

2.2 Cell counting using a haemocytometer

To calculate the number of cells in a cell suspension, a haemocytometer was used, which consists of two chambers: chamber A and chamber B (**Figure 2.3**). Two coverslips were placed onto each chamber. The suspension was mixed thoroughly, and 10µl of cell content were transferred into each chamber. The total number of cells in four gridded squares was counted in both chambers under a microscope (4 × objective magnification). The gridded area is 1 x 1 mm (1 mm^2) squares. The raised edges of the hemocytometer hold the coverslip 0.1 mm off the marked grid, giving each square a defined volume. The density of cells was calculated as the following formula:

$$Cell\ concentration = (N_A + N_B) \div 2 \div 4 \div 1\ (mm^2) \div 0.1\ (mm)$$

$$= (N_A + N_B) \div 8 \times 10^4\ (cells/ml)$$

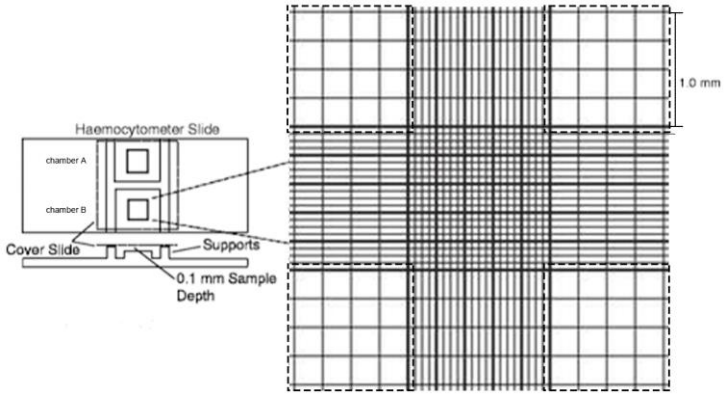

Figure 2.3 Cell number determination using haemocytometer.
The haemocytometer contains two chambers: chamber A and chamber B. For counting cells, the total number of cells in four gridded squares (marked by dashed lines) in chamber A was counted as the value N_A. The same counting was performed in chamber B, obtaining a value of N_B. The number of cells was calculated by the formula: $(N_A + N_B) \div 8 \times 10^4$ (cells/ml).

2.3 Bicinchoninic acid protein assay for immunoblotting

The bicinchoninic acid (BCA) protein assay is a colourmetric assay which is used to determine the protein concentration of samples, by comparing their absorbance to a standard curve of known protein concentrations (Smith et al., 1985). BCA reagents contain cupric sulphate. In the presence of peptide bonds in proteins samples, cupric sulphate is converted to Cu^+. Two molecules of BCA then chelate each Cu^+ molecule forming a purple coloured product, with an absorbance that can be detected at 562nm. The proportion of Cu^{2+} reduced (Abs 562nm) relates to the protein concentration, which is a linear relationship. The BCA reaction is carried out at 37°C to minimise variation due to presence of cysteine, tyrosine and tryptophan side chains (**Figure 2.4A**).

For each assay, a standard curve was generated by running a set of bovine serum albumin (BSA) standards in parallel. A representative standard curve is shown in **Figure 2.4B**. Samples were boiled for 7min at 95°C. 5µl of sodium dodecyl sulfate (SDS) lysis buffer (see

Appendix 2) were added in duplicate to a clear 96-well plate followed by 5µl of each standard (or 5µl ddH_2O for zero), stored at 4°C from when cells were treated. 5µl of ddH_2O per well was added in duplicate and 5µl of each sample. To all wells containing samples or standards were added 200µl of BCA solution (Thermo Fisher Scientific, 23225), consisting of a 1 in 50 dilution of reagent B (4% cupric sulphate, C2715) to reagent A (sodium carbonate, sodium bicarbonate, BCA detection reagent, and sodium tartrate in 0.1N sodium hydroxide, UF287195). The plate was covered by a piece of clingfilm wrap and incubated for 20 min at 37°C before reading absorbance at 562nm, which was measured by a plate reader (TECAN, Sunrise, UK).

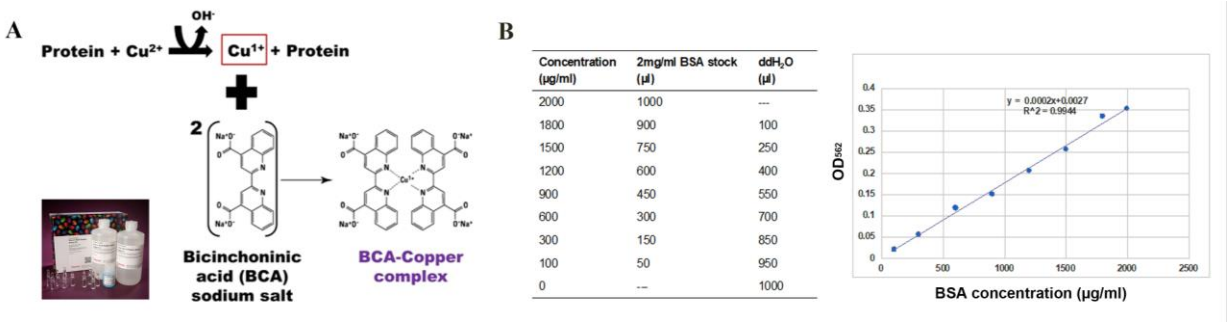

Figure 2.4 Reaction of BCA protein assay and representative standard curve.
(A) Reaction of BCA protein assay. Under an alkaline environment, protein reduces Cu^{2+} to Cu^{+}. Two molecules of BCA then chelate each Cu^{+} molecule forming a purple coloured product, which can be quantified by reading the absorbance at 562nm. (**B**) Standards using BSA and representative standard curve for a BCA assay.

2.4 Measurement of cell proliferation

In order to measure HCASMCs proliferation, changes in cells number were determined by cell counting and protein content as well as using a RTCA iCELLigence™ instrument (ACEA Biosciences, USA).

2.4.1 Measurement of cell proliferation using cell counting

HCASMCs were cultured in 18 or 5kPa O_2 for 5 days and then seeded at 3500 cells/well into a 96-well plate in SMC basal medium 2 with supplement pack. Medium was changed every two days. Cells were counted each day, and the average of three wells was quantified using a haemocytometer.

2.4.2 Measurement of cell proliferation by comparing protein content

Cells were seeded in a 96-well plate in triplicate at a seeding density of 3500 cells/well. Complete medium was used and changed every two days. Cells were lysed using SDS lysis buffer (40µl/well) and stored at -20℃. Then protein content was measured by BCA protein assay as described in **Section 2.3**, with changes in protein content monitored for 5 days.

2.4.3 Measurement of cell proliferation using an iCELLigence™ platform

In addition, cell proliferation was assessed using an iCELLigence™ platform, which uses noninvasive electrical impedance to quantify cell proliferation in a label-free, real-time manner (Toedebusch et al., 2018). As illustrated in **Figure 2.5**, the cellular impedance platform has a set of gold microelectrodes fused to the bottom surface of well in a microtiter plate (E-Plates®). In an electrically conductive solution such as culture medium the application of an electric potential across these electrodes causes electrons to exit from the negative terminal, pass through medium, and deposit onto the positive terminal. The presence of adherent cells at the electrode-solution interface impedes electron flow, and the magnitude

of impedance is dependent on the number of cells. The impedance of electron flow caused by adherent cells is referred to as Cell Index (CI), which can be used to monitor cell number during cell proliferation (Turker Sener et al., 2017).

HCASMCs were seeded in E-Plates® in a triplicate at a concentration of 7000 cells/well. Cell adhesion occurs in the first 2h to reach a baseline CI. Cell proliferation was recorded as CI measured in over a period of 6 days with media changed every 2 days.

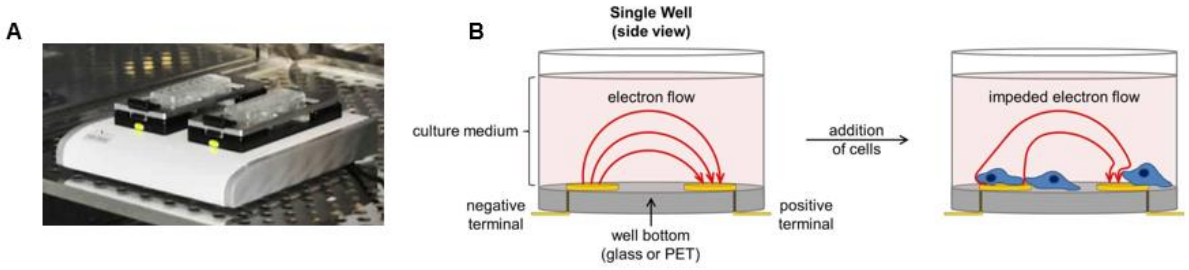

Figure 2.5 Overview of cellular impedance apparatus.
(**A**) iCELLigence™ instrument. (**B**) A side view of a single well is shown before and after cells have been added. In the absence of cells, electric current flows freely through culture medium to complete the circuit between the electrodes. As cells adhere to and proliferate on the electrodes, current flow is impeded, which provides a readout of cell number, cell size/morphology, and cell-substrate attachment quality (Turker Sener et al., 2017).

2.5 MTT assay

The thiazolyl blue tetrazolium bromide (MTT) assay is a colorimetric assay for cell metabolic activity and can be used as an index of cell viability and proliferation (Freimoser et al., 1999; Mosmann, 1983). NAD(P)H-dependent dehydrogenase enzymes in living cells are capable of changing MTT (a yellow, water-soluble tetrazolium salt) to formazan (an insoluble purple crystal). The absorbance of this coloured solution can be detected at a certain wavelength (usually 500-600 nm) using a spectrophotometer.

HCASMCs pre-adapted to 18, 5 or 1kPa O_2 for 5d were seeded into 24-well plates in triplicate and cultured to ~80%. Cells were then treated with different concentrations of N,N,N′,N′-tetrakis (2-pyridylmethyl) ethylenediamine (TPEN) (0-1.5µM, Sigma-Aldrich, P4413) or 2-mercaptopyridine N-oxide sodium salt (a Zn^{2+} ionophore, 0-1µM, Sigma-Aldrich, 329061) with $ZnCl_2$ (10-14µM, Sigma-Aldrich, Z0152) for 16h, respectively. HCASMCs incubated with media were used as controls. 1h before the end of treatment period untreated cells were treated with hydrogen peroxide (H_2O_2, 500 mM) (Sigma-Aldrich, 31642) as a positive marker of cell death. Subsequently, media was aspirated and 100µl/well of 10% MTT stock solution (5mg/ml in PBS) (Sigma, M5655) were added and incubated for 4h at 37°C respectively at 18, 5 or 1kPa O_2 in the Sci-tive workstation. 50µl/well of dimethylsulfoxide (DMSO) (Sigma-Aldrich, D8418) were directly added after aspirating the 10% MTT, and plates were placed on a shaker at room temperature for 10min to solubilise the purple formazan crystals. The optical density (OD) value was measured at 562 nm (see **Figure 2.6**).

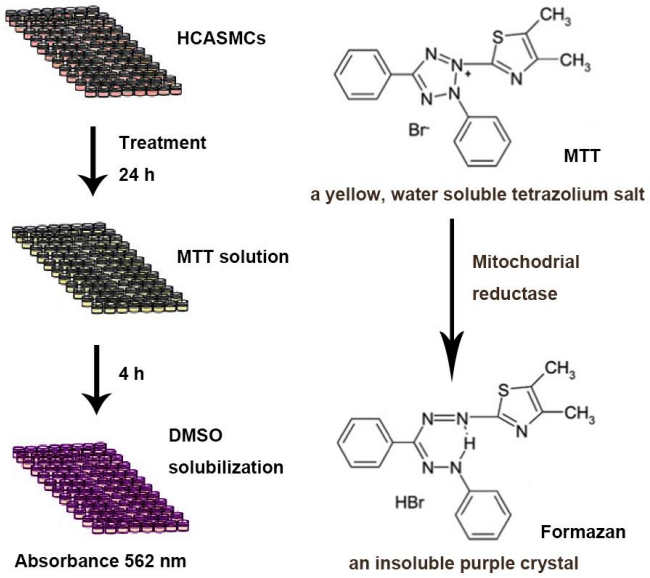

Figure 2.6 Schematic of MTT assay
HCASMCs were seeded and cultured at 18, 5 or 1kPa O_2 in the Sci-tive workstation. Cells were treated with different concentrations of drugs. Media was then aspirated and 100µl/well of 10% MTT were added and incubated for 4h. 50µl/well DMSO were directly added after aspirating MTT, and plates were placed on a shaker at room temperature for 10min. MTT, a yellow, water-soluble tetrazolium salt is reduced to formazan, an insoluble purple crystal.The OD value was measured at 562 nm.
Abbreviations: MTT, chloride 3-(4,5-dimethylthiazol-2-yl)-2,5-diphenyltetrazolium bromide; HCASMCs, human coronary artery smooth muscle cells; DMSO, dimethyl sulfoxide; OD, optical density.

2.6 Firefly lantern extract chemiluminescence-based ATP assay

Adenosine triphosphate (ATP) plays a fundamental role in cellular energetics, serving as an indicator of metabolically active cells (Bonora et al., 2012). Cell viability can be assessed based on quantifying intracellular ATP levels in culture (Garewal et al., 1986). The firefly lantern extract chemiluminescence-based ATP assay employs the luciferin-luciferase system to quantitatively determine ATP levels (Chida et al., 2012). Firefly luciferase catalyses the two-step oxidation of luciferin to oxyluciferin along with a burst of light (see **Figure 2.7**). The amount of light generated is linearly proportional to the amount of ATP, and thus ATP levels in cell lysates can be quantified following calibration of the luminescence signal with standards of known ATP concentration (Jenner et al., 2002; Srivastava et al., 2016).

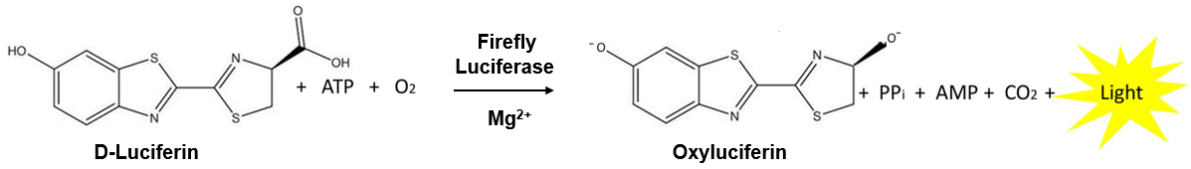

Figure 2.7 Bioluminescent reactions catalysed by firefly luciferase
The extract from firefly lanterns contains the enzymes luciferase and its substrate luciferin. In the presence of ATP, the firefly luciferase catalyses luciferin to oxyluciferin along with generating a bioluminescent signal.
Abbreviations: ATP, adenosine triphosphate; AMP, adenosine monophosphate; CO_2, carbon dioxide; PP_i, pyrophosphate.

Basal ATP levels in HCASMCs were determined in cells were adapted for 5d to 18, 5 or 1kPa O_2. Cells were seeded into 24-well plates in duplicate and cultured to ~70%. When collecting samples for an ATP assay, 100µl 6.5% trichloroacetic acid (TCA) (Sigma-Aldrich, T9159) were added into each well after washing twice ice-cold PBS washing and banging the plate dry rapidly and placing it on ice for 10min. TCA extracts were transferred into ice cold Eppendorf tubes and stored at -80℃ for subsequent ATP assay. 50µl SDS lysis buffer was added into each well for collecting protein and left on ice for 5min. The proteins were stored at -20℃, with protein concentrations determined using the BCA assay, as described in **Section 2.3**.

Fresh ATP (Sigma-Aldrich, A2383) standards (0µM, 2.5 µM, 5µM, 10µM, 15µM, 20µM, 30µM, 40µM) were prepared in 6.5% TCA on ice and run in parallel with each assay in a 96-well white microtiter plate. 5µl 6.5%TCA were added into a 96-well plate in duplicate as a blank. 5µl ATP standards or sample acid extracts was added into the same plate in duplicate. 15µl ddH_2O was added to each blank, ATP standards and samples to dilute the acid concentration because this strongly inhibits the firefly extract. The plate reader (CLARIOstar, BMG Labtech., UK) was set to 27℃ and the entire vial firefly extracts (Sigma-Aldrich, FLE250) was placed in plate reader and allowed to equilibrate to the new temperature. The 96-well plate was placed in plate reader and the luciferase ATP protocol was edited with our

desired layout and concentrations of standards. Each well takes 10s to read when the plate reader starts to measure. Measurements were corrected for the concentration of protein to obtain ATP in nmol/mg protein.

2.7 Measurement of intracellular reduced glutathione by fluorometric assay

Glutathione (GSH) plays a critical role in the cellular defense against oxidative stress (Forman et al., 2009; Meister, 1995; Meister and Anderson, 1983). Glutathione exists in two free forms, reduced form (GSH) and oxidized form (glutathione disulfide, GSSG), and there are various established methods to measure cellular levels (Rousar et al., 2012). Under physiological conditions, the ratio of GSH to GSSG generally remains above 99%, whilst the ratio can change under oxidative stress (Lu, 1999). In the present work, intracellular reduced GSH levels were measured using a fluorometric assay, which provides an index of the basal redox status of cells (Siow et al., 1998; Warpsinski et al., 2020). The fluorescent probe, *o*-phthalaldehyde (phthalic dicarboxaldehyde, OPA) (Sigma-Aldrich, 79760) reacts directly with GSH and is non-fluorescent until it reacts as a heterobifunctional reagent with a primary amine and thiol provided by GSH to a fluorescent isoindole (OPA-GSH) (see **Figure 2.8**) (Hissin and Hilf, 1976; Michaelsen et al., 2009), which can be detected by the plate reader (CLARIOstar, BMG Labtech., UK).

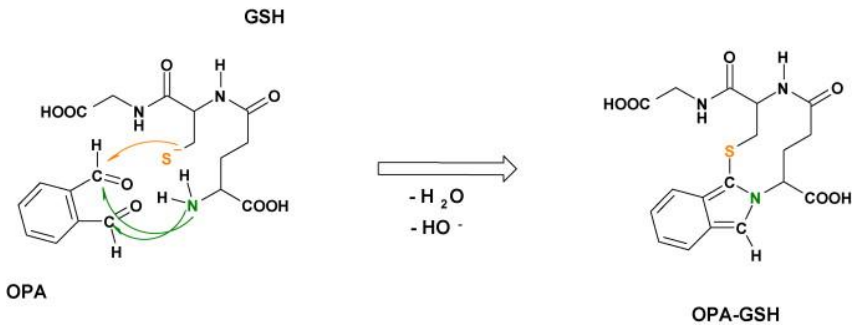

Figure 2.8 The reaction of OPA with GSH
Reaction of GSH with OPA to form a highly fluorescent and stable isoindole derivative OPA-GSH. Taken from (Michaelsen et al., 2009).
Abbreviations: OPA, *o*-phthalaldehyde; GSH, glutathione; GSSG, glutathione disulfide.

To assess basal GSH levels in HCASMCs under 18, 5 or 1kPa O_2, cells were pre-adapted to 18, 5 or 1kPa O_2 for 5d. HCASMCs were then seeded into 24-well plates in duplicate and cultured to ~70% confluence in air (18kPa O_2), 5 kPa O_2 or 1 kPa O_2 in a Sci-tive workstation (Baker-Ruskinn, UK). Samples and protein were collected using protocols for an ATP assay, as highlighted in **Section 2.6.** The acid extracts collected for an ATP assay were used to measure intracellular GSH levels.

Fresh GSH (Sigma-Aldrich, G4251) standards (0µM, 2.5µM, 5µM, 7.5µM, 10µM, 15µM, 20µM, 30µM) were prepared in 6.5% TCA on ice and run in parallel with each assay in a 96-well black microtiter plate. TCA (7.5µl 6.5%) was added into a 96-well plate in duplicate as a blank. 7.5µl GSH standards or sample (acid extracts) were added into the same plate in duplicate. Then 277.5µl phosphate/Ethylenediaminetetraacetic acid (EDTA) + NaOH buffer (pH>8) (see **Appendix 3**) were added to each well before 15µl fresh OPA solution (Sigma-Aldrich, 79760) was added. The 96-well plate was left in the dark at room temperature for 25min and fluorescence read at 350nm excitation and 420nm emission. Values were corrected for the absorbance of standard GSH concentrations to give GSH concentrations in nmol/mg protein for sample (Siow et al., 1998).

2.8 Immunostaining

To investigate the phenotype of cultured HCASMCs under different O_2 levels, vascular smooth muscle cell contractile type markers were probed by immunostaining. HCASMCs were pre-adapted to 18, 5 or 1kPa O_2 for 5d and then seeded into 8-chambered coverslips (Ibidi, Germany) for 48h. Cells were then washed twice with PBS and fixed with 4% formaldehyde solution (Fisher Chemical™, UK, 1340771) for 15min at room temperature. If necessary, cells were permeabilized using 0.2% Triton X-100 (Sigma-Aldrich, T9284) in PBS for 5min at room temperature. Cells were then blocked with 3% BSA for 30min at room temperature with constant rocking. Cells were incubated with primary antibodies (**Table 2.1**) against target protein overnight at 4°C. All primary antibodies were made up in 3% BSA PBS-T (see **Appendix 4**). Primary antibodies were diluted in blocking solution according to manufacturer's information. After washing cells thrice with PBS for 5min each, cells were stained with Alexa Fluor 488 or DyLight® 488 conjugated secondary antibody (**Table 2.2**) (recognizing the host species of the primary antibody) diluted with 3% BSA and PBS-T according to manufacturer's instructions for 1h with constant rocking, followed by thrice washes with PBS. Staining for endothelial nitric oxide synthase (eNOS) with Alexa Fluor 488 was only performed to confirm no contamination of endothelial cells. Fluorescence was visualized at ×40 magnification using a fluorescence microscope (Etaluma LS720 Microscopes, USA) and appropriate filters. All immunofluorescence images were merged with the nuclear stain 4,6-diamidino-2-phenylinde (DAPI, Sigma, D9542).

Table 2.1 List of primary antibodies for immunostaining

Antigen	Molecular Weight (kDa)	Dilution	Manufacturer	Host Species	Catalog number
SM22-α	23	1:100	Abcam	goat	Ab10135
Calponin 1	34	1:5000	Abcam	rabbit	ab46794
eNOS	140	1:500	Santa Cruz	mouse	SC-376751

Abbreviations: SM22-α, Smooth muscle protein 22-alpha; eNOS, endothelial nitric oxide synthase.

Table 2.2 List of secondary antibodies for immunostaining

Antigen	Manufacturer	Catalog number	concentration	Dilution	Conjugated Fluorophore	Emission colour
Donkey Anti-Rabbit	Bethyl Laboratories	A120-216D2	0.5mg/ml	1:900	DyLight® 488	green
Goat Anti-Mouse	Invitrogen™	A-10680	2mg/ml	1:900	Alexa 488	green
Donkey Anti-Goat	Abcam	Ab150129	2mg/ml	1:900	Alexa 488	green

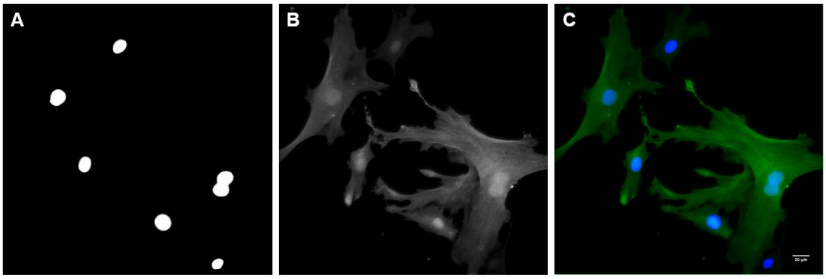

Figure 2.9 Representative images of HCASMCs immunostained for SM22-α.
(A) Representative image of HCASMCs nucleus stained with DAPI. (**B**) Representative image of HCASMCs stained with SM22-α using an Alexa Fluor 488 conjugated secondary antibody. (**C**) SM22-α positive immunofluorescence image was merged with nuclear stain DAPI. Images were taken at ×40 magnification using an Etaluma microscope (LS720 Microscopes, USA). Scale bar is 20µm.

2.9 Nuclear translocation of Nrf2

To assess translocation of Nrf2 to the nucleus after activation by different drugs, HCASMCs were pre-adapted to 18, 5 or 1kPa O_2 for 5d and then seeded into 8-chambered coverslips (Ibidi, Germany) for 48h. Cells were then treated with vehicle (veh, 0.005% dimethyl sulfoxide (DMSO) (Sigma-Aldrich, D8418), sulforaphane (SFN, 2.5µM, Sigma-Aldrich, S4441), N,N,N′,N′-tetrakis (2-pyridylmethyl) ethylenediamine (TPEN, 1.25µM, Sigma-Aldrich, P4413) or 2-mercaptopyridine N-oxide sodium salt (a Zn^{2+} ionophore, 0.5µM, Sigma-Aldrich, 329061) with $ZnCl_2$ (10µM, Sigma-Aldrich, Z0152) for 16h, respectively.

Immunostaining protocols are the same as described in **Section 2.8**. The primary antibodies and DyLight® 488 conjugated secondary antibodies are summarised in **Table 2.2 and 2.3**. Nrf2 immunofluorescence was quantified as the ratio of nuclear to cytoplasmic Nrf2 immunofluorescence.

Table 2.3 Nrf2 antibody for immunostaining

Antigen	Molecular Weight (kDa)	Dilution	Manufacturer	Host Species	Catalog number
Nrf2	95-110	1:500	Santa Cruz	rabbit	sc-722

Abbreviations: Nrf2, nuclear factor erythroid 2-related factor 2.

2.10 Quantification of mRNA expression using quantitative reverse transcription polymerase chain reaction (qRT-PCR)

2.10.1 Extraction of ribonucleic acid (RNA) using RNeasy® Mini Kit

In order to measure mRNA expression, total RNA from HCASMCs was extracted using a RNeasy® Mini Kit (Qiagen, Germany, 74106), which combines the stringency of guanidine-isothiocyanate lysis with the speed of microspin technology and the purity of silica-gel-based membrane purification. The kit consists of four steps: lysing, binding, washing and eluting.

HCASMCs were pre-adapted to 18, 5 or 1kPa O_2 for 5d and then seeded into 6-well plates and cultured to ~80%. Cells were then treated with vehicle (Veh, 0.005% DMSO), SFN (2.5μM), TPEN (1.25μM) or 2-mercaptopyridine N-oxide sodium salt (a Zn^{2+} ionophore, 0.5μM) with $ZnCl_2$ (10μM) for 6h, respectively. Cells were then washed twice with cold PBS and lysed with β-mercaptoethanol (1%) and RLT lysis buffer (350ul/well), which is a

guanidine isothiocyanate (GITC)-containing buffer leading to efficient RNA lysis, protein denaturation and ribonuclease (RNase) inactivation. Lysates were transferred into RNase-free Eppendorfs and stored at -80°C before extraction (Chapple et al., 2016).

As shown in **Figure 2.10**, frozen lysates were defrosted at room temperature for 5min and then 70% ethanol (350ul/per sample) added to provide appropriate binding conditions. The mixed well solution was transferred into a RNeasy spin column placed in a 2ml collection tube and centrifuged for 15s at 13,000rpm at room temperature. The total RNA binds to the membrane, and the flow-through in the collection tube was discarded. The columns were washed with RW1 buffer (a washing buffer that efficiently removes biomolecules such as carbohydrates, proteins, fatty acids) (700ul/per column) and centrifuged for 15s at 13,000rpm at room temperature. The columns were then washed by RPE buffer (a mild washing buffer to remove salts used before) (700ul/per column) twice, followed by centrifugation at 13,000rpm at room temperature for 15s and 2min, with flow-through discarded. The columns were subsequently centrifuged for 1min at 13,000rpm at room temperature and then transferred to a new 1.5 ml collection tube. To elute RNA, 40µl RNase-free H_2O was directly added to center of the spin column membrane and centrifuged for 1min at 13,000rpm. 30ul eluate was then added to center of membrane and centrifuged again and the eluted RNA was collected.

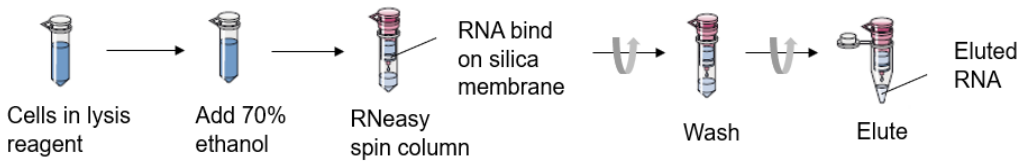

Figure 2.10 Example of RNeasy® Mini Kit procedure
Cultured and treated HCASMCs were lysed with RLT lysis buffer including 1% β-mercaptoethanol. Ethanol provides optimal conditions leading to total RNA binding to the silica membrane. The silica membrane was washed 3 times with RW1 buffer or RPE buffer to remove contaminants and cellular material. 40µl RNase-free H_2O was added and eluted RNA.

The concentration and purity of RNA were measured using a NanoDrop DN-100 spectrophotometer (NanoDrop Technologies, USA), with 1ul per sample used for measurement. The contamination was assessed by the ratio of absorbance 260/280 ($A_{260/280}$) and 260/230 ($A_{260/230}$). $A_{260/280}$ of around 2.0, and $A_{260/230}$ of 2.0-2.2 are generally accepted as 'pure' for RNA. The concentration of RNA was expressed in ng/µl. RNA samples were stored at -80℃ before reverse transcription polymerase chain reaction (RT-PCR).

2.10.2 Complementary DNA (cDNA) synthesis

The original RNA was reverse transcribed to complementary DNA (cDNA). cDNA was synthesized using High-Capacity cDNA Reverse Transcription Kit (Applied Biosystems, 4368814, USA). 13µl of each RNA sample was mixed with 7µl cDNA Master Mix containing the following components: 10× reverse transcription (RT) buffer (2µl), 100mM 25× deoxy-ribonucleoside triphosphate (dNTP) mix (0.8µl), 10× RT random primers (1.6µl), 500ng/µl oligo dT primers (0.4µl), MultiScribe™ reverse transcriptase (1µl) and Nuclease (DNase)-free H_2O (1.2µl). Reaction was performed using the GeneAmp® PCR System 9700 thermal cycler (Applied Biosystems, USA), as follows: The reaction was incubated at 25℃ for 10min, then stored at 37℃ for 120min, stopped at 85℃ for 5min before the system cooled down and held at 4℃. cDNA products were diluted as 20ng/µl before they were used in further qPCR procedures.

2.10.3 Primer design and qRT-PCR

The design of primers was based on gene sequences in the National Centre for Biotechnology Information (NCBI). The specificity and complementarity of primers were assessed by

Oligonucleotide Properties Calculator and In-Silico PCR, and a list of the primers used is tabulated in **Table 2.4**. All primers were obtained from Sigma-Aldrich.

The master mix (10ul) was prepared before qPCR and contained enzyme (5ul, SensiFAST™ SYBR® No-ROX Kit, Bio-98005), cDNA (20ng/ul, 0.5ul), primers (6µM, 1ul) and Nuclease free H_2O (3.5µl). The master mix was added into a 384-well plate and the fluorescence signal were detected and quantitated nucleic acid sequences by the 7900HT Fast Real-Time PCR System (Applied Biosystems™, Instrument Serial number 279003048). The DNA templates were amplified by 3 repeating steps with 40 cycles: denaturation (95℃, 5s), annealing (60℃, 15s) and extension (72℃, 15s) after polymerase activation (95℃, 2min). In dye-based qPCR, fluorescent labelling quantified the amplified DNA molecules by non-specific fluorescent dyes intercalating with double-stranded DNA (dsDNA) (Bustin, 2000). The fluorescence signal increased proportionally to the amount of replicated DNA. Relative mRNA levels were calculated using the threshold cycles (Ct) and normalized to three house-keeping gene (ribosomal protein lateral stalk subunit P0 (RPLP0), TATA-binding protein (TBP), succinate dehydrogenase complex, subunit A (SDHA)). The calculation formula is as follows: amount of target = $2^{-\Delta Ct}$.

Table 2.4 List of qPCR primers

No	Gene name	Forward (5'→3')	Reverse (3'→5')	Amplicon(bp)
1	RPLP0	CAGATTGGCTACCCAACTGTT	GGGAAGGTGTAATCCGTCTCC	98
2	TBP	CACGAACCACGGCACTGATT	TTTTCTTGCTGCCAGTCTGGAC	89
3	SDHA	CTACAAGGTGCGGATTGATG	ATAGGACAGGGTGTGCTTCC	100
4	HO1	GGCTTCAAGCTGGTGATGG	AGTAGACAGGGGCGAAGACTG	100
5	GCLC	CACAAGGACGTTCTCAAGTGG	AGGATGGTTTGGGTTTGTCC	150
6	GCLM	CCAGATGTCTTGGAATGCAC	GACTGAACAGGCCATGTCAAC	150
7	NQO1	GCACTGATCGTACTGGCTCA	GGTCCTTCAGTTTACCTGTGATG	172
8	MT1	ATGGACCCCAACTGCTCCTG	AGCAGCTCTTCTTGCAGGAG	100

Abbreviations: RPLP0, ribosomal protein lateral stalk subunit P0; TBP, TATA-binding protein; SDHA, succinate dehydrogenase complex, subunit A; HO-1, heme oxygenase-1, GCLC, glutamate-cysteine ligase catalytic subunit; GCLM, glutamate-cysteine ligase modifier subunit; NQO1, NAD(P)H quinone dehydrogenase 1; MT1, metallothionein-1.

2.11 Immunoblotting

Immunoblotting is used for the detection of protein expression by exploiting the specificity inherent in antigen-antibody recognition. Firstly, whole cell lysates were prepared. After aspirating medium, cell monolayers were washed twice with cold PBS. Cell lysates were collected using SDS lysis buffer supplemented with protease inhibitor cocktail (Sigma-Aldrich, 42484600). All steps were performed on ice and lysates stored at -80ºC.

The SDS-PAGE gel contains a resolving gel (see **Appendix 5**) that separates proteins by molecular weight and a stacking gel (see **Appendix 6**) that "stacks" all of proteins in sample into a narrow band, so that they all enter the resolving gel at essentially the same time, with 10µg of each sample were loaded in sodium dodecyl sulfate-polyacrylamide (SDS-PAGE) gel. The loading volume for each sample was calculated from protein concentration determined using the BCA assay as described in **Section 2.2**. Loading buffer (0.02% bromophenol blue + 1% 2-mercaptoethanol) was added into each sample at a ratio of 1:9 to the original sample volume. Electrophoresis was conducted at 120V for 1.0-1.5h in gel tank with running buffer (see **Appendix 7**). Afterwards, separated proteins were transferred onto a polyvinylidene difluoride (PVDF) membrane (Millipore, IPVH00010) by electrophoresis using semi-dry transfer with transfer buffer (see **Appendix 8**) for 2.5h at 20V. The protein binding sites on PVDF membrane were blocked by PBS-T containing 5% skimmed milk (Marvel, UK) with constant rocking for 1h at room temperature. The membrane was then incubated with primary antibody (**Table 2.5**) targeted against tested protein overnight at 4°C. All primary antibodies were made up in 3% BSA PBS-T and a few granules of sodium azide were added to prevent contamination and allow multiple use of the antibody. The primary antibodies were diluted in blocking solution according to manufacturer’s information for

different antibodies. After washing membrane thrice with PBS-T for 10min each, the membrane was incubated with a suitable horseradish peroxidases (HRP)-conjugated secondary antibody (**Table 2.6**) (recognizing the host species of the primary antibody) diluted with 3% skimmed milk and PBS-T according to the instructions for 1h with constant rocking, followed by three times washes with PBS-T. The membrane was subjected to development with enhanced chemiluminescence (ECL) (Immobilon® classico western HRP substrate (Millipore, Lot.192265) or Immobilon® crescendo western HRP substrate (Millipore, Lot. 190465)). Immunoblot data were analysed by ImageJ 1.49c (National Institute of health, USA). The immunoblotting protocols are illustrated in **Figure 2.11.**

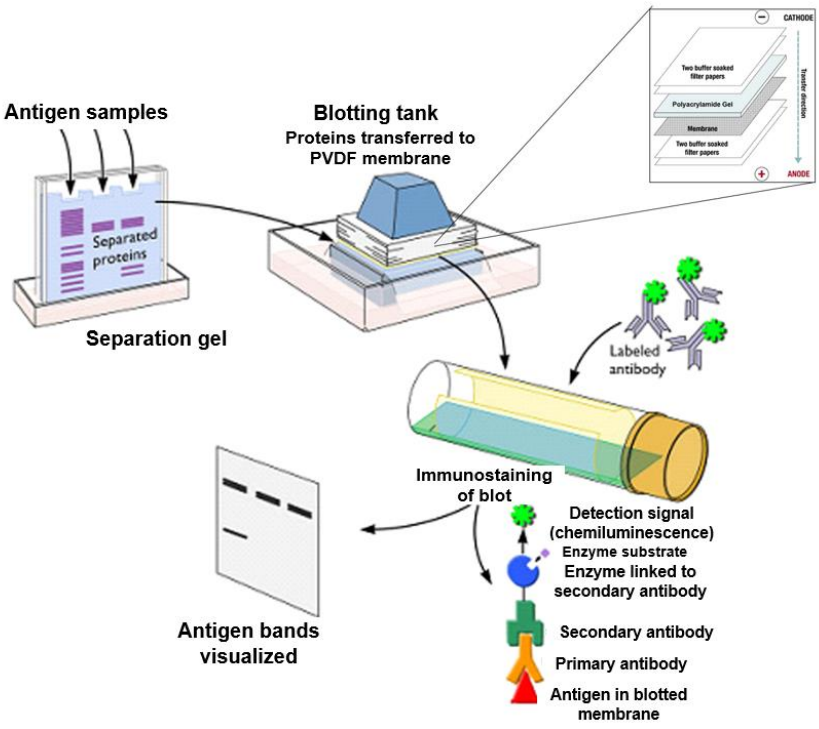

Figure 2.11 Immunoblotting
Cell lysates were run through electrophoresis on SDS-PAGE to separate proteins based on their molecular weight. Proteins were transferred onto a PVDF membrane, which was then blocked with skimmed milk. The membrane was incubated with primary antibody and the corresponding secondary antibody conjugated with HRP. Substrates were added to react with the HRP to generate light that can be detected using a G: Box system (Syngene, UK). Densitometry was performed using Image J software (National Institute of Health, USA).

Table 2.5 List of primary antibodies for immunoblotting

Antigen	Molecular Weight (kDa)	Dilution	Manufacturer	Host Species	Catalog number
β-actin	45	1:8000	Sigma-Aldrich	mouse	A1978
HIF-1α	110	1:1000	Abcam	rabbit	Ab179483
HO-1	32	1:500	BD Biosciences	mouse	610713
NQO1	29	1:500	Santa Cruz	mouse	sc-32973
GCLC	73	1:10,000	N/A	rabbit	N/A
GCLM	31	1:10,000	N/A	rabbit	N/A
Bach1	110	1:500	Santa Cruz	mouse	sc-271211
MT	10	1:500	Abcam	mouse	Ab12228
MT	10	1:1000	GeneTex	mouse	GTX12228
ZnT1	55	1:500	Abcam	rabbit	Ab123139
CAT	~60-65	1:8000	Sigma-Aldrich	rabbit	219010
CuZnSOD	17	1:2000	Abcam	rabbit	Ab16831
MnSOD	22	1:1000	R&D systems	mouse	MAB3419
SM22-α	23	1:100	Abcam	goat	Ab10135
Calponin 1	34	1:5000	Abcam	rabbit	Ab46794
eNOS	140	1:500	Santa Cruz	mouse	SC-376751

Abbreviations: Nrf2, nuclear factor erythroid-2-related factor 2; HIF-1α, hypoxia-inducible factor 1-alpha; HO-1, heme oxygenase 1; NQO1, NAD(P)H quinone oxidoreductase; GCLC, glutamate-cysteine ligase catalytic subunit; GCLM, glutamate-cysteine ligase modifier subunit; Bach1, BTB and CNC homology 1; ZnT1, zinc transporter 1; MT, metallothionein; CAT, catalase; CuZnSOD (SOD1), superoxide dismutase [Cu-Zn]; MnSOD (SOD2), superoxide dismutase [Mn]; *GCLC and GCLM were gifts from Prof. T. Kavanagh (University of Washington, WA, USA).

Table 2.6 List of secondary antibodies for immunoblotting

Antigen	Manufacturer	Catalog number	Dilution
Goat Anti-Rabbit	MilliporeSigma	401315	1:2000
Goat Anti-Mouse	MilliporeSigma	401215	1:2000
Goat Anti-Goat	MilliporeSigma	AB324P	1:2000

2.12 siRNA Nrf2 silencing of Nrf2

HCASMCs were pre-adapted to 18, 5 or 1kPa O_2 for 5d and then seeded into 24-well plates and cultured to ~80%. HCASMCs were transfected with 2.5nM of either scrambled siRNA (Santa Cruz, USA, sc-37007) or Nrf2 siRNA (Santa Cruz, USA, sc-37030) for 24h using DharmaFECT 4 transfection reagent (Thermo Scientific, UK, T2004-02) before treatment with before treatment with SFN (2.5 mmol/L) or vehicle for 16h, followed by measurements of HO-1, NQO1 MT and ZnT1 protein or metal concentrations.

2.13 Nrf2 overexpression

HCASMC were pre-adapted to 18, 5 and 1kPa for 5d in 24-well plates and then transfected with control vector pcDNA3.1 (3.1C) or pcDNA3.1-hNrf2 (hNrf2) vector at 400ng per well for 24 hours using FuGENE transfection reagent (Promega, UK) according to the manufacturer's instructions, followed by measurements of HO-1, NQO1 MT and ZnT1 protein or metal concentrations. **Appendix 9** provides further vector information.

2.14 Phosphorescence lifetime measurements of O_2 levels in HCASMCs cytosol and medium

Intracellular O_2 levels in living cells were monitored using MitoXpress®-INTRA (Agilent Technologies, MX-300-4), which is a cell-penetrating phosphorescent platinum-porphyrin based nanoparticle probe (Chapple et al., 2016; Fercher et al., 2011; Warpsinski et al., 2020; Zhdanov et al., 2014). The probe can emit a phosphorescence signal at 655±55 nm when excited at 355±55 nm. The probe traverses the plasma membrane and binds to O_2, quenching phosphorescence emission, which can be detected in an oxygen-controlled plate reader (CLARIOstar, BMG Labtech, UK). The signal decay is inversely proportional to the concentration of O_2. The assay, equipped with an atmospheric control unit attachment, enables measurements of cytosolic and medium O_2 levels under defined ambient O_2 levels (Chapple et al., 2016; Fercher et al., 2011; Warpsinski et al., 2020).

HCASMCs were seeded into black clear bottomed 96-well plates in quadruplicate and cultured to ~80% confluence in air (18kPa) and loaded with the nanoparticle probe (10µg/ml)

for 16h in complete medium. Phosphorescence intensity after excitation was measured after 30μs (D1) and 70μs (D2) with a 30μs window and converted to probe lifetime (T) [$T=(D2–D1)/\ln(l_{w1}/l_{w2})$], where T represents emission lifetime and l_{w1} and l_{w2} represent signals measured at window 1 and window 2 . Averaged lifetime measured at 7 ambient O_2 tensions (18, 15, 10, 7.5, 5, 2.5, 1kPa) were plotted against the known O_2 tension and subjected to an exponential fit analysis. Lifetime values were then converted to $\%O_2$ by a curve based on the parameters of the fit. Lifetime values were then interpolated from this curve to give the dissolved intracellular O_2 level in HCASMCs cytosol. Dissolved O_2 level in culture medium was also measured in parallel by diluting MitoXpress®-INTRA (2.5μg/ml) in complete medium.

2.15 Measurement of intracellular free radical generation by L-012 chemiluminescence

L-012 (8-amino-5-chloro-7-phenylpyridol[3,4-d]pyridazine-1,4-(2H,3H)dione), a luminol-based chemiluminescent probe, is widely used to measure oxidants in biological systems, specifically O_2^- (Warpsinski et al., 2020; Zielonka et al., 2013). O_2^- alone does not react with L-012 to emit luminescence. The first step of the reaction is oxidation of the probe to its radical. Reaction of the luminol radical with self-generated O_2^- during oxidation of L-012 leads to the emission of blue light, which can be inhibited by superoxide dismutase (SOD) (Zielonka and Kalyanaraman, 2018; Zielonka et al., 2013).

HCASMCs were seeded into white clear bottomed 96-well plates in quadruplicate and adapted for 5d under 18 or 5kPa O_2. Cell monolayers (~80% confluence) were incubated in the absence or presence of polyethylene glycol SOD (pSOD, 20U/ml, Sigma-Aldrich, S9549), polyethylene glycol catalase (pCAT, 200U/ml, Sigma-Aldrich, C4963) and then the L-012

sodium salt (L-012, 10μM, TOCRIS, 5085). Cells adapted to 18 or 5kPa O_2 were rapidly transferred to an O_2-regulated plate reader (CLARIOstar, BMG Labtech, UK) at 37°C and exposed to hypoxia (1kPa O_2) for 1h and reoxygenation under 18 or 5 kPa O_2, respectively. O_2 changes between 18kPa or 5kPa and 1kPa took ~30 minutes. Chemiluminescence was measured at 60s intervals over 3h and data expressed as mean light units×10^4/mg protein.

Meanwhile, to measure the effects of the Nrf2 inducer sulforaphane (SFN), Zn^{2+} and TPEN treatment on intracellular free radical generation, HCASMCs were seeded into 96-well plates in quadruplicate and adapted for 5d under 18 or 5kPa O_2. HCASMCs were treated with vehicle (veh, 0.005% DMSO), SFN (2.5μM), TPEN (1.25μM) or 2-mercaptopyridine N-oxide sodium salt (a Zn^{2+} ionophore, 0.5μM) with $ZnCl_2$ (10μM) respectively for 16h. Cells were then incubated with L-012 sodium salt (L-012, 10μM, TOCRIS). Cells adapted to 18 or 5kPa O_2 were rapidly transferred to an O_2-regulated plate reader (CLARIOstar, BMG Labtech) at 37°C and exposed to hypoxia (1kPa O_2) for 1h and reoxygenation under 18 or 5kPa O_2, respectively. Chemiluminescence was measured at 60s intervals over 3h and data expressed as mean light units×10^4/mg protein.

2.16 Metallomic profiling in HCASMCs using inductively coupled plasma mass spectrometry (ICP-MS)

The London Metallomics Facility, funded by a Wellcome Trust Multi-user Equipment Grant and King's College London, enables the imaging and speciation of trace metal elements in biological samples. In collaboration with Dr Theodora Stewart , Dr Alex Griffiths and Prof Wolfgang Maret, we conducted metal profiling in HCASMCs adapted to physiological normoxia (5kPa), hypoxia (1kPa) and reoxygenation using ICP-MS (Mittal et al., 2017;

Stewart, 2019). ICP-MS uses an inductively coupled plasma to ionize the sample, and ions are detected in a NexION 350D mass spectrometer with concentrations of metals proportional to the ion signals according to their mass-charge ratio (Wilschefski and Baxter, 2019).

HCASMCs were cultured long-term (5d) in air (18kPa O_2) or in an O_2-regulated Sci-tive workstation under physiological normoxia (5kPa O_2) or hypoxia (1kPa O_2) or 1h hypoxia following re-exposure to 18 or 5kPa O_2 for 1 and 9h. O_2 changes between 18kPa or 5kPa and 1kPa took 30 minutes. HCASMCs in 6-well plates were treated with vehicle (veh, 0.005% DMSO), SFN (2.5μM), TPEN (1.25μM) or 2-mercaptopyridine N-oxide sodium salt (0.5μM) with $ZnCl_2$ (10μM) for 16h, respectively. Cells were washed with PBS twice and metal-free ddH_2O (500μl/well) were added to each well. 6-well plates were kept in a humidified environment at 4℃ for 4 h, and subsequently lysis solution was collected into an Eppendorf tube and stored at -80℃. Samples were then thawed and subjected to 95℃ for 20 min. Protein concentrations were obtained using the BCA assay. Cells lysed in water were subjected to three freeze-thawing cycles and sonication for 20min before heating with 10% Suprapur® nitric acid (Merck Millipore, UK) to 95℃ for 2h. Subsequently, the lysis solution was cooled and diluted with metal-free ddH_2O to a final concentration of 0.5% nitric acid. The lysis solution was centrifuged to collect samples at the bottom of the tube and sent for ICP-MS analysis to obtain subcellular measurements of total zinc (Zn), iron (Fe), copper (Cu), manganese (Mn) and magnesium (Mg) in HCASMCs adapted to 18, 5 or 1kPa O_2 and reoxygenation.

2.17 Statistical analysis

All experimental data were analyzed using GraphPad Prism software version 8 (GraphPad Software, USA) and presented as mean ± S.E.M. All experiments were repeated in 3-6 independent HCASMCs cultures. Statistical analyses of multiple groups were evaluated using one-way ANOVA analyses. Statistical comparisons of multiple groups involving treatments, two-way ANOVA analyses of variances with Tukey or Bonferroni post-test were performed, with significant values of *P<0.05, **P<0.01, ***P<0.001 and ****P<0.0001.

Chapter 3 – Results

Redox phenotype of HCASMCs under 18, 5 and 1kPa O_2

Coronary arteries are responsible for suppling blood and O_2 to the myocardium (Goodwill et al., 2017) and involved in myocardial IR injury. Coronary artery SMCs, located in tunica media layer of vessel walls, exhibit contractile functions and maintain blood pressure and tissue perfusion (Owens et al., 2004) and play an important role in IR injury, which is associated with atherosclerotic plaque instability and rupture (Durham et al., 2018). Thus, in the present study primary HCASMCs were used to investigate Nrf2-regulated redox signalling pathways under normoxia and IR injury. This chapter describes the characterizations of HCASMCs adapted to 18, 5 and 1kPa O_2, including morphology, phenotype, proliferation and cytosolic O_2 levels. Moreover, basal ATP, GSH, catalase, CuZnSOD and MnSOD levels and Nrf2-targeted protein and mRNA expression were measured in HCASMCs adapted for 5d to 18, 5 and 1kPa O_2. Knock-down of Nrf2 transcriptional activity using siRNA was used to confirm the involvement of Nrf2.

3.1 Characterisation of HCASMCs under 18, 5 and 1kPa O_2

3.1.1 Morphology of HCASMCs under 18, 5 and 1kPa O_2

HCASMCs maintained under 18, 5 and 1kPa O_2 exhibited the typical morphology of smooth muscle cells, characterized by a ‘hill and valley’ appearance (see **Figure 3.1**). Experiments were carried out using HCASMCs cultures in passage 5-8. Vascular SMCs (VSMCs) can exhibit contractile and synthetic functions with two different phenotypes (contractile and synthetic phenotype) (Durham et al., 2018; Owens, 1995; Rensen et al., 2007). VSMCs in

blood vessel walls *in vivo* are normally in a quiescent contractile phenotype to maintain vascular tone via contraction under physiological conditions (Rensen et al., 2007). In various pathologies, VSMCs undergo a rapid and reversible change to a proliferative and synthetic phenotype characterised by increased proliferation and extracellular matrix (ECM) synthesis (Owens et al., 2004). **Figure 3.1** shows the morphology of around 80% confluent HCASMCs cultured for 5 days under 18, 5 and 1kPa O_2. Cells spread randomly on culture plates in a rhomboid-like proliferative and synthetic state.

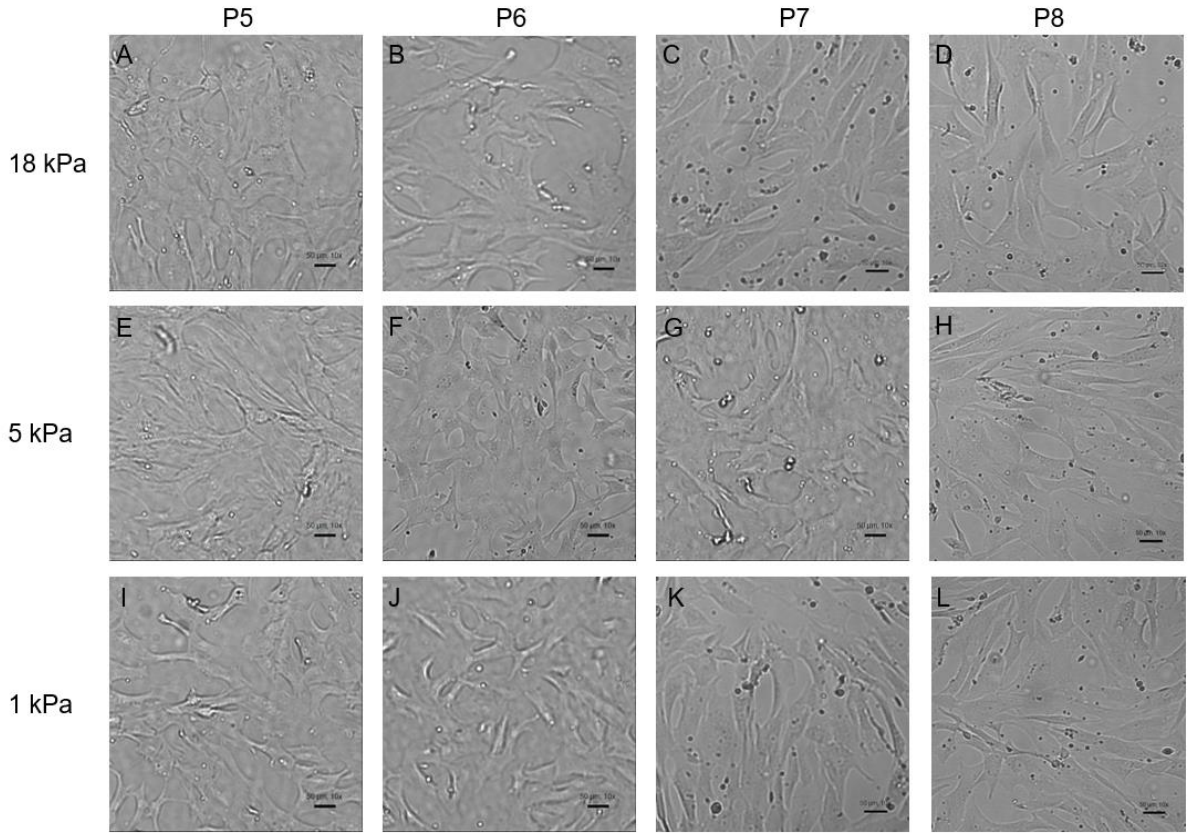

Figure 3.1 Phase images of HCASMCs cultures
(A)-(D) Representative images of passage HCASMCs cultured in smooth muscle cell basal medium 2 (SMC BM2) (PromoCell, C-22262), supplemented with supplement pack smooth muscle cell growth medium 2 (PromoCell, C-39262) under 18kPa. **(E)-(H)** Representative images of passage HCASMCs cultured in complete medium under 5kPa. **(I)-(L)** Representative images of passage HCASMCs cultured in complete medium under 1kPa. Images were taken at ×10 magnification using an Etaluma microscope (LS720 Microscopes, USA). Scale bar is 50µm.

3.1.2 Characterization of HCASMCs by immunostaining and immunoblotting

SMCs exist in a contractile or synthetic phenotype, and the degree of differentiation can be detected by the expression VSMCs specific markers. Markers of contractile phenotype are widely reported in the literature and are divided into early (SMαA, myocardin and SM22-α), mid-term (H-caldesmon and calponin-1) and late (SMMHC-1 and -2 and smoothelin) via their appearance during embryonic development or during differentiation of stem cells toward VSMCs (Babij et al., 1992b; Han et al., 2008; Rashidi et al., 2018; Rodriguez et al., 2006).

In the present study, SM22-α and calponin-1 expression was detected in HCASMCs cultured for 5d under 18, 5 or 1kPa O_2 by immunostaining and immunoblotting. Endothelial nitric oxide synthase (eNOS) expression was used as a negative control to confirm the absence of endothelial cells. Information for the antibodies used for immunostaining and immunoblotting are summarised in **Tables 2.1, 2.2 and 2.5.**

Figure 3.2A-C and **Figure 3.2E-G** show representative fluorescence images of SM22-α and Calponin-1 staining of HCASMCs under 18, 5 and 1kPa O_2, respectively. Protein expression of SM22-α and Calponin-1 was confirmed in HCASMCs cultured under 18, 5 and 1kPa by immunoblotting (**Figure 3.2D and H**). Expression of eNOS was not detected, indicating negligible endothelial contamination. Furthermore, expression of calponin-1 was significantly increased in HCASMCs under 5 kPa and 1 kPa O_2 compared to 18kPa O_2, whilst SM22-α protein expression was not altered significantly under different O_2 levels.

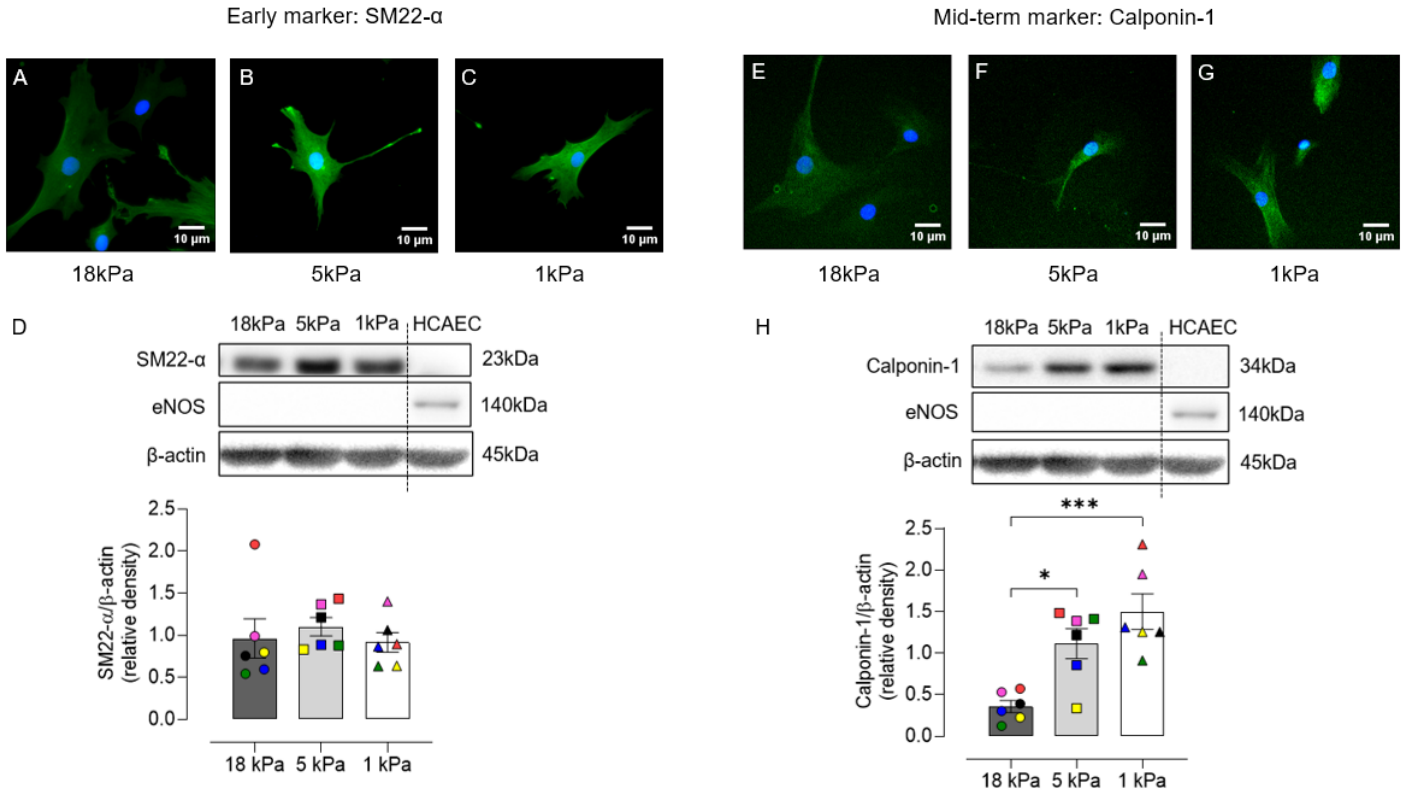

Figure 3.2 Characterization of HCASMCs by immunostaining and immunoblotting
(A)-(C) Representative fluorescence images of HCASMCs stained with SM22-α following culture for 5d under 18, 5 and 1kPa O_2, respectively. **(D)** SM22-α protein expression determined by immunoblotting, with densitometric analysis of SM22-α relative to β-actin. **(E)-(G)** Representative fluorescence images of HCASMCs stained with Calponin1 following culture under 18, 5 and 1kPa O_2, respectively. **(H)** Calponin-1 protein expression determined by immunoblotting with densitometric analysis of Calponin-1 relative to β-actin. Data denote mean ± SEM, n=6 independent HCASMCs cultures, *P<0.05, ***P < 0.001, One-way ANOVA with Tukey's multiple comparisons test. Images were taken at ×40 magnification using an Etaluma microscope (LS720 Microscopes, USA). Scale bar is 10µM. The 6 different HCASMCs cultures are colour-coded to highlight changes in SM22-α and Calponin1 expression in a given culture.
Abbreviation: SM22-α, smooth muscle protein 22-alpha.

3.1.3 Proliferation of HCASMCs

To compare the proliferation of HCASMCs cultured under 18, 5 and 1kPa O_2, cell number, protein content and doubling time were determined as described in **Section 2.4**. As shown in **Figure 3.3 and 3.4**, HCASMCs proliferated continuously over 5 days. Compared to cells cultured under 18 kPa O_2, the rate of proliferation was increased in cells cultured under 5 and 1kPa O_2 level. There are significant differences between cell number and cell protein in cells cultured for 4 and 5 days under 5 and 1kPa compared to cells adapted to 18kPa O_2. The doubling time is markedly lower in cells adapted to 5 and 1kPa O_2 compared to 18kPa O_2, consistent with results for cell number and protein content.

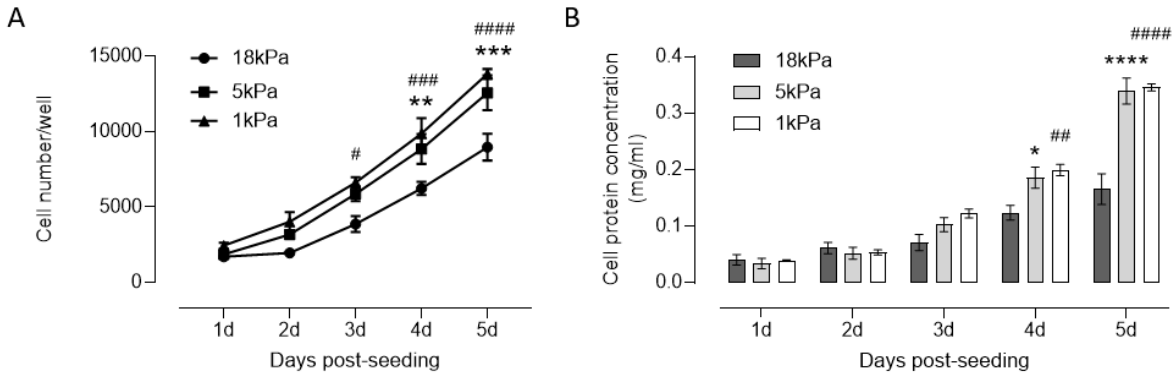

Figure 3.3 Proliferation of HCASMCs under 18, 5 and 1 kPa O_2
Cells were seeded at 3500 cells/well into 96-well plates and proliferation monitored continuously over 5 days. (**A**) Cell counting using a haemocytometer. (**B**) Protein content measured using a BCA assay. Data denote mean ± S.E.M., n=3-4 independent cultures, *P < 0.05, **P < 0.01, ***P < 0.001, ****P < 0.0001, 5kPa vs 18kPa group. $^{\#}$P < 0.05, $^{\#\#}$P < 0.01, $^{\#\#\#}$P < 0.001, $^{\#\#\#\#}$P < 0.0001, 1kPa vs 18kPa group. Two-way ANOVA with Tukey's multiple comparisons test.

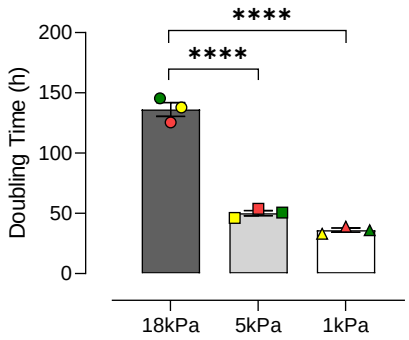

Figure 3.4 Doubling time of HCASMCs under 18, 5 and 1kPa O_2 level
Cells were pre-adapted for 5 days to either 18, 5 or 1kPa O_2 and then seeded at 7000 cells/well in a E-Plates® and proliferation monitored continously over 5 days in the iCelligence platform. One-way ANOVA with Tukey's multiple comparisons test. Data denote mean ± S.E.M., n=3 independent cultures, ****$P \leq 0.0001$. The 3 cultures are colour-coded to highlight changes in a given culture.

3.2 Real-time measurement of O_2 levels in HCASMCs cytosol and medium

Previous studies have reported the O_2 gradients between the intracellular and medium environment in HUVECs and mouse brain microvascular endothelial cells (bEnd.3), enabling the selection of O_2 levels *in vitro* to recapitulate values measured in *in vivo* (Chapple et al., 2016; Warpsinski et al., 2020). In the present study, real-time cytosolic O_2 levels were monitored in HCASMCs preloaded with the cell-penetrating phosphorescent nanoparticle probe MitoXpress®-INTRA (Chapple et al., 2016). When cells were adapted from 18kPa to 1kPa, phosphorescence lifetime in cells and medium was increased, as measured in real-time in an O_2-controlled CLARIOstar plate reader (**Figure 3.5A**). The relationship between ambient O_2 levels and phosphorescence lifetime is illustrated in **Figure 3.5B**. Cells adapted to 5kPa achieved an intracellular O_2 level of 3.98±0.11kPa (**Figure 3.5B**). Notably, the cytosolic O_2 level was slightly lower than dissolved O_2 in the medium above the cell monolayer.

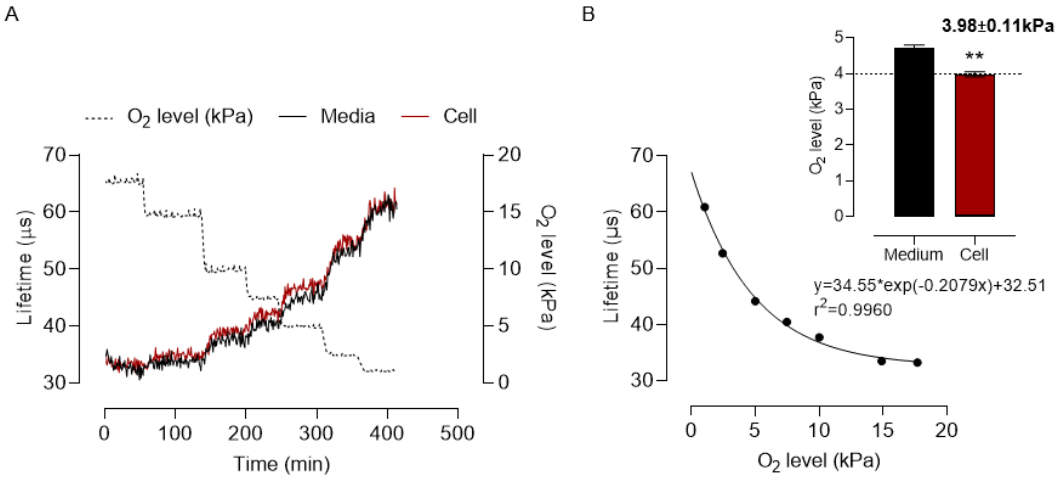

Figure 3.5 Cytosolic and medium O_2 level in HCASMCs under 5kPa O_2
Intracellular O_2 levels in HCASMCs were monitored using MitoXpress®-INTRA. **(A)** Representative traces show phosphorescence lifetime measurements in cells and medium. **(B)** Relationship between phosphorescence lifetime and O_2 level and intracellular O_2 level in HCASMCs. Interpolated O_2 content in HCASMCs cytosol and medium under 5 kPa O_2 (dashed line). Data denote mean ± S.E.M., n=3 independent cultures, Student's t-test, **P≤0.01.

3.3 Stabilization of HIF-1α in HCASMCs adapted to 1kPa O_2

Hypoxia-inducible factor-1 (HIF-1) is a transcription factor sensitive to hypoxia, and consists of two subunits, α (active oxygen-regulated subunit) and β (oxygen-independent subunit) (Bhattarai et al., 2018; Ratcliffe, 2007; Salceda and Caro, 1997; Semenza, 2001). Hypoxia decreases the hydroxylation of HIF-1α, resulting in limitation of proteolytic degradation (Jaakkola et al., 2001; Zimna and Kurpisz, 2015). Under physiological normoxia, HIF-1α is hydroxylated to suppress transcriptional activation (Semenza, 2014; Srinivas et al., 1999). In the present study, stabilization of HIF-1α was only observed in HCASMCs adapted to 1 kPa O_2 and cells adapted to 5kPa O_2 did not exhibit a hypoxic phenotype (**Figure 3.6**).

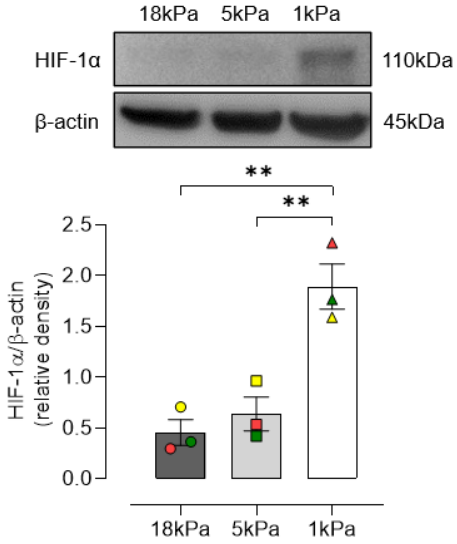

Figure 3.6 Effect of different ambient O_2 levels on HIF-1α expression in HCASMCs
HIF-1α protein expression was determined by immunoblotting with densitometric analysis of HIF-1α relative to β-actin. Data denote mean ± S.E.M., n=3 independent cultures, *P<0.05, One-way ANOVA with Tukey's multiple comparisons test. The 3 cultures are colour-coded to highlight changes in a given culture.
Abbreviation: HIF-1α, hypoxia-inducible factor-1.

3.4 Basal ATP levels in HCASMCs cultured under 18, 5 and 1kPa O_2

To determine how hyperoxia, normoxia and hypoxia regulate cellular ATP utilization, basal ATP levels were examined in HCASMCs adapted for 5d to 18, 5 and 1kPa O_2. Intracellular ATP levels had negligible effect by pericellular O_2 level in HCASMCs, Several studies have described these cardiomyocytes exposed to prolonged hypoxia (1min to 16h) exhibit a reversible inhibition of ATP demand, ATP consumption and O_2 uptake, reflecting a self-protection response associated with a reversible suppression of cytochrome-*c* oxidase (Budinger et al., 1996; Budinger et al., 1998).

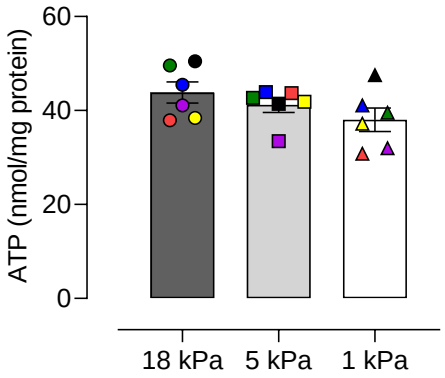

Figure 3.7 Intracellular ATP levels in HCASMCs cultured under 18, 5 and 1kPa O_2
Basal intracellular ATP levels in HCASMCs adapted to 18, 5 and 1kPa O_2 for 5d and expressed as nmol/mg protein. Data denote mean ± S.E.M., n=6 independent cultures, One-way ANOVA with Tukey's multiple comparisons test. The 6 cultures are colour-coded to highlight changes in a given culture.
Abbreviation: ATP, adenosine 5′-triphosphate.

3.5 Effects of different ambient O_2 levels on intracellular GSH and antioxidant enzyme levels in HCASMCs

The basal redox status of HCASMCs cultured under 18, 5 and 1kPa O_2 for at least 5 days was assessed prior to further experimentation. Basal intracellular glutathione (GSH) levels in HCASMCs were not altered when cells were cultured under 18 and 5 kPa O_2 (13.76 ±0.58 versus 13.77 ±0.47 nmol/mg protein respectively), consistent with our previous findings in HUVECs (Chapple et al., 2016). However, intracellular GSH levels were significantly lower in HCASMCs adapted to 1kPa O_2, namely 11.41 ±0.58 nmol/mg protein (**Figure 3.8**).

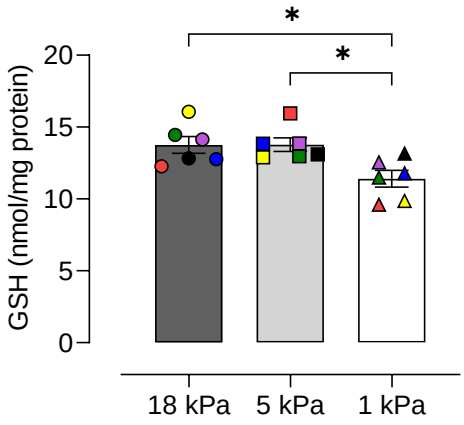

Figure 3.8 Intracellular GSH levels in HCASMCs cultured under 18, 5 and 1kPa O_2
Basal intracellular total GSH levels in HCASMCs adapted to 18, 5 and 1kPa O_2 for 5d and expressed as nmol/mg protein. Data derived from same cultures for ATP determinations in Fig.3.7 and denote mean ± S.E.M., n=6 independent cultures, *P ≤ 0.05, One-way ANOVA with Tukey's multiple comparisons test. The 6 cultures are colour-coded to highlight changes in a given culture.
Abbreviation: GSH, glutathione.

Although long-term adaptation of HCASMCs to 18kPa O_2 had no effect on protein expression of catalase (CAT) compared to cells under 5kPa O_2, CAT expression trended to be lower under 1kPa O_2. Protein expression of CuZnSOD and MnSOD decreased as ambient O_2 levels decreased from 18 to 1kPa O_2, with a significant difference measured between cells cultured under 18kPa and 1kPa O_2 (**Figure 3.9**), consistent with other studies in human fibroblasts adapted to 1kPa for 72h (Sgarbi et al., 2017).

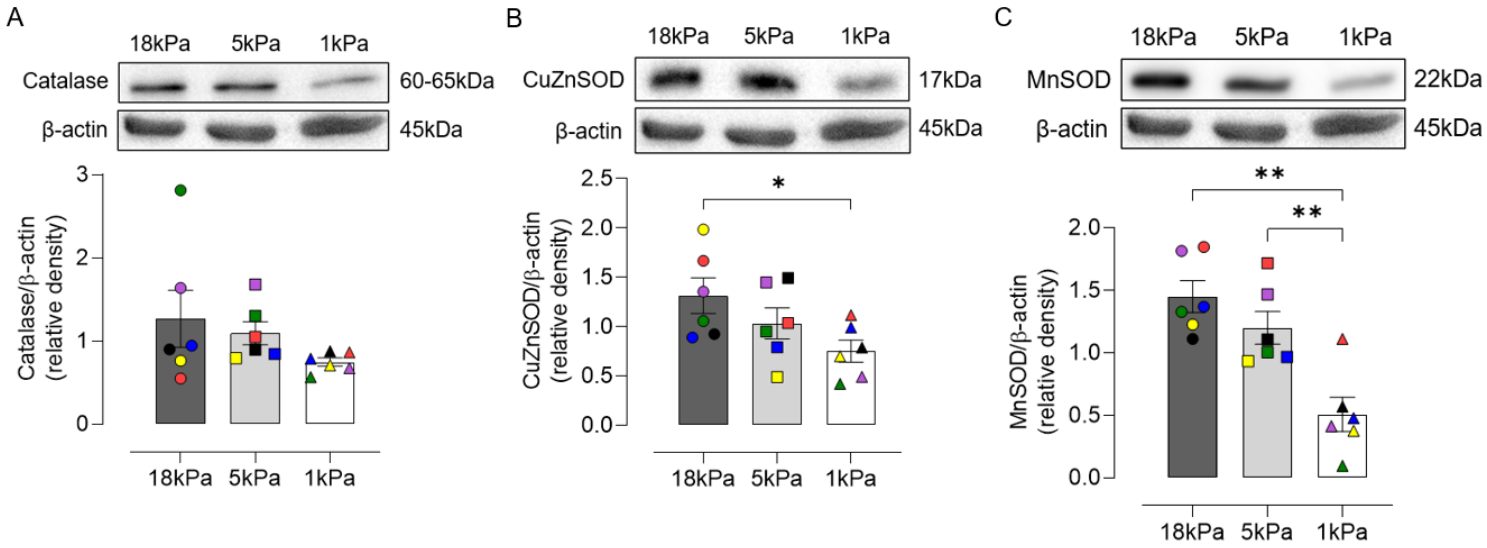

Figure 3.9 Effects of different ambient O_2 levels on CAT, CuZnSOD and MnSOD expression in HCASMCs
Basal protein expression of catalase, CuZnSOD and MnSOD in HCASMCs adapted to 18, 5 and 1kPa O_2 were determined by immunoblotting, with densitometric analysis of catalase, CuZnSOD and MnSOD expressed relative to β-actin. Data denote mean ± S.E.M., n=6 independent cultures, *P < 0.05, **P < 0.01, ***P < 0.001, One-way ANOVA with Tukey's multiple comparisons test. The 6 cultures are colour-coded to highlight changes in a given culture.
Abbreviations: CAT, catalase; CuZnSOD, SOD1, superoxide dismutase [Cu-Zn]; MnSOD, SOD2, superoxide dismutase [Mn].

3.6 Sulforaphane induces Nrf2 nuclear translocation

Activation of Nrf2 by sulforaphane (SFN), a classic activator known to modify Cys151 on Keap1 (Baird and Yamamoto, 2020; Robledinos-Anton et al., 2019), was assessed by immunostaining and quantifying Nrf2 nuclear: cytoplasmic ratios. As shown in **Figure 3.10**, SFN (2.5µM) significantly induced Nrf2 nuclear accumulation in HCASMCs under 18, 5 and 1kPa O_2.

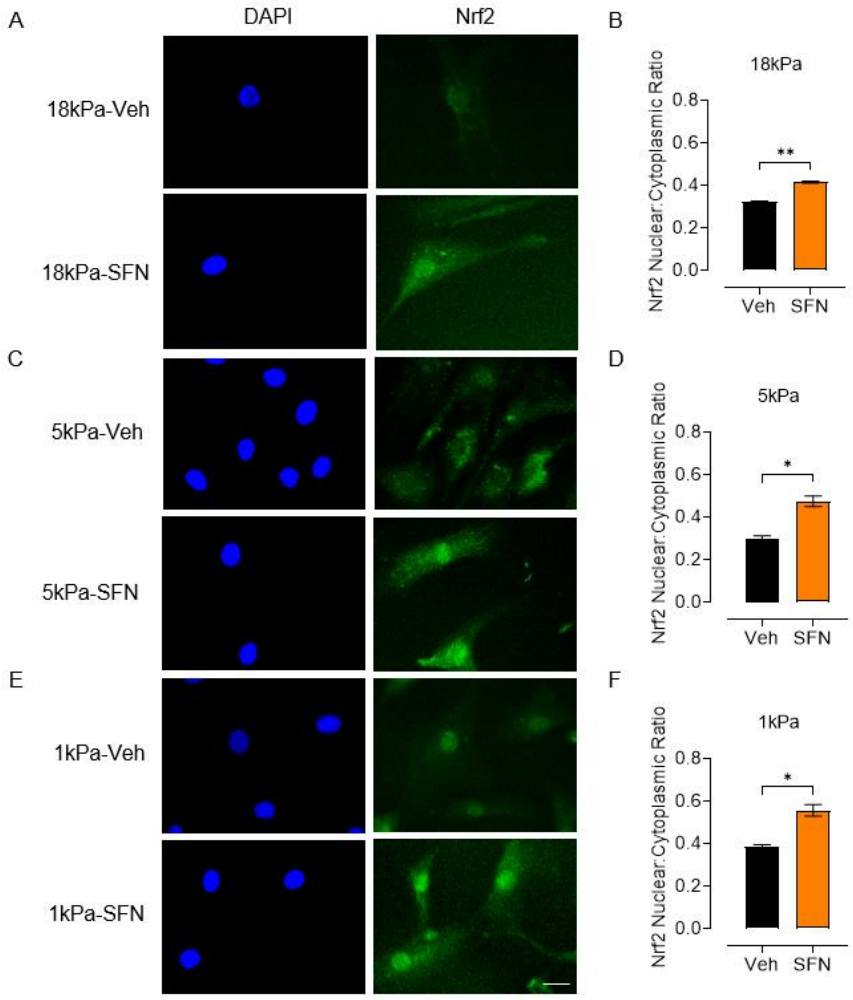

Figure 3.10 Sulforaphane induced Nrf2 nuclear translocation in HCASMCs under 18, 5 and 1kPa O_2
(A, C, E) Representative Nrf2 positive immunofluorescence images of HCASMCs and nucleus stained with DAPI following pre-treatment of cells with Vehicle (Veh, 0.005% DMSO, 16h) or SFN (2.5µM, 16h). **(B, D, F)** Quantification of Nrf2 nuclear: cytoplasmic ratio in HCASMCs treated with Veh or SFN under 18, 5 and 1kPa O_2, respectively. Data denote mean ± S.E.M., n = 3 independent cultures, *P<0.05, **P<0.01, Two-way ANOVA with Tukey's multiple comparisons test. Images were taken at ×40 magnification using an Etaluma microscope (LS720 Microscopes, USA). Scale bar: 20µM.
Abbreviations: SFN, sulforaphane; Nrf2, nuclear factor erythroid 2- related factor 2.

3.7 Nrf2-regulated target protein and mRNA expression under 18, 5 and 1kPa O_2

To determine whether long-term adaptation to different O_2 levels affects Nrf2 signalling, the effects of hyperoxia (18kPa), normoxia (5kPa) and hypoxia (1kPa) on Nrf2-regulated target protein and mRNA expression were examined.

Previous studies in our group have shown that SFN (2.5 μM) upregulates Nrf2 target proteins over 8-24h (Warpsinski et al., 2020). The present study examined the effects of SFN (2.5μM) on protein (16h) and mRNA (6h) expression of key Nrf2 downstream targets GCLM, HO-1 and NQO1 (**Figure 3.11 and 3.12**). Basal GCLC and GCLM protein expression had negligible change in HCASMCs cultured for 5d under 18 or 5kPa O_2, with a trend for lower expression under 1kPa O_2 (**Figure 3.11A and B**). These findings are consistent with GSH results, as GCL catalyzes the first and rate-limiting step in GSH production (Forman et al., 2009). Meanwhile, Basal mRNA expression of GCLC and GCLM had no significant change in cells treated with vehicle (0.005% DMSO, 6h) (**Figure 3.12A and B)**.

In contrast to our previous studies in human venous umbilical and brain microvascular endothelial cells (Chapple et al., 2016; Warpsinski et al., 2020), SFN induced activation of Nrf2-HO-1 signalling was not significantly attenuated in cells under 5kPa O_2 with the consistent results of HO-1 mRNA expression (**Figure 3.11C and 3.12C**). There was negligible difference of HO-1 protein and mRNA expression in cells after pre-treated with SFN across the different O_2 level. Meanwhile, the NQO1 protein decreased as ambient O_2 levels from 18 to 1kPa O_2 (**Figure 3.11D and 3.12D**).

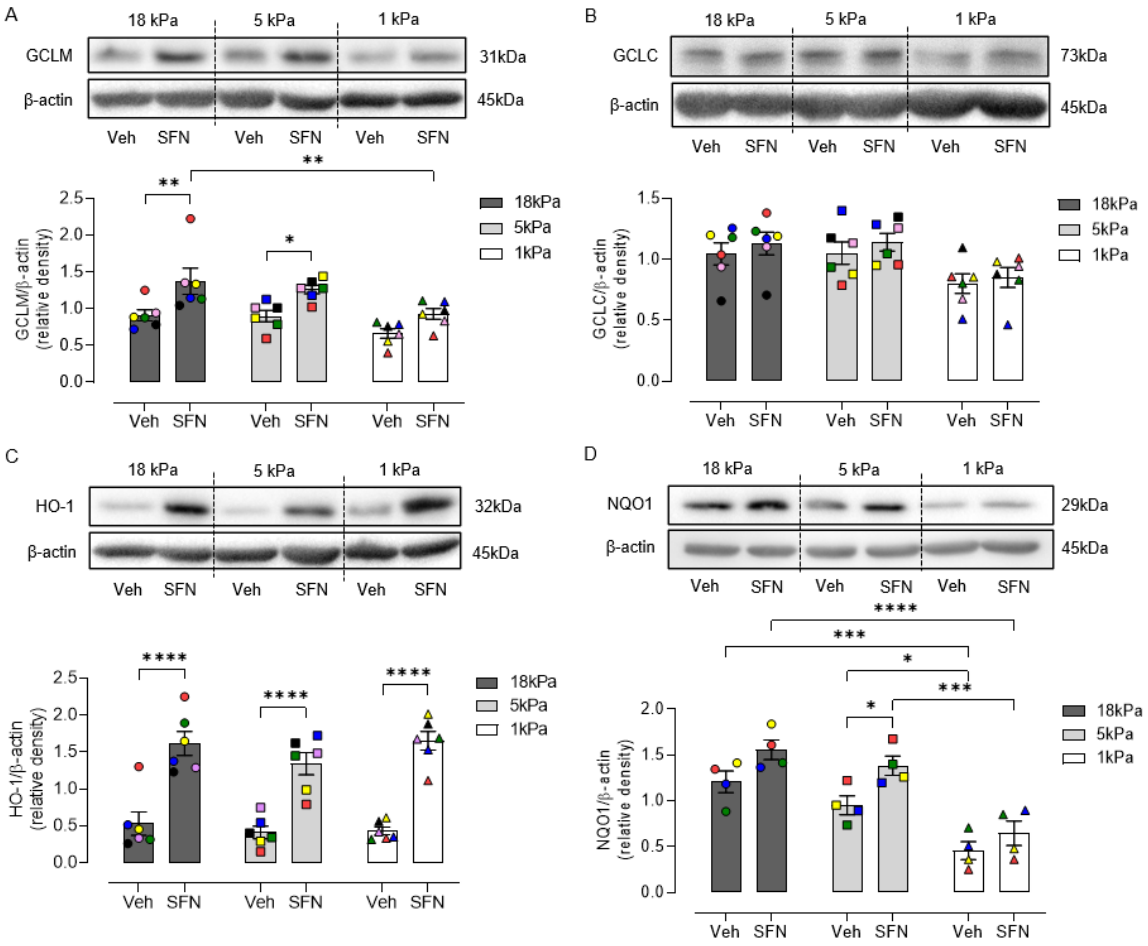

Figure 3.11 Nrf2-regulated target protein expression in HCASMCs under 18, 5 and 1kPa O_2
Representative GCLM (A), GCLC (B), HO-1 (C) and NQO1 (D) immunoblots of HCASMCs treated with Veh (0.005% DMSO, 16h) or SFN (2.5µM, 16h) after adaptation to 18kPa, 5kPa and 1kPa O_2 for 5d. Densitometric analyses of GCLM, GCLC, HO-1 or NQO1 protein expression relative to β-actin. Data denote mean ± S.E.M., n=4-6 independent cultures, *P<0.05, **P<0.01, ***P<0.001, ****P<0.0001, Two-way ANOVA with Tukey's multiple comparisons test. The 4-6 cultures are colour-coded to highlight changes within a given culture.
Abbreviations: SFN, sulforaphane; GCLM, glutamate-cysteine ligase modifier subunit; GCLC, glutamate-cysteine ligase catalytic subunit; HO-1, heme oxygenase-1; NQO1, NAD(P)H quinone dehydrogenase 1.

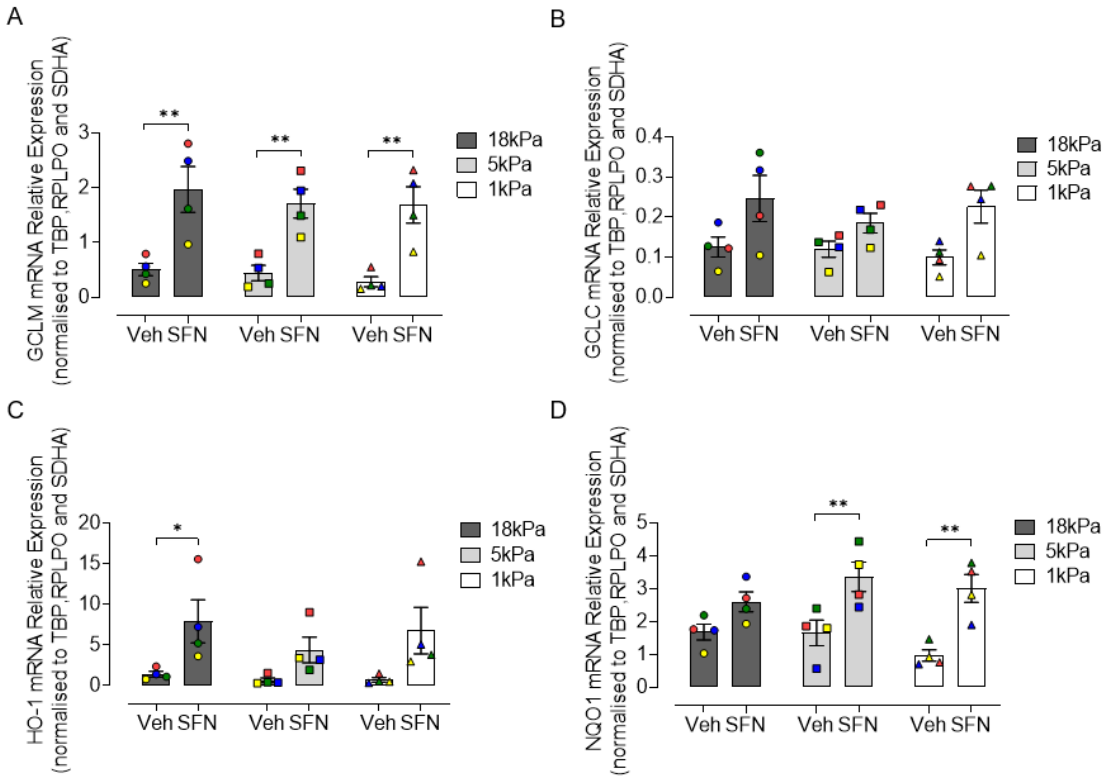

Figure 3.12 Nrf2-regulated target mRNA expression in HCASMCs under 18, 5 and 1kPa O_2
mRNA expression of GCLM (A), GCLC (B), HO-1 (C) or NQO1 (D) in HCASMCs treated with Veh (0.005% DMSO, 6h) or SFN (2.5µM, 6h) after adapted to 18kPa, 5kPa and 1kPa O_2 level for 5d. Data were normalized to three housekeeping genes (TBP, RPLPO and SDHA). Data denote mean ± S.E.M., n=4 independent cultures, *P<0.05, **P<0.01, Two-way ANOVA with Tukey's multiple comparisons test. The 4 cultures are colour-coded to highlight changes within a given culture.
Abbreviations: SFN, sulforaphane; GCLM, glutamate-cysteine ligase modifier subunit; GCLC, glutamate-cysteine ligase catalytic subunit; HO-1, heme oxygenase-1; NQO1, NAD(P)H Quinone Dehydrogenase 1; TBP, TATA box binding protein; RPLPO, ribosomal protein lateral stalk subunit P0; SDHA, succinate dehydrogenase complex, subunit A.

Notably, BTB and CNC homology 1 (Bach1), a negative regulator of NQO1 and HO-1 expression was shown to be downregulated in HUVECs adapted to 18kPa for 5d compared to 5kPa O_2 (Chapple et al., 2016; Kimura et al., 2007). Prolonged hypoxia upregulates Bach1 expression in HUVECs and other cell types compared to 18kPa O_2 (Kitamuro et al., 2003). In the present study, protein and mRNA expression of Bach1 were reduced in cells under 18kPa O_2 compared to 5 and 1kPa O_2 (**Figure 3.13**). Notably, knockdown of Bach1 did not increase GCLM expression in HUVECs adapted to 5 kPa O_2, indicating that the expression of GSH-related genes under physiological O_2 may be independent of Bach1 (Chapple et al., 2016). Moreover, SFN treatment significantly upregulated Bach1 protein expression in cells under 18 and 1kPa O_2(**Figure 3.13A**).

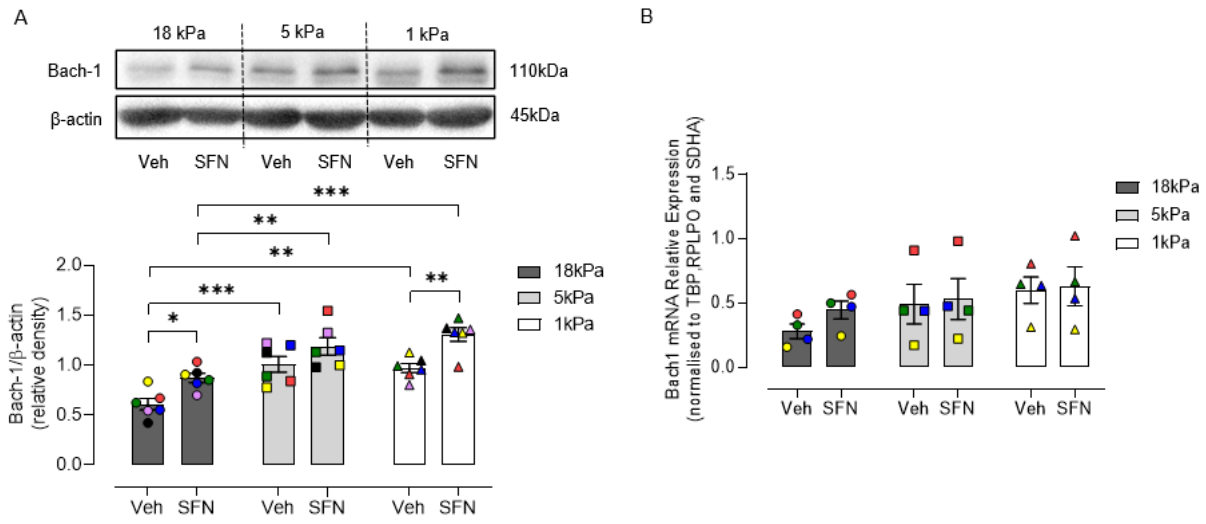

Figure 3.13 Protein and mRNA expression of Bach1 in HCASMCs under 18, 5 and 1kPa O_2
(A) Representative Bach1 immunoblots of HCASMCs treated with Vehicle (Veh, 0.005% DMSO, 16h) or SFN (2.5μM, 16h) after adapted to 18kPa, 5kPa and 1kPa O_2 level for 5d. Densitometric analyses of Bach1 protein expression relative to β-actin. Data denote mean ± S.E.M., n=6 independent cultures. Whole-cell lysates are the same as those analysed in Fig. 3.12. (B) mRNA expression of Bach1 in HCASMCs treated with Vehicle (Veh, 0.005% DMSO, 6h) or SFN (2.5μM, 6h) after adaptation to 18kPa, 5kPa and 1kPa O_2 level for 5d. Data were normalized to three housekeeping genes (TBP, RPLPO and SDHA). Data denote mean ± S.E.M., n=4 independent cultures, *P<0.05, **P<0.01, ***P<0.0001, Two-way ANOVA with Tukey's multiple comparisons test. The 4-6 cultures are colour-coded to highlight changes within a given culture.
Abbreviation: SFN, sulforaphane,; Bach1, BTB and CNC homology 1; TBP, TATA box binding protein; RPLPO, ribosomal protein lateral stalk subunit P0; SDHA, succinate dehydrogenase complex, subunit A.

3.8 Effects of silencing Nrf2 on antioxidant protein expression

To confirm that HO-1 and NQO1 protein expression are regulated by Nrf2, HCASMCs were cultured with scrambled (control) or Nrf2 siRNA to knockdown transcriptional activity before treatment with SFN or vehicle. As shown in **Figure 3.14**, compared to scrambled siRNA transfection, 2.5nM Nrf2 siRNA obviously knock-down Nrf2-targeted HO-1 protein expression, which is the transfection concentration used in subsequent experiments. Notably,Nrf2 gene silencing had negligible effects on basal HO-1 or NQO1 protein levels but significantly abrogated SFN-induced upregulation of HO-1 and NQO1 (**Figure 3.15**) protein expression, confirming that activation of Nrf2 is involved in SFN-induced upregulation of HO-1 and NOQ1 expression in HCASMCs. These additional experiments further support the upregulation of HO-1 and NQO1 showed in **Figure. 3.12**.

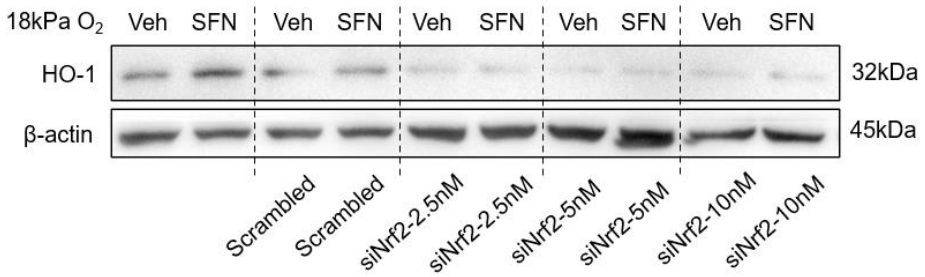

Figure 3.14 Preliminary experiment with scrambled (control) or Nrf2 siRNA to knockdown Nrf2 transcriptional activity
HO-1 immunoblots of HCASMCs transfected with different concentrations of scrambled or Nrf2 siRNA for 24h before treatment with SFN (2.5μM) or vehicle (0.005% DMSO) for 16h after 5d adaptation to 18kPa O_2. The preliminary experiment shows one cell culture result.
Abbreviations: Veh, vehicle; SFN, sulforaphane; HO-1, heme oxygenase-1.

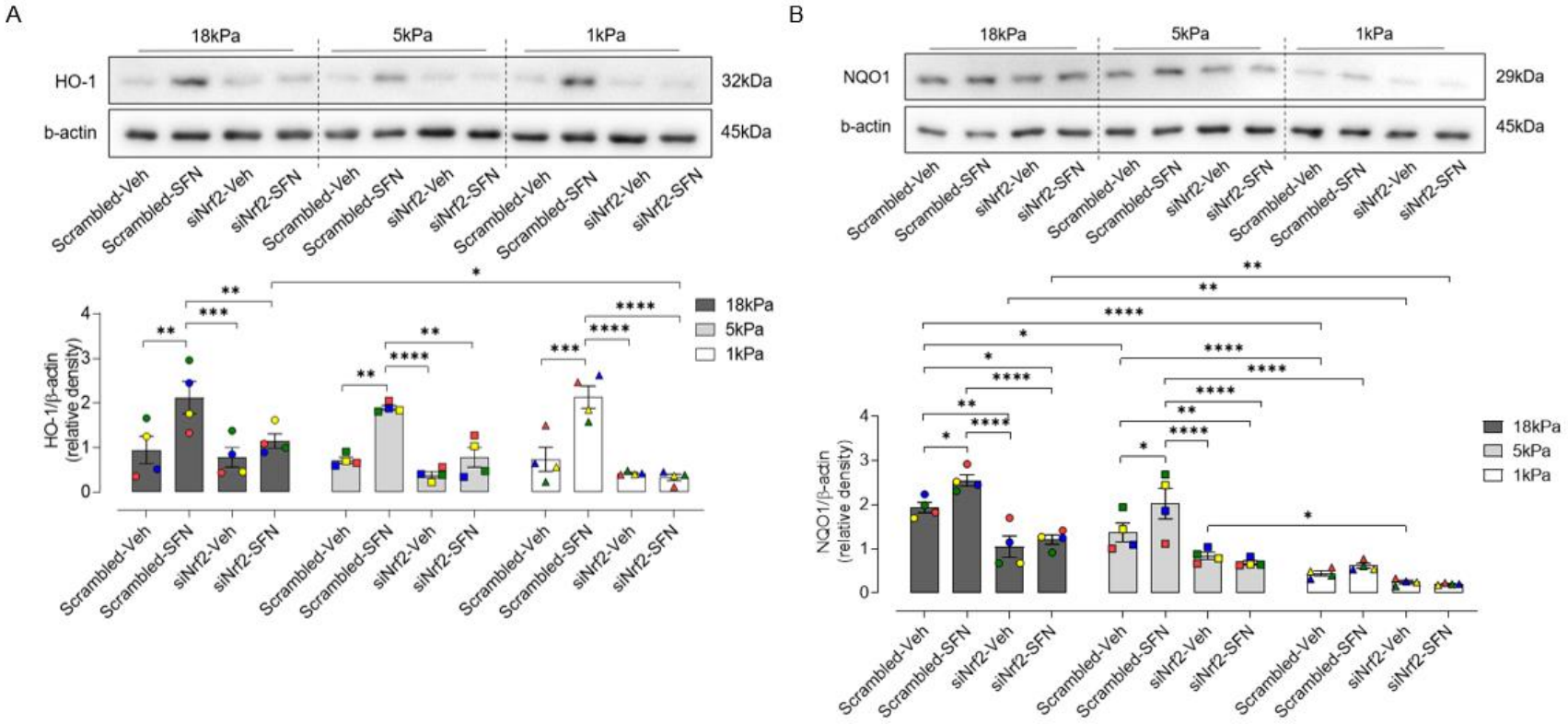

Figure 3.15 Nrf2 silencing downregulates SFN-induced HO-1 and NQO1 protein expression

Representative HO-1 (A) and NQO1 (B) immunoblots of HCASMCs transfected with scrambled or Nrf2 siRNA for 24h before treatment with SFN (2.5μM) or vehicle (0.005% DMSO) for 16h after 5d adaptation to 18kPa, 5kPa and 1kPa O_2 level. Densitometric analyses of protein expression relative to β-actin. Data denote mean ± S.E.M., n=4 independent cultures, *P<0.05, **P<0.01, ***P<0.001, ****P<0.0001, Two-way ANOVA with Tukey's multiple comparisons test. The 4 cultures are colour-coded to highlight changes within a given culture.

Abbreviations: Veh, vehicle; SFN, sulforaphane; HO-1, heme oxygenase-1; NQO1, NAD(P)H quinone dehydrogenase 1

Chapter 3 – Discussion

In this chapter the phenotype of HCASMCs in culture was characterised, including cell morphology, contractile markers, proliferation rates and cytosolic O_2 levels under hyperoxia, physiological normoxia and hypoxia. Importantly, lack of eNOS expression (used as a negative control) confirmed the absence of endothelial cell contamination (**Figure 3.2D** and **H**). Cells exhibited a similar morphology under the light microscope after 5d culture under 18, 5 and 1kPa O_2. Although expression of contractile markers SM22-α was affected negligibly during long-term culture under 18, 5 and 1kPa O_2, Calponin1 levels were elevated significantly under 5 and 1 kPa O_2. As shown in **Figure 3.1,** HCASMCs exhibited a classic 'hills and valleys' shape under 18, 5 and 1kPa O_2, which is a typical of a synthetic phenotype (Proudfoot and Shanahan, 2012). The majority of cells had a spindle elongated shape at confluence but as previously reported, cells develop into spherical multicellular nodules if allowed to become over-confluent, as encountered in studies of vascular apoptosis and calcification (Bennett et al., 1997).

In mature and healthy vessels, vascular smooth muscle cells (VSMCs) exhibit a differentiated and contractile phenotype, a low rate of proliferation and expression of unique contractile proteins to maintain the integrity of the vessel wall and regulation of contraction and relaxation (Owens, 1995). Meanwhile, VSMCs within injured vessels or in culture *in vitro* exhibit a dedifferentiated and synthetic phenotype, retaining remarkable plasticity, capable of proliferation and synthesis of the extracellular matrix components (Owens et al., 2004). The degree of VSMCs differentiation can be determined by the expression level of contractile (e.g. calponin-1 and SM22-α) or synthetic (e.g. CRBP-1 and Smemb) markers (Rensen et al., 2007). According to their appearance during embryonic development or during

differentiation of stem cells towards VSMCs, contractile markers include early (SMαA, myocardin and SM22-α), mid-term (H-caldesmon and calponin-1) and late (SMMHC-1 and -2 and smoothelin) markers (Babij et al., 1992b; Dong et al., 2012).

In this present study, expression of an early marker, SM22-α (an actin-binding protein of the calponin family), and a mid-term marker, calponin-1 (an actin filament- associated regulatory protein) was monitored as an index of changes in HCASMCs phenotype. As shown in **Figure 3.2**, expression of calponin-1 was significantly increased in HCASMCs under 5 kPa compared to 18kPa O_2 with SM22-α protein expression affected negligibly by changes in O_2 within the workstation. These results suggest that 5kPa O_2 more accurately replicate physiological normoxia *in vitro*, as discussed by Badran and Eid. in their review (Badran et al., 2020). Notably, reactive oxygen species (ROS) are main contributors to modulation of VSMCs phenotype (see **Figure 3.16**) (Badran et al., 2020; Clempus and Griendling, 2006). Basal and physiological ROS levels influence the transition of quiescent VSMCs into a contractile phenotype (Su et al., 2001). In contrast, excessive ROS generation induce a synthetic phenotype associated with disease and pathologies model such as atherosclerosis and diabetes (Byon et al., 2008; Carrillo-Sepulveda and Matsumoto, 2014). Thus, the recapitulating physiological normoxia *in vitro* cell culture models is of particular importance for generation of ROS and modulation of VSMCs phenotype.

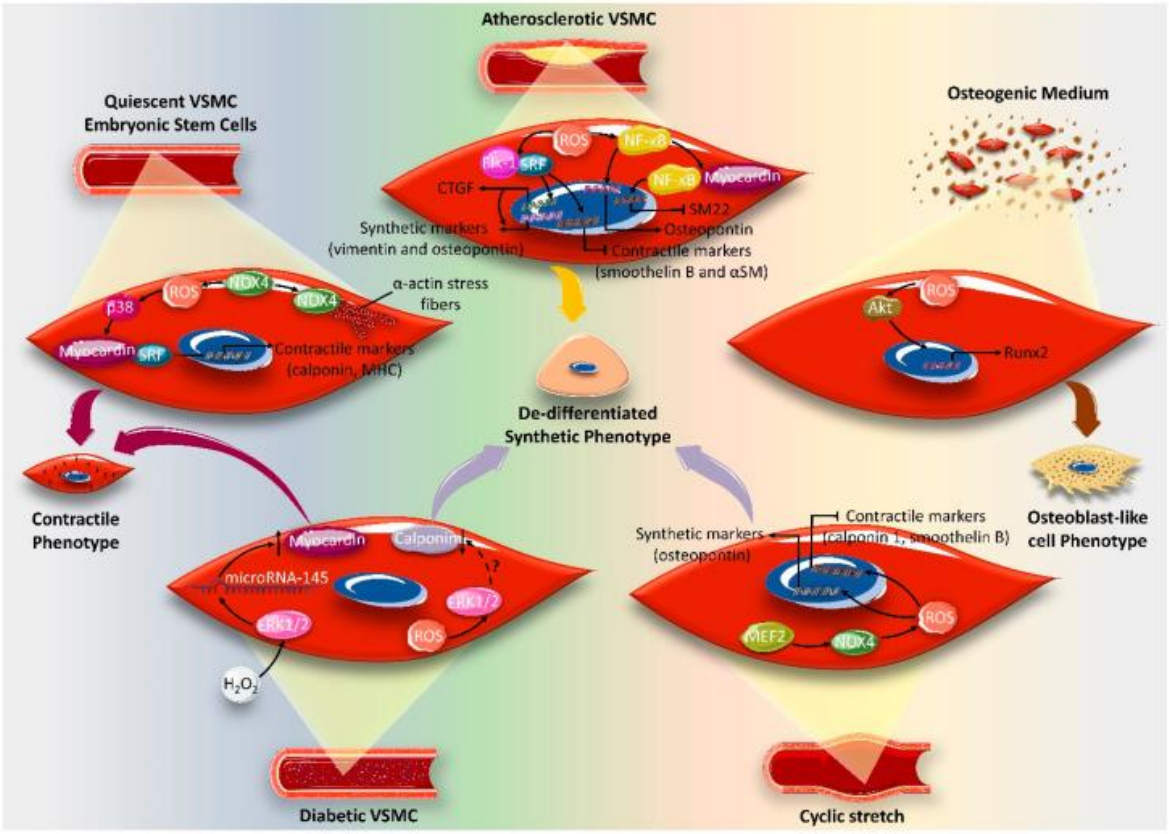

Figure 3.16 The effect of reactive oxygen species on modulation of vascular smooth muscle cell phenotypes
Basal ROS levels induce the switch of quiescent VSMCs or embryonic stem cells to a contractile phenotype, with an upregulation of contractile markers (e.g. calponin1 and SMMHC) expression. However, dysregulated ROS generation in atherosclerotic, diabetic or cyclic stretch VSMCs induces the switch to a dedifferentiated synthetic phenotype, with loss of contractile markers (e.g. calponin1, SM22-α and smoothelin). Taken from Badran and Eid review (Badran et al., 2020).
Abbreviations: ROS, reactive oxygen species; SM22-α, smooth muscle protein 22-alpha; MHC, SMMHC, smooth muscle myosin heavy chain; H_2O_2, hydrogen peroxide; Akt, protein kinase B; ERK1/2, extracellular signal-regulated protein kinase 1/2; NOX4, NADPH oxidase 4; CTGF, connective tissue growth factor; SFR, serum response factor; NF-κB, nuclear factor kappa B; Runx2, runt-related transcription factor 2.

Notably, in present study, expression of calponin-1, a key marker of smooth muscle contractile phenotype, was increased in HCASMCs under 1kPa O_2 (**Figure 3.2**) and associated with increased HIF-1α protein levels (**Figure 3.6**). Previous studies have reported that hypoxia promotes differentiation of epicardial cells into VSMCs and silencing HIF-1α decreases the expression of contractile markers (e.g. SMαA and SM22-α) (Tao et al., 2018; Wiafe et al., 2017). As forementioned, HIF-1α is hydroxylated and degraded under normoxic conditions, whilst it is stablised under hypoxia (Salceda and Caro, 1997; Semenza, 2014). Previous studies with human umbilical vein endothelial cells (HUVECs) established that at

least 5d culture under 5 kPa O_2 is required to achieve a physiological oxygen phenotype in the absence of HIF-1α protein stabilisation (Keeley et al., 2017). In my study, stabilisation of HIF-1α was only observed in HCASMCs under 1 kPa O_2, whilst cells under 5kPa O_2 did not exhibit a hypoxic phenotype (**Figure 3.6**), consistent with increased calponin-1 protein expression in cells under 1kPa O_2 (**Figure 3.2**). Moreover, Veber et al. have been reported that factors driving the expression of the myogenic transcription factor myocardin, such as type IV collagen culture, low serum culture, hypoxia, or TGF-β1 treatment, contribute the modulation of VSMCs contractile phenotype (Veber et al., 2018).

To further characterize HCASMCs during long-term (5d) culture under hyperoxia, normoxia and hypoxia, proliferation rates were measured using three different methods, including continuously counting cells using a haemocytometer, measuring protein content using a BCA assay and calculating doubling time using an iCELLigence^{TM} platform (**Figure 3.3 and 3.4**). HCASMCs exposed to hyperoxia (18kPa) exhibited significantly slower growth compared to those under normoxia (5kPa) and hypoxia (1kPa), contrary to findings reported in mouse brain microvascular endothelial (bEnd.3) cells (Warpsinski et al., 2020). Moreover, rates of proliferation were higher in HCASMCs cultured under 5 and 1kPa O_2 compared to 18 kPa O_2. The evidence for a correlation between hypoxia and VSMCs proliferation was first demonstrated in pulmonary hypertension, which is often triggered by chronic hypoxia (Meyrick and Reid, 1978; Wohrley et al., 1995). Acute hypoxia-promoted VSMCs proliferation and death are associated with mitochondria ROS generation and activation of HIF-1α, leading to a decrease of G0/G1 phase and an increase of G2/M and S phase of the cell cycle, which may contribute to vascular remodeling (Bhansali et al., 2021; Griendling and Ushio-Fukai, 1998; Meng and Yu, 2011; Ray et al., 2008). Moreover, Cooper and Beasley have reported that proliferation of human pulmonary artery, aortic, and saphenous

vein smooth muscle cells is increased during culture under 5kPa O_2 compared to room air, and increased proliferation of human VSMCs under 1kPa O_2 is associated with IL-1α production (Cooper and Beasley, 1999).

In addition, the present study provided the first measurements of O_2 content in the cytosol and medium during culture of HCASMCs *in vitro*. Cells exposed to 5kPa achieved an intracellular O_2 level of 3.98 ± 0.11kPa (**Figure 3.5**). Notably, the cytosolic O_2 level was lower than dissolved O_2 in the medium above the cell monolayer, consistent with our previous studies in HUVECs and bEnd.3 cells (Chapple et al., 2016; Warpsinski et al., 2020).

There is a pressing need to re-define concept of physiological normoxia in cell culture *in vitro* to recapitulate the O_2 level of organs, tissues and cells *in vivo*. Notably, O_2 levels vary throughout the body as a consequence of differences in cell metabolism and O_2 consumption and diffusion limitation (Keeley and Mann, 2019). As pericellular O_2 levels will influence the cellular redox status, it is important to investigate the redox status of cells *in vitro* under physiological normoxia (O_2 levels of tissues/cells *in vivo*). In this context, the majority of studies have investigated redox signalling in cells in standard cell culture incubators gassed with 5% CO_2 and room air (18 kPa O_2) known to induce oxidative stress (Keeley and Mann, 2019; Sies et al., 2022).

In this study, the redox phenotype of HCASMCs during long-term culture under hyperoxia (18kPa), normoxia (5kPa) and hypoxia (1kPa) was characterised by measuring GSH levels, antioxidant enzymes and Nrf2-regulated redox signalling pathway. Firstly, the effects of different O_2 on HCASMCs viability was measured by assaying intracellular ATP levels. ATP levels had negligible change in HCASMCs adapted to 18, 5 or 1kPa O_2 for 5d. Previous

findings have reported in HCASMCs and cardiomyocytes that ATP:ADP ratio was significantly reduced by exposure to hypoxia due to opening ATP-sensitive potassium channels (Yang et al., 2020). Moreover, hypoxia diminishes ATP production due to lower activity of the electron transport chain and slows oxygen consumption to prevent anoxia (Wheaton and Chandel, 2011). Adaptation of cells to 18 kPa O_2 did not affect cell viability compared to 5kPa O_2, as evidenced by negligible changes in intracellular ATP levels (5kPa O_2: 41.18 ± 1.59 vs 18 kPa O_2: 43.82 ± 2.25 nmol/mg protein) (**Figure 3.7**). Previous studies have reported intracellular GSH increase in cells acutely exposed to hypoxia or hyperoxia, which is associated with oxidative stress (Bogdanova et al., 2010; Lin and Miller, 1992), whilst HCASMCs cultured long-term under hypoxia, normoxia and hyperoxia in present study exhibited a different pattern. Adaptation of cells to 18 kPa O_2 did not alter basal intracellular GSH levels compared to these under 5kPa O_2 (5kPa O_2: 13.77 ± 0.47 vs 18 kPa O_2: 13.76 ± 0.58 nmol/mg protein), consistent with similar range of values in other VSMCs types (see **Table 3.1)**. However, intracellular GSH levels (11.41 ± 0.58 nmol/mg protein) were significantly lower in HCASMCs adapted to 1kPa O_2 (**Figure 3.8**), consistent with previous findings that GSH levels are lower in hepatocarcinoma cell lines cultured at lower pO_2 for 6-30d (Trepiana et al., 2017). Limited O_2 may impair de novo glutamine synthesis and activity of γ-glutamyl cycle, leading to a reduction of GSH (Rajpurohit et al., 1996).

Table 3.1 Studies of intracellular GSH levels in vascular smooth muscle cells

Species	SMC cell type	Intracellular GSH+GSSG levels (nmol/mg protein)	Measurement method	Reference
Human	coronary artery	~13.76	Fluorometric assay (OPA as a florescent reagent)	Present study
Human	umbilical artery	~11	High-performance liquid chromatography (HPLC) and total GSH levels by spectrophotometry	(Siow et al., 1998)
Human	umbilical artery	~7.5	Fluorometric assay (OPA as a florescent reagent)	(Ruiz et al., 2003)
Human	aorta	~33	Fluorometric assay (OPA as a florescent reagent)	(Anwar et al., 2005)
Human	aorta	~57	Fluorometric assay (OPA as a florescent reagent)	(Zhu et al., 2007)
Human	aorta	22.7	Enzymatic method, which is based on the catalytic action of glutathione in the reduction of 5,5/-dithiobis- (2-nitrobenzoic acid) by a mixture of NADPH and glutathione reductase	(Maltese et al., 2017)
Human	aorta	~ 130-155µM	Commercial kit (BIOXYTECH GSH/GSSG-412 assay kit; OXISResearch, a division of Oxis Health Product, Portland, OR)	(Sinha-Hikim et al., 2010)
Mouse	aorta	~25 (WT) (GSH:21 nmol/mg protein; GSSG:4 nmol/mg protein) ~44 (MsrA-/-) (GSH:40 nmol/mg protein; GSSG:4 nmol/mg protein)	The 5-sulfosalicylic acid treatment, BCA protein assay kit	(Pennington et al., 2018)
Embryonic rat	aorta	~11µM	NDA assay	(Belcastro et al., 2017)
Rat	aorta	~17.5	Commercial kits (Jian Cheng Biological Engineering Institute, Nanjing, China)	(Guo et al., 2014)
Rat	aorta	~58	Tietze recycling assay	(Hill et al., 2010)
Rat	aorta	~25	Fluorometric assay (OPA as a florescent reagent)	(Cao and Li, 2004)

Abbreviation: GSH, reduced glutathione; GSSH, oxidized glutathione; HPLC, high-performance liquid chromatography; OPA, o-phthaladehyde; MsrA, methionine sulfoxide reductase A; NDA, naphthalene dicarboxaldehyde.

Moreover, antioxidant enzymes participate in maintaining the redox phenotypes. In my study, catalase (CAT), converting H_2O_2 to H_2O and O_2, and superoxide dismutase (SOD), converting O_2^- to H_2O_2 and O_2, were measured by immunoblotting. Long-term adaptation of HCASMCs to 18kPa O_2 had no effect on CAT compared to cells under 5kPa O_2, whilst protein levels of CAT trended to be lower under 1kPa, consistent with results in human fibroblasts exposed to hypoxia for 72h (Sgarbi et al., 2017). SOD1 (CuZnSOD) located in cytosol, and SOD2 (MnSOD) located in mitochondria, decreased as ambient O_2 levels decreased from 18 to 1kPa O_2 with significant differences observed between 18kPa and 1kPa O_2 groups. Overall, antioxiant enzymes and GSH levels were significant lower in HCASMCs under 1kPa O_2.

Accumulating evidence suggests that ROS are hypoxia signalling molecules, as ROS production is increased in ischaemia (Becker et al., 1999; Mansfield et al., 2004). Nevertheless, there is controversy due to a decrease in the required substrate O_2 in ischaemia (Sgarbi et al., 2017). Understanding how different O_2 levels affect the redox phenotype of HCASMCs is important for measurements of ROS during long-term *in vitro* culture. To further address redox sensitive responses in HCASMCs, the Nrf2 antioxidant signalling pathway was investigated. The transcription factor Nrf2 is a master regulator of antioxidant defences and translocates into nucleus under oxidative stress or upon activation by electrophiles such as sulforaphane (SFN), known to modify Cys151 on its cytosolic binding partner Keap1 (Chapple et al., 2015; Robledinos-Anton et al., 2019; Suzuki and Yamamoto, 2015). Nrf2 signalling upregulates antioxidant gene expression, including GCLC, GCLM, NOQ1 and HO-1 (Chapple et al., 2016). As assessed by Nrf2 nuclear: cytoplasmic immunostaining (see **Figure 3.10**), sulforaphane (SFN, 2.5µM) significantly induced Nrf2 nuclear accumulation in HCASMCs under 18, 5 and 1kPa O_2. Moreover, SFN increased

protein and mRNA expression of key Nrf2 downstream targets GCLM, GCLC, HO-1 and NQO1 (**Figure 3.11 and 3.12**). In the present study, GCLC and GCLM protein expression were lower in cells adapted to 1kPa, with a significant decrease in GCLM protein expression in cells treated with SFN, a finding consistent with lower GSH levels (see **Figure 3.8**), since GCL catalyzes the first and rate-limiting step in GSH production (Forman et al., 2009). mRNA expression of GCLC and GCLM were similar in vehicle groups, with negligible differences in detected. GCLC and GCLM expression in cells challenged with SFN under 18 or 5kPa.

In addition, NQO1 protein in vehicle groups significantly decreased as ambient O_2 levels decreased from 18 to 1kPa O_2, although there were negligible differences in cells with following SFN treatment under 18 or 5kPa. Basal HO-1 protein and mRNA expression were affected negligibly in HCASMCs across the different O_2 levels. Unlike our findings in HUVECs (Chapple et al., 2016), SFN induced upregulation of HO-1 expression was maintained in HCASMCs cultured under 18, 5 and 1 kPa O_2 (see **Figure 3.11**). In this context, our previous findings in HUVECs implicated Bach 1, a competitor of Nrf2 to heterodimerisation with small Maf proteins, in the attenuation of HO-1 expression in cells under 5kPa O_2 (Chapple et al., 2016; Kimura et al., 2007). In HUVECs, Bach1 negatively regulates the select Nrf2 targeted genes (e.g. NQO1 and HO-1), whilst GSH-related genes (e.g. GCLM and GCLC) are independent of Bach1 (Chapple et al., 2016; Fischhuber et al., 2020). In my study, protein and mRNA expression of Bach1 were significantly enhanced in HCASMCs under 5 and 1kPa O_2 compared to cells under 18kPa (**Figure 3.13**), explaining potentially the decrease in NQO1 protein expression in vehicle groups across the O_2 change. Unlike HUVECs, upregulated protein expression of HO-1 with SFN treatment was not inhibited by Bach1 in HCASMCs under 5kPa O_2. Previous studies found that hypoxia

induces HO-1 protein expression in rat pulmonary VSMCs and rat aortic VSMCs (Hartsfield et al., 1999), but reduces HO-1 protein expression in HUVECs and HCAECs (Nakayama et al., 2000). This may be due to feedback regulation involving HO-1, Bach1 and heme (Ogawa et al., 2001; Shibahara et al., 2007). Ogawa et al. has reported that heme inhibits repressor Bach1 in human embryonic kidney HEK293 cells, abrogating its repression of HO-1 expression (Ogawa et al., 2001). Moreover, HO-1 may be regulated by other signalling pathways and factors, such as the metal zinc (Kaufman et al., 2020; Li et al., 2014), which will be detailed in later chapters.

SFN significantly increased Bach1 protein expression in HCASMCs under 18, 5 and 1kPa O_2 (**Figure 3.13**), which has been explained by Jyrkkänen and colleagues (Jyrkkanen et al., 2011). Bach1 is a Nrf2 targeted gene and has a functional Maf recognition element site near the transcription start site of Bach1 transcript variant 2, which can be upregulated by Nrf2 overexpression and Nrf2 activators in HUVECs and human hepatoblastoma HepG2 cells (Jyrkkanen et al., 2011; Kaspar and Jaiswal, 2010). Nrf2-induced Bach1 upregulation is considered as a feedback-inhibitory mechanism for ARE-mediated gene regulation (Jyrkkanen et al., 2011; Zhang et al., 2018). In addition, to confirm that HO-1 and NQO1 protein expression are regulated by Nrf2, HCASMCs were transfected with scrambled (control) or Nrf2 siRNA to knockdown transcriptional activity before treatment with SFN or vehicle. Nrf2 gene silencing significantly abrogated SFN-induced upregulation of HO-1 and NQO1 under 18, 5 and 1kPa O_2 (**Figure 3.15**) protein expression, suggesting these enzymes in this cell typey are highly regulated by Nrf2. Overall, the Nrf2 targeted antioxidant protein expression was significantly lower in HCASMCs under 1kPa O_2.

As summaried in **Figure 3.17**, physiological normoxia promoted contractile phenotype modulation and proliferation in HCASMCs, whilst hyperoxia induced synthetic phenotype and slow proliferation. Compared to 5kPa O_2, redox phenotype of HCASMCs adapted long-term to 18 kPa O_2 did not alter intracellular GSH levels, antioxidant enzymes nor induction of Nrf2 target proteins except for NQO1. The present findings in HCASMCs appear to be cell-type specific, as umbilical vein (Chapple et al., 2016) and coronary artery endothelial cells exhibit enhanced Nrf2 activation under 18 kPa O_2 (Smith et al., 2023).

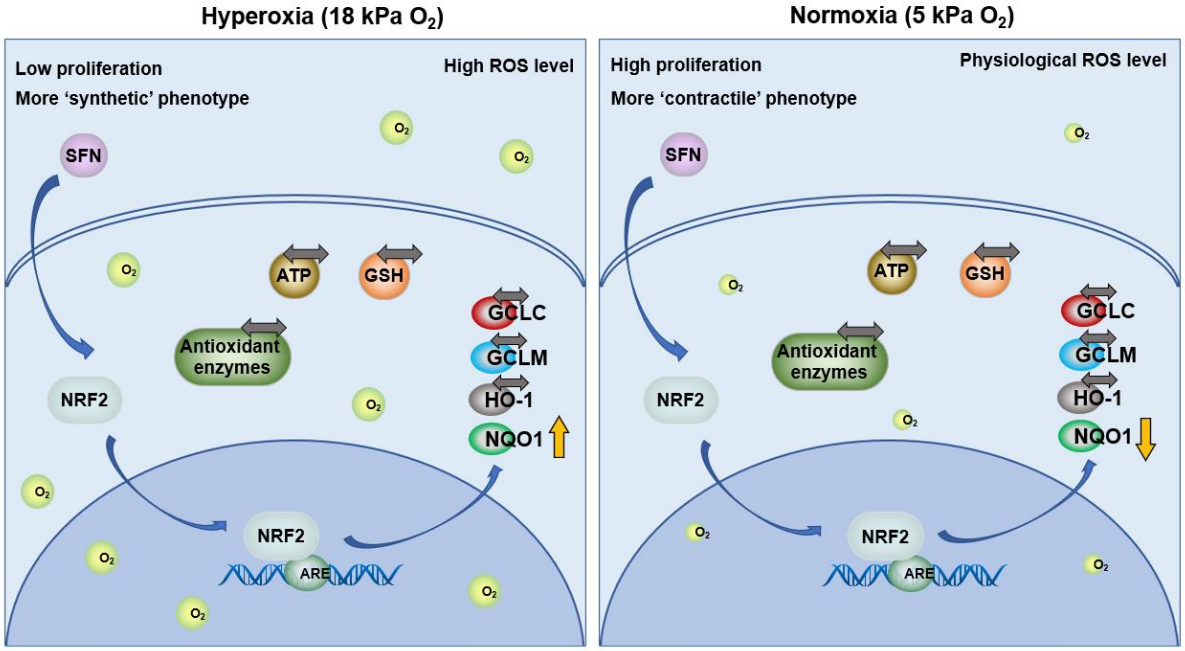

Figure 3.17 Graphical abstract of Chapter 3
Redox phenotype of HCASMCs adapted long-term to 18kPa O_2 did not alter intracellular GSH levels, antioxidant enzymes nor induction of Nrf2 target proteins except for NQO1 compared to physiological normoxia.

Chapter 4 – Results

Metal profiles of HCASMCs under 18, 5 and 1kPa O_2 and crosstalk between Nrf2 signaling and Zn

Over the past two decades, the field of metallomics has provided new insights into mechanisms underlying pro-oxidant and antioxidant pathological processes (Maret, 2018). Both redox-active (e.g. Fe and Cu) and redox-inert (e.g. Zn and Mg) metals play key roles in modulating cellular redox balance during ischaemia-reperfusion (IR) injury (Jomova and Valko, 2011; Maret, 2019). This chapter investigates the total content of metals in HCASMCs adapted long-term (5d) to hyperoxia (18kPa O_2), physiological normoxia (5kPa O_2) or hypoxia (1kPa O_2). Metallomic profiling of HCASMCs lysates was conducted using inductively coupled plasma mass spectrometry (ICP-MS) (Mittal et al., 2017; Wilschefski and Baxter, 2019). In addition, crosstalk between Zn and Nrf2 signalling was investigated, as well as the role of ZnT1 (main exporter of Zn) and metallothionein (MT, main storage of Zn in cells) in Zn handling by HCASMCs.

4.1 Metal profiling under 18, 5 and 1kPa O_2 levels in HCASMCs using ICP-MS

ICP-MS is widely used to measure multiple elements in a single analysis of samples (Stewart, 2019; Sussulini et al., 2017). The liquid samples are atomized and ionized by high-temperature plasma into ions and then separated by in a mass analyzer according to their mass-charge ratio. In collaboration with the London Metallomics Facility at King's College London, I have characterised metal profiles in HCASMCs adapted for 5d to hyperoxia, physiological normoxia and hypoxia. In cells adapted to 18 kPa O_2, total Zn levels were

0.345 ± 0.037ng/µg protein and had no significant changes under 5 kPa and 1 kPa O_2 (0.298 ± 0.020 ng/µg protein and 0.441 ± 0.06 ng/µg protein, respectively) (**Figure 4.1A**). Notably, the concentration of Cu was dramatically higher in cells under 1kPa (0.026 ± 0.004 ng/µg protein) compared to cells under 18 and 5kPa O_2 (18kPa: 0.008 ± 0.002 ng/µg protein vs 5kPa: 0.010 ± 0.002 ng/µg protein) (**Figure 4.1B**). Meanwhile, ambient O_2 levels did not influence total concentrations of Fe and Mg in HCASMCs (**Figure 4.1C and E**). Mn content trended to be lower in cells under 1kPa O_2 (**Figure 4.1D)**. The concentration of these metals measured in the complete culture medium (SMC basal medium 2 + supplement pack SMC growth medium 2) is shown in **Figure 4.1F**.

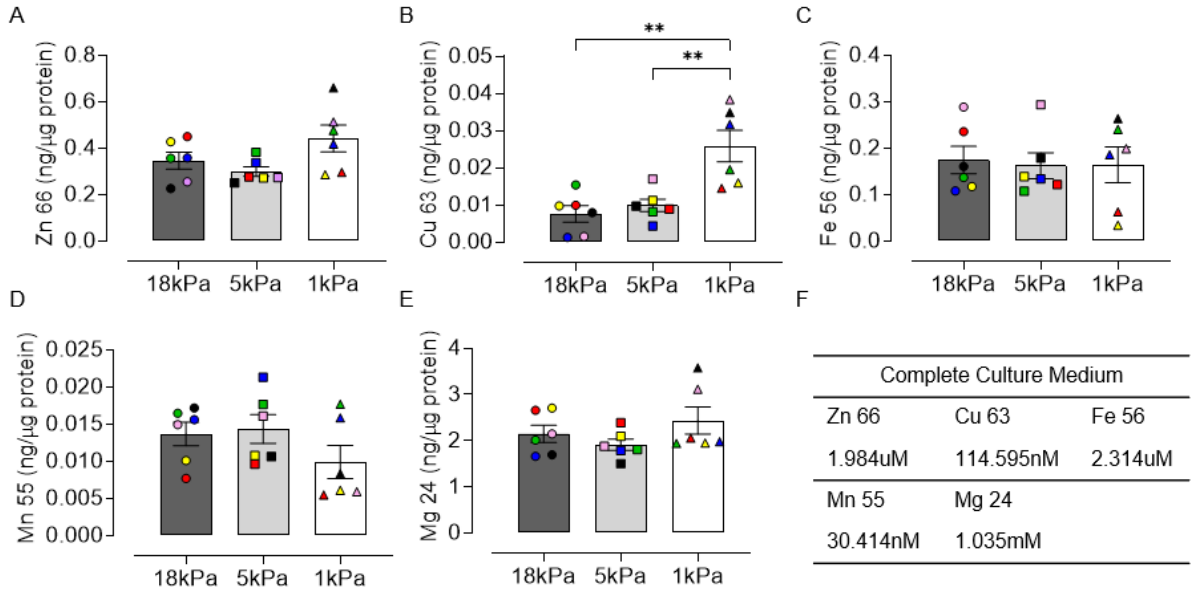

Figure 4.1 Total content of different metals in HCASMCs or culture medium following long-term adaptation of cells to 18, 5 and 1kPa O_2

Total Zn (A), Cu (B), Fe (C), Mn (D) and Mg (E) content in HCASMCs adapted for 5 days under hypoxia, physiological normoxia and hyperoxia was measured by ICP-MS. The different metal concentrations in complete culture medium are summarised in panel F. Data denote mean ± S.E.M., n=4 independent cultures, **P<0.01, One-way ANOVA with Tukey's multiple comparisons test. The 4 cultures are colour-coded to highlight changes within a given culture.

Abbreviations: Zn, zinc; Cu, cooper; Fe, iron; Mn, manganese; Mg, magnesium; ICP-MS, inductively coupled plasma mass spectrometry.

4.2 Zn supplementation increases total Zn content in HCASMCs

Zn, a redox-inactive metal, plays an important role in the defence against oxidative stress in an indirect way by stabilising thiol groups against free radical attack (Maret, 2003; Marreiro et al., 2017). In a previous study, treatment of rats heart with zinc pyrithione (pyrithione, Zn ionophore) (Ischia et al., 2019) at onset of reperfusion was shown to exacerbate myocardial infarction (MI) (Lien et al., 2018). In order to establish appropriate concentrations for supplementation of culture media with $ZnCl_2$ with pyrithione or TPEN (a chelator of Zn), cell viability was measured using an MTT assay (see **Section 2.5**). These experiments established that maximum concentrations of $ZnCl_2$ and pyrithione (10µM and 0.5µM) had negligible effects on the viability of HCASMCs, confirming concentrations used in other studies (Bodiga et al., 2015; Karagulova et al., 2007; Kasi et al., 2011). Moreover, TPEN (0-1.5µM) had a negligible effect on cell viability and further experiments were conducted using 1.25µM TPEN.

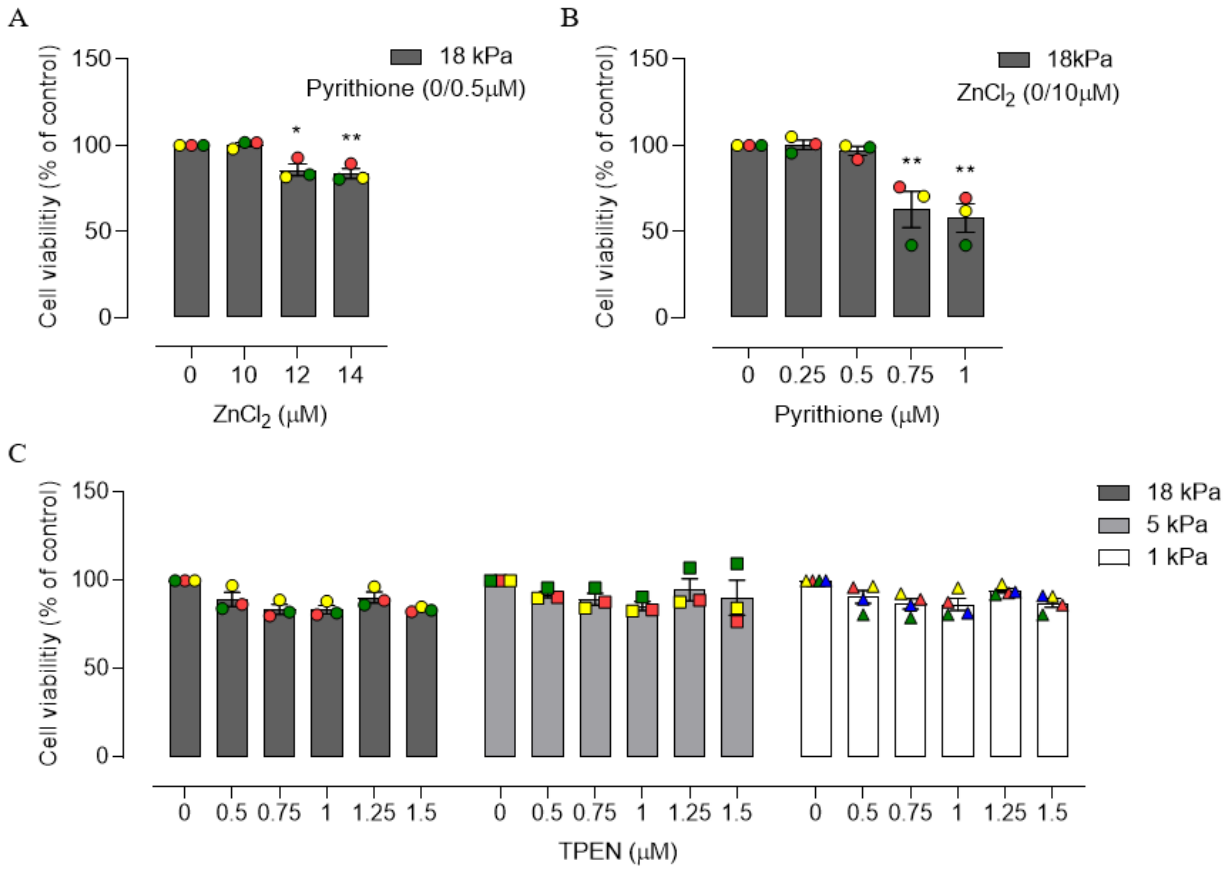

Figure 4.2 Viability of HCASMCs following supplemented with $ZnCl_2$ and pyrithione or treated with TPEN

HCASMCs pre-adapted to 18kPa O_2 for 5d were seeded in a triplicate at a concentration of 10^4 cells/well in 96-well plate and cultured for 48h. Cells were then treated with different concentrations of pyrithione, $ZnCl_2$ or TPEN respectively for 16h. (A) The concentration of pyrithione was 0.5μM in $ZnCl_2$ treatment groups. The concentration of $ZnCl_2$ was 10, 12 or 14 μM respectively. (B) The concentration of $ZnCl_2$ was 10μM in pyrithione treatment groups. The concentration of pyrithione was 0.25, 0.5, 0.75 or 1μM respectively. (C) The concentration of TPEN was 0.5, 0.75, 1.0, 1.25 or 1.5μM. HCASMCs incubated with medium were used as controls. Data denote mean ± S.E.M., n=3-4 independent cultures, *P<0.05, **P<0.01, One-way or Two-way ANOVA with Tukey's multiple comparisons test. The 3-4 cultures are colour-coded to highlight changes within a given culture.

Abbreviations: $ZnCl_2$, zinc chloride; TPEN, N,N,N′,N′-tetrakis (2-pyridylmethyl) ethylenediamine.

In the present studies, cellular Zn concentration was upregulated by exogenous Zn addition ($ZnCl_2$ (10μM) + pyrithione (0.5μM), 16h), with significant differences noted between Veh and Zn supplementation groups in HCASMCs under 18kPa and TPEN (1.25μM, 16h) and Zn supplementation groups in cells under 18 and 1kPa O_2 (**Figure 4.3**). Compared with the significant increase of total Zn content in cells induced by Zn supplementation under 18 O_2, increases of total Zn content in cells under 5 or 1 kPa O_2 were less.

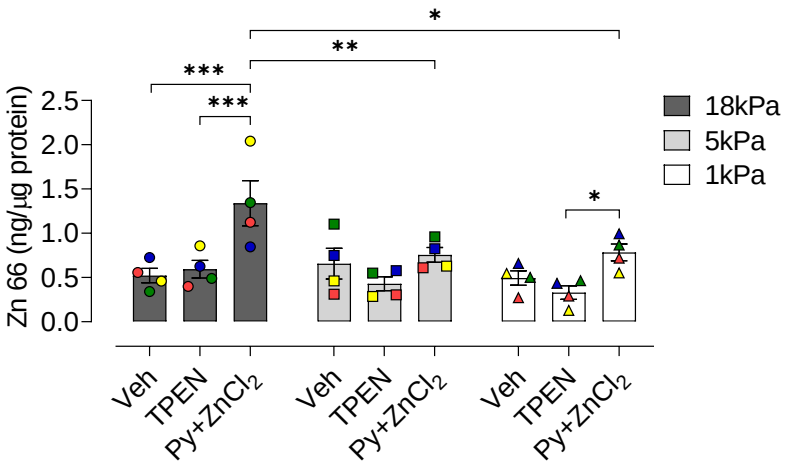

Figure 4.3 Total Zn content in HCASMCs supplemented with Zn or treated with TPEN under 18, 5 and 1kPa O_2

Total Zn content in HCASMCs following treatments with (Vehicle (Veh, 0.005% DMSO,16h), TPEN (a Zn^{2+} chelotor, 1.25μM, 16h) or 2-mercaptopyridine N-oxide sodium salt (pyrithione, a Zn^{2+} ionophore, 0.5μM) with $ZnCl_2$ (10μM) (Py+$ZnCl_2$, 16h)) under 18, 5 and 1kPa O_2 measured by ICP-MS. Data denote mean ± S.E.M., n=4 independent cultures, *P<0.05, **P<0.01, ***P<0.001, Two-way ANOVA with Bonferroni's multiple comparisons test. The 4 cultures are colour-coded to highlight changes within a given culture.

Abbreviations: Zn, zinc; ICP-MS, inductively coupled plasma mass spectrometry; Veh, vehicle; TPEN, N,N,N′,N′-tetrakis(2-pyridinylmethyl)-1,2-ethanediamine; Py, pyrithione; $ZnCl_2$, zinc chloride.

4.3 Effects of Zn on Nrf2 signalling in HCASMCs under 18, 5 and 1kPa O_2

Several studies have reported that Zn supplementation promotes functional recovery after spinal cord injury by activating the Nrf2-HO-1 defense pathway and inducing HO-1 expression in cancer cells (Li et al., 2020a; Xue et al., 2013). The present study in HCASMCs showed that HO-1 protein and mRNA expression were upregulated by Zn addition ($ZnCl_2$ (10μM) + pyrithione (0.5μM), 16h/6h) in cells adapted for 5d to 18, 5 and 1kPa O_2 (**Figure 4.4A and C**). Similar trends were detected for NQO1 protein (**Figure 4.4B**). No differences HO-1 or NQO1 protein and mRNA expression was detected in cells treated with Veh (Vehicle, 0.005% DMSO,16h) or TPEN (a Zn^{2+} chelator, 1.25μM, 16h). In addition, Zn supplementation significantly induced Nrf2 nuclear translocation in HCASMCs under 18, 5 and 1kPa O_2 (**Figure 4.5**), noting basal Nrf2 nuclear: cytoplasmic ratio had negligible change in HCASMCs.

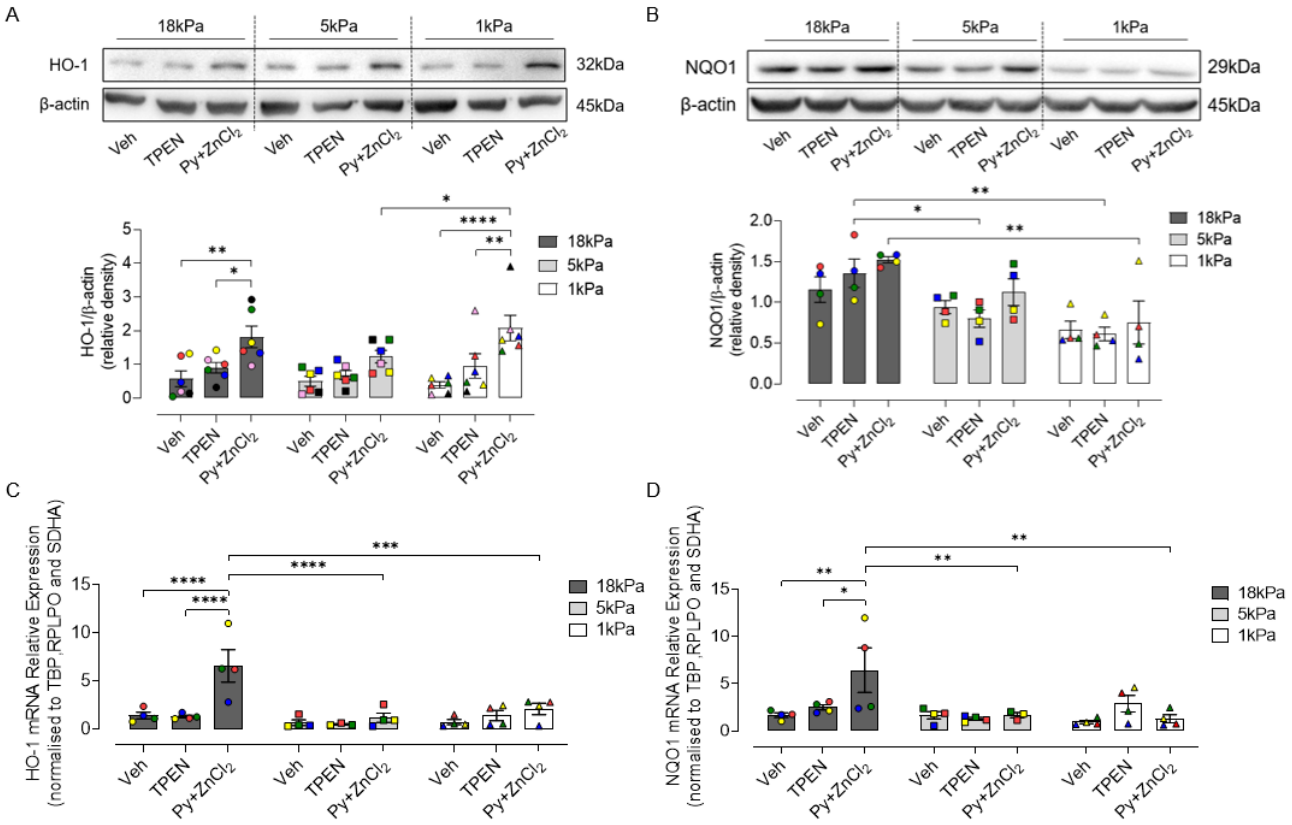

Figure 4.4 HO-1 and NQO1 protein and mRNA expression in HCASMCs supplemented with Zn or treated with TPEN under 18, 5 and 1kPa O_2

HO-1 (A) and NQO1 (B) protein expression in HCASMCs following treatment with Zn (2-mercaptopyridine N-oxide sodium salt (pyrithione, a Zn^{2+} ionophore, 0.5μM) and $ZnCl_2$ (10μM) (Py+$ZnCl_2$, 16h)) under 18, 5 and 1kPa O_2. Densitometric analysis of protein expression relative to β-actin. Data denote mean ± S.E.M., n=4-6 independent cultures. mRNA expression of HO-1 (C) or NQO1 (D) in HCASMCs treated with Veh (0.005% DMSO, 6h), TPEN (1.25μM, 6h) or Py+$ZnCl_2$ (0.5μM+10μM, 6h) under 18kPa, 5kPa and 1kPa O_2. Values were normalized to three housekeeping genes (TBP, RPLPO and SDHA). Data denote mean ± S.E.M., n=4 independent cultures, *P<0.05, **P<0.01, ****P<0.0001, Two-way ANOVA with Bonferroni's multiple comparisons test. The 4-6 cultures are colour-coded to highlight changes within a given culture.

Abbreviations: HO-1, heme oxygenase-1; NQO1, NAD(P)H Quinone Dehydrogenase 1; Veh, vehicle; TPEN, N,N,N′,N′-tetrakis(2-pyridinylmethyl)-1,2- ethanediamine; Py, pyrithione; $ZnCl_2$, zinc chloride; TBP, TATA box binding protein; RPLPO, ribosomal protein lateral stalk subunit P0; SDHA, succinate dehydrogenase complex, subunit A.

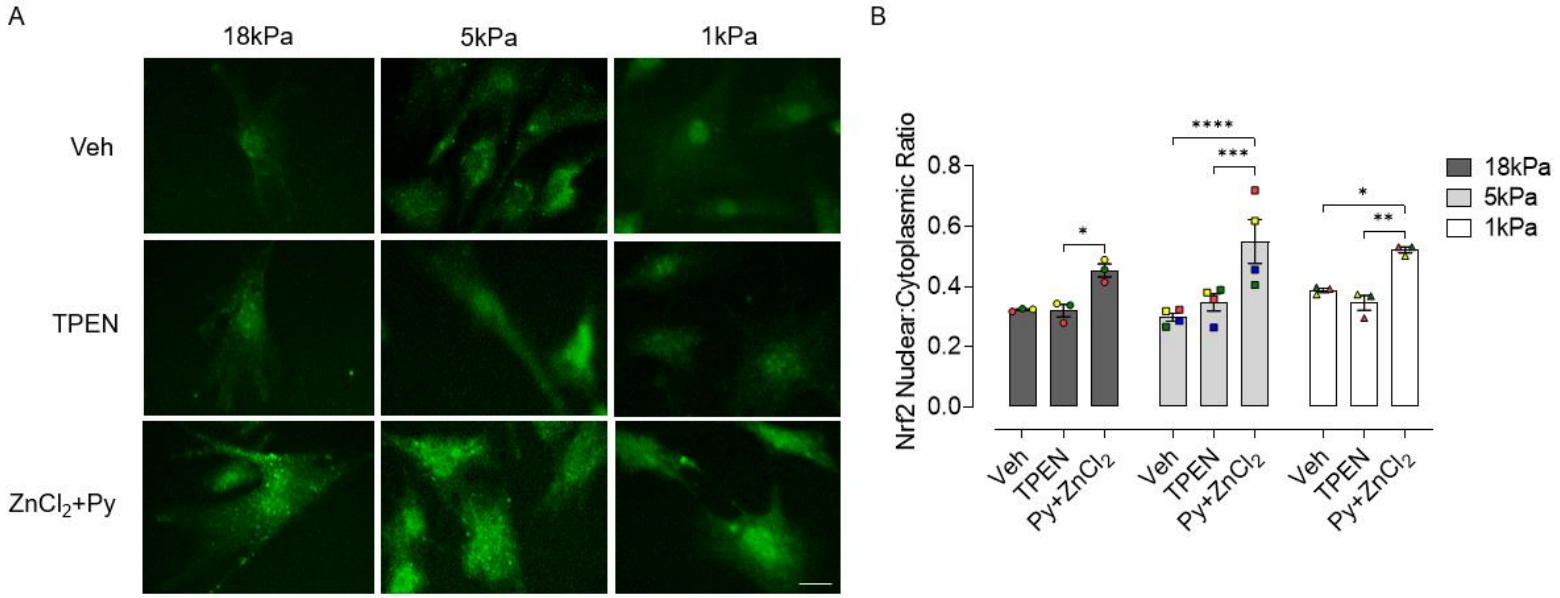

Figure 4.5 Zn supplementation induces Nrf2 nuclear translocation in HCASMCs under 18, 5 and 1kPa O_2

(A) Representative Nrf2 positive immunofluorescence images in HCASMCs under 18, 5 and 1kPa O_2 after 16h treatment with Vehicle (Veh, 0.005% DMSO), Py+$ZnCl_2$ (0.5µM+10µM) or TPEN (1.25µM), respectively. **(B)** Quantification of the Nrf2 nuclear: cytoplasmic ratio in HCASMCs treated with Veh, Py+$ZnCl_2$ or TPEN under 18, 5 and 1kPa O_2, respectively. Data denote mean ± S.E.M., n=3-4 independent cultures, *P<0.05, **P<0.01, ***P<0.001, ****P<0.0001, Two-way ANOVA with Bonferroni's multiple comparisons test. Images were taken at ×40 magnification using an Etaluma microscope (LS720 Microscopes, USA). Scale bar: 20µM. The 3-4 cultures are colour-coded to highlight changes within a given culture.

Abbreviations: Veh, vehicle; TPEN, N,N,N′,N′-tetrakis(2-pyridinylmethyl)-1,2- ethanediamine; Py, pyrithione; $ZnCl_2$, zinc chloride; Nrf2, nuclear factor erythroid 2- related factor 2.

4.4 Effects of Zn on MT1 and ZnT1 expression in HCASMCs

Metallothionein (MT) is a cysteine-rich low-molecular weight protein with a low affinity for Zn, and can store 5-15% of the total cellular Zn pool (Coyle et al., 2002). When intracellular Zn^{2+} increases, the activation of the metal responsive transcription factor 1 (MTF-1), a regulator of metal homeostasis, results in upregulation of MTs gene expression, which can bind excessive Zn^{2+} (Maret, 2006). Meanwhile, an antioxidant response element (ARE) exists in the promoter region of MT genes. Moreover, few studies have shown that Nrf2 translocates into nucleus and binds to AREs, inducing for example expression of MTs in bovine aortic endothelial cells and mouse liver (Fujie et al., 2016; Ohtsuji et al., 2008). There are four isoforms of MTs in humans, and MT-1 and MT-2 widely expressed in various tissues (Ghoshal and Jacob, 2001). In the present study, negligible differences in MT (1 and 2) protein expression were observed in HCASMCs under 18 and 5kPa O_2, but expression decreased significantly in cells under 1kPa compared to 5kPa O_2 (**Figure 4.6A**). MT1 mRNA expression was significantly enhanced by Zn supplementation ($ZnCl_2$ (10μM) + pyrithione (0.5μM), 6h) in HCASMCs adapted to 18, 5 and 1kPa O_2 (**Figure 4.6B**) compared to cells treated with those in cells with Veh or TPEN.

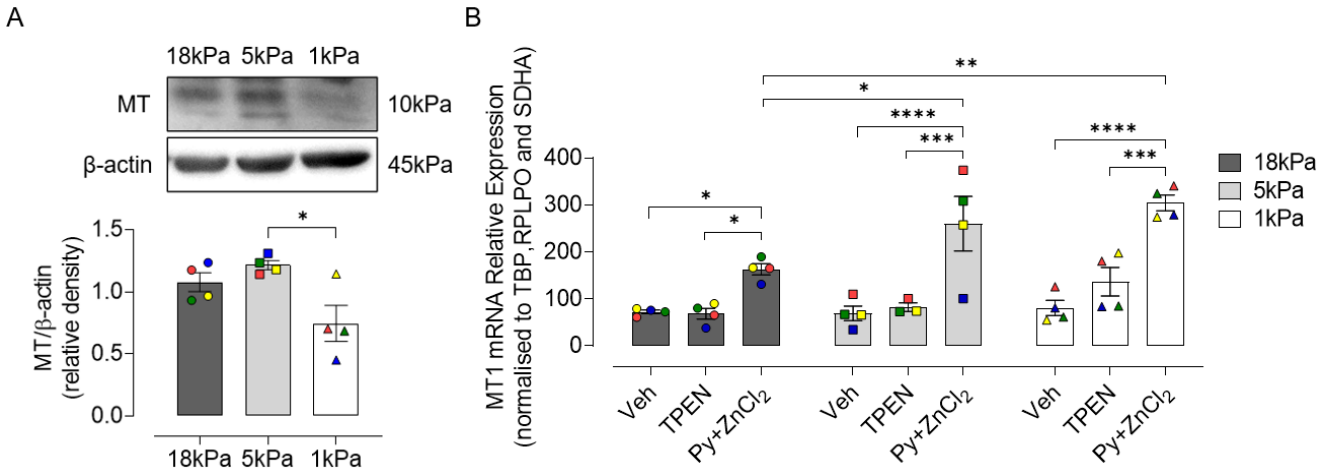

Figure 4.6 MT protein and mRNA expression in HCASMCs supplemented with Zn or treated with TPEN under 18, 5 and 1kPa O_2

(A) Representative immunoblot of combined MT1/2 protein expression with densitometric analysis of protein expression relative to β-actin. (B) MT1 mRNA was after 6h supplementation with Zn (2-mercaptopyridine N-oxide sodium salt (pyrithione, a Zn^{2+} ionophore, 0.5μM) and $ZnCl_2$ (10μM) (Py+$ZnCl_2$)) in HCASMCs under 18, 5 and 1kPa O_2. Data were normalized to three housekeeping genes (TBP, RPLPO and SDHA). Data denote mean ± S.E.M., n=3-4 independent cultures, *P<0.05, **P<0.01, ***P<0.001, ****P<0.0001, One-way or Two-way ANOVA with Tukey's or Bonferroni's multiple comparisons test. The 3-4 cultures are colour-coded to highlight changes within a given culture.

Abbreviations: MT, metallothionein; Veh, vehicle; TPEN, N,N,N′,N′-tetrakis (2-pyridinylmethyl)-1,2- ethanediamine; Py, pyrithione; $ZnCl_2$, zinc chloride; TBP, TATA box binding protein; RPLPO, ribosomal protein lateral stalk subunit P0; SDHA, succinate dehydrogenase complex, subunit A.

ZnT1 is the main exporter of Zn and mainly located in cells membranes (Nishito and Kambe, 2019). It exports cytosolic Zn to the extracellular space or from the cytosol to the organelles, thereby contributing to the regulation intracellular Zn levels (Fukada et al., 2011). Basal ZnT1 protein expression in HCASMCs was not affected by changes in ambient O_2 levels. Moreover, ZnT1 protein expression was not influenced by Zn supplementation in HCASMCs under 18, 5 and 1kPa O_2 (**Figure 4.7**).

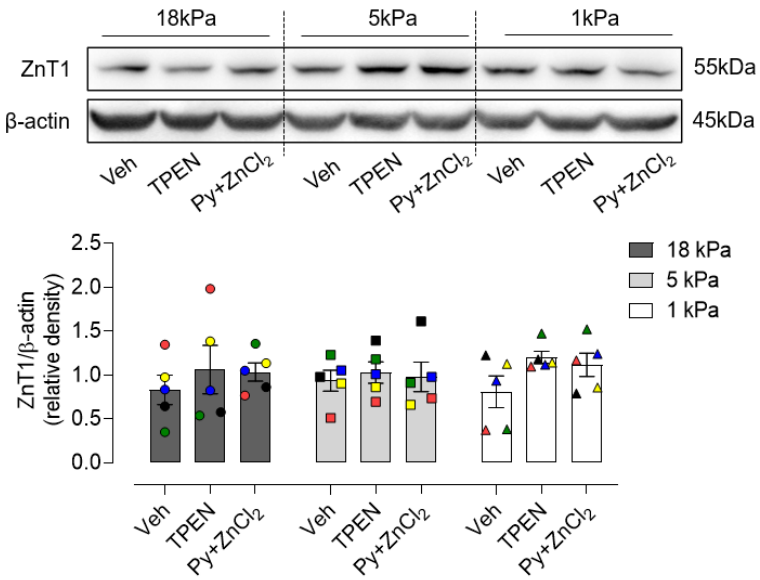

Figure 4.7 ZnT1 protein expression in HCASMCs supplemented with Zn or treated with TPEN under 18, 5 and 1kPa O_2

ZnT1 protein expression was not affected by supplementation of the medium with Zn (2-mercaptopyridine N-oxide sodium salt (pyrithione, a Zn^{2+} ionophore, 0.5μM) and $ZnCl_2$ (10μM) (Py+$ZnCl_2$, 16h)) in HCASMCs under 18, 5 and 1kPa O_2. Densitometric analyses of protein expression relative to β-actin. Data denote mean ± S.E.M., n=5 independent cultures, Two-way ANOVA with Bonferroni's multiple comparisons test. The 5 cultures are colour-coded to highlight changes within a given culture.

Abbreviations: ZnT1, zinc transporter 1; Veh, vehicle; TPEN, N,N,N′,N′-tetrakis(2-pyridinylmethyl)-1,2-ethanediamine; Py, pyrithione; $ZnCl_2$, zinc chloride.

4.5 Effects of silencing Nrf2 on total Zn levels in HCASMCs under 18, 5 and 1kPa O_2

As shown in **Figure 3.14**, compared to scrambled siRNA transfection, 2.5nM Nrf2 siRNA obviously know-down Nrf2-targeted HO-1 protein expression, which is the transfection concentration used in subsequent experiments. When HCASMCs were transfected with scrambled or Nrf2 siRNA for 24h after adaptation for 5d to 18, 5 or 1kPa O_2 (**Figure 4.8**), siNrf2 had negligible effects on intracellular total zinc levels. As shown in **Figure 4.9A**, Nrf2 protein expression trended to be decreased in cells with silencing Nrf2 activity. As the efficiency of Nrf2 antibody is not good, Nrf2-targeted HO-1 and NQO1 protein expression were significantly downregulated in Nrf2 silenced cells, confirming knock-down of Nrf2 (**Figure 4.9B and C**). NQO1 protein expression in cells transfected with scrambled RNA decreased as ambient O_2 levels were lowered from 18 to 1kPa O_2, consistent with the basal NQO1 protein expression pattern (see **Figure 3.11D**). Negligible differences in HO-1 protein expression were detected in cells transfected with scrambled RNA, consistent with initial findings for basal HO-1 protein expression (see **Figure 3.11C**). Silencing Nrf2 decreased basal HO-1 protein levels under 18 and 1kPa O_2, underpinning earlier findings that Nrf2 silencing led to downregulation of SFN induced HO-1 expression (**Figure 3.15A**). Meanwhile, protein expression of MT was not altered under any oxygen condition tested (**Figure 4.10A**). ZnT1 protein expression was unaffected by Nrf2 knockdown under 18 and 5 kPa O_2 but was significantly reduced under 1 kPa O_2 (**Figure 4.10B**).

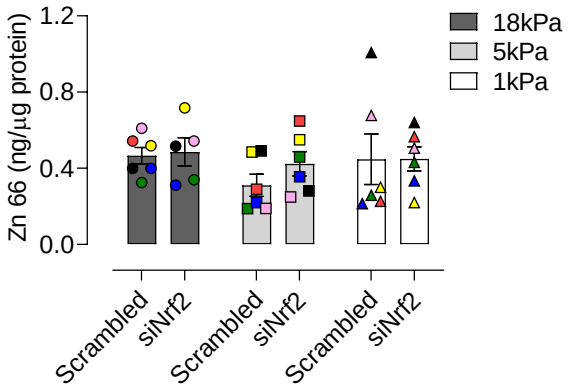

Figure 4.8 Silencing Nrf2 transcriptional activity has a negligible effect on total Zn levels in HCASMCs
ICP-MS analysis of total Zn content in HCASMCs transfected with scrambled or Nrf2 siRNA for 24h after 5 days adaptation to 18, 5 and 1kPa O_2. Data denote mean ± S.E.M., n=5-6 independent cultures, Two-way ANOVA with Tukey's multiple comparisons test. The 5-6 cultures are colour-coded to highlight changes within a given culture.
Abbreviations: Zn, zinc; ICP-MS, inductively coupled plasma mass spectrometry.

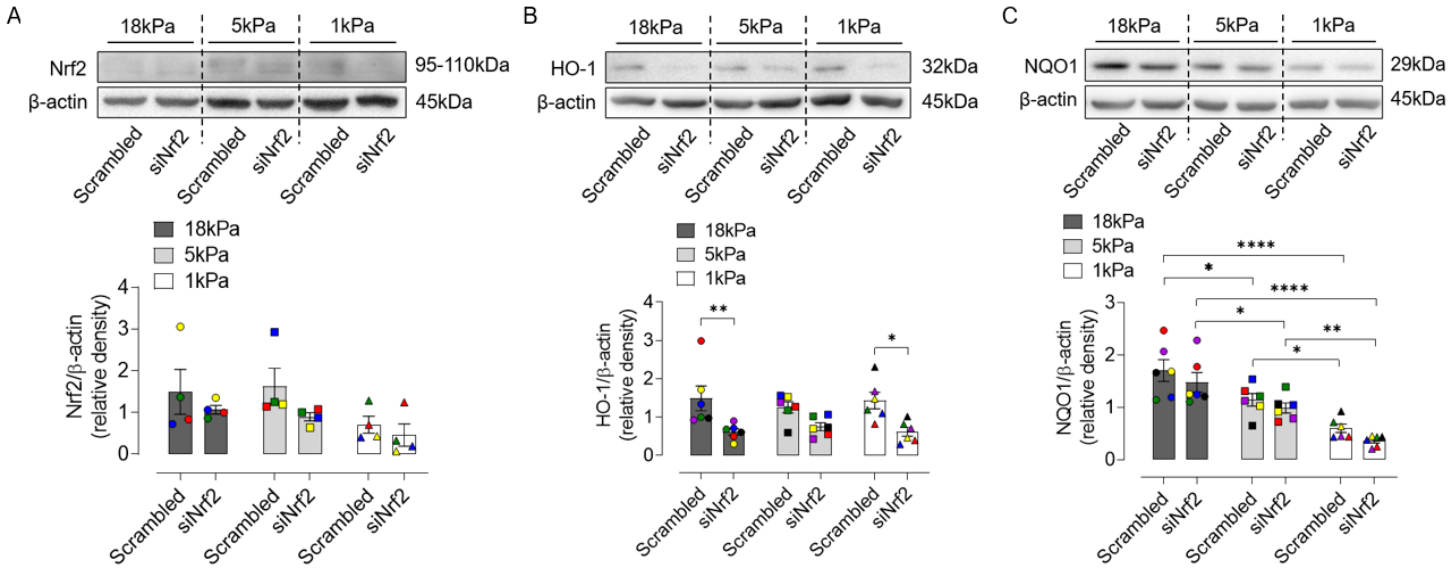

Figure 4.9 Nrf2, HO-1 and NQO1 protein expression in HCASMCs with Nrf2 silencing

HCASMCs were transfected with scrambled or Nrf2 siRNA for 24h after 5d adaptation to 18, 5 and 1kPa O_2. Representative immunoblots of Nrf2 (A), HO-1 (B) and NQO1 (C) in HCASMCs with densitometric analyses of protein expression relative to β-actin. Data denote mean ± S.E.M., n=4-6 independent cultures, *P<0.05, **P<0.01, ****P<0.0001, Two-way ANOVA with Tukey's multiple comparisons test. The 4-6 cultures are colour-coded to highlight changes within a given culture.

Abbreviations: Nrf2, nuclear factor-erythroid factor 2-related factor 2; HO-1, heme oxygenase-1; NQO1, NAD(P)H quinone dehydrogenase 1; MT, metallothionine; ZnT1, zinc transporter 1.

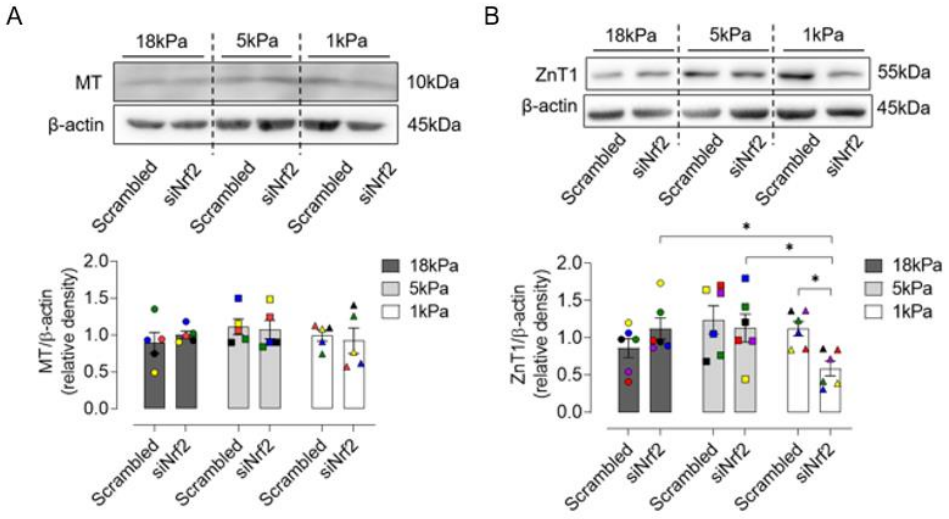

Figure 4.10 Silencing Nrf2 transcriptional activity does not affect MT and ZnT1 protein expression in HCASMCs

HCASMCs were transfected with scrambled or Nrf2 siRNA for 24h after 5d adaptation to 18, 5 and 1kPa O_2. Representative immunoblots of MT1/2 (A) and ZnT1 (B) in HCASMCs with densitometric analyses of protein expression relative to β-actin. Data denote mean ± S.E.M., n=5-6 independent cultures, *P<0.05, Two-way ANOVA with Tukey's multiple comparisons test. The 5-6 cultures are colour-coded to highlight changes within a given culture.

Abbreviations: MT, metallothionine; ZnT1, zinc transporter 1.

4.6 Effects of Nrf2 overexpression on Zn levels in HCASMCs under 18, 5 and 1kPa O_2

As shown in **Figure 4.11**, compared to control vector 3.1C transfection, 400ng per well (in 24-well-plate) hNrf2 vector enhanced Nrf2-targeted NQO-1 protein expression, which is the transfection concentration used in subsequent experiments. HCASMCs were transfected with control vector 3.1C and hNrf2 vector respectively for 24h to investigate the effects of Nrf2 overexpression on total Zn content measured by ICP-MS. Nrf2 overexpression had negligible effects on total Zn levels in HCASMCs under different O_2 levels (**Figure 4.12**). As the efficiency of Nrf2 antibody is bad (see **Figure 4.9A**), Nrf2 protein expression with hNrf2 vector transfection in HCASMCs were not detected. However, Nrf2-targeted NQO1 protein expression was significantly upregulated by hNrf2 vector, validating Nrf2 overexpression (**Figure 4.13A**), and underpinning a similar trend for NQO1 protein expression in cells treated with SFN under 18, 5 or 1kPa O_2 (**Figure 3.13D**). In contrast, MT and ZnT1 protein

expression were not altered in HCASMCs transfected with hNrf2 vector under 18, 5 or 1kPa O_2 (**Figure 4.13B and C**).

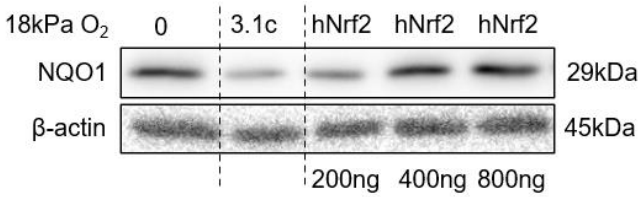

Figure 4.11 Preliminary experiment with control vector 3.1C and hNrf2 vector induce Nrf2 overexpression
NQO1 immunoblot of HCASMCs transfected with different concentrations of control vector 3.1C and hNrf2 vector for 24h after 5d adaptation to 18kPa O_2. The preliminary experiment shows one cell culture result.
Abbreviations: NQO1, NAD(P)H quinone dehydrogenase 1.

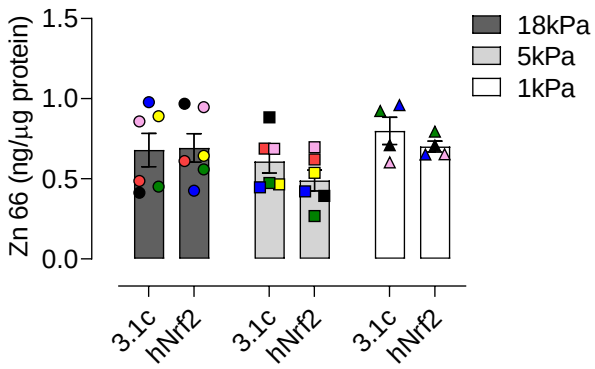

Figure 4.12 Nrf2 overexpression does not alter total Zn content in HCASMCs
ICP-MS analysis of total Zn content in HCASMCs transfected with control vector 3.1C or hNrf2 vector respectively for 24h under 18, 5 or 1kPa O_2. Data denote mean ± S.E.M., n=6 independent cultures. Two-way ANOVA with Tukey's multiple comparisons test. The 4-6 cultures are colour-coded to highlight changes within a given culture.
Abbreviations: Zn, zinc; ICP-MS, inductively coupled plasma mass spectrometry.

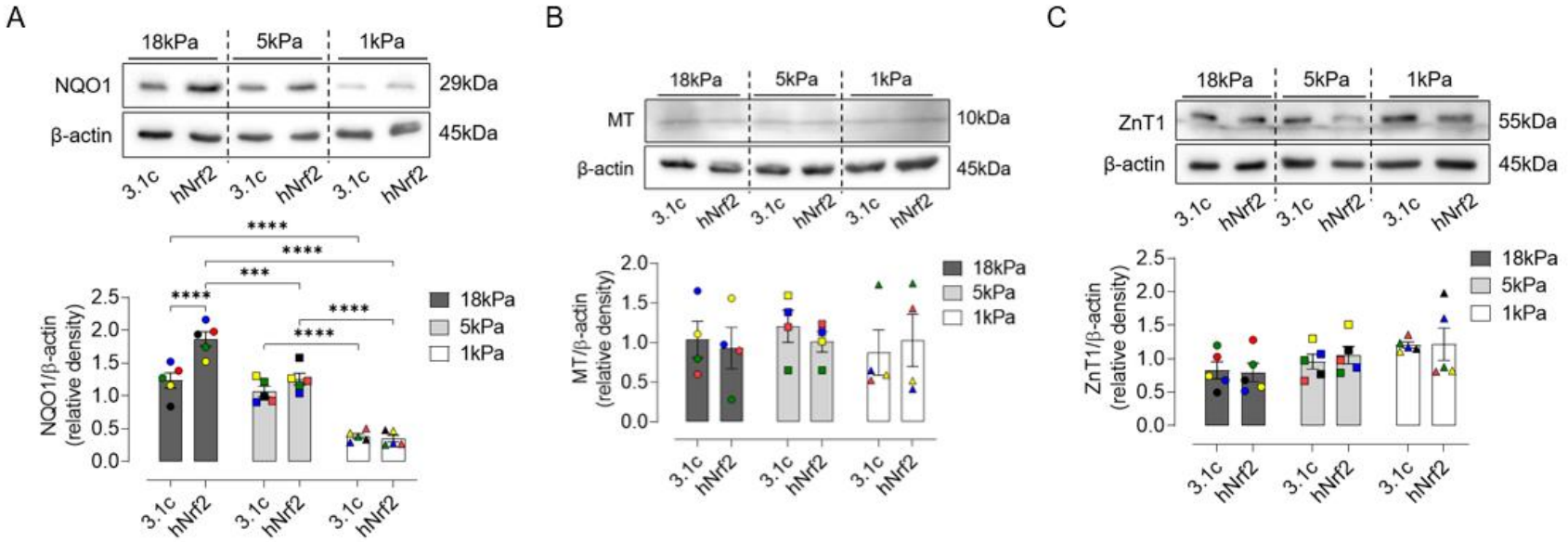

Figure 4.13 Nrf2 overexpression does not affect MT and ZnT1 protein expression in HCASMCs

HCASMCs were transfected with control vector 3.1C and hNrf2 vector respectively for 24 after adaptation for 5d to 18, 5 or 1kPa O_2. Representative immunoblots for NQO1 (A), MT (B) and ZnT1 (C) expression in immunoblots of HCASMCs transfected with control vector 3.1C and hNrf2 vector. Densitometric analyses of protein expression relative to β-actin. Data denote mean ± S.E.M., n=4-5 independent cultures, ***P<0.001, ****P<0.0001, Two-way ANOVA with Tukey's multiple comparisons test. The 4-5 cultures are colour-coded to highlight changes within a given culture.

Abbreviations: NQO1, NAD(P)H quinone dehydrogenase 1; MT, metallothionine; ZnT1, zinc transporter 1.

4.7 Effects of Nrf2 inducer sulforaphane on total Zn content in HCASMCs under 18, 5 and 1kPa O_2

Previous results in this thesis have shown that Nrf2 inducer sulforaphane (SFN) significantly upregulates Nrf2 regulated expression of NQO1 and HO-1 (**Figure 3.11 and 3.14**). However, when HCASMCs were treated with SFN the total cellular Zn content was not altered (**Figure 4.14A**), consistent with the finding that overexpression of Nrf2 did not change Zn levels (**Figure 4.12**). Although MT protein expression was unaffected in vehicle groups under 18 and 5kPa O_2, it trended to decrease under 1kPa O_2 (**Figure 4.14B**). Notably, MT and ZnT1 protein expression were not altered by SFN treatment in HCASMCs under 18, 5 or 1kPa O_2 (**Figure 4.14B and C**), consistent with the finding in cells with Nrf2 overexpression (**Figure 4.13**).

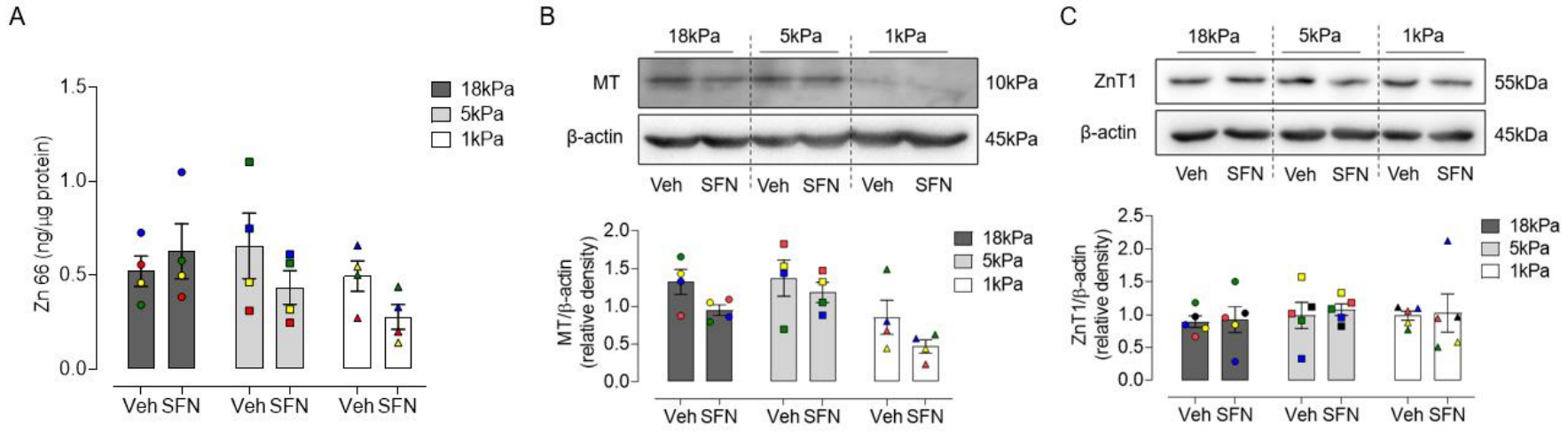

Figure 4.14 The Nrf2 inducer sulforaphane does not alter total Zn content or MT and ZnT1 protein expression in HCASMCs

ICP-MS analysis of total Zn (A) in HCASMCs adapted for 5d to 18, 5, or 1kPa O_2 and treated with SFN (2.5µM, 16h). Data denote mean ± S.E.M., n=4 independent cultures. Two-way ANOVA with Tukey's or Bonferroni's multiple comparisons test. Representative immunoblots of MT [1/2] (B) and ZnT1 (C) expression in HCASMCs treated with SFN (2.5µM, 16h), densitometric analyses of protein expression relative to β-actin. Data denote mean ± S.E.M., n=4-5 independent cultures. Two-way ANOVA with Tukey's multiple comparisons test. The 4-5 cultures are colour-coded to highlight changes within a given culture.

Abbreviations: SFN, sulforaphane, MT, metallothionine; ZnT1, zinc transporter 1.

Chapter 4 – Discussion

Over the past two decades, our increased understanding of metallomics has been paralleled by the growing number of primary research publications, providing insights into the role of metals in pro-oxidant and antioxidant pathological processes (Maret, 2018). Findings presented in this chapter provide the first metal profiles in HCASMCs adapted long-term to hyperoxia, physiological normoxia and hypoxia and the crosstalk between Zn and Nrf2 signalling.

In this study, metallomic profiling of HCASMCs adapted for 5d to 18, 5 or 1kPa O_2 was conducted by ICP-MS using a NexION 350D mass spectrometer (**Figure 4.1**). Total Zn levels were 0.345±0.037ng/µg protein in HCASMCs adapted to 18 kPa O_2 with similar values measured in cells under 5kPa and 1kPa O_2, highlighting cell specific differences in human coronary artery endothelia cells (HCAECs) (Smith et al., 2023) and mouse brain endothelial cell (bEnd.3) (unpublished data done by Dr Gabriela Warpsinki, King's College London). There was a significant increase in Cu under 1kPa O_2 compared to 18 or 5kPa O_2 groups. Meanwhile, changes in O_2 levels did not affect the concentrations of total Fe and Mg in HCASMCs. Total intracellular Mn content trented to decrease under 1kPa O_2. Parat et al. reported similar intracellular Zn content (0.394ng/µg protein) in HaCaT keratinocytes (Parat et al., 1997). In the context of this thesis, **Table 4.1** summarises metal distributions in different regions of the human heart. Establishing unique metal profiles in HCASMCs under relevant O_2 levels provides a basis for further studies of different metals in disease models and creates opportunities for new clinical tools relating perturbations in Zn with disease progression.

Table 4.1 The metal content in human heart tissue

Tissue/cell type	Measurement method	Disease status	Metal	Concentration	Reference
Heart	Inductively coupled plasma atomic emission spectroscopy	Normal + dilated or hypertrophied	Fe Cu Mn Zn	46.9 µg/g. wet weight 2.99 µg/g. wet weight 0.172 µg/g. wet weight 30 µg/g. wet weight	(Rahil-Khazen et al., 2002)
Heart	Inductively coupled plasma atomic emission spectroscopy	-	Fe Cu Mn Zn	52 µg/g. wet weight S.D.12 2.7 µg/g. wet weight S.D.0.64 0.29 µg/g. wet weight S.D.0.09 23 µg/g. wet weight S.D.4.9	(Yoo et al., 2002)
Heart Left ventricle	Atomic absorption spectrophotometry	Normal controls	Mg Fe Cu Mn	186 µg/g. wet weight S.D.25 46.8 µg/g. wet weight S.D.9.6 3.32 µg/g. wet weight S.D.0.66 1.07 µg/g. wet weight S.D.0.31	(Chipperfield and Chipperfield, 1978)
		Sudden heart death	Mg Fe Cu Mn	154 µg/g. wet weight S.D.27 38.5 µg/g. wet weight S.D.11 3.11 µg/g. wet weight S.D.0.44 0.96 µg/g. wet weight S.D.0.18	
		Late heart death	Mg Fe Cu Mn	173 µg/g. wet weight S.D.17 48.6 µg/g. wet weight S.D.8.1 2.84 µg/g. wet weight S.D.0.36 0.76 µg/g. wet weight S.D.0.23	
Heart Lateral wall of the left ventricle	Atomic absorption spectrophotometry	Normal controls	Mg Ca Cu Zn	177.06 µg/g. wet weight S.D.32.71 36.06 µg/g. wet weight S.D.10.72 3.22 µg/g. wet weight S.D.0.37 26.53 µg/g. wet weight S.D.3.99	(Shakibi et al., 1982)
		Cyanotic congenital heart disease	Mg Ca Cu Zn	155.66 µg/g. wet weight S.D.14.79 43.22 µg/g. wet weight S.D.7.01 2.94 µg/g. wet weight S.D.0.22 26.00 µg/g. wet weight S.D.4.15	
		Acute rheumatic heart disease, active carditis and severe congestive heart failure	Mg Ca Cu Zn	149.00 µg/g. wet weight S.D.13.29 46.30 µg/g. wet weight S.D.4.85 2.56 µg/g. wet weight S.D.0.32 26.40 µg/g. wet weight S.D.3.53	

(**Table 4.1** continued)

Tissue/cell type	Measurement method	Disease status	Metal	Concentration	Reference
Heart	Atomic absorption	Normal controls	Mg	114 µg/g. wet weight S.D.28	(Oster et al., 1993)
Right atrium	spectrophotometry		Fe	100 µg/g. wet weight S.D.25	
			Cu	3.2 µg/g. wet weight S.D.1.5	
			Zn	15 µg/g. wet weight S.D.4	
		Coronary heart disease	Mg	133 µg/g. wet weight S.D.38	
			Fe	129 µg/g. wet weight S.D.62	
			Cu	4.1 µg/g. wet weight S.D.2.0	
			Zn	18 µg/g. wet weight S.D.4	

Abbreviations: Fe, iron; Cu, copper; Zn, zinc; Mg, magnesium; Mn, manganese; S.D., standard deviation. Collaborated with Dr. Matthew Smith, King's College London.

Although zinc is a redox-inert metal, physiological concentrations of zinc have antioxidant, anti-inflammatory and anti-proliferative properties (Berger et al., 2004; Korichneva, 2006; Powell, 2000), whilst zinc deficiency or overload generates oxidative stress (Maret, 2006). Meanwhile, Nrf2 as an antioxidant transcription factor participates in maintaining redox homeostasis, which is influenced by intracellular zinc in human renal tubule cells (Li et al., 2014), human neuroblastoma cells (Kaufman et al., 2020) and murine spinal cord neurons (Ge et al., 2021; Li et al., 2020a). To investigate the effect of Zn on the Nrf2 signaling pathway in HCASMCs, pyrithione, a well-known ionophore for Zn, and TPEN, a chelator of Zn, were used (Karagulova et al., 2007; Parat et al., 1997). Compared to Zn alone, pyrithione can increase Zn uptake nearly 10-fold in rat oligodendrocyte progenitor cells (Ischia et al., 2019; Law et al., 2003). Based on cell viability experiments, 10μM $ZnCl_2$ and 0.5μM pyrithione were used to supply exogenous Zn in present study, and ICP-MS analysis confirmed a significant increase in intracellular Zn content in treated cells (**Figure 4.2**). Previous studies have reported that increased Zn levels in zebrafish cells and dendritic cells seconds or minutes after exogenous supplementation, whilst a change in labile Zn signal change is also observed hours after addition, both of which are associated with transcriptional regulation of transporters expression (Murakami and Hirano, 2008). Although increases of total Zn content in HCASMCs induced by Zn supplementation for 16h under 5 or 1kPa O_2 were less compared to 18kPa O_2, an early Zn wave may significantly increase intracellular Zn in cells under 18, 5 or 1kPa O_2 based on Zn supplementation induced Nrf2 nuclear accumulation. Meanwhile, labile Zn levels can enhance in cells within seconds or minutes and have been linked with transcriptional regulation of Zn transporters in hours after Zn supplementation (Maret, 2011, 2017b). Zn 'muffling' reaction modulate transient changes of cytosolic Zn after Zn supplementation via Zn transporters and zinc-binding proteins into a new balance by shuttling zinc ions into subcellular stores or by removing zinc ions from the

cell (Colvin et al., 2010). In cells treated with TPEN to chelate intracellular Zn, no statistical difference was detected between Veh and TPEN groups. Zn content was significantly lower in cells with TPEN treatment compared to cells supplemented with Zn under 18 and 1kPa (**Figure 4.3**). The inability of cells to tolerate higher concentrations of TPEN may in part account for the negligible difference in Zn content between Veh and TPEN groups.

Notably, Zn supplementation ($ZnCl_2$ (10μM) + pyrithione (0.5μM)) for 16h significantly induced Nrf2 nuclear accumulation in HCASMCs under 18, 5 and 1kPa O_2 (**Figure 4.4**). Xu et al. showed that punicalagin enhances Nrf2 nuclear translocation over 3-12h in a dose-dependent manner in rat small intestine epithelial IEC-6 cells (Xu et al., 2016), whilst Liang et al. found that pulmonary arterial SMCs treated with 5mM methamphetamine induces Nrf2 nuclear translocation at 24h and 36h but decreases at 48 h (Liang et al., 2020). It indicates that Nrf2 nucleus translocation is in a time and dose-dependent manner. Meanwhile, Zn addition significantly upregulated Nrf2 mediated HO-1 protein and mRNA expression with a similar trend observed for NQO1 expression under 18kPa O_2, whilst were markedly attenuated in cells under 5kPa O_2 (**Figure 4.5**). These findings are consistent with findings in rat testicular tissues, prostate cancer cells and spinal neuronal cells in air (Kwok, 2013; Li et al., 2020b; Qin et al., 2019). Overall, these data suggest that the Nrf2 signaling pathway is activated by Zn supplementation in HCASMCs adapted to 18kPa O_2 but to a lesser extent under 5 kPa O_2, which can be abrogated by TPEN addition.

Zinc is one of the most remarkable metals found in tissues because more than 3000 proteins in humans contain functional zinc-binding sites, with an estimate that ~10% of proteins are zinc proteins (Andreini et al., 2006; Maret, 2019). Zn plays structural, catalytic or signalling functions in numerous biological processes (Kambe et al., 2015). Previous studies reported that increased intracellular Zn^{2+} can modify both Keap1 and GSK3β, result in repression of

ubiquitination and stabilisation of Nrf2, which may in part explain our data (Kambe et al., 2015; Maret, 2006). Nrf2 protein levels are maintained relatively low under physiological condition due to rapid ubiquitination and proteasomal degradation mediated by Keap1 (Suzuki and Yamamoto, 2015). Meanwhile, GSK3β phosphorylates Nrf2, leading to β transducin repeats-containing proteins (βTrCP)-mediated degradation and Fyn-mediated nuclear exclusion (Culbreth and Aschner, 2018). Zn^{2+} can be sensed by histidine 225, cysteine 226 and 613 residues of Keap1, causing a change in Keap1 conformation (Jenkitkasemwong et al., 2012). It indicates that Zn^{2+} actives Nrf2 signaling indirectly through the loss of Keap1-mediated Nrf2 ubiquitination and degradation (McMahon et al., 2010; McMahon et al., 2018). Moreover, ZIP6-induced Zn influx inactivates GSK-3β, resulting in Snail dephosphorylation and leading to loss of cell adherence (Hogstrand et al., 2013). Protein kinases are involved in regulation of transcription factors and protein activity (Sun et al., 2009). Li et al. have described that Zn supplementation increases Akt and GSK-3β phosphorylation with a decrease in Nrf2 nuclear exporter, Fyn, in human renal tubular (HK11) cells, suggesting a role for Zn in Nrf2 expression and transcription function (Li et al., 2014). Moreover, Kaufman and Hou implicated Bach1, the mammalian repressor of HO-1, in Zn-induced protein upregulation of HO-1 due to Zn-mediated degradation of Bach1 (Hou et al., 2008; Kaufman et al., 2020).

Due to the importance of Zn in oxidative stress and cardiovascular disease, we further interrogated the effects of O_2 on zinc homeostasis by investigating levels of some of the key factors involved in zinc storage and transport. As forementioned in **Section 1.5.5**, tight control of cellular Zn levels via zinc transporters (ZIP1-14, importers and ZnT1-10, exporters), zinc-binding proteins (MT) and metal regulatory transcription factor 1 (MTF-1), zinc-sensing transcription factors (Maret, 2017a; Plum et al., 2010b). Oxidative stress and

hypoxia induce release of Zn from MT, a key transition metal ion-binding protein in cells (Maret, 2006), leading to the activation of MTF-1 and increased MT and ZnT1, the main Zn exporter in plasma membrane, gene expression, causing sequestration and extrusion of transiently increased labile zinc (Dalton et al., 1996; Gunther et al., 2012). MT-1 is widely expressed in human various tissues and participates in protection against stress responses due to its cysteinyl thiolate groups (Palmiter, 1987; Ruttkay-Nedecky et al., 2013). In the present study, there appears to be a no difference between 18 and 5kPa O_2, but a statistically significant reduction in MT protein expression between 1kPa and 5kPa (**Figure 4.6A**). MT1 mRNA expression was significantly upregulated by Zn supplementation in HCASMCs under 18, 5 and 1kPa O_2 (**Figure 4.6B**) compared to Veh or TPEN treatment, consistent with previous studies (Abdo et al., 2021; Dalton et al., 1996; Gu et al., 2017). There were no changes in total intracellular Zn, nor was basal ZnT1 protein expression affected by changes in pericellular O_2 levels as well. Moreover, ZnT1 protein expression was not altered by Zn supplementation in HCASMCs under 18, 5 and 1kPa O_2 (**Figure 4.7**).

Previous studies have shown that culturing cells under different O_2 levels has significant effects on the Keap1-Nrf2 signalling pathway (Chapple et al., 2016; Warpsinski et al., 2020), and it is known that Nrf2 can modulate zinc homeostasis (Ishida and Takechi, 2016b; Schwarz et al., 2019). For instance, mRNA levels of ZnT-1, 3 and 6 are significantly increased and ZnT10 and ZIP3 mRNA levels were significantly decreased by activation of Nrf2 in HepG2 Cells (Ishida and Takechi, 2016a). We therefore decided to determine whether intracellular total Zn levels were affected by Nrf2 signaling pathway in HCASMCS following long-term (5d) culture under hyperoxia, physiological normoxia or hypoxia. As shown in **Figure 4.8, 4.12 and 4.14**, HCASMCs showed negligible changes in total intracellular Zn levels following Nrf2 knockdown with siRNA or Nrf2 overexpression or

Nrf2 activation by SFN under 18, 5 or 1kPa O_2. Moreover, MT1 and ZnT1 protein expression were not significantly altered by Nrf2 knockdown or overexpression or SFN induced activation, with the exception that ZnT1 expression was decreased by Nrf2 knockdown in HCASMCs under 1kPa O_2 (**Figure 4.10, 13 and 14**). Although the efficiency of Nrf2 antibody is not good, induction of Nrf2-targeted HO-1 and NQO1 protein expression confirmed the success of knockdown and overexpression protocols.

As summaried in **Figure 4.15**, the Nrf2 signalling pathway was activated by Zn supplementation in HCASMCs adapted to 18, 5 and 1kPa O_2, whilst knockdown or overexpression or activation of Nrf2 signalling caused negligible changes in total intracellular Zn levels. In HCASMCs no significant differences in Zn levels were measured across different O_2 conditions tested.

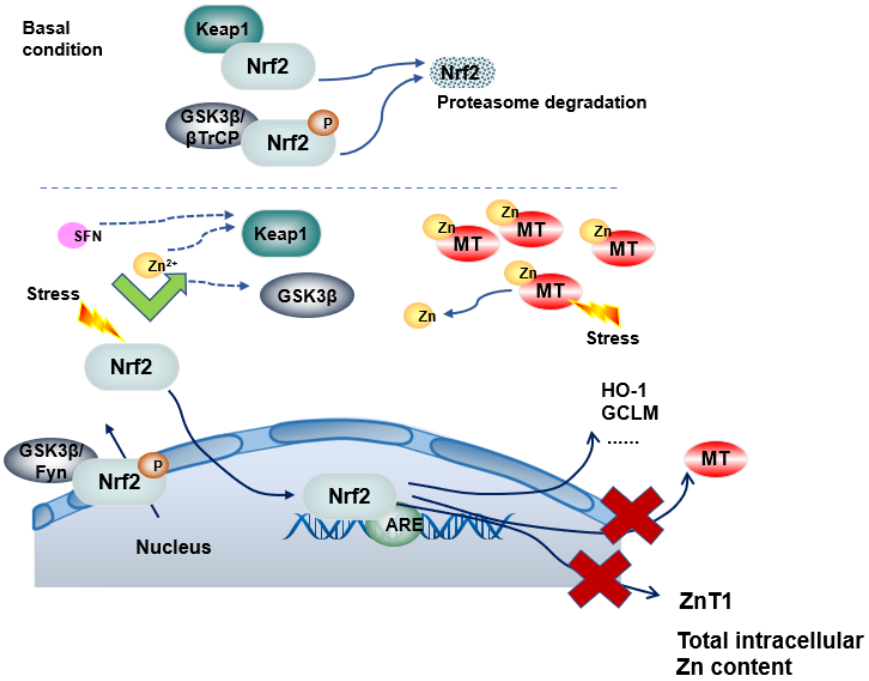

Figure 4.15 Graphical abstract of Chapter 4
Zn supplementation activated Nrf2 signalling pathway in HCASMCs under 18 and 5kPa O_2. Silencing or overexpressing Nrf2 did not alter total intracellular zinc content in HCASMCs and paralleled with MT and ZnT1 protein expression.

Chapter 5 – Results

Hypoxia-reoxygenation effect on HCASMCs under 18 or 5kPa O_2

Coronary IR injury is the key cause of morbidity and mortality, accounting for > 9 million deaths annually worldwide (Nowbar et al., 2019). The initial ischaemic and hypoxic damage is exacerbated by more severe injury caused by reperfusion and reoxygenation, mainly involving oxidative stress (Carden and Granger, 2000; Granger and Kvietys, 2015; Maxwell and Lip, 1997). This chapter studies reoxygenation induced free radical generation in HCASMCs under 18 and 5kPa O_2, and following pre-treatment with Zn or SFN to protect cells against the free radical burst during hypoxia-reoxygenation (HR). In addition, intracellular reduced GSH levels and total Zn levels were measured in HCASMCs under HR.

5.1 Reoxygenation induced free radical generation in HCASMCs under 18 and 5kPa O_2

To determine ROS generation during HR, HCASMCs pre-adapted to 18 or 5kPa were loaded with the luminescence probe L-012 and exposed to hypoxia (1h) and reoxygenation. As shown in **Figure 5.1**, ROS production was only detected on reoxygenation. In a similar experimental protocol, PEG- superoxide dismutase (pSOD) and PEG- catalase (pCAT) have been shown to inhibit superoxide dismutase and catalase, respectively, in brain microvascular endothelial cell line (bEnd.3) (Warpsinski et al., 2020). pSOD significantly inhibited reoxygenation-induced free radical generation in HCASMCs adapted to 18kPa, whilst pCAT had a negligible effect, indicating that reoxygenation most likely increases superoxide generation. As negligible changes in L-012 luminescence were detected after reoxygenation of cells pre-adapted to 5kPa for 5d, it is possible that the radical generation was too low to be

detected by L-012 probe or the probe lacked sensitivity to monitor low levels of radical generation at lower O_2 levels (**Figure 5.1C and D**).

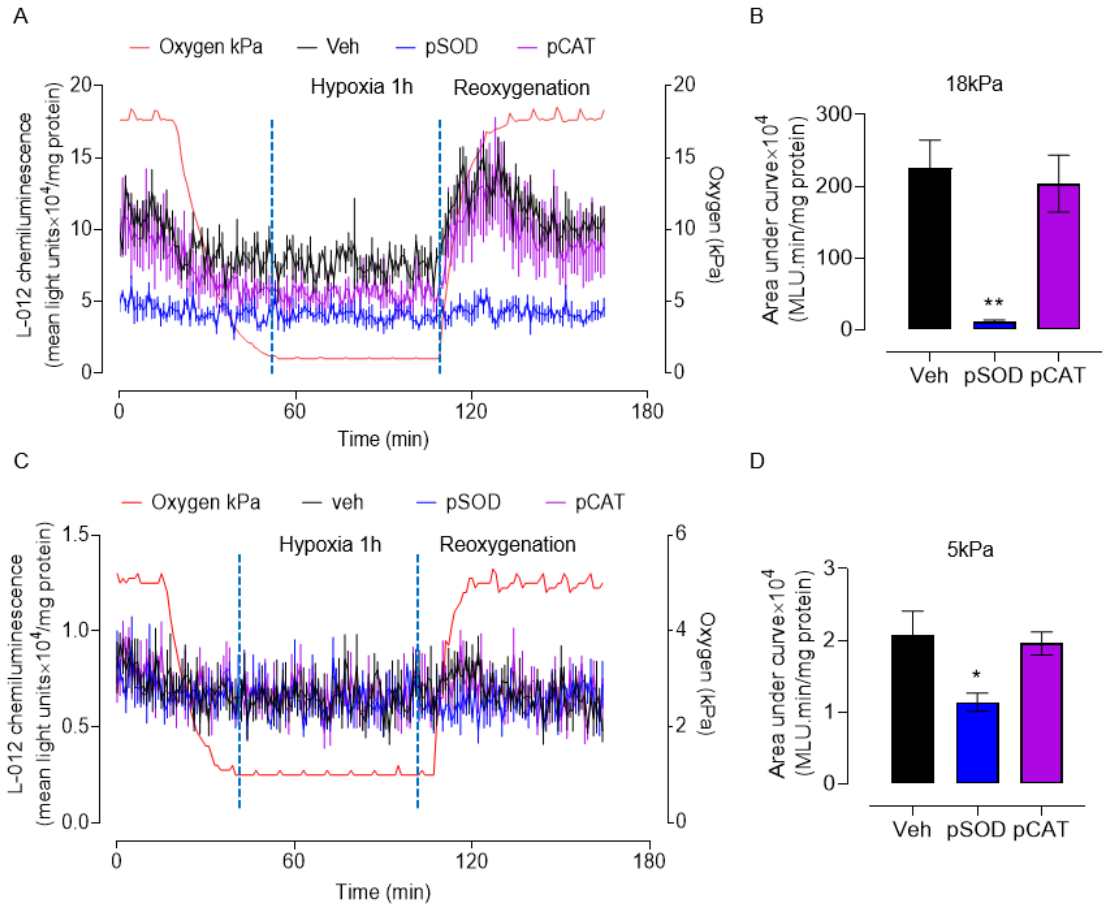

Figure 5.1 Reoxygenation induced ROS generation in HCASMCs under 18 and 5kPa O_2
(A and C) Representative L-012 traces in HCASMCs adapted to 18 or 5kPa O_2 for 5d. Cells were incubated with luminescence probe L-012 and treated with vehicle (0.005% DMSO), PEG-superoxide dismutase (pSOD, 20U/ml) or PEG-catalase (pCAT, 200U/ml). Cells were then rapidly transferred to an O_2-regulated plate reader and exposed to hypoxia (1h) and reoxygenation. The luminescence signal was detected in a plate reader gassed initially with 18 or 5kPa O_2. (CLARIOstar, BMG Labtech). (B and D) Area under curve summary of reoxygenation-induced luminescence changes. Data denote mean ± S.E.M., n=6 independent cultures, *P<0.05, **P<0.01, One-way ANOVA with Tukey's multiple comparisons test.
Abbreviations: Veh, vehicle; pSOD, PEG-superoxide dismutase; pCAT, PEG-catalase.

5.2 Effects of SFN, Zn or TPEN on superoxide production under hypoxia-reoxygenation

To investigate whether activation of the Nrf2 signaling pathway or Zn supplementation attenuates reoxygenation-induced free radical generation, cells were adapted long-term (5d) to 18 or 5kPa O_2 and incubated with the luminescence probe L-012 and exposed to HR after pre-treatment with SFN, Zn supplementation or a Zn^{2+} chelator, TPEN. **Figure 5.2 A and B** show that SFN or Zn significantly attenuate reoxygenation-induced superoxide generation under 18kPa O_2, with the effect of Zn supplementation abolished by TPEN. Negligible changes in L-012 luminescence were detected after reoxygenation in HCASMCs pre-adapted for 5d to 5kPa O_2 (**Figure 5.2C and D**).

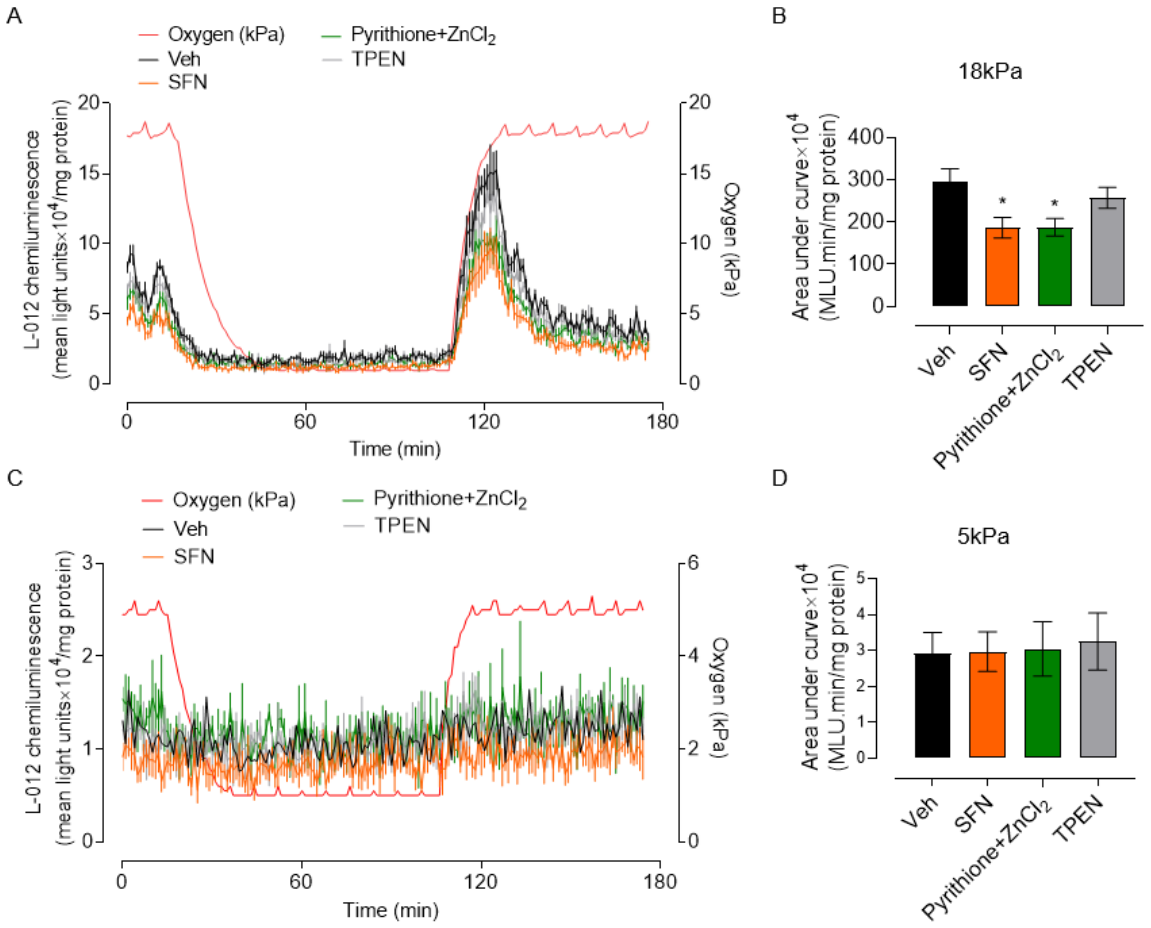

Figure 5.2 SFN or Zn supplementation attenuate reoxygenation-induced ROS production in HCASMCs
(A and C) Representative L-012 traces in HCASMCs adapted for 5d to 18 or 5kPa O_2 following with pre-treatment for 16h with (Vehicle (Veh, 0.005% DMSO), sulforaphane (SFN, a Nrf2 inducer, 2.5µM), TPEN (a Zn^{2+} chelator, 1.25µM) or 2-mercaptopyridine N-oxide sodium salt (pyrithione, a Zn^{2+} ionophore, 0.5µM) with $ZnCl_2$ (10µM) (Py+$ZnCl_2$)). Cells were then incubated with L-012 sodium salt. L-012 luminescence was detected by in a plate reader (CLARIOstar, BMG Labtech) gassed initially with 18 or 5kPa O_2. (B and D) Area under curve summary of reoxygenation-induced luminescence changes. Data denote mean ± S.E.M., n=4 independent cultures, *P<0.05, One-way ANOVA with Tukey's multiple comparisons test.
Abbreviations: Veh, vehicle; SFN, sulforaphane; TPEN, N,N,N′,N′-tetrakis(2-pyridinylmethyl)-1,2-ethanediamine; Py, pyrithione; $ZnCl_2$, zinc chloride.

5.3 Effects of hypoxia-reoxygenation on total Zn concentration in HCASMCs

Previous studies in this thesis established have indicated that HCASMCs have a similar total Zn content under 18, 5 and 1kPa O_2 level (see **Figure 4.1**). To determine whether total Zn levels in HCASMCs adapted (5d) to physiological normoxia (5kPa) or hyperoxia (18kPa) are altered by hypoxia-reoxygenation (HR) and cells lysates were analysed by ICP-MS. As shown in **Figure 5.3**, total Zn levels were not altered significantly by hypoxia (1h) and reoxygenation for 1h and 9h in cells pre-adapted to either 18kPa or 5kPa O_2.

A

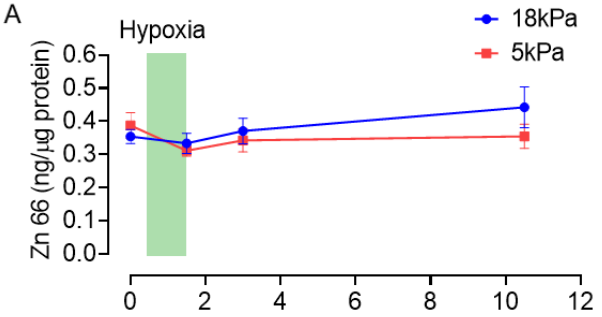

B

Zn66 (ng/µg protein)	18kPa O_2	5kPa O_2
Basal	0.354 ± 0.021	0.387 ± 0.039
Hypoxia 1h	0.334 ± 0.031	0.311 ± 0.016
Reoxygenation 1h	0.371 ± 0.038	0.343 ± 0.035
Reoxygenation 9h	0.443 ± 0.062	0.355 ± 0.037

Figure 5.3 Total Zn content in HCASMCs pre-adapted to 18 or 5kPa O_2 and exposed to hypoxia-reoxygenation
(A) Total Zn content under basal conditions, hypoxia (1h), hypoxia-reoxygenation (1h and 9h) in HCASMCs pre-adapted to 18 or 5kPa O_2 was measured by ICP-MS. O_2 changes between 18kPa or 5kPa and 1kPa take 30 minutes. (B) Summary table of values for each time point. Data denote mean ± S.E.M., n=4-10 independent cultures. Two-way ANOVA with Tukey's multiple comparisons test.
Abbreviations: Zn, zinc; ICP-MS, inductively coupled plasma mass spectrometry.

5.4 Intracellular reduced GSH levels in HCASMCs under hypoxia-reoxygenation

GSH, as an antioxidant, is capable of protecting cells preventing against IR injury (Meister and Anderson, 1983). GSH is rich in thiol groups, which can bind Zn^{2+} through non-enzymatic conjugation to maintain Zn^{2+} homeostasis. GSH inhibits Zn^{2+} release from cells in the absence of GSSG, with GSH/GSSG working as a redox cycle (Gonzalez-Iglesias et al., 2014; Higashi et al., 2021; Oteiza, 2012). To investigate whether intracellular reduced

GSH levels were affected by HR, HCASMCs pre-adapted to 18 or 5kPa O_2 were exposed to hypoxia (1h) and short-term (1h) or longer-term (24h) reoxygenation and GSH levels were measured. Basal intracellular glutathione (GSH) levels in HCASMCs were not altered by O_2 (18kPa O_2: 25.82 ±2.67 nmol/mg protein versus 5kPa O_2: 21.34 ±1.32 nmol/mg protein), consistent with measurements in **Figure 3.8**. Compared to negligible changes under 5kPa O_2, GSH levels in HCASMCs adapted to 18kPa showed a significant increase under hypoxia (44.24 ±7.53 nmol/mg protein) and gradually decreased during reoxygenation for 1h (38.09 ±5.33 nmol/mg protein) and 24h (31.86 ±4.60 nmol/mg protein) (see **Figure 5.4**). Notably, GSH levels were significantly lower in cells under hypoxia after pre-adaptation to 5kPa compared to 18kPa O_2.

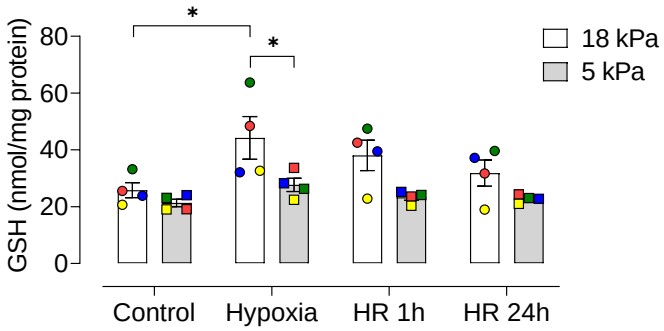

Figure 5.4 Intracellular reduced GSH levels in HCASMCs under hypoxia-reoxygenation
GSH levels under hypoxia (1h) and reoxygenation (1h and 24h) in HCASMCs pre-adapted to 18 or 5kPa O_2 measured using a fluorometric assay. Data denote mean ± S.E.M. n=4 independent cultures. *P<0.05, Two-way ANOVA with Tukey's multiple comparisons test. Independent cultures are coded by coloured data points.
Abbreviations: GSH, glutathione; HR, hypoxia-reoxygenation.

5.5 Effects of hypoxia-reoxygenation on Nrf2-regulated target protein expression

Previous experiments suggested that activation of Nrf2 by SFN pre-treatment abrogated the reoxygenation-induced superoxide generation in HCASMCs under 18kPa O_2, whilst negligible changes in L-012 luminescence were detected in cells under 5kPa O_2 (see **Figure 5.2**). We thus further investigated whether Nrf2-regulated target protein expression is altered

by HR. As shown in **Figure 5.5**, basal NQO1 protein decreased in HCASMCs as ambient O_2 levels from 18 to 5kPa O_2, whilst basal GCLM protein expression had negligible change in cells under 18 or 5kPa O_2, consistent with results in **Figure 3.11**. Moreover, NQO1 protein expression trended to increase after reoxygenation in cells under 18kPa O_2, and GCLM trended to increase after hypoxia in cells under 18kPa O_2. Notably, both NQO1 and GCLM expression were affected negligibly in cells pre-adapted to 5kPa O_2 and then exposed to hypoxia-reoxygenation.

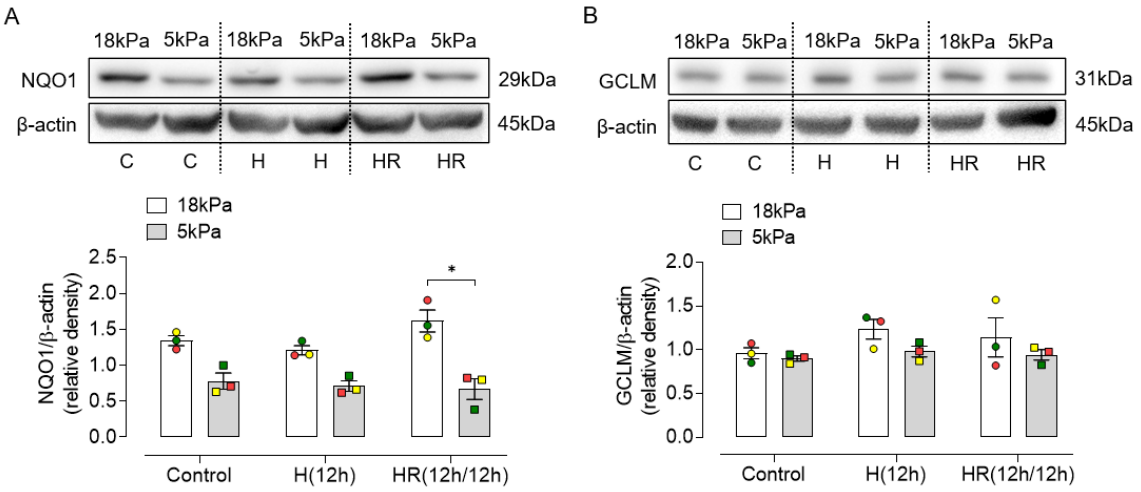

Figure 5.5 NQO1 and GCLM protein expression in HCASMCs under hypoxia-reoxygenation
NQO1 and GCLM expression in HCASMCs pre-adapted for 5d to 18 or 5kPa O_2 and then subjected to hypoxia (12h) and reoxygenation (12h) under 18 or 5kPa O_2. Densitometric analyses of protein expression relative to β-actin. Data denote mean ± S.E.M. n=3 independent cultures, Two-way ANOVA with Tukey's multiple comparisons test. Independent cultures are coded by coloured data points.
Abbreviations: NQO1, NAD(P)H quinone dehydrogenase; GCLM, glutamate-cysteine ligase modifier subunit; H, hypoxia; HR, hypoxia-reoxygenation.

5.6 Effects of hypoxia-reoxygenation injury on ZnT1 protein expression in HCASMCs

As shown in **Figure 5.3**, exposure of HCASMCs to hypoxia (1h) and reoxygenation (1h and 9h) had no effect on total intracellular Zn level. It is known that free Zn^{2+} accumulates in cardiomyocytes after hypoxia, whilst reoxygenation reduces free Zn^{2+} concentration,

resulting from cytosolic and mitochondrial Zn^{2+} release (Bodiga et al., 2017; Karagulova et al., 2007; Lin et al., 2011b). We therefore determined whether ZnT1 protein expression in HCASMCs was altered by HR. Although there were negligible changes in cells under 5kPa O_2, ZnT1 protein expression trended to increase after reoxygenation for 12h in HCASMCs adapted to 18kPa O_2 (**Figure 5.6**), potentially reflecting increased efflux of Zn after reoxygenation.

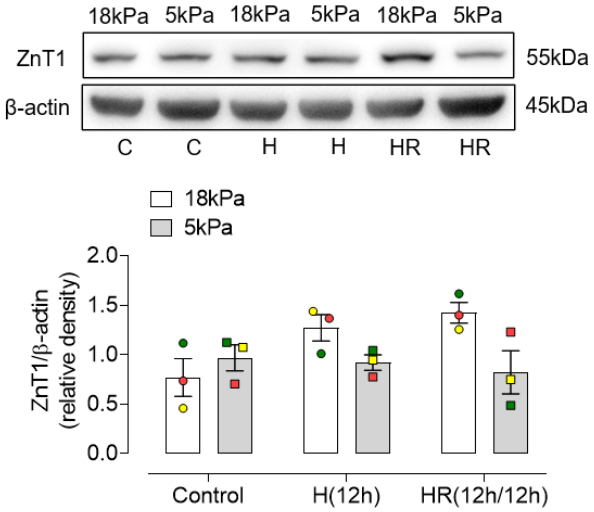

Figure 5.6 ZnT1 protein expression in HCASMCs under hypoxia-reoxygenation
ZnT1 expression under hypoxia (12h) and reoxygenation (12h) in HCASMCs pre-adapted for 5d to 18 or 5kPa O_2. Densitometric analyses of protein expression relative to β-actin. Data denote mean ± S.E.M., n=3 independent cultures, Two-way ANOVA with Tukey's multiple comparisons test. Independent cultures are coded by coloured data points.
Abbreviations: ZnT1, zinc transporter 1; H, hypoxia; HR, hypoxia-reoxygenation.

Chapter 5 – Discussion

IR injury occurs in a variety of pathophysiological processes such as myocardial infarction and stroke. As the basal redox phenotypes and metal profiles of HCASMCs under hyperoxia, physiological normoxia and hypoxia were described in Chapters 3 and 4, a model of HR injury was established to further investigate changes in ambient O_2 levels on redox signalling. HR injury is complex, involving not only changes in ROS generation but also disruption of

Zn^{2+} homeostasis (Feng et al., 2012; Higashi et al., 2021). Findings in this chapter are the first to examine how the Nrf2 signalling pathway and GSH levels are altered by HR in HCASMCs. Furthermore, the present study highlights (i) a protective function of Zn supplementation in HCASMCs exposed to HR, (ii) total intracellular Zn levels under HR and (iii) links Zn with redox responses under HR.

To characterize the effects of HR on HCASMCs, ROS generation was measured using the luminescence probe L-012 probe (Zielonka et al., 2013). It is well known that free radicals are generated after reoxygenation and play a key role in the pathogenesis of reoxygenation injury (Granger and Kvietys, 2015; Kalogeris et al., 2012). The present study demonstrated for the first time that changes in L-012 luminescence provide a useful measure of reoxygenation-induced ROS in HCASMCs under 18kPa O_2. As shown in **Figure 5.1**, the ROS burst was significantly diminished by pSOD but not pCAT, indicating that ROS are predominantly superoxide anions. These data are consistent with previous findings in HCASMCs, brain microvascular endothelial (bEnd.3) cells and human aortic endothelial cells (ECs) (Feng et al., 2012; Warpsinski et al., 2020; Zweier et al., 1994). In contrast to previous findings reporting increased ROS generation in rat pulmonary microvascular ECs under hypoxia for 1h and 4h (Kayyali et al., 2001), no significant ROS generation was observed in HCASMCs exposed to hypoxia for 1h in present study. It is possible that this is due to the low level of O_2 substrates available for ROS production. In this context, Kelmanson et al. reported only a slight decrease in H_2O_2 levels in the cytosol and mitochondria of neurons exposed to hypoxia for 30min using genetically encoded fluorescent biosensors (Kelmanson et al., 2021), finding consistent with our results. In HCASMCs, reoxygenation-induced superoxide generation was not detectable in cells adapted to 5kPa O_2, suggesting that radical

generation is too low to be detected by L-012 probe or the probe itself lacks sensitivity to monitor low levels of radical generation (Warpsinski et al., 2020).

As described in Chapter 3, SFN, a classic activator of Nrf2, significantly enhanced Nrf2-targeted protein expression (e.g. NQO1, HO-1 and GCLM) under hypoxic, normoxic and hyperoxic conditions. In **Figure 5.2**, activation of Nrf2 by SFN significantly attenuated reoxygenation-induced superoxide generation in cells pre-adapted to 18kPa O_2, suggesting a protective role of Nrf2 signalling pathway in HR injury. Meanwhile, Zn supplementation activates Nrf2 in HCASMCs under hypoxia, normoxia and hyperoxia (see **Figure 4.4** and **4.5**), and pre-treatment with Zn for 16h diminished reoxygenation-induced superoxide generation in cells, which was abrogated by TPEN, the classic chelator of Zn (see **Figure 5.2)**. Although the mechanisms of Zn mediated protection against oxidative stress are complex and overlapping as described in **Figure 1.12**, the present study suggests Zn mediates protection against HR injury in HCASMCs via activation of the Nrf2-HO-1 pathway. Interestingly, only a few studies have reported that combined SFN and Zn treatment potentiates Nrf2 targeted protein expression compared to a single treatment in human renal tubule cells *in vitro* and mouse kidney *in vivo* under the diabetic conditions (Li et al., 2014; Wang et al., 2019).

We further investigated whether the intracellular Zn content changes under HR, as previous studies have demonstrated that the plasma magnesium (Mg), calcium (Ca), potassium (K), zinc (Zn) and nickel (Ni) were significantly lower in acute coronary syndrome (ACS) patients (Ising et al., 1987; Solini et al., 2006; Yin et al., 2017). As shown in **Figure 5.3**, Zn levels were affected negligibly by hypoxia (1h) and reoxygenation (1h and 9h) in HCASMCs pre-adapted to 5kPa and 18kPa O_2. Although ZnT1 protein expression were affected negligibly in cells under 5kPa O_2, ZnT1 protein expression trended to increase after

reoxygenation for 12h in HCASMCs adapted to 18kPa O_2, suggesting that reoxygenation may be associated with enhanced Zn efflux (**Figure 5.6**). Notably, it is known that labile Zn^{2+} actually participates in redox cycles and binds thiols of the amino acid cysteine (Krezel et al., 2007; Maret, 2006). The effect of HR or IR on labile Zn^{2+} were summarized in **Table 5.1**. At present, *in vitro* labile Zn^{2+} content in cells under HR injury adapted to physiological normoxia is poorly understood and thus merits future experiments.

Table 5.1 Effect of hypoxia-reoxygenation or ischaemia-reperfusion on Zn content

Species	Cell type/ Tissue	HR/IR duration	Measurement method of labile Zn^{2+} level	Main findings	Reference
Human	Pulmonary artery smooth muscle cells	48h H	eCALWY-4 fluorescence probe	Labile Zn^{2+} ↑ under hypoxia- mediated by ZIP12	(Zhao et al., 2015)
Rat	Cardiomyocytes	6h H/18h R	FluoZin-3 fluorescence probe	Labile Zn^{2+} ↑ under hypoxia- enhanced expression of ZIPs; labile Zn^{2+} ↓ during reoxygenation- lowered expression of all ZIPs, elevated levels of ZnT2 and 5	(Bodiga et al., 2017)
Rat	Cardiomyocytes	15-30min I/30min R	TSQ fluorescence probe	labile Zn^{2+} ↓ under ischaemia	(Karagulova et al., 2007)
Rat	Cardiomyocytes	Intermittent 30min H/30min R	FluoZin-3 and RhodZin3 fluorescence probe	Labile Zn^{2+} ↑ under intermittent HR	(Lien et al., 2018)
Rat	Heart	30min I/2h R	FluoZin-3 and RhodZin3 fluorescence probe	Labile Zn^{2+} ↑ under ischaemia; Labile Zn^{2+} ↑↑ under reperfusion	(Lin et al., 2011b)
Rat	Heart	30min I/2h R	Inductively coupled plasma optical emission spectroscopy	Total Zn^{2+} ↓ under IR	(Xu et al., 2014b)
Mouse	Neuron	0-15min OGD	FluoZin-3 fluorescence probe	Labile Zn^{2+} ↑ after ~6–8min of oxygen-glucose deprivation, which is taken up by mitochondria	(Medvedeva et al., 2009)
Mouse	Heart	45min I/10min R	Zinpyr-1 fluorescence probe	Labile Zn^{2+} ↑ under IR- mediated by ZIP7	(Zhang et al., 2021)
Mouse	Heart	30min I/2h R	Inductively coupled plasma optical emission spectroscopy	Total Zn^{2+} ↓ under IR- induce ZIP2 upregulation	(Du et al., 2019)

Abbreviations: HR, hypoxia-reoxygenation; IR, ischaemia-reperfusion; OGD, oxygen-glucose deprivation; ZIP, Zrt- and Irt-like proteins; ZnTs, zinc transporter proteins.

In addition, as summarized in **Figure 5.7**, GSH plays a protective role against oxidative stress as a free radical scavenger, and the thiol group of GSH have a high affinity for Zn^{2+} affording protection against Zn^{2+} dysregulation (Higashi et al., 2021). In **Figure 5.4**, although there was negligible change under 5kPa, GSH levels in HCASMCs adapted to 18kPa showed a significant increase under hypoxia and a gradual decrease after reoxygenation over 1h to 24h, indicating elevated levels of GSH in response to hypoxia and restoration of basal GSH levels under reoxygenation. Similarly, Makarov et.al. reported that in astroglial-rich cultures total GSH levels are not altered significantly after hypoxia (1h) but decrease gradually after reoxygenation (Makarov et al., 2002). Geihs et al. found that GSH content in locomotor muscle of the crab decreases during 3h hypoxia (65%) and 30 min (62%) and 2h (65%) of reoxygenation (Geihs et al., 2016). Moreover, GSH/GSSH content decreases in calf pulmonary artery tissue under hypoxia for 14d (Hartney et al., 2011). Although there were no significant changes in total Zn levels under HR, changes in GSH levels may reflect changes in labile Zn^{2+} accumulation under hypoxia and reoxygenation, as Zn^{2+} binds to thiol cysteines residues of GSH and consumes GSH, consistent with previous findings that labile Zn^{2+} increases under hypoxia and decreases after reoxygenation (Bodiga et al., 2017; Karagulova et al., 2007; Lin et al., 2011b). Moreover, oxidized GSH (GSSH) mediates release of Zn from MT and other Zn-thiol clusters (Oteiza, 2012).

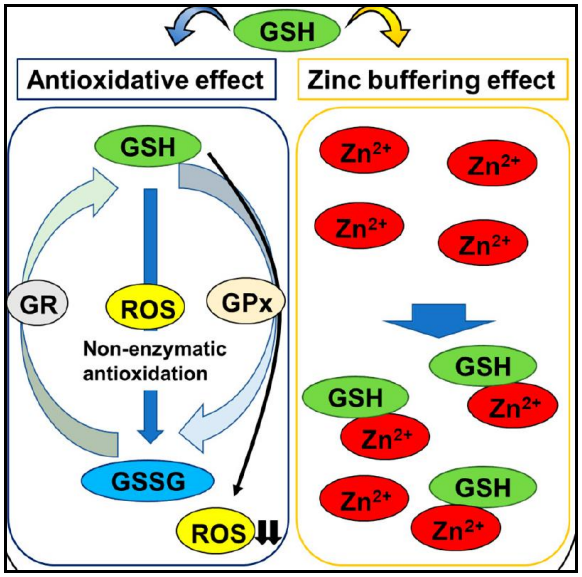

Figure 5.7 Effects of GSH on cellular antioxidant status and Zn buffering in neurons following brain ischaemia
GSH is oxidized and converted into GSSG by glutathione peroxidase (GPx), which is subsequently reduced to GSH by glutathione reductase (GR). GSH acts as an intrinsic factor that buffers intracellular Zn^{2+} concentrations and protects against dysregulation of Zn levels under brain ischaemia. Taken from (Higashi et al., 2021).
Abbreviations: GSH, glutathione; GSSH, glutathione disulfide; GR, GSH reductase; GPx, GSH peroxidase; ROS, reactive oxygen species; Zn^{2+}, labile zinc.

Although it is well known that Nrf2, as an antioxidant transcription factor, plays an important cardioprotective role in myocardial IR injury (Cadenas, 2018; Chen and Maltagliati, 2018), in the present study NQO1 and GCLM protein expression were affected negligibly under HR in HCASMCs pre-adapted to 5kPa O_2 (see **Figure 5.5**), consistent with the negligible in change of L-012 luminescence in cells under 5kPa. NQO1 protein expression trended to be enhanced after reoxygenation in cells under 18kPa O_2, and GCLM trended to be increased after hypoxia in cells under 18kPa O_2 (see **Figure 5.5**), suggesting that upregulation of Nrf2 downstream antioxidant proteins may potentially afford protection against IR injury *in vivo*. A previous report has shown that hypoxia for 16h followed by reoxygenation led to Nrf2 nuclear accumulation (within 2h) and increased NQO1 expression in human renal and colonic epithelial cells (Leonard et al., 2006), which is consistent with the trends for Nrf2 target enzymes in the present study. HR is widely used in *in vitro* experimental models to replicate *in vivo* IR injury. On the one hand, Allison et al. reported that IR and HR showed similar

effects in dog lungs, with a modest increase in vascular permeability and predominantly an increase in vascular resistance (Allison et al., 1990). Hypoxia accompanied by glucose and serum deprivation in HR models of freshly isolated adult mouse cardiomyocytes showed similar characteristics to *in vivo* IR conditions (Portal et al., 2013). On the other hand, findings obtained under HR in cell culture models *in vitro* may differ from actual changes induced by IR injury. For instance, Kelmanson et al. reported that the pH decreases from 7.25 to 6.7 in the first few minutes after ischaemia in the core zone of ischaemia stroke in rats and remains at a low level for much longer after reperfusion compared to pH dynamics in cultured mouse neurons during HR (Kelmanson et al., 2021). Foy et al. reported that pH in porcine coronary artery SMCs is not altered significantly under HR using the fluorescent pH indicator BCECF-AM (Foy et al., 1997). Previous measurements performed in our laboratory by Dr. Matthew smith showed pH in cytoplasm and mitochondria of human embryonic kidney HEK293 cell line were not altered under HR using the fluorescent pH sensor SypHer (unpublished data). In present study, Compared to physiological normoxia, HR under hyperoxia hyperoxia enhanced ROS generation, Nrf2-targeted protein expression or GSH levels, suggesting a higher oxidative stress-induced antioxidant responses in cells under 18kPa O_2. Moreover, a potential limitation of the HR model in the current study is that cells were not deprived of glucose and serum, as we also investigated Zn profiles in this study, and these cells typically obtain Zn from serum in the culture medium. Alternatively, it is likely that any HR induced changes under 5kPa O_2 are too low to be detected. Regardless, further experiments are warranted to investigate redox signalling in HCASMCs, and other cell types adapted to physiological normoxia.

As summarized in **Figure 5.8**, a ROS burst, mainly superoxide was detected in first 20min after reoxygenation in HCASMCs under 18kPa O_2 and was significantly attenuated by

pre-treatment of cells with SFN or Zn. Although these findings implicate activation of Nrf2 and Zn supplementation in the protection against HR injury, HR had a negligible effect on intracellular total Zn levels in HCASMCs under 18 or 5kPa O_2.

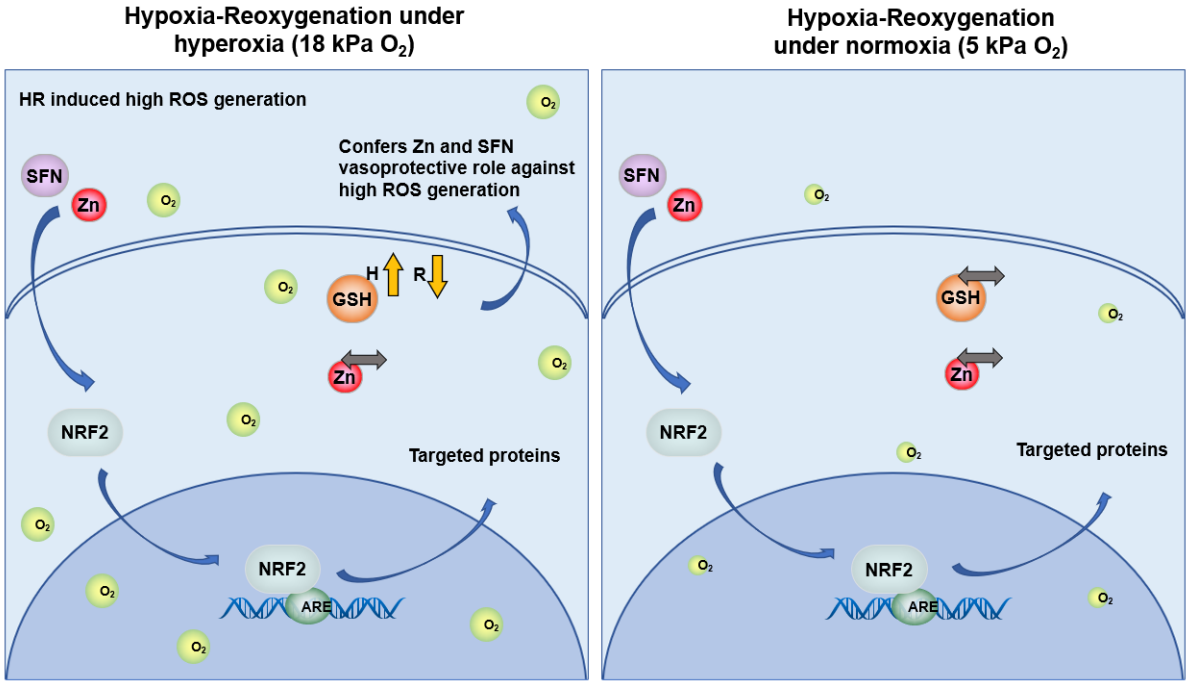

Figure 5.8 Graphical abstract for Chapter 5
Reoxygenation induces higher ROS generation in HCASMCs adapted to 18kPa O_2 compared to 5kPa O_2. Zn and SFN have protective effects against oxidative stress under hypoxia-reoxygenation.

Chapter 6 – General Discussion

6.1 Summary and significance

The present study aimed to further establish the importance of physiological O_2 levels for investigating the redox phenotype and metal profile of *in vitro* cell culture models, thereby recapitulating *in vivo* oxygen levels to improve translation of findings from bench to bedside. Moreover, the present study aimed to investigate antioxidant mechanisms involved in ischaemia-reperfusion (IR) injury under physiological O_2 levels, and to highlight protective roles of sulforaphane (SFN), an activator of Nrf2, and metal Zn in IR injury and crosstalk between these redox signalling pathways.

6.2 Adaptation to physiological normoxia alters the redox phenotype and metal profile in a cell-type specific manner

HCASMCs were cultured under hyperoxia (18kPa), physiological normoxia (5kPa) or hypoxia (1kPa) for at least 5 days to stabilize HIF-1α protein expression (Keeley and Mann, 2019), as confirmed in this study. Monolayer cells cultured *in vitro* under 5kPa O_2 replicates O_2 levels in blood perfusing in human coronary artery, and an intracellular O_2 level of 3.98 ±0.11kPa was measured in HCASMCs. Findings in Chapter 3 demonstrate that HCASMCs adapted to hyperoxia (18kPa O_2) exhibit a lower proliferation rate and synthetic phenotype differentiation compared to cells maintained under physiological normoxia (5kPa O_2), indicating that pericellular O_2 levels affect migration, proliferation and the spreading of VSMCs, which are associated with disease mechanisms such as angiogenesis and atherosclerosis.

In the present study, intracellular ATP levels, reduced GSH, catalase (CAT) protein expression, SFN-induced Nrf2-targeted, GCLM, GCLC and HO-1 expression were not significantly altered by long-term adaptation to 18kPa O_2 compared to cells under 5kPa O_2, suggesting that pre-adaptation to hyperoxia does not significantly alter the redox phenotype of HCASMCs. These findings appear to be cell-type specific, as umbilical vein, mouse brain microvascular and coronary artery endothelial cells exhibit enhanced Nrf2 activation under 18kPa O_2 compared to 5 kPa O_2 (Chapple et al., 2016; Warpsinski et al., 2020). Additionally, Stuart and colleagues have reported that pericellular O_2 levels (5 or 18kPa O_2 for 14d) affect the transcript abundance of hundreds of genes (e.g. mitochondrially-encoded genes and HIF-1 targeted genes) in human cancer cell line in a cell-type specific manner with overlap (Alva et al., 2022). Thus, it is important to recapitulate hypoxia and physiological normoxia for different cell types, especially for studies aimed at defining antioxidant defense mechanisms in cellular models *in vitro*.

Interestingly, intracellular homeostasis of metals such as Zn, Fe and Cu are interrelated with cellular responses to oxygen tension and oxidative stress, which may serve as new biomarkers for diagnosis and therapeutic drugs (Maret, 2018; Yin et al., 2017). As highlighted in Chapter 4, the present study reports the first metal profiling in HCASMCs adapted long-term to 18, 5 and 1kPa O_2. There were negligible changes in total Zn content in cells under 18, 5 and 1kPa O_2. Total intracellular Cu content increased in cells under 1kPa O_2 compared to 18 or 5kPa O_2, whilst there were no significant differences in total Fe and Mg content across the O_2 conditions and Mn content trended to be lower in cells under 1kPa O_2. In contrast, in parallel studies in human coronary artery endothelial cells (HCAECs), Zn and Cu levels trended to decrease as pericellular O_2 levels were lowered (unpublished data),

indicating that compared to physiological normoxia, adaptation to hyperoxia (cultured in air) changes cellular metal profile in a cell-specific manner.

6.3 Crosstalk between Zn and Nrf2 and Zn homeostasis regulation

In present study, antioxidant characteristics of Zn and crosstalk between Zn and Nrf2 were investigated. As previously discussed, Zn can modify Keap1 and GSK3β conformation, inducing Nrf2 translocation into nucleus and upregulating antioxidant gene expression (Hogstrand et al., 2013; Jenkitkasemwong et al., 2012). As described in Chapter 4, Nrf2 signalling activated by Zn supplementation in HCASMCs adapted long-term to 18, 5 and 1kPa O_2, as evidenced by Nrf2 nuclear accumulation. However, Zn supplementation significantly increased total Zn content, HO-1 mRNA and protein expression in HCASMCs under 18kPa O_2, which was markedly attenuated in cells under 5kPa O_2. Interestingly, Nrf2 nucleus translocation and upregulation of HO-1 and NQO1 protein expression had negligible change in HCASMCs treated with SFN under 18 or 5kPa O_2, and Nrf2 gene silencing significantly abrogated SFN-induced upregulation of HO-1 and NQO1. These novel findings suggest that compared to 5kPa O_2, HCASMCs have more Zn antioxidant capacity to against oxidative stress than SFN induced Nrf2 antioxidant capacity under 18kPa O_2. Furthermore, both SFN and Zn enhance HO-1 and NQO1 protein expression by activating Nrf2. Previous studies have shown that both of SFN and Zn can trigger activity of ERK1/2, a Nrf2 upstream kinase, which can induce Nrf2 dissociation from Keap1 and Nrf2 translocation into nucleus and then upregulate antioxidant gene expression such as HO-1 and NQO1 (Anson et al., 2021; Shin et al., 2019; Sindreu et al., 2011; Sun et al., 2009; Ye et al., 2022).

Notably, metal homeostasis is maintained by tight regulation of uptake, storage and secretion. Zinc homeostasis is mainly mediated by zinc transporters (ZnT1-10 (exporter of Zn) and ZIP1-14 (importer of Zn)), zinc-binding proteins such as metallothionein (MT) and metal regulatory transcription factor 1 (MTF-1), zinc-sensing transcription factors, many of which are differentially altered by oxidative stress or ambient oxygen levels (see **Table 6.1**) (Maret, 2017a; Plum et al., 2010b). In addition to two ZnTs (ZnT1 and ZnT10) located in the plasma membrane, most ZIPs transporters are found on the plasma membrane, indicating that the importance of ZIPs in regulating Zn supply from extracellular environment (Bosomworth et al., 2012; Maret, 2017a). ZIPs have been known to mainly transport Zn, but some such as ZIP8 and ZIP14 can also transport Fe, Mn and Cd (Fujishiro et al., 2012; Jenkitkasemwong et al., 2012). Subcellular localization of zinc transporters are shown in **Figure 6.1**. Moreover, Tran et al. have shown that Zn transporters located differentially among ECs and SMCs in human subcutaneous microvessels. ZIP10 and 14 are approximately equally expressed in ECs and SMCs, ZIP1, 2, 8 and 12 are relatively more abundant in ECs and ZIP14 is richer in SMCs (Tran et al., 2022). In addition, Zn storage has a characteristic membrane-bound vesicle structure termed zincosomes, which function similarly to ferritin storage of iron (Beyersmann and Haase, 2001; Haase and Maret, 2003).

Table 6.1 Zinc regulating genes and relation to oxygen

Gene name	Gene symbol	Tissue of major expression	Cellular localisation	Mechanism of zinc regulation	References	Oxygen or oxidative stress regulated	References
ATPase cation transporting 13A2/ PARK9	ATP13A2	Brain	Cytoplasm, intracellular membrane	Facilitates transport of zinc into membrane-bound compartments or vesicles	(Kong et al., 2014; Tsunemi et al., 2014)	PHD2-HIF-1α regulated in response to hypoxia	(Rajagopalan et al., 2016)
Adaptor related protein complex 3 subunit beta 1	AP3B1	Ubiquitous	Nucleus, Golgi, intracellular membrane	Facilitates vesicular zinc accumulation	(Yang et al., 2000)	No evidence	
ATPase copper transporting beta	ATP7B	Liver, gallbladder, brain	Golgi	Transporter that has low affinity for zinc and possibly regulates several zinc transporters	(Meacham et al., 2018)	No evidence	
Fc fragment of IgE receptor I (tetrameric)	FCER1-A/G and MS4A2	Langerhans cells, eosinophils, mast cells, basophils	Plasma membrane	Stimulates a 'zinc wave' by release from the endoplasmic reticulum via Ca^{2+} and Erk1/2	(Yamasaki et al., 2007)	No evidence	
Metal regulatory transcription factor 1	MTF1	Ubiquitous	Cytoplasm, nucleus	Zinc sensitive transcription factor that regulates several zinc transporters such as ZnT1, ZIP10 and MT1	(Gunther et al., 2012)	Activity is induced by oxidative stress and contributes to HIF1 activity	(Grzywacz et al., 2015; Murphy et al., 2005)
S100 calcium binding protein A8	S100A8	Proximal digestive tract, bone	Cytoplasm, cell junctions, intermediate filaments	Dimerises with S100A8/9 to form calprotectin, a zinc chelator that acts primarily as an antimicrobial agent	(Heizmann and Cox, 1998; Kerkhoff et al., 1999)	Inhibited by oxidative stress	(Hoskin et al., 2019)
S100 calcium binding protein A9	S100A9	Proximal digestive tract, bone	Cytoplasm, cell junctions, intermediate filaments				

(**Table 6.1** continued)

Gene name	Gene symbol	Tissue of major expression	Cellular localisation	Mechanism of zinc regulation	References	Oxygen or oxidative stress regulated	References
Metallothionein-1A	MT1A	Ubiquitous	Cytoplasm, nucleus	Primary protein involved in zinc metabolism, storage, transport and detoxification	(Krezel and Maret, 2017)	1. ROS scavenger that releases zinc upon oxidation, stimulating MTF-1 activity and further MT expression 2. Transcriptionally regulated by antioxidant master-regulator Nrf2 3. Induced in hypoxia via HIF1α regulation 4. Induced by hyperoxia 5. Hypobaric hypoxia increases MT3 expression	(Dalton et al., 1996; Eck and Pallauf, 2001; Gu et al., 2017; Kojima et al., 2009; Malairaman et al., 2014; Murphy et al., 2008; Veness-Meehan et al., 1991)
Metallothionein-1B	MT1B	Liver	Cytoplasm				
Metallothionein-1E	MT1E	Ubiquitous	Nucleus				
Metallothionein-1F	MT1F	Kidney, liver, thyroid gland	Cytoplasm				
Metallothionein-1G	MT1G	Intestine, liver, kidney, pancreas, thyroid gland	Cytoplasm				
Metallothionein-1H	MT1H	Intestine, liver, kidney, pancreas, thyroid gland	Cytoplasm				
Metallothionein-1H-like-1	MT1HL1	Heart muscle, liver	Cytoplasm				
Metallothionein-1L	MT1L						
Metallothionein-1X	MT1X	Liver, skeletal muscle	Cytoplasm				
Metallothionein-2A	MT2A	Liver	Cytoplasm				
Metallothionein-3	MT3	Brain	Cytoplasm				
Metallothionein-4	MT4	Skin	Cytoplasm				
Signal transducer and activator of transcription 3	STAT3	Ubiquitous	Cytoplasm, nucleus	Regulates the expression of ZIP6 and ZIP10	(Miyai et al., 2014; Yamashita et al., 2004)	Activated by ischaemia	(Lei et al., 2011)
Toll-like receptor 4	TLR4	Ubiquitous, immune cells	Plasma membrane, Golgi	Stimulates a transient 'zinc wave' possibly as a second messenger and inhibits ZIP6/10 expression whilst upregulating ZnT1/4/6	(Haase et al., 2008; Kitamura et al., 2006)	Upregulated in acute ischaemia but downregulated by chronic hypoxia via mitochondrial ROS	(Ishida et al., 2002; Kim et al., 2010)

(**Table 6.1** continued)

Gene name	Gene symbol	Tissue of major expression	Cellular localisation	Mechanism of zinc regulation	References	Oxygen or oxidative stress regulated	References
Transient receptor potential cation channel subfamily M member 2	TRPM2	Bone, brain	Nuclear membrane, plasma membrane	Channel that increases intracellular calcium and zinc when activated	(Li et al., 2016)	Molecular ROS sensor and activated by acute ischaemia	(Li et al., 2016; Zhan et al., 2016)
Transient receptor potential cation channel	TRP-A1, -C3, -C6, -M2, -M3, -M6, -M7, -V5, -V6	Ubiquitous	Plasma membrane, intracellular membranes	Participate in zinc transport at plasma membrane	(Chevallet et al., 2016)	Molecular oxygen sensors, activated by ROS and acute ischaemia	(Li et al., 2016; Mori et al., 2016; Numata et al., 2013; Zhan et al., 2016)
Transmembrane channel-like 6	TMC6	Bone, intestine, brain, lymphoid tissue	Nuclear membrane, ER, Golgi	Interacts with ZnT1 to affect intracellular zinc distribution (homolog of TMC6)	(Lazarczyk et al., 2008)	No evidence	
Transmembrane channel-like 8	TMC8	Bone, intestine, brain, lymphoid tissue	Nuclear membrane, ER, Golgi	Interacts with ZnT1 to affect intracellular zinc distribution (homolog of TMC8)		No evidence	
Transmembrane protein 163	TMEM163	Brain, pancreas, lung, testis	Plasma membrane, endosome, lysosome, vesicles, ER, Golgi, mitochondria	Zinc efflux protein	(Cuajungco et al., 2014; Sanchez et al., 2019)	Colocalises and binds with redox sensor TRPML1	(Cuajungco et al., 2014)

(**Table 6.1** continued)

Gene name	Gene symbol	Tissue of major expression	Cellular localisation	Mechanism of zinc regulation	References	Oxygen or oxidative stress regulated	References
Zinc transporter 1 (ZnT1)	SLC30A1	Ubiquitous	Plasma membrane, ER	Exports cytosolic zinc to extracellular space and from the cytosol to the ER	(Fukada et al., 2011; Kimura and Kambe, 2016)	1. ZnT1 and ZnT2 are upregulated by redox-sensitive MTF-1 2. Both increased and decreased ZnT1 expression reported after ischaemia-reperfusion injury (possibly time/cell dependent) 3. ZnT2 and ZnT4 upregulated after ischaemia-reperfusion injury 4. ZnT1 is upregulated by acute hypoxia, whilst ZnT2 and ZnT5 are upregulated by reoxygenation 5. Hypoxia reduces ZnT8 expression 6. Hypobaric hypoxia increases ZnT1 expression 7. ZnT1 mRNA is upregulated in response to increase in cellular zinc levels in transient forebrain ischaemia 8. ZnT3 and ZnT10 downregulation by siRNA increases ROS 9. mRNA expression of ZnT1, ZnT3 and ZnT6 are upregulated and ZnT10 is downregulated by the Nrf2-ARE signal pathway	(Aguilar-Alonso et al., 2008; Bodiga et al., 2017; Gerber et al., 2014; Gunther et al., 2012; Ishida and Takechi, 2016a; Malairaman et al., 2014; Pan and Liu, 2016; Patrushev et al., 2012; Tsuda et al., 1997)
Zinc transporter 2 (ZnT2)	SLC30A2	Mammary gland, pancreas, retina, intestine, kidney	Endosome, lysosome, secretory vesicle, plasma membrane, mitochondria	Facilitates zinc export into secretory vesicles			
Zinc transporter 3 (ZnT3)	SLC30A3	Brain, pancreas, testis	Synaptic vesicles	Facilitates zinc export into synaptic vesicles			
Zinc transporter 4 (ZnT4)	SLC30A4	Mammary gland, placenta, prostate, kidney, brain	Endosome, secretory vesicle, plasma membrane, Golgi	Facilitates zinc export into secretory vesicles			
Zinc transporter 5 (ZnT5)	SLC30A5	Heart, placenta, prostate, ovary, testis, intestine, thymus, bone	Golgi, vesicles, plasma membrane	Facilitates zinc export to Golgi			
Zinc transporter 6 (ZnT6)	SLC30A6	Brain, lung, intestine	Golgi, vesicles	Facilitates zinc export to Golgi			
Zinc transporter 7 (ZnT7)	SLC30A7	Intestine, stomach, pancreas, prostate, placenta, testis, retina, muscle	Golgi, vesicles	Facilitates zinc export to Golgi			
Zinc transporter 8 (ZnT8)	SLC30A8	Pancreas, adrenal gland, thyroid, testis	Secretory granules	Facilitates zinc export into secretory vesicles			
Zinc transporter 9 (ZnT9)	SLC30A9	Brain, muscle, kidney	ER, nucleus	Facilitates zinc export to ER			
Zinc transporter 10 (ZnT10)	SLC30A10	Brain, retina, liver	Golgi, plasma membrane	Facilitates zinc export into early endosomes			

(**Table 6.1** continued)

Gene name	Gene symbol	Tissue of major expression	Cellular localisation	Mechanism of zinc regulation	References	Oxygen or oxidative stress regulated	References
Zinc transporter (ZIP1)	SLC39A1	Prostate, small intestine, kidney, liver, pancreatic a cells	Plasma membrane, ER	Facilitates zinc influx into cytoplasm from extracellular space	(Fukada et al., 2011; Kimura and Kambe, 2016)	1. ZIP10 is downregulated by redox-sensitive MTF-1. 2.Oxidative stress increases ZIP1 expression 3.ZIP1, 2, 3, 7, 9, 10, 11, 13, and 14 are downregulated by hypoxia 4. Hypobaric hypoxia increases ZIP6 expression 5. ZIP8 is upregulated by HIF2a 6. Genetic disruption of ZIP12 attenuates hypoxia-associated pulmonary hypertension 7. ZIP3 are downregulated by the Nrf2-ARE signal pathway	(Bodiga et al., 2017; Furuta et al., 2016; Gunther et al., 2012; Ishida and Takechi, 2016a; Lee et al., 2016; Malairaman et al., 2014; Zhao et al., 2015)
Zinc transporter (ZIP2)	SLC39A2	Prostate, uterine, epithelial cells, ovary, liver, skin	Plasma membrane	Facilitates zinc influx into cytoplasm from extracellular space			
Zinc transporter (ZIP3)	SLC39A3	Testes, pancreatic b cells	Plasma membrane	Facilitates zinc influx into cytoplasm from extracellular space			
Zinc transporter (ZIP4)	SLC39A4	Small intestine, stomach, colon, cecum, skin, kidney, pancreatic b cells	Plasma membrane	Facilitates zinc influx into cytoplasm from extracellular space			
Zinc transporter (ZIP5)	SLC39A5	Liver, kidney, spleen, colon, pancreas	Plasma membrane	Facilitates zinc influx into cytoplasm from extracellular space			
Zinc transporter (ZIP6)	SLC39A6	Testis, pancreatic b cells	Plasma membrane	Facilitates zinc influx into cytoplasm from extracellular space			
Zinc transporter (ZIP7)	SLC39A7	Brain, liver, pancreatic b cells	Golgi, ER	Facilitates zinc influx from ER into the cytoplasm			
Zinc transporter (ZIP8)	SLC39A8	Pancreas, placenta, lung, liver, testis, thymus, erythrocytes	Plasma membrane, lysosome, endosome	Facilitates zinc influx into cytoplasm from extracellular space and from endosomes and lysosomes			
Zinc transporter (ZIP9)	SLC39A9	Prostate	Golgi	Facilitates zinc influx into cytoplasm from extracellular space and from Golgi			
Zinc transporter (ZIP10)	SLC39A10	Testis, kidney, breast, pancreatic a cells, erythrocytes	Plasma membrane	Facilitates zinc influx into cytoplasm from extracellular space			

(**Table 6.1** continued)

Gene name	Gene symbol	Tissue of major expression	Cellular localisation	Mechanism of zinc regulation	References	Oxygen or oxidative stress regulated	References
Zinc transporter (ZIP11)	SLC39A11	Mammary gland, testis, stomach, ileum and cecum	Golgi, nucleus	Facilitates zinc influx into cytoplasm from Golgi			
Zinc transporter (ZIP12)	SLC39A12	Neurons, endothelial cells, smooth muscle cells and interstitial cells	Plasma membrane	Facilitates zinc influx into cytoplasm from extracellular space			
Zinc transporter (ZIP13)	SLC39A13	Retinal pigment endothelial cells, osteoblasts	ER, Golgi	Facilitates zinc influx into cytoplasm from Golgi			
Zinc transporter (ZIP14)	SLC39A14	Liver, heart, placenta, lung, brain, pancreatic a cells	Plasma membrane, mitochondria, endosome, lysosome	Facilitates zinc influx into cytoplasm from extracellular space			
Zinc Finger Protein 658	ZNF658	Ubiquitous	Nucleus	Zinc sensitive transcription factor that downregulates ZnT5 and ZnT10	(Ogo et al., 2015)	No evidence	
Nuclear factor erythroid 2-related factor 2 (Nrf2)	NFE2L2	Ubiquitous	Cytoplasm, nucleus	Transcriptionally upregulates, MT, ZnT1/3/6 and downregulates ZnT10/ZIP3	(Ishida and Takechi, 2016a)	Master regulator of transcriptional anti-oxidant response to oxidative stress	(Vomund et al., 2017)
Kelch-like ECH-associated protein 1 (Keap1)	KEAP1	Ubiquitous	Cytoplasm, nucleus, ER	The increases of intracellular Zn^{2+} inactivate both Keap1 and keap1 can release Zn^{2+} during the oxidation process	(Kambe et al., 2015; Maret, 2006)	Keap1 can release Zn^{2+} during the oxidation process	(Kambe et al., 2015; Maret, 2006)

Abbreviations: PHD, prolyl hydroxylase domain; HIF, hypoxia-inducible factor; ER, endoplasmic reticulum; ARE, antioxidant response element; TRPML1, transient receptor potential mucolipin 1; ROS, reactive oxygen species.
Data search in Ccollaborationed with Dr. Matthew Smith, King's College London.

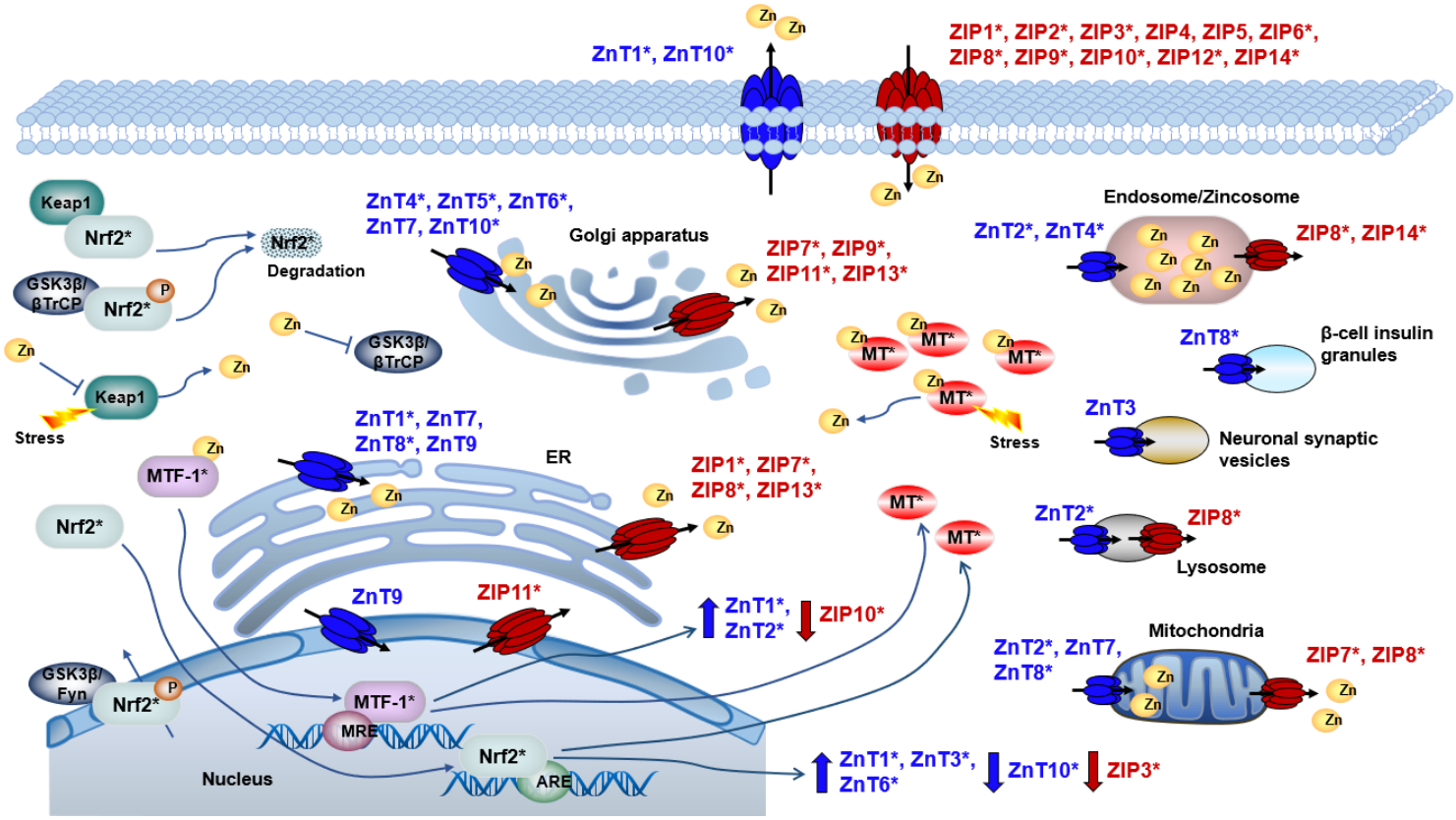

Figure 6.1 Subcellular localisation of ZnTs and ZIPs

ZnTs (blue) efflux zinc out of cells or into organelles, including ER, Golgi apparatus and mitochondria, whilst ZIPs (red) take zinc into cells or out of subcellular compartments. Asterisk (*) indicates that it is influenced by oxygen or oxidative stress. ZnT-1, 3 and 6 increases and ZnT10 and ZIP3 decreases after activation of Nrf2 signalling pathway. ZnT1 and ZnT2 are upregulated and ZIP10 is downregulated by MTF-1. Nrf2 is targeted for proteasomal degradation and ubiquitination in basal state via the dual actions of GSK3β/βTrCP and Keap1. Zn^{2+} increases can inhibit Keap1 and GSK3β. Schematic researched in collaboration with Dr. Matthew Smith, King's College London.

Abbreviations: ZnT, zinc transporter; ZIP, Zrt- and Irt- like protein; ER, Endoplasmic reticulum; ARE, antioxidant response element; Keap1, Kelch-like ECH-associated protein 1; Nrf2, nuclear factor erythroid 2-related factor 2; GSK3β, glycogen synthase kinase 3β; βTrCP, β transducin repeats-containing proteins; MRE, metal response elements; MTs, metallothionines; MTF-1, metal regulatory transcription factor 1; P, phosphorylation.

Ishida and his colleagues have described that mRNA levels of ZnT-1, 3 and 6 significantly increase and ZnT10 and ZIP3 mRNA levels significantly decrease after activation of Nrf2 signaling pathway in HepG2 Cells (Ishida and Takechi, 2016a). However, as shown in Chapter 4, knockdown with siRNA or overexpression with vector or activation of Nrf2 signalling pathway by SFN had negligible effects on total intracellular Zn content in HCASMCs under 18, 5 or 1kPa O_2. MT1 and ZnT1 protein expression were not significantly altered in cells by Nrf2 knockdown or overexpression/ activation, with the exception that Nrf2 silencing reduced ZnT1 expression decreased in cells under 1kPa O_2. HO-1 and NQO1 protein expression levels confirmed the success of knockdown, overexpression or activation protocols. In contrast, silencing Nrf2 decreased total Zn content in HCAECs under 18kPa O_2 but had negligible effects in these cells adapted to 5kPa O_2 (Smith et al., 2023). Together these findings suggest that intracellular Zn content is affected by O_2 in a cell-type specific manner. In addition, total intracellular Zn content did not change in HCASMCs under hypoxia-reoxygenation (HR) pre-adapted to 5kPa and 18kPa condition. ZnT1 protein expression trended to increase after reoxygenation for 12h in HCASMCs adapted to 18kPa O_2 but not in cells under 5kPa O_2, suggesting that Zn efflux may be affected by reoxygenation under room air. Although not investigated in the present study, ZIPs may mediate influx of Zn or other factors release Zn into the cytosol to achieve a constant total intracellular Zn level under HR injury. Furuta et al. demonstrated that expression levels of ZIP1 were significantly increased by oxidative stress in cultured mouse astrocytes (Furuta et al., 2016). Besides, Keap1, acting as a Zn sensor and Zn-binding factor, can release Zn from cysteine 273 and 288 under oxidative stress (Dinkova-Kostova et al., 2005; McMahon et al., 2010; Suzuki and Yamamoto, 2015).

6.4 Evidence of free radical generation under hypoxia- reoxygenation

In present study, we also reported indirect evidence for enhanced oxidative stress in HCASMCs under 1kPa O_2 based on lower GSH levels, antioxidant enzyme expression (e.g. CAT, SOD1 and SOD2) and SFN-induced Nrf2-targeted GCLM, GCLC, HO-1 and NQO1 expression. These data in cells after long-term adaptation to defined O_2 levels indicate that there is a new balance and antioxidants in cells under hypoxia. Furthermore, in order to establish the effect of hypoxia-reoxygenation (HR) on free radical generation, we used L-012 probe to assess reactive oxygen species (ROS) as previously reviewed (Zielonka et al., 2013). As discussed in Chapter 5, reoxygenation-induced ROS generation was much higher in HCASMCs under 18kPa O_2 compared to cells adapted to physiological normoxia , emphasizing the importance of *in vitro* cell culture models under physiological normoxia. Besides, reoxygenation-induced ROS generation was significantly attenuated by pSOD (not pCAT), suggests that the predominant ROS are superoxide, consistent with previous studies (Warpsinski et al., 2020).

6.5 Clinical significance of SFN and Zn

In the present study, SFN, a classic activator of Nrf2 signalling, was used to activate Nrf2 in HCASMCs adapted long-term to 18, 5 or 1kPa O_2, as previously reported (Chapple et al., 2016; Warpsinski et al., 2020). Notably, Zn supplementation was shown to activate Nrf2-HO-1 signalling in HCASMCs under basal conditions, consistent with previous findings that Zn supplementation triggers GSH and Nrf2-mediated protection in rat aorta ECs, rat pheochromocytoma cells and human neuroblastoma cells (Cortese et al., 2008; Hossain et al., 2021; Kaufman et al., 2020; Omata et al., 2013). Moreover, pre-treating HCASMCs with

SFN or Zn successfully attenuated superoxide generation after reoxygenation under 18kPa O_2, which was abolished by Zn chelator TPEN, indicating the protective role of Zn and SFN against oxidative stress under HR. Previous studies have reported that zinc prevents HR-induced mitochondrial superoxide generation in cardiac cells, alleviates HR-induced endoplasmic reticulum stress and improves cardiomyocyte survival (Bodiga et al., 2020; Salazar et al., 2017). Furthermore, the present study provides the first evidence protective effects of Zn and SFN cannot be detected in HCASMCs adapted long-term to 5kPa O_2 probably due to lower oxidative stress in cells under physiological normoxia.

SFN is abundant in broccoli, cauliflower, and cabbage (Liang et al., 2006) and Zn is rich in nuts, shellfish, and mushroom (Fallah et al., 2018). Thus, the present study provides insights into potential novel dietary therapeutic approaches that could be employed to protect against coronary ischaemia-reperfusion injury. So far, high throughput screening is widely established to unbiasedly assess cellular function and track the efficacy or toxicity of drugs (Panusatid et al., 2022). It would be worthwhile to evaluate SFN or Zn therapy in different cell types in different physiological or pathological models using high-throughput screening. Although most high throughput screening is currently conducted in cell culture models in air (hyperoxia), Fridman and her colleagues have combined a high throughput microfluidic device with different gradient oxygen levels in studies of breast tumor spheroids strategies, as oxygen gradients affect the ROS generation and the drugs cytotoxicity (Berger Fridman et al., 2021). Thus, further experiments in this field are warranted to consider the effects of oxygen and particularly to investigate cell signalling under physiological normoxia.

6.6 Limitations of the study

The present study has a few potential limitations. Firstly, all experiments were not conducted with cells subjected to serum deprivation. Notably, serum starvation is regarded as a commonly performed procedure to synchronise the cells cycle before studies of molecular mechanisms (Chen et al., 2012; Cooper and Gonzalez-Hernandez, 2009; Epstein et al., 1975). Moreover, serum deprivation provides more reproducible experimental conditions due to the known contribution of serum factors to cell biology (Pirkmajer and Chibalin, 2011). However, as metal contents were measured as well in this study, it is important to consider that *in vitro* cells take up metals such as Zn mainly from serum (Messer et al., 1982). Thus, serum deprivation was not employed to enable correlation of redox signaling and metal profiling.

Secondly, findings in Chapter 5 demonstrated that HCASMCs pre-adapted to physiological normoxia exhibited negligible ROS generation under HR. It is possible that the radical generation is too low to be detected by L-012 probe or the probe is lack of sensitivity to monitor low levels of radical generation. Furthermore, GSH levels and Nrf2-targeted protein expression such as NQO1 and GCLM showed negligible changes in cells under HR pre-adapted to 5kPa O_2. On the one hand, oxidative stress under HR was much less in HCASMCs adapted to physiological normoxia compared to cells under 18kPa O_2, as supported by a lower antioxidant response with hardly detectable changes. On the other hand, it is possible a limitation of the present HR model is that cells were not deprived of glucose and serum. Notably, some studies have used serum and glucose deprivation combined with hypoxia- reoxygenation as an *in vitro* cell model to mimic IR clinical conditions (Pirkmajer and Chibalin, 2011). Thus, further experiments are warranted to determine whether effects of HR are enhanced by glucose deprivation.

Finally, we investigated the total intracellular Zn content long-term adaptation to hyperoxia, normoxia and hypoxia and the effects of HR on total Zn content in this study. However, it is well known that labile Zn^{2+} is the form that participates in oxidative and redox responses. At present, *in vitro* research of changes in labile Zn^{2+} in HCASMCs under HR injury adapted to normoxia remains to be investigated. In fact, Dr. Matthew Smith and I attempted to measure labile Zn^{2+} changes in cells under 18kPa for 1h or under HR using the fluorescence probe FluoZin3, which is a common labile Zn^{2+} indicator (Zhao et al., 2008). However, leakage of FluoZin3 from cells into the medium limited interpretation. This field of detecting labile Zn^{2+} deserves further investigation in future experiments.

6.7 Statement about the impact of Covid restrictions on the research

The COVID-19 pandemic and the restrictions had some impact on my PhD thesis research. These restrictions avoiding the spread of the virus brought about numerous challenges and disruptions to the research process over 2 years, including the 3-4 months interruption of experiments in the first year and the strict restriction in the following 1-2 years.

One of the major challenges of COVID restrictions on PhD thesis research was the limitation on access to our laboratories. We were unable to carry out our planned experiments due to restricted access to Franklin Wilkins Building and complete lockdown. This resulted in delays and interruption of the collaboration with Dr. Joose Kreutzer at Tampere university in Finland to set up the mechanical stretch system. It forced us to reconsider methodologies and modify our research to do metallomics instead. Furthermore, travel restrictions imposed during the pandemic blocked opportunities for attending conferences, workshops, and

seminars. These academic events provide valuable platforms for knowledge sharing, networking, and receiving critical feedback on research work. A lack of these opportunities limits our PhD researchers' access to diverse and valuable insights, which may affect the quality and depth of our work.

Another big influence is the use of online virtual communication. The lack of in-person interactions and face-to-face collaborations affected on the research experience and our mental health due to the isolation and uncertainties. I would like to thank my supervisor Prof. Giovanni Mann, Dr. Matthew Smith and other colleagues. We supported each other during and after COVID, which really gave me a lot of confidence and accompany.

Overall, the COVID restrictions had some impact on my PhD thesis research but did not ruin it. The limitations on access to research laboratories, travel restrictions, and the shift to online virtual communication have disrupted the research process, delayed progress, and affected the quality of research outcomes.

6.8 Future directions

The current experiments have established an *in vitro* HCASMCs culture model under physiological normoxia to investigate HR as a model of IR injury and characterise antioxidant mechanisms related to Nrf2 signalling and Zn. To obviate individual differences, primary HCASMCs sourced from a male Caucasian were purchased commercially. Physiological normoxia was used to more accurately mimic *in vivo* O_2 conditions. To better replicate physiological and pathological models, mechanotransduction needs to be considered, as vascular SMCs are exposed to cyclic stretch *in vivo*, namely contraction and relaxation

(Jensen et al., 2021; Osol, 1995). Mechanotransduction describes how cells respond to their environment by converting physical or mechanical stimuli into biochemical signals (Chatterjee and Fisher, 2014). These forces regulate the proliferation, apoptosis, migration, phenotype and alignment of vascular cells, and activate downstream signalling pathways, which are important to maintain homeostasis in blood vessels and are relevant to vascular remodelling in pathological conditions (Haga et al., 2007; Jufri et al., 2015). For instance, mechanical stretch has been shown to affect many transcription factors such as Nrf2 and nuclear factor-κB (NFκB) (Chaqour et al., 1999; Li et al., 2018; Papaiahgari et al., 2007). Furthermore, mechanical stretch is associated with ROS generation (Birukov, 2009; Chatterjee and Fisher, 2014). Hishikawa and colleagues have reported that 1Hz, 10% cyclic stretch to human coronary artery SMCs in culture stimulates the production of superoxide, whilst a cyclic stretch of 6% did not (Hishikawa et al., 1997). Thus, mechanical stress needs to be considered in defining antioxidant mechanism for improved translation of findings into clinical applications.

In addition, as introduced in Chapter 1 (Section 1.2.3), there are numerous interactions between vascular endothelial (ECs) and smooth muscle cells (SMCs) (see **Figure 1.6**). Vascular ECs can communicate with vascular SMCs by releasing bioactive agents such as NO, which is important for homeostasis and regulation of vascular tone (Gao et al., 2016; Moncada and Higgs, 1993; Tousoulis et al., 2005). Chiu et al. reported that vascular SMCs induce expression of the adhesion molecule E-selection in ECs by in endothelial/smooth muscle co-cultures and that shear stress inhibited its expression (Chiu et al., 2007). In a mouse aortic aneurysm model, elevated endoplasmic reticulum stress and microparticles production in vascular SMC induce vascular EC dysfunction and apoptosis (Jia et al., 2017). Thus, it is critical to establish a co-culture system of vascular ECs and SMCs in future

experiments, to replicate *in vitro* antioxidant mechanisms under physiological O_2 and interaction between vascular ECs and SMCs exposed to shear and cyclic stretch, respectively.

In summary, the present study highlights the critical importance of adapting cells *in vitro* to physiological O_2 levels to correlate the redox phenotype and metal profile in HCASMCs under 18kPa O_2 and 5kPa O_2. Moreover, the novel findings on antioxidant mechanisms explored in HR models demonstrate a protective role of SFN and Zn supplementation in HR injury. Thus, this study provides valuable insights into the design of new therapeutic targets in coronary ischaemia-reperfusion as well as regenerative medicine and ecotoxicology.

Appendices

Appendix 1- Composition of supplement pack Smooth Muscle Cell Growth Medium 2

Supplement pack smooth muscle cell growth medium 2, C-39262, PromoCell, UK

Media supplement	Final supplement concentration
Fetal Calf Serum	0.05 ml/ml
Epidermal Growth Factor (recombinant human)	0.5 ng/ml
Basic Fibroblast Growth Factor (recombinant human)	2 ng/ml
Insulin (recombinant human)	5 µg/ml

Appendix 2- Composition of SDS lysis buffer

Component	Concentration	Amount required to make 200ml
Tris base (pH 6.8)	50mM	1.2g in 100ml ddH_2O
Glycerol	10%	20g
Sodium dodecyl sulfate (SDS)	2%	40ml
ddH_2O	-	up to 200ml

Appendix 3- Composition of Phosphate/EDTA + NaOH buffer

Component	Concentration
Monopotassium phosphate (KH_2PO_4)	100.0mM
Ethylenediaminetetraacetic acid (EDTA)	6.3mM
Adjust pH > 8	

Appendix 4- Composition of PBS-T

Component	Concentration
10×PBS tablets (OXOID, BR0014C)	1×
TWEEN® (Sigma, P5927-500)	0.1%

Appendix 5- Composition of resolving gel for mini-SDS-PAGE

Component	10%	Final concentration
4×Tris-SDS (pH 8.8)	4.8ml	1× Tris (375mM) + 0.1%SDS
30%Acrylamide	6.4ml	10%
ddH_2O	8ml	-
10%APS	70µl	0.04%
N,N,N',N'- Tetramethylethylenediamine (Temed)	15µl	0.08%

Appendix 6- Composition of stacking gel for mini-SDS-PAGE

Component	Amount	Final concentration
4× Tris-SDS (pH 6.8)	3ml	1×Tris (125mM) + 0.1%SDS
30%Acrylamide	1.56 ml	4%
ddH_2O	7.32ml	-
10%APS	60µl	0.05%
N,N,N',N'- Tetramethylethylenediamine (Temed)	7.5µl	0.06%

Appendix 7- Composition of running buffer for SDS-PAGE electrophoresis

Component	Amount
SDS PAGE Tank Buffer (10X) Tris-Glycine SDS	100ml
ddH_2O	900ml

Composition of Tris-Glycine-SDS PAGE Buffer (10X)

Component	Concentration
Tris base	0.25M
Glycine	1.92M
SDS	1%

Appendix 8- Composition of transfer buffer for immunoblotting

Component	Amount	Final concentration
Tris base	6.06g	25mM
Glycine	28.8g	192mM
Methanol	400ml	20%
ddH_2O	1600ml	-

Appendix 9- Plasmid vector information

pcDNA3.1 backbone

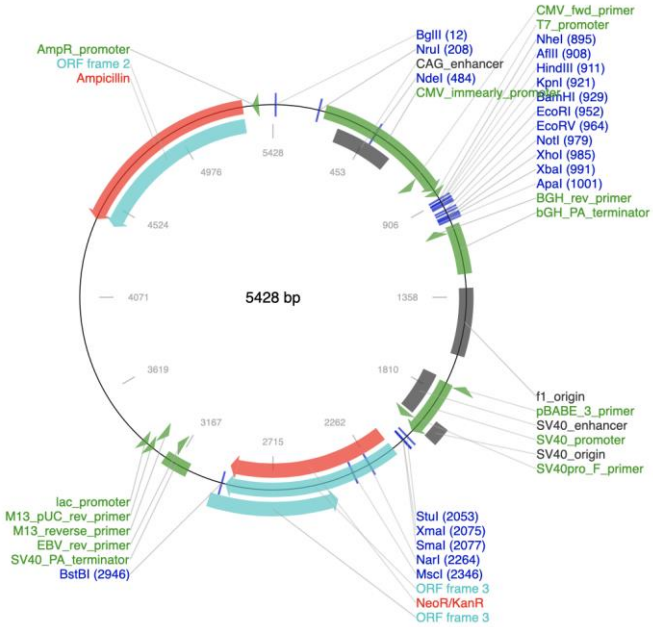

Human NFE2L2 (NM_006164.5) cDNA including putative kozak sequence was inserted between NheI and ApaI site

Insert sequence

gctcat catgatggac ttggagctgc cgccgccggg actcccgtcc cagcaggaca tggatttgat tgacatactt tggaggcaag atatagatct tggagtaagt cgagaagtat ttgacttcag tcagcgacgg aaagagtatg agctggaaaa acagaaaaaa cttgaaaagg aaagacaaga acaactccaa aaggagcaag agaaagcctt tttcgctcag ttacaactag atgaagagac aggtgaattt ctcccaattc agccagccca gcacatccag tcagaaacca gtggatctgc caactactcc caggttgccc acattcccaa atcagatgct ttgtactttg atgactgcat gcagcttttg gcgcagacat tcccgtttgt agatgacaat gaggtttctt cggctacgtt tcagtcactt gttcctgata ttcccggtca catcgagagc ccagtcttca ttgctactaa tcaggctcag tcacctgaaa cttctgttgc tcaggtagcc cctgttgatt tagacggtat gcaacaggac attgagcaag tttgggagga gctattatcc attcctgagt tacagtgtct taatattgaa aatgacaagc tggttgagac taccatggtt ccaagtccag aagccaaact gacagaagtt gacaattatc atttttactc atctataccc tcaatggaaa aagaagtagg taactgtagt ccacattttc ttaatgcttt tgaggattcc ttcagcagca tcctctccac agaagacccc aaccagttga cagtgaactc attaaattca gatgccacag tcaacacaga ttttggtgat gaattttatt ctgctttcat agctgagccc agtatcagca acagcatgcc ctcacctgct actttaagcc attcactctc tgaacttcta aatgggccca ttgatgtttc tgatctatca ctttgcaaag ctttcaacca aaaccaccct gaaagcacag cagaattcaa tgattctgac tccggcattt cactaaacac aagtcccagt gtggcatcac cagaacactc agtggaatct tccagctatg gagacacact acttggcctc agtgattctg aagtggaaga gctagatagt gcccctggaa gtgtcaaaca gaatggtcct aaaacaccag tacattcttc tggggatatg gtacaaccct tgtcaccatc tcaggggcag agcactcacg tgcatgatgc ccaatgtgag aacacaccag agaaagaatt gcctgtaagt cctggtcatc ggaaaacccc attcacaaaa gacaaacatt caagccgctt ggaggctcat ctcacaagag atgaacttag ggcaaaagct ctccatatcc cattccctgt agaaaaaatc attaacctcc ctgttgttga cttcaacgaa atgatgtcca aagagcagtt caatgaagct caacttgcat

References

Abdo, A.I., Tran, H.B., Hodge, S., Beltrame, J.F., and Zalewski, P.D. (2021). Zinc Homeostasis Alters Zinc Transporter Protein Expression in Vascular Endothelial and Smooth Muscle Cells. Biol Trace Elem Res *199*, 2158-2171.

Adachi, T., Fukushima, T., Usami, Y., and Hirano, K. (1993). Binding of human xanthine oxidase to sulphated glycosaminoglycans on the endothelial-cell surface. Biochem J *289 (Pt 2)*, 523-527.

Adams, D.J., Barakeh, J., Laskey, R., and Van Breemen, C. (1989). Ion channels and regulation of intracellular calcium in vascular endothelial cells. FASEB J *3*, 2389-2400.

Adkison, D., Hollwarth, M.E., Benoit, J.N., Parks, D.A., McCord, J.M., and Granger, D.N. (1986). Role of free radicals in ischemia-reperfusion injury to the liver. Acta Physiol Scand Suppl *548*, 101-107.

Aguilar-Alonso, P., Martinez-Fong, D., Pazos-Salazar, N.G., Brambila, E., Gonzalez-Barrios, J.A., Mejorada, A., Flores, G., Millan-Perezpena, L., Rubio, H., and Leon-Chavez, B.A. (2008). The increase in zinc levels and upregulation of zinc transporters are mediated by nitric oxide in the cerebral cortex after transient ischemia in the rat. Brain Res *1200*, 89-98.

Ahn, Y.H., Hwang, Y., Liu, H., Wang, X.J., Zhang, Y., Stephenson, K.K., Boronina, T.N., Cole, R.N., Dinkova-Kostova, A.T., Talalay, P., *et al.* (2010). Electrophilic tuning of the chemoprotective natural product sulforaphane. P Natl Acad Sci USA *107*, 9590-9595.

Aikawa, M., Sivam, P.N., Kuroo, M., Kimura, K., Nakahara, K., Takewaki, S., Ueda, M., Yamaguchi, H., Yazaki, Y., Periasamy, M., *et al.* (1993). Human Smooth-Muscle Myosin Heavy-Chain Isoforms as Molecular Markers for Vascular Development and Atherosclerosis. Circulation Research *73*, 1000-1012.

Akgur, F.M., Kilinc, K., Aktug, T., and Olguner, M. (1994). The effect of allopurinol pretreatment before detorting testicular torsion. J Urol *151*, 1715-1717.

Akhter, S.A. (2011). The heart and pericardium. Thorac Surg Clin *21*, 205-217, viii.

Allison, R.C., Kyle, J., Adkins, W.K., Prasad, V.R., McCord, J.M., and Taylor, A.E. (1990). Effect of ischemia reperfusion or hypoxia reoxygenation on lung vascular permeability and resistance. J Appl Physiol (1985) *69*, 597-603.

Allwork, S.P. (1987). The applied anatomy of the arterial blood supply to the heart in man. J Anat *153*, 1-16.

Altamirano, F., Wang, Z.V., and Hill, J.A. (2015). Cardioprotection in ischaemia-reperfusion injury: novel mechanisms and clinical translation. J Physiol *593*, 3773-3788.

Alva, R., Moradi, F., Liang, P., and Stuart, J.A. (2022). Culture of Cancer Cells at Physiological Oxygen Levels Affects Gene Expression in a Cell-Type Specific Manner. Biomolecules *12*.

Andreini, C., Banci, L., Bertini, I., and Rosato, A. (2006). Counting the zinc-proteins encoded in the human genome. Journal of Proteome Research *5*, 196-201.
Andrews, G.K. (2000). Regulation of metallothionein gene expression by oxidative stress and metal ions. Biochemical Pharmacology *59*, 95-104.
Anson, K.J., Corbet, G.A., and Palmer, A.E. (2021). Zn2+ influx activates ERK and Akt signaling pathways. P Natl Acad Sci USA *118*.
Anwar, A.A., Li, F.Y., Leake, D.S., Ishii, T., Mann, G.E., and Siow, R.C. (2005). Induction of heme oxygenase 1 by moderately oxidized low-density lipoproteins in human vascular smooth muscle cells: role of mitogen-activated protein kinases and Nrf2. Free Radic Biol Med *39*, 227-236.
Atkuri, K.R., Herzenberg, L.A., and Herzenberg, L.A. (2005). Culturing at atmospheric oxygen levels impacts lymphocyte function. Proc Natl Acad Sci U S A *102*, 3756-3759.
Atkuri, K.R., Herzenberg, L.A., Niemi, A.K., Cowan, T., and Herzenberg, L.A. (2007). Importance of culturing primary lymphocytes at physiological oxygen levels. Proc Natl Acad Sci U S A *104*, 4547-4552.
Auld, D.S. (2001). Zinc coordination sphere in biochemical zinc sites. Biometals *14*, 271-313.
Auscher, C., Amory, N., van der Kemp, P., and Delbarre, F. (1979). Xanthine oxidase activity in human intestines. Histochemical and radiochemical study. Adv Exp Med Biol *122B*, 197-201.
Babij, P., Kawamoto, S., White, S., Adelstein, R.S., and Periasamy, M. (1992a). Differential Expression of Sm1 and Sm2 Myosin Isoforms in Cultured Vascular Smooth-Muscle. American Journal of Physiology *262*, C607-C613.
Babij, P., Kawamoto, S., White, S., Adelstein, R.S., and Periasamy, M. (1992b). Differential expression of SM1 and SM2 myosin isoforms in cultured vascular smooth muscle. Am J Physiol *262*, C607-613.
Badran, A., Nasser, S.A., Mesmar, J., El-Yazbi, A.F., Bitto, A., Fardoun, M.M., Baydoun, E., and Eid, A.H. (2020). Reactive Oxygen Species: Modulators of Phenotypic Switch of Vascular Smooth Muscle Cells. Int J Mol Sci *21*.
Bai, Y., Cui, W.P., Xin, Y., Miao, X., Barati, M.T., Zhang, C., Chen, Q., Tan, Y., Cui, T.X., Zheng, Y., *et al.* (2013). Prevention by sulforaphane of diabetic cardiomyopathy is associated with up-regulation of Nrf2 expression and transcription activation. Journal of Molecular and Cellular Cardiology *57*, 82-95.
Bai, Y., Wang, X., Zhao, S., Ma, C., Cui, J., and Zheng, Y. (2015). Sulforaphane Protects against Cardiovascular Disease via Nrf2 Activation. Oxid Med Cell Longev *2015*, 407580.
Baird, L., and Yamamoto, M. (2020). The Molecular Mechanisms Regulating the KEAP1-NRF2 Pathway. Mol Cell Biol *40*.

Beamish, J.A., He, P., Kottke-Marchant, K., and Marchant, R.E. (2010). Molecular Regulation of Contractile Smooth Muscle Cell Phenotype: Implications for Vascular Tissue Engineering. Tissue Eng Part B-Re *16*, 467-491.
Becker, L.B., vanden Hoek, T.L., Shao, Z.H., Li, C.Q., and Schumacker, P.T. (1999). Generation of superoxide in cardiomyocytes during ischemia before reperfusion. Am J Physiol *277*, H2240-2246.
Bedard, K., and Krause, K.H. (2007). The NOX family of ROS-generating NADPH oxidases: physiology and pathophysiology. Physiol Rev *87*, 245-313.
Belcastro, E., Wu, W., Fries-Raeth, I., Corti, A., Pompella, A., Leroy, P., Lartaud, I., and Gaucher, C. (2017). Oxidative stress enhances and modulates protein S-nitrosation in smooth muscle cells exposed to S-nitrosoglutathione. Nitric Oxide *69*, 10-21.
Bellezza, I., Giambanco, I., Minelli, A., and Donato, R. (2018). Nrf2-Keap1 signaling in oxidative and reductive stress. Biochim Biophys Acta Mol Cell Res *1865*, 721-733.
Bennett, M.R., Littlewood, T.D., Schwartz, S.M., and Weissberg, P.L. (1997). Increased sensitivity of human vascular smooth muscle cells from atherosclerotic plaques to p53-mediated apoptosis. Circ Res *81*, 591-599.
Berger Fridman, I., Ugolini, G.S., VanDelinder, V., Cohen, S., and Konry, T. (2021). High throughput microfluidic system with multiple oxygen levels for the study of hypoxia in tumor spheroids. Biofabrication *13*.
Berger, M., Rubinraut, E., Barshack, I., Roth, A., Keren, G., and George, J. (2004). Zinc reduces intimal hyperplasia in the rat carotid injury model. Atherosclerosis *175*, 229-234.
Bergstrom, P., Andersson, H.C., Gao, Y., Karlsson, J.O., Nodin, C., Anderson, M.F., Nilsson, M., and Hammarsten, O. (2011). Repeated transient sulforaphane stimulation in astrocytes leads to prolonged Nrf2-mediated gene expression and protection from superoxide-induced damage. Neuropharmacology *60*, 343-353.
Berry, C.E., and Hare, J.M. (2004). Xanthine oxidoreductase and cardiovascular disease: molecular mechanisms and pathophysiological implications. J Physiol *555*, 589-606.
Beyersmann, D., and Haase, H. (2001). Functions of zinc in signaling, proliferation and differentiation of mammalian cells. Biometals *14*, 331-341.
Bhansali, S., Sohi, K., and Dhawan, V. (2021). Hypoxia-induced mitochondrial reactive oxygen species (mtROS) differentially regulates smooth muscle cell (SMC) proliferation of pulmonary and systemic vasculature. Mitochondrion *57*, 97-107.
Bhattarai, D., Xu, X., and Lee, K. (2018). Hypoxia-inducible factor-1 (HIF-1) inhibitors from the last decade (2007 to 2016): A "structure-activity relationship" perspective. Med Res Rev *38*, 1404-1442.
Bian, X., Teng, T., Zhao, H., Qin, J., Qiao, Z., Sun, Y., Liun, Z., and Xu, Z. (2018). Zinc prevents mitochondrial superoxide generation by inducing mitophagy in the setting of hypoxia/reoxygenation in cardiac cells. Free Radic Res *52*, 80-91.

Birukov, K.G. (2009). Cyclic stretch, reactive oxygen species, and vascular remodeling. Antioxid Redox Signal *11*, 1651-1667.
Bodiga, V.L., Thokala, S., Kovur, S.M., and Bodiga, S. (2017). Zinc Dyshomeostasis in Cardiomyocytes after Acute Hypoxia/Reoxygenation. Biol Trace Elem Res *179*, 117-129.
Bodiga, V.L., Thokala, S., Vemuri, P.K., and Bodiga, S. (2015). Zinc pyrithione inhibits caspase-3 activity, promotes ErbB1-ErbB2 heterodimerization and suppresses ErbB2 downregulation in cardiomyocytes subjected to ischemia/reperfusion. J Inorg Biochem *153*, 49-59.
Bodiga, V.L., Vemuri, P.K., Nimmagadda, G., and Bodiga, S. (2020). Zinc-dependent changes in oxidative and endoplasmic reticulum stress during cardiomyocyte hypoxia/reoxygenation. Biological Chemistry *401*, 1257-1271.
Bogdanova, A., Heinicke, I., Gassmann, M., and Heinicke, K. (2010). Oxygen-induced regulation of the intracellular glutathione levels in erythrocytes. European Journal of Applied Physiology *109*, 575-576.
Bonaventura, P., Benedetti, G., Albarede, F., and Miossec, P. (2015). Zinc and its role in immunity and inflammation. Autoimmunity Reviews *14*, 277-285.
Bonora, M., Patergnani, S., Rimessi, A., De Marchi, E., Suski, J.M., Bononi, A., Giorgi, C., Marchi, S., Missiroli, S., Poletti, F., *et al.* (2012). ATP synthesis and storage. Purinergic Signal *8*, 343-357.
Bosomworth, H.J., Thornton, J.K., Coneyworth, L.J., Ford, D., and Valentine, R.A. (2012). Efflux function, tissue-specific expression and intracellular trafficking of the Zn transporter ZnT10 indicate roles in adult Zn homeostasis. Metallomics *4*, 771-779.
Bost, M., Houdart, S., Oberli, M., Kalonji, E., Huneau, J.F., and Margaritis, I. (2016). Dietary copper and human health: Current evidence and unresolved issues. J Trace Elem Med Bio *35*, 107-115.
Bouche, D., Chauveau, C., Roussel, J.C., Mathieu, P., Braudeau, C., Tesson, L., Soulillou, J.P., Iyer, S., Buelow, R., and Anegon, I. (2002). Inhibition of graft arteriosclerosis development in rat aortas following heme oxygenase-1 gene transfer. Transpl Immunol *9*, 235-238.
Boveris, A., and Chance, B. (1973). The mitochondrial generation of hydrogen peroxide. General properties and effect of hyperbaric oxygen. Biochem J *134*, 707-716.
Braunwald, E., and Kloner, R.A. (1982). The stunned myocardium: prolonged, postischemic ventricular dysfunction. Circulation *66*, 1146-1149.
Bryan, H.K., Olayanju, A., Goldring, C.E., and Park, B.K. (2013). The Nrf2 cell defence pathway: Keap1-dependent and -independent mechanisms of regulation. Biochem Pharmacol *85*, 705-717.
Bubb, K.J., Kok, C., Tang, O., Rasko, N.B., Birgisdottir, A.B., Hansen, T., Ritchie, R., Bhindi, R., Reisman, S.A., Meyer, C., *et al.* (2017). The NRF2 activator DH404 attenuates

adverse ventricular remodeling post-myocardial infarction by modifying redox signalling. Free Radic Biol Med *108*, 585-594.
Budinger, G.R., Chandel, N., Shao, Z.H., Li, C.Q., Melmed, A., Becker, L.B., and Schumacker, P.T. (1996). Cellular energy utilization and supply during hypoxia in embryonic cardiac myocytes. Am J Physiol *270*, L44-53.
Budinger, G.R., Duranteau, J., Chandel, N.S., and Schumacker, P.T. (1998). Hibernation during hypoxia in cardiomyocytes. Role of mitochondria as the O2 sensor. J Biol Chem *273*, 3320-3326.
Bunn, H.F., and Poyton, R.O. (1996). Oxygen sensing and molecular adaptation to hypoxia. Physiol Rev *76*, 839-885.
Bustin, S.A. (2000). Absolute quantification of mRNA using real-time reverse transcription polymerase chain reaction assays. J Mol Endocrinol *25*, 169-193.
Byon, C.H., Javed, A., Dai, Q., Kappes, J.C., Clemens, T.L., Darley-Usmar, V.M., McDonald, J.M., and Chen, Y.B. (2008). Oxidative stress induces vascular calcification through modulation of the osteogenic transcription factor Runx2 by AKT signaling. Journal of Biological Chemistry *283*, 15319-15327.
Cadenas, S. (2018). ROS and redox signaling in myocardial ischemia-reperfusion injury and cardioprotection. Free Radic Biol Med *117*, 76-89.
Cai, H. (2005). NAD(P)H oxidase-dependent self-propagation of hydrogen peroxide and vascular disease. Circ Res *96*, 818-822.
Cao, Z., and Li, Y. (2004). Protecting against peroxynitrite-mediated cytotoxicity in vascular smooth muscle cells via upregulating endogenous glutathione biosynthesis by 3H-1,2-dithiole-3-thione. Cardiovasc Toxicol *4*, 339-353.
Carden, D.L., and Granger, D.N. (2000). Pathophysiology of ischaemia-reperfusion injury. J Pathol *190*, 255-266.
Carrillo-Sepulveda, M.A., and Matsumoto, T. (2014). Phenotypic Modulation of Mesenteric Vascular Smooth Muscle Cells from Type 2 Diabetic Rats is Associated with Decreased Caveolin-1 Expression. Cellular Physiology and Biochemistry *34*, 1497-1506.
Chai, Y.C., Ashraf, S.S., Rokutan, K., Johnston, R.B., and Thomas, J.A. (1994). S-Thiolation of Individual Human Neutrophil Proteins Including Actin by Stimulation of the Respiratory Burst - Evidence against a Role for Glutathione Disulfide. Archives of Biochemistry and Biophysics *310*, 273-281.
Chakravarthy, M.V., Spangenburg, E.E., and Booth, F.W. (2001). Culture in low levels of oxygen enhances in vitro proliferation potential of satellite cells from old skeletal muscles. Cell Mol Life Sci *58*, 1150-1158.
Chambers, D.E., Parks, D.A., Patterson, G., Roy, R., McCord, J.M., Yoshida, S., Parmley, L.F., and Downey, J.M. (1985). Xanthine oxidase as a source of free radical damage in myocardial ischemia. J Mol Cell Cardiol *17*, 145-152.

Chang, H.C., Wu, R.X., Shang, M., Sato, T., Chen, C.L., Shapiro, J.S., Liu, T., Thakur, A., Sawicki, K.T., Prasad, S.V.N., *et al.* (2016). Reduction in mitochondrial iron alleviates cardiac damage during injury. Embo Molecular Medicine *8*, 247-267.
Chapple, S.J., Keeley, T.P., Mastronicola, D., Arno, M., Vizcay-Barrena, G., Fleck, R., Siow, R.C.M., and Mann, G.E. (2016). Bach1 differentially regulates distinct Nrf2-dependent genes in human venous and coronary artery endothelial cells adapted to physiological oxygen levels. Free Radic Biol Med *92*, 152-162.
Chapple, S.J., Puszyk, W.M., and Mann, G.E. (2015). Keap1-Nrf2 regulated redox signaling in utero: Priming of disease susceptibility in offspring. Free Radic Biol Med *88*, 212-220.
Chapple, S.J., Siow, R.C., and Mann, G.E. (2012). Crosstalk between Nrf2 and the proteasome: therapeutic potential of Nrf2 inducers in vascular disease and aging. Int J Biochem Cell Biol *44*, 1315-1320.
Chaqour, B., Howard, P.S., Richards, C.F., and Macarak, E.J. (1999). Mechanical stretch induces platelet-activating factor receptor gene expression through the NF-kappaB transcription factor. J Mol Cell Cardiol *31*, 1345-1355.
Chatterjee, S., and Fisher, A.B. (2014). Mechanotransduction: forces, sensors, and redox signaling. Antioxid Redox Signal *20*, 868-871.
Chen, B., Lu, Y., Chen, Y., and Cheng, J. (2015). The role of Nrf2 in oxidative stress-induced endothelial injuries. J Endocrinol *225*, R83-99.
Chen, M.F., Huang, J.J., Yang, X.J., Liu, B.Q., Zhang, W.Z., Huang, L., Deng, F., Ma, J., Bai, Y.J., Lu, R., *et al.* (2012). Serum Starvation Induced Cell Cycle Synchronization Facilitates Human Somatic Cells Reprogramming. Plos One *7*.
Chen, Q.M., and Maltagliati, A.J. (2018). Nrf2 at the heart of oxidative stress and cardiac protection. Physiol Genomics *50*, 77-97.
Chen, R.L., Lai, U.H., Zhu, L.L., Singh, A., Ahmed, M., and Forsyth, N.R. (2018). Reactive Oxygen Species Formation in the Brain at Different Oxygen Levels: The Role of Hypoxia Inducible Factors. Frontiers in Cell and Developmental Biology *6*.
Chen, Y.R., and Zweier, J.L. (2014). Cardiac mitochondria and reactive oxygen species generation. Circ Res *114*, 524-537.
Cheng, X., Chapple, S.J., Patel, B., Puszyk, W., Sugden, D., Yin, X., Mayr, M., Siow, R.C., and Mann, G.E. (2013). Gestational diabetes mellitus impairs Nrf2-mediated adaptive antioxidant defenses and redox signaling in fetal endothelial cells in utero. Diabetes *62*, 4088-4097.
Chevallet, M., Gallet, B., Fuchs, A., Jouneau, P.H., Um, K., Mintz, E., and Michaud-Soret, I. (2016). Metal homeostasis disruption and mitochondrial dysfunction in hepatocytes exposed to sub-toxic doses of zinc oxide nanoparticles. Nanoscale *8*, 18495-18506.

Chida, J., Yamane, K., Takei, T., and Kido, H. (2012). An efficient extraction method for quantitation of adenosine triphosphate in mammalian tissues and cells. Anal Chim Acta *727*, 8-12.
Chipperfield, B., and Chipperfield, J.R. (1978). Differences in metal content of the heart muscle in death from ischemic heart disease. Am Heart J *95*, 732-737.
Chiu, J.J., Chen, L.J., Lee, C.I., Lee, P.L., Lee, D.Y., Tsai, M.C., Lin, C.W., Usami, S., and Chien, S. (2007). Mechanisms of induction of endothelial cell E-selectin expression by smooth muscle cells and its inhibition by shear stress. Blood *110*, 519-528.
Choi, A.M.K., and Alam, J. (1996). Heme oxygenase-1: Function, regulation, and implication of a novel stress-inducible protein in oxidant-induced lung injury. Am J Resp Cell Mol *15*, 9-19.
Choi, S., Liu, X., and Pan, Z. (2018). Zinc deficiency and cellular oxidative stress: prognostic implications in cardiovascular diseases. Acta Pharmacol Sin *39*, 1120-1132.
Chorley, B.N., Campbell, M.R., Wang, X., Karaca, M., Sambandan, D., Bangura, F., Xue, P., Pi, J., Kleeberger, S.R., and Bell, D.A. (2012). Identification of novel NRF2-regulated genes by ChIP-Seq: influence on retinoid X receptor alpha. Nucleic Acids Res *40*, 7416-7429.
Chouchani, E.T., Pell, V.R., Gaude, E., Aksentijevic, D., Sundier, S.Y., Robb, E.L., Logan, A., Nadtochiy, S.M., Ord, E.N.J., Smith, A.C., *et al.* (2014). Ischaemic accumulation of succinate controls reperfusion injury through mitochondrial ROS. Nature *515*, 431-435.
Chowdhry, S., Zhang, Y., McMahon, M., Sutherland, C., Cuadrado, A., and Hayes, J.D. (2013). Nrf2 is controlled by two distinct beta-TrCP recognition motifs in its Neh6 domain, one of which can be modulated by GSK-3 activity. Oncogene *32*, 3765-3781.
Clempus, R.E., and Griendling, K.K. (2006). Reactive oxygen species signaling in vascular smooth muscle cells. Cardiovasc Res *71*, 216-225.
Cohen, P., and Frame, S. (2001). The renaissance of GSK3. Nat Rev Mol Cell Biol *2*, 769-776.
Collard, C.D., Lekowski, R., Jordan, J.E., Agah, A., and Stahl, G.L. (1999). Complement activation following oxidative stress. Mol Immunol *36*, 941-948.
Colvin, R.A., Holmes, W.R., Fontaine, C.P., and Maret, W. (2010). Cytosolic zinc buffering and muffling: Their role in intracellular zinc homeostasis. Metallomics *2*, 306-317.
Cooper, A.L., and Beasley, D. (1999). Hypoxia stimulates proliferation and interleukin-1 alpha production in human vascular smooth muscle cells. Am J Physiol-Heart C *277*, H1326-H1337.
Cooper, S., and Gonzalez-Hernandez, M. (2009). Experimental reconsideration of the utility of serum starvation as a method for synchronizing mammalian cells. Cell Biol Int *33*, 71-77.
Cortese, M.M., Suschek, C.V., Wetzel, W., Kroncke, K.D., and Kolb-Bachofen, V. (2008). Zinc protects endothelial cells from hydrogen peroxide via Nrf2-dependent stimulation of glutathione biosynthesis. Free Radical Bio Med *44*, 2002-2012.

Coverdale, J.P.C., Barnett, J.P., Adamu, A.H., Griffiths, E.J., Stewart, A.J., and Blindauer, C.A. (2019). A metalloproteomic analysis of interactions between plasma proteins and zinc: elevated fatty acid levels affect zinc distribution. Metallomics *11*, 1805-1819.
Coyle, P., Philcox, J.C., Carey, L.C., and Rofe, A.M. (2002). Metallothionein: the multipurpose protein. Cell Mol Life Sci *59*, 627-647.
Cuajungco, M.P., Basilio, L.C., Silva, J., Hart, T., Tringali, J., Chen, C.C., Biel, M., and Grimm, C. (2014). Cellular zinc levels are modulated by TRPML1-TMEM163 interaction. Traffic *15*, 1247-1265.
Cui, Z.W., Zhong, Z.H., Yang, Y., Wang, B.F., Sun, Y.H., Sun, Q.F., Yang, G.Y., and Bian, L.G. (2016). Ferrous Iron Induces Nrf2 Expression in Mouse Brain Astrocytes to Prevent Neurotoxicity. J Biochem Mol Toxic *30*, 396-403.
Culbreth, M., and Aschner, M. (2018). GSK-3beta, a double-edged sword in Nrf2 regulation: Implications for neurological dysfunction and disease. F1000Res *7*, 1043.
D'Amico, R., Fusco, R., Gugliandolo, E., Cordaro, M., Siracusa, R., Impellizzeri, D., Peritore, A.F., Crupi, R., Cuzzocrea, S., and Di Paola, R. (2019). Effects of a new compound containing Palmitoylethanolamide and Baicalein in myocardial ischaemia/reperfusion injury in vivo. Phytomedicine *54*, 27-42.
D'Autreaux, B., and Toledano, M.B. (2007). ROS as signalling molecules: mechanisms that generate specificity in ROS homeostasis. Nat Rev Mol Cell Bio *8*, 813-824.
Dalton, T.P., Li, Q., Bittel, D., Liang, L., and Andrews, G.K. (1996). Oxidative stress activates metal-responsive transcription factor-1 binding activity. Occupancy in vivo of metal response elements in the metallothionein-I gene promoter. J Biol Chem *271*, 26233-26241.
Davies, P.F. (1995). Flow-mediated endothelial mechanotransduction. Physiol Rev *75*, 519-560.
Davies, P.F., Dewey, C.F., Jr., Bussolari, S.R., Gordon, E.J., and Gimbrone, M.A., Jr. (1984). Influence of hemodynamic forces on vascular endothelial function. In vitro studies of shear stress and pinocytosis in bovine aortic cells. J Clin Invest *73*, 1121-1129.
Davis, C., Fischer, J., Ley, K., and Sarembock, I.J. (2003). The role of inflammation in vascular injury and repair. J Thromb Haemost *1*, 1699-1709.
Davis, M.J., Donovitz, J.A., and Hood, J.D. (1992). Stretch-activated single-channel and whole cell currents in vascular smooth muscle cells. Am J Physiol *262*, C1083-1088.
De Pascali, F., Hemann, C., Samons, K., Chen, C.A., and Zweier, J.L. (2014). Hypoxia and reoxygenation induce endothelial nitric oxide synthase uncoupling in endothelial cells through tetrahydrobiopterin depletion and S-glutathionylation. Biochemistry *53*, 3679-3688.
Della Corte, E., Gozzetti, G., Novello, F., and Stirpe, F. (1969). Properties of the xanthine oxidase from human liver. Biochim Biophys Acta *191*, 164-166.
DiNicolantonio, J.J., Mangan, D., and O'Keefe, J.H. (2018). Copper deficiency may be a leading cause of ischaemic heart disease. Open Heart *5*.

Dinkova-Kostova, A.T., Holtzclaw, W.D., and Wakabayashi, N. (2005). Keap1, the sensor for electrophiles and oxidants that regulates the phase 2 response, is a zinc metalloprotein. Biochemistry *44*, 6889-6899.
Dodge, J.T., Jr., Brown, B.G., Bolson, E.L., and Dodge, H.T. (1992). Lumen diameter of normal human coronary arteries. Influence of age, sex, anatomic variation, and left ventricular hypertrophy or dilation. Circulation *86*, 232-246.
Dodson, M., de la Vega, M.R., Cholanians, A.B., Schmidlin, C.J., Chapman, E., and Zhang, D.D. (2019). Modulating NRF2 in Disease: Timing Is Everything. Annu Rev Pharmacol *59*, 555-575.
Dong, L.H., Lv, P., and Han, M. (2012). Roles of SM22alpha in cellular plasticity and vascular diseases. Cardiovasc Hematol Disord Drug Targets *12*, 119-125.
Dora, K.A. (2001). Cell-cell communication in the vessel wall. Vasc Med *6*, 43-50.
Downey, J.M. (1990). Free radicals and their involvement during long-term myocardial ischemia and reperfusion. Annu Rev Physiol *52*, 487-504.
Downey, J.M., Miura, T., Eddy, L.J., Chambers, D.E., Mellert, T., Hearse, D.J., and Yellon, D.M. (1987). Xanthine oxidase is not a source of free radicals in the ischemic rabbit heart. J Mol Cell Cardiol *19*, 1053-1060.
Droge, W. (2002). Free radicals in the physiological control of cell function. Physiol Rev *82*, 47-95.
Drummond, G.R., Selemidis, S., Griendling, K.K., and Sobey, C.G. (2011). Combating oxidative stress in vascular disease: NADPH oxidases as therapeutic targets. Nat Rev Drug Discov *10*, 453-471.
Drummond, G.R., and Sobey, C.G. (2014). Endothelial NADPH oxidases: which NOX to target in vascular disease? Trends Endocrinol Metab *25*, 452-463.
Du, L.P., Zhang, H.L., Zhao, H.H., Cheng, X.X., Qin, J.Y., Teng, T.M., Yang, Q., and Xu, Z.L. (2019). The critical role of the zinc transporter Zip2 (SLC39A2) in ischemia/reperfusion injury in mouse hearts. Journal of Molecular and Cellular Cardiology *132*, 136-145.
Duncker, D.J., and Bache, R.J. (2008). Regulation of coronary blood flow during exercise. Physiol Rev *88*, 1009-1086.
Durante, W., Johnson, F.K., and Johnson, R.A. (2007). Arginase: a critical regulator of nitric oxide synthesis and vascular function. Clin Exp Pharmacol Physiol *34*, 906-911.
Durham, A.L., Speer, M.Y., Scatena, M., Giachelli, C.M., and Shanahan, C.M. (2018). Role of smooth muscle cells in vascular calcification: implications in atherosclerosis and arterial stiffness. Cardiovasc Res *114*, 590-600.
Eck, P., and Pallauf, J. (2001). Induction of metallothionein by exposure to normobaric 100% oxygen atmosphere in rats with different zinc supply. J Trace Elem Med Biol *15*, 229-235.

Eddy, L.J., Stewart, J.R., Jones, H.P., Engerson, T.D., McCord, J.M., and Downey, J.M. (1987). Free radical-producing enzyme, xanthine oxidase, is undetectable in human hearts. Am J Physiol *253*, H709-711.
Eelen, G., de Zeeuw, P., Treps, L., Harjes, U., Wong, B.W., and Carmeliet, P. (2018). Endothelial Cell Metabolism. Physiol Rev *98*, 3-58.
Eide, D.J. (2011a). The oxidative stress of zinc deficiency. Metallomics *3*, 1124-1129.
Eide, D.J. (2011b). The oxidative stress of zinc deficiency. Metallomics *3*, 1124-1129.
El Alami, M., Vina-Almunia, J., Gambini, J., Mas-Bargues, C., Siow, R.C., Penarrocha, M., Mann, G.E., Borras, C., and Vina, J. (2014). Activation of p38, p21, and NRF-2 mediates decreased proliferation of human dental pulp stem cells cultured under 21% O2. Stem Cell Reports *3*, 566-573.
Eleutherio, E.C.A., Magalhaes, R.S.S., Brasil, A.D., Neto, J.R.M., and Paranhos, L.D. (2021). SOD1, more than just an antioxidant. Archives of Biochemistry and Biophysics *697*.
Ellmark, S.H., Dusting, G.J., Fui, M.N., Guzzo-Pernell, N., and Drummond, G.R. (2005). The contribution of Nox4 to NADPH oxidase activity in mouse vascular smooth muscle. Cardiovasc Res *65*, 495-504.
Elrod, J.W., Duranski, M.R., Langston, W., Greer, J.J., Tao, L., Dugas, T.R., Kevil, C.G., Champion, H.C., and Lefer, D.J. (2006). eNOS gene therapy exacerbates hepatic ischemia-reperfusion injury in diabetes: a role for eNOS uncoupling. Circ Res *99*, 78-85.
Eltzschig, H.K., and Collard, C.D. (2004). Vascular ischaemia and reperfusion injury. Br Med Bull *70*, 71-86.
Epstein, D., Elias-Bishko, S., and Hershko, A. (1975). Requirement for protein synthesis in the regulation of protein breakdown in cultured hepatoma cells. Biochemistry *14*, 5199-5204.
Ernster, L. (1958). Diaphorase Activities in Liver Cytoplasmic Fractions. Federation Proceedings *17*, 216-216.
Ernster, L., and Navazio, F. (1958). Soluble Diaphorase in Animal Tissues. Acta Chem Scand *12*, 595-595.
Erusalimsky, J.D., and Moncada, S. (2007). Nitric oxide and mitochondrial signaling: from physiology to pathophysiology. Arterioscler Thromb Vasc Biol *27*, 2524-2531.
Fahey, J.W., Wade, K.L., Wehage, S.L., Holtzclaw, W.D., Liu, H., Talalay, P., Fuchs, E., and Stephenson, K.K. (2017). Stabilized sulforaphane for clinical use: Phytochemical delivery efficiency. Mol Nutr Food Res *61*.
Fallah, A., Mohammad-Hasani, A., and Colagar, A.H. (2018). Zinc is an Essential Element for Male Fertility: A Review of Zn Roles in Men's Health, Germination, Sperm Quality, and Fertilization. J Reprod Infertil *19*, 69-81.
Fatigati, V., and Murphy, R.A. (1984). Actin and tropomyosin variants in smooth muscles. Dependence on tissue type. J Biol Chem *259*, 14383-14388.
Feigl, E.O. (1983). Coronary physiology. Physiol Rev *63*, 1-205.

Feng, G.M., Chen, J.H., Lin, C.I., and Yang, J.M. (2012). Effect of docosahexaenoic acid on hypoxia/reoxygenation injury in human coronary arterial smooth muscle cells. Eur J Nutr *51*, 987-995.
Fercher, A., Borisov, S.M., Zhdanov, A.V., Klimant, I., and Papkovsky, D.B. (2011). Intracellular O2 sensing probe based on cell-penetrating phosphorescent nanoparticles. ACS Nano *5*, 5499-5508.
Fischhuber, K., Matzinger, M., and Heiss, E.H. (2020). AMPK Enhances Transcription of Selected Nrf2 Target Genes via Negative Regulation of Bach1. Front Cell Dev Biol *8*, 628.
Fisher, A.B., Al-Mehdi, A.B., and Muzykantov, V. (1999). Activation of endothelial NADPH oxidase as the source of a reactive oxygen species in lung ischemia. Chest *116*, 25S-26S.
Forman, H.J., Zhang, H., and Rinna, A. (2009). Glutathione: overview of its protective roles, measurement, and biosynthesis. Mol Aspects Med *30*, 1-12.
Foster, M., and Samman, S. (2010). Zinc and redox signaling: perturbations associated with cardiovascular disease and diabetes mellitus. Antioxid Redox Signal *13*, 1549-1573.
Foy, R.A., Shimizu, S., and Paul, R.J. (1997). The effects of hypoxia on pH(i) in porcine coronary artery endothelium and smooth muscle - A novel method for measurements in endothelial cells in situ. Circulation Research *80*, 21-27.
Fraenkel, M., Ketzinel-Gilad, M., Ariav, Y., Pappo, O., Karaca, M., Castel, J., Berthault, M.F., Magnan, C., Cerasi, E., Kaiser, N., *et al.* (2008). mTOR inhibition by rapamycin prevents beta-cell adaptation to hyperglycemia and exacerbates the metabolic state in type 2 diabetes. Diabetes *57*, 945-957.
Frame, S., and Cohen, P. (2001). GSK3 takes centre stage more than 20 years after its discovery. Biochem J *359*, 1-16.
Freimoser, F.M., Jakob, C.A., Aebi, M., and Tuor, U. (1999). The MTT [3-(4,5-dimethylthiazol-2-yl)-2,5-diphenyltetrazolium bromide] assay is a fast and reliable method for colorimetric determination of fungal cell densities. Appl Environ Microb *65*, 3727-3729.
Fu, H., Luo, F., Yang, L., Wu, W., and Liu, X. (2010). Hypoxia stimulates the expression of macrophage migration inhibitory factor in human vascular smooth muscle cells via HIF-1alpha dependent pathway. BMC Cell Biol *11*, 66.
Fujie, T., Segawa, Y., Yoshida, E., Kimura, T., Fujiwara, Y., Yamamoto, C., Satoh, M., Naka, H., and Kaji, T. (2016). Induction of metallothionein isoforms by copper diethyldithiocarbamate in cultured vascular endothelial cells. J Toxicol Sci *41*, 225-232.
Fujishiro, H., Yano, Y., Takada, Y., Tanihara, M., and Himeno, S. (2012). Roles of ZIP8, ZIP14, and DMT1 in transport of cadmium and manganese in mouse kidney proximal tubule cells. Metallomics *4*, 700-708.

Fukada, T., Yamasaki, S., Nishida, K., Murakami, M., and Hirano, T. (2011). Zinc homeostasis and signaling in health and diseases: Zinc signaling. J Biol Inorg Chem *16*, 1123-1134.
Furuta, T., Ohshima, C., Matsumura, M., Takebayashi, N., Hirota, E., Mawaribuchi, T., Nishida, K., and Nagasawa, K. (2016). Oxidative stress upregulates zinc uptake activity via Zrt/Irt-like protein 1 (ZIP1) in cultured mouse astrocytes. Life Sci *151*, 305-312.
Gao, L., Fan, Y., Zhang, X., Yang, L., Huang, W., Hang, T., Li, M., Du, S., and Ma, J. (2019). Zinc supplementation inhibits the high glucoseinduced EMT of peritoneal mesothelial cells by activating the Nrf2 antioxidant pathway. Mol Med Rep *20*, 655-663.
Gao, Y.S., Chen, T.J., and Raj, J.U. (2016). Endothelial and Smooth Muscle Cell Interactions in the Pathobiology of Pulmonary Hypertension. Am J Resp Cell Mol *54*, 451-460.
Garewal, H.S., Ahmann, F.R., Schifman, R.B., and Celniker, A. (1986). ATP assay: ability to distinguish cytostatic from cytocidal anticancer drug effects. J Natl Cancer Inst *77*, 1039-1045.
Ge, M.H., Tian, H., Mao, L., Li, D.Y., Lin, J.Q., Hu, H.S., Huang, S.C., Zhang, C.J., and Mei, X.F. (2021). Zinc attenuates ferroptosis and promotes functional recovery in contusion spinal cord injury by activating Nrf2/GPX4 defense pathway. CNS Neurosci Ther.
Geihs, M.A., Vargas, M.A., Maciel, F.E., Vakkuri, O., Meyer-Rochow, V.B., Allodi, S., and Nery, L.E.M. (2016). Effects of hypoxia and reoxygenation on the antioxidant defense system of the locomotor muscle of the crab Neohelice granulata (Decapoda, Varunidae). J Comp Physiol B *186*, 569-579.
Gerber, P.A., Bellomo, E.A., Hodson, D.J., Meur, G., Solomou, A., Mitchell, R.K., Hollinshead, M., Chimienti, F., Bosco, D., Hughes, S.J., *et al.* (2014). Hypoxia lowers SLC30A8/ZnT8 expression and free cytosolic Zn2+ in pancreatic beta cells. Diabetologia *57*, 1635-1644.
Ghoshal, K., and Jacob, S.T. (2001). Regulation of metallothionein gene expression. Prog Nucleic Acid Res Mol Biol *66*, 357-384.
Gonzalez-Flecha, B., and Boveris, A. (1995). Mitochondrial sites of hydrogen peroxide production in reperfused rat kidney cortex. Biochim Biophys Acta *1243*, 361-366.
Gonzalez-Flecha, B., Cutrin, J.C., and Boveris, A. (1993). Time course and mechanism of oxidative stress and tissue damage in rat liver subjected to in vivo ischemia-reperfusion. J Clin Invest *91*, 456-464.
Gonzalez-Iglesias, H., Alvarez, L., Garcia, M., Petrash, C., Sanz-Medel, A., and Coca-Prados, M. (2014). Metallothioneins (MTs) in the human eye: a perspective article on the zinc-MT redox cycle. Metallomics *6*, 201-208.
Goodwill, A.G., Dick, G.M., Kiel, A.M., and Tune, J.D. (2017). Regulation of Coronary Blood Flow. Compr Physiol *7*, 321-382.

Gough, P.J., Gomez, I.G., Wille, P.T., and Raines, E.W. (2006). Macrophage expression of active MMP-9 induces acute plaque disruption in apoE-deficient mice. J Clin Invest *116*, 59-69.
Granger, D.N., and Kvietys, P.R. (2015). Reperfusion injury and reactive oxygen species: The evolution of a concept. Redox Biol *6*, 524-551.
Granger, D.N., Rutili, G., and McCord, J.M. (1981). Superoxide radicals in feline intestinal ischemia. Gastroenterology *81*, 22-29.
Griendling, K.K., and Ushio-Fukai, M. (1998). Redox control of vascular smooth muscle proliferation. Journal of Laboratory and Clinical Medicine *132*, 9-15.
Grzywacz, A., Gdula-Argasinska, J., Muszynska, B., Tyszka-Czochara, M., Librowski, T., and Opoka, W. (2015). Metal responsive transcription factor 1 (MTF-1) regulates zinc dependent cellular processes at the molecular level. Acta Biochim Pol *62*, 491-498.
Gu, J., Cheng, Y., Wu, H., Kong, L., Wang, S., Xu, Z., Zhang, Z., Tan, Y., Keller, B.B., Zhou, H., *et al.* (2017). Metallothionein Is Downstream of Nrf2 and Partially Mediates Sulforaphane Prevention of Diabetic Cardiomyopathy. Diabetes *66*, 529-542.
Guarnieri, C., Flamigni, F., and Caldarera, C.M. (1980). Role of oxygen in the cellular damage induced by re-oxygenation of hypoxic heart. J Mol Cell Cardiol *12*, 797-808.
Gundry, S.R., Wang, N., Sciolaro, C.M., Van Arsdell, G.S., Razzouk, A.J., Hill, A.C., and Bailey, L.L. (1996). Uniformity of perfusion in all regions of the human heart by warm continuous retrograde cardioplegia. Ann Thorac Surg *61*, 33-35.
Gunther, V., Lindert, U., and Schaffner, W. (2012). The taste of heavy metals: gene regulation by MTF-1. Biochim Biophys Acta *1823*, 1416-1425.
Guo, R., Li, W., Liu, B., Li, S., Zhang, B., and Xu, Y. (2014). Resveratrol protects vascular smooth muscle cells against high glucose-induced oxidative stress and cell proliferation in vitro. Med Sci Monit Basic Res *20*, 82-92.
Gute, D., Fraga, C., Laughlin, M.H., and Amann, J.F. (1996). Regional changes in capillary supply in skeletal muscle of high-intensity endurance-trained rats. J Appl Physiol (1985) *81*, 619-626.
Guzik, T.J., Sadowski, J., Guzik, B., Jopek, A., Kapelak, B., Przybylowski, P., Wierzbicki, K., Korbut, R., Harrison, D.G., and Channon, K.M. (2006). Coronary artery superoxide production and nox isoform expression in human coronary artery disease. Arterioscler Thromb Vasc Biol *26*, 333-339.
Ha, K.N., Chen, Y., Cai, J.Y., and Sternberg, P. (2006). Increased glutathione synthesis through an ARE-Nrf2-dependent pathway by zinc in the RPE: Implication for protection against oxidative stress. Invest Ophth Vis Sci *47*, 2709-2715.
Haase, H., and Maret, W. (2003). Intracellular zinc fluctuations modulate protein tyrosine phosphatase activity in insulin/insulin-like growth factor-1 signaling. Experimental Cell Research *291*, 289-298.

Haase, H., Ober-Blobaum, J.L., Engelhardt, G., Hebel, S., Heit, A., Heine, H., and Rink, L. (2008). Zinc signals are essential for lipopolysaccharide-induced signal transduction in monocytes. J Immunol *181*, 6491-6502.
Haga, J.H., Li, Y.S., and Chien, S. (2007). Molecular basis of the effects of mechanical stretch on vascular smooth muscle cells. J Biomech *40*, 947-960.
Han, Y.L., Xiao, Y.P., Qi, Y.M., Kang, J., and Yan, C.H. (2008). [Expression of vascular smooth muscle cell markers during early stage of embryonic stem cell-derived embryoid bodies differentiation]. Zhongguo Ying Yong Sheng Li Xue Za Zhi *24*, 385-390.
Harrison, R. (2002). Structure and function of xanthine oxidoreductase: where are we now? Free Radic Biol Med *33*, 774-797.
Hart, B.J., Bian, X., Gwirtz, P.A., Setty, S., and Downey, H.F. (2001). Right ventricular oxygen supply/demand balance in exercising dogs. Am J Physiol Heart Circ Physiol *281*, H823-830.
Hartney, T., Birari, R., Venkataraman, S., Villegas, L., Martinez, M., Black, S.M., Stenmark, K.R., and Nozik-Grayck, E. (2011). Xanthine Oxidase-Derived ROS Upregulate Egr-1 via ERK1/2 in PA Smooth Muscle Cells; Model to Test Impact of Extracellular ROS in Chronic Hypoxia. Plos One *6*.
Hartsfield, C., Alam, J., and Choi, A.M.K. (1999). Differential signaling pathways of HO-1 gene expression in pulmonary and systemic vascular cells. Am J Physiol-Lung C *277*, L1133-L1141.
Hausenloy, D.J., Chilian, W., Crea, F., Davidson, S.M., Ferdinandy, P., Garcia-Dorado, D., van Royen, N., Schulz, R., and Heusch, G. (2019). The coronary circulation in acute myocardial ischaemia/reperfusion injury: a target for cardioprotection. Cardiovasc Res *115*, 1143-1155.
Hayashi, S., Omata, Y., Sakamoto, H., Higashimoto, Y., Hara, T., Sagara, Y., and Noguchi, M. (2004). Characterization of rat heme oxygenase-3 gene. Implication of processed pseudogenes derived from heme oxygenase-2 gene. Gene *336*, 241-250.
Hearse, D.J., Maxwell, L., Saldanha, C., and Gavin, J.B. (1993). The myocardial vasculature during ischemia and reperfusion: a target for injury and protection. J Mol Cell Cardiol *25*, 759-800.
Heizmann, C.W., and Cox, J.A. (1998). New perspectives on S100 proteins: a multi-functional Ca(2+)-, Zn(2+)- and Cu(2+)-binding protein family. Biometals *11*, 383-397.
Heusch, G. (2016). The Coronary Circulation as a Target of Cardioprotection. Circ Res *118*, 1643-1658.
Heywood, H.K., and Lee, D.A. (2010). Low oxygen reduces the modulation to an oxidative phenotype in monolayer-expanded chondrocytes. J Cell Physiol *222*, 248-253.

Higashi, Y., Aratake, T., Shimizu, T., Shimizu, S., and Saito, M. (2021). Protective Role of Glutathione in the Hippocampus after Brain Ischemia. Int J Mol Sci *22*.
Hill, B.G., Higdon, A.N., Dranka, B.P., and Darley-Usmar, V.M. (2010). Regulation of vascular smooth muscle cell bioenergetic function by protein glutathiolation. Biochim Biophys Acta *1797*, 285-295.
Hishikawa, K., Oemar, B.S., Yang, Z., and Luscher, T.F. (1997). Pulsatile stretch stimulates superoxide production and activates nuclear factor-kappa B in human coronary smooth muscle. Circ Res *81*, 797-803.
Hissin, P.J., and Hilf, R. (1976). A fluorometric method for determination of oxidized and reduced glutathione in tissues. Anal Biochem *74*, 214-226.
Hogstrand, C., Kille, P., Ackland, M.L., Hiscox, S., and Taylor, K.M. (2013). A mechanism for epithelial-mesenchymal transition and anoikis resistance in breast cancer triggered by zinc channel ZIP6 and STAT3 (signal transducer and activator of transcription 3). Biochem J *455*, 229-237.
Holland, R., and Fishbein, J.C. (2010). Chemistry of the cysteine sensors in Kelch-like ECH-associated protein 1. Antioxid Redox Signal *13*, 1749-1761.
Holmstrom, K.M., Kostov, R.V., and Dinkova-Kostova, A.T. (2016). The multifaceted role of Nrf2 in mitochondrial function. Curr Opin Toxicol *1*, 80-91.
Horie, N., So, K., Moriya, T., Kitagawa, N., Tsutsumi, K., Nagata, I., and Shinohara, K. (2008). Effects of oxygen concentration on the proliferation and differentiation of mouse neural stem cells in vitro. Cell Mol Neurobiol *28*, 833-845.
Hoskin, T.S., Crowther, J.M., Cheung, J., Epton, M.J., Sly, P.D., Elder, P.A., Dobson, R.C.J., Kettle, A.J., and Dickerhof, N. (2019). Oxidative cross-linking of calprotectin occurs in vivo, altering its structure and susceptibility to proteolysis. Redox Biol *24*, 101202.
Hossain, K.F.B., Hosokawa, T., Saito, T., and Kurasaki, M. (2021). Zinc-pretreatment triggers glutathione and Nrf2-mediated protection against inorganic mercury-induced cytotoxicity and intrinsic apoptosis in PC12 cells. Ecotox Environ Safe *207*.
Hotter, G., Closa, D., Gelpi, E., Prats, N., and Rosello-Catafau, J. (1995). Role of xanthine oxidase and eicosanoids in development of pancreatic ischemia-reperfusion injury. Inflammation *19*, 469-478.
Hou, W., Shan, Y., Zheng, J., Lambrecht, R.W., Donohue, S.E., and Bonkovsky, H.L. (2008). Zinc mesoporphyrin induces rapid and marked degradation of the transcription factor Bach1 and up-regulates HO-1. Biochim Biophys Acta *1779*, 195-203.
Huang, H.C., Nguyen, T., and Pickett, C.B. (2000). Regulation of the antioxidant response element by protein kinase C-mediated phosphorylation of NF-E2-related factor 2. P Natl Acad Sci USA *97*, 12475-12480.
Huber, D., Oskooei, A., Casadevall, I.S.X., Andrew, d., and Kaigala, G.V. (2018). Hydrodynamics in Cell Studies. Chem Rev *118*, 2042-2079.

Ichikawa, H., Takagi, T., Uchiyama, K., Higashihara, H., Katada, K., Isozaki, Y., Naito, Y., Yoshida, N., and Yoshikawa, T. (2004). Rotenone, a mitochondrial electron transport inhibitor, ameliorates ischemia-reperfusion-induced intestinal mucosal damage in rats. Redox Rep *9*, 313-316.
Ichimura, Y., Waguri, S., Sou, Y.S., Kageyama, S., Hasegawa, J., Ishimura, R., Saito, T., Yang, Y., Kouno, T., Fukutomi, T., *et al.* (2013). Phosphorylation of p62 activates the Keap1-Nrf2 pathway during selective autophagy. Mol Cell *51*, 618-631.
Ikeda, Y., Young, L.H., Scalia, R., Ross, C.R., and Lefer, A.M. (2001). PR-39, a proline/arginine-rich antimicrobial peptide, exerts cardioprotective effects in myocardial ischemia-reperfusion. Cardiovasc Res *49*, 69-77.
Im, M.J., Shen, W.H., Pak, C.J., Manson, P.N., Bulkley, G.B., and Hoopes, J.E. (1984). Effect of allopurinol on the survival of hyperemic island skin flaps. Plast Reconstr Surg *73*, 276-278.
Ischia, J., Bolton, D.M., and Patel, O. (2019). Why is it worth testing the ability of zinc to protect against ischaemia reperfusion injury for human application. Metallomics *11*, 1330-1343.
Ishida, I., Kubo, H., Suzuki, S., Suzuki, T., Akashi, S., Inoue, K., Maeda, S., Kikuchi, H., Sasaki, H., and Kondo, T. (2002). Hypoxia diminishes toll-like receptor 4 expression through reactive oxygen species generated by mitochondria in endothelial cells. J Immunol *169*, 2069-2075.
Ishida, T., and Takechi, S. (2016a). Nrf2-ARE-Dependent Alterations in Zinc Transporter mRNA Expression in HepG2 Cells. PLoS One *11*, e0166100.
Ishida, T., and Takechi, S. (2016b). Nrf2-ARE-Dependent Alterations in Zinc Transporter mRNA Expression in HepG2 Cells. Plos One *11*.
Ishii, T., Itoh, K., Ruiz, E., Leake, D.S., Unoki, H., Yamamoto, M., and Mann, G.E. (2004). Role of Nrf2 in the regulation of CD36 and stress protein expression in murine macrophages: activation by oxidatively modified LDL and 4-hydroxynonenal. Circ Res *94*, 609-616.
Ishii, T., Itoh, K., Takahashi, S., Sato, H., Yanagawa, T., Katoh, Y., Bannai, S., and Yamamoto, M. (2000). Transcription factor Nrf2 coordinately regulates a group of oxidative stress-inducible genes in macrophages. J Biol Chem *275*, 16023-16029.
Ishikawa, K., Sugawara, D., Wang, X., Suzuki, K., Itabe, H., Maruyama, Y., and Lusis, A.J. (2001). Heme oxygenase-1 inhibits atherosclerotic lesion formation in ldl-receptor knockout mice. Circ Res *88*, 506-512.
Ising, H., Gunther, T., Bertschat, F., Ibe, K., Stoboy, V., and Heldman, E. (1987). Alterations of Electrolytes in Serum and Erythrocytes after Myocardial-Infarction. Magnesium *6*, 192-200.

Itoh, K., Wakabayashi, N., Katoh, Y., Ishii, T., Igarashi, K., Engel, J.D., and Yamamoto, M. (1999). Keap1 represses nuclear activation of antioxidant responsive elements by Nrf2 through binding to the amino-terminal Neh2 domain. Genes Dev *13*, 76-86.
Jaakkola, P., Mole, D.R., Tian, Y.M., Wilson, M.I., Gielbert, J., Gaskell, S.J., von Kriegsheim, A., Hebestreit, H.F., Mukherji, M., Schofield, C.J., *et al.* (2001). Targeting of HIF-alpha to the von Hippel-Lindau ubiquitylation complex by O-2-regulated prolyl hydroxylation. Science *292*, 468-472.
Jain, R.K. (2003). Molecular regulation of vessel maturation. Nat Med *9*, 685-693.
Jain, T., Nikolopoulou, E.A., Xu, Q., and Qu, A. (2018). Hypoxia inducible factor as a therapeutic target for atherosclerosis. Pharmacol Ther *183*, 22-33.
Jang, H.S., Kim, J.I., Kim, J., Na, Y.K., Park, J.W., and Park, K.M. (2012). Bone marrow derived cells and reactive oxygen species in hypertrophy of contralateral kidney of transient unilateral renal ischemia-induced mouse. Free Radic Res *46*, 903-911.
Jatho, A., Zieseniss, A., Brechtel-Curth, K., Yamamoto, A., Coleman, M.L., Leon, A.M.V., Biggs, D., Davies, B., Pugh, C.W., Ratcliffe, P.J., *et al.* (2021). Precisely Tuned Inhibition of HIF Prolyl Hydroxylases Is Key for Cardioprotection After Ischemia. Circulation Research *128*, 1208-1210.
Jenkitkasemwong, S., Wang, C.Y., Mackenzie, B., and Knutson, M.D. (2012). Physiologic implications of metal-ion transport by ZIP14 and ZIP8. Biometals *25*, 643-655.
Jenner, A.M., Ruiz, J.E., Dunster, C., Halliwell, B., Mann, G.E., and Siow, R.C. (2002). Vitamin C protects against hypochlorous Acid-induced glutathione depletion and DNA base and protein damage in human vascular smooth muscle cells. Arterioscler Thromb Vasc Biol *22*, 574-580.
Jensen, L.F., Bentzon, J.F., and Albarran-Juarez, J. (2021). The Phenotypic Responses of Vascular Smooth Muscle Cells Exposed to Mechanical Cues. Cells *10*.
Jia, L.X., Zhang, W.M., Li, T.T., Liu, Y., Piao, C.M., Ma, Y.C., Lu, Y., Wang, Y., Liu, T.T., Qi, Y.F., *et al.* (2017). ER stress dependent microparticles derived from smooth muscle cells promote endothelial dysfunction during thoracic aortic aneurysm and dissection. Clin Sci *131*, 1287-1299.
Jiang, S., Yang, Y., Li, T., Ma, Z., Hu, W., Deng, C., Fan, C., Lv, J., Sun, Y., and Yi, W. (2016). An overview of the mechanisms and novel roles of Nrf2 in cardiovascular diseases. Expert Opin Ther Targets *20*, 1413-1424.
Johnson, J.A., Johnson, D.A., Kraft, A.D., Calkins, M.J., Jakel, R.J., Vargas, M.R., and Chen, P.C. (2008). The Nrf2-ARE pathway: an indicator and modulator of oxidative stress in neurodegeneration. Ann N Y Acad Sci *1147*, 61-69.
Jomova, K., and Valko, M. (2011). Advances in metal-induced oxidative stress and human disease. Toxicology *283*, 65-87.

Juan, S.H., Lee, T.S., Tseng, K.W., Liou, J.Y., Shyue, S.K., Wu, K.K., and Chau, L.Y. (2001). Adenovirus-mediated heme oxygenase-1 gene transfer inhibits the development of atherosclerosis in apolipoprotein E-deficient mice. Circulation *104*, 1519-1525.
Jufri, N.F., Mohamedali, A., Avolio, A., and Baker, M.S. (2015). Mechanical stretch: physiological and pathological implications for human vascular endothelial cells. Vasc Cell *7*, 8.
Jyrkkanen, H.K., Kuosmanen, S., Heinaniemi, M., Laitinen, H., Kansanen, E., Mella-Aho, E., Leinonen, H., Yla-Herttuala, S., and Levonen, A.L. (2011). Novel insights into the regulation of antioxidant-response-element-mediated gene expression by electrophiles: induction of the transcriptional repressor BACH1 by Nrf2. Biochemical Journal *440*, 167-174.
Kaelin, W.G. (2002). How oxygen makes its presence felt. Gene Dev *16*, 1441-1445.
Kahles, T., Kohnen, A., Heumueller, S., Rappert, A., Bechmann, I., Liebner, S., Wittko, I.M., Neumann-Haefelin, T., Steinmetz, H., Schroeder, K., *et al.* (2010). NADPH oxidase Nox1 contributes to ischemic injury in experimental stroke in mice. Neurobiol Dis *40*, 185-192.
Kalogeris, T., Baines, C.P., Krenz, M., and Korthuis, R.J. (2012). Cell biology of ischemia/reperfusion injury. Int Rev Cell Mol Biol *298*, 229-317.
Kambe, T., Tsuji, T., Hashimoto, A., and Itsumura, N. (2015). The Physiological, Biochemical, and Molecular Roles of Zinc Transporters in Zinc Homeostasis and Metabolism. Physiological Reviews *95*, 749-784.
Kansanen, E., Kuosmanen, S.M., Leinonen, H., and Levonen, A.L. (2013). The Keap1-Nrf2 pathway: Mechanisms of activation and dysregulation in cancer. Redox Biol *1*, 45-49.
Karagulova, G., Yue, Y., Moreyra, A., Boutjdir, M., and Korichneva, I. (2007). Protective role of intracellular zinc in myocardial ischemia/reperfusion is associated with preservation of protein kinase C isoforms. J Pharmacol Exp Ther *321*, 517-525.
Kasi, V., Bodiga, S., Kommuguri, U.N., Sankuru, S., and Bodiga, V.L. (2011). Zinc pyrithione salvages reperfusion injury by inhibiting NADPH oxidase activation in cardiomyocytes. Biochem Biophys Res Commun *410*, 270-275.
Kaspar, J.W., and Jaiswal, A.K. (2010). Antioxidant-induced Phosphorylation of Tyrosine 486 Leads to Rapid Nuclear Export of Bach1 That Allows Nrf2 to Bind to the Antioxidant Response Element and Activate Defensive Gene Expression. Journal of Biological Chemistry *285*, 153-162.
Kato, M., Narematsu, M., and Nakajima, Y. (2018). Anatomy of the coronary artery and cardiac vein in the quail ventricle: patterns are distinct from those in mouse and human hearts. Anat Sci Int *93*, 533-539.
Kaufman, Z., Salvador, G.A., Liu, X., and Oteiza, P.I. (2020). Zinc and the modulation of Nrf2 in human neuroblastoma cells. Free Radic Biol Med *155*, 1-9.
Kaushal, S., Amiel, G.E., Guleserian, K.J., Shapira, O.M., Perry, T., Sutherland, F.W., Rabkin, E., Moran, A.M., Schoen, F.J., Atala, A., *et al.* (2001). Functional small-diameter

neovessels created using endothelial progenitor cells expanded ex vivo. Nat Med *7*, 1035-1040.
Kayyali, U.S., Donaldson, C., Huang, H., Abdelnour, R., and Hassoun, P.M. (2001). Phosphorylation of xanthine dehydrogenase/oxidase in hypoxia. J Biol Chem *276*, 14359-14365.
Keeley, T.P., and Mann, G.E. (2019). Defining Physiological Normoxia for Improved Translation of Cell Physiology to Animal Models and Humans. Physiol Rev *99*, 161-234.
Keeley, T.P., Siow, R.C.M., Jacob, R., and Mann, G.E. (2017). A PP2A-mediated feedback mechanism controls Ca(2+)-dependent NO synthesis under physiological oxygen. FASEB J *31*, 5172-5183.
Kelmanson, I.V., Shokhina, A.G., Kotova, D.A., Pochechuev, M.S., Ivanova, A.D., Kostyuk, A.I., Panova, A.S., Borodinova, A.A., Solotenkov, M.A., Stepanov, E.A., *et al.* (2021). In vivo dynamics of acidosis and oxidative stress in the acute phase of an ischemic stroke in a rodent model. Redox Biol *48*, 102178.
Kensler, T.W., Egner, P.A., Agyeman, A.S., Visvanathan, K., Groopman, J.D., Chen, J.G., Chen, T.Y., Fahey, J.W., and Talalay, P. (2013). Keap1-Nrf2 Signaling: A Target for Cancer Prevention by Sulforaphane. Top Curr Chem *329*, 163-177.
Kerins, M.J., and Ooi, A. (2018). The Roles of NRF2 in Modulating Cellular Iron Homeostasis. Antioxid Redox Signal *29*, 1756-1773.
Kerkhoff, C., Vogl, T., Nacken, W., Sopalla, C., and Sorg, C. (1999). Zinc binding reverses the calcium-induced arachidonic acid-binding capacity of the S100A8/A9 protein complex. FEBS Lett *460*, 134-138.
Keyse, S.M., and Tyrrell, R.M. (1989). Heme Oxygenase Is the Major 32-Kda Stress Protein-Induced in Human-Skin Fibroblasts by Uva Radiation, Hydrogen-Peroxide, and Sodium Arsenite. P Natl Acad Sci USA *86*, 99-103.
Kim, S.Y., Choi, Y.J., Joung, S.M., Lee, B.H., Jung, Y.S., and Lee, J.Y. (2010). Hypoxic stress up-regulates the expression of Toll-like receptor 4 in macrophages via hypoxia-inducible factor. Immunology *129*, 516-524.
Kimura, M., Yamamoto, T., Zhang, J., Itoh, K., Kyo, M., Kamiya, T., Aburatani, H., Katsuoka, F., Kurokawa, H., Tanaka, T., *et al.* (2007). Molecular basis distinguishing the DNA binding profile of Nrf2-Maf heterodimer from that of Maf homodimer. J Biol Chem *282*, 33681-33690.
Kimura, T., and Kambe, T. (2016). The Functions of Metallothionein and ZIP and ZnT Transporters: An Overview and Perspective. Int J Mol Sci *17*, 336.
Kissen, R., Rossiter, J.T., and Bones, A.M. (2009). The 'mustard oil bomb': not so easy to assemble?! Localization, expression and distribution of the components of the myrosinase enzyme system. Phytochem Rev *8*, 69-86.

Kitamura, H., Morikawa, H., Kamon, H., Iguchi, M., Hojyo, S., Fukada, T., Yamashita, S., Kaisho, T., Akira, S., Murakami, M., *et al.* (2006). Toll-like receptor-mediated regulation of zinc homeostasis influences dendritic cell function. Nat Immunol *7*, 971-977.
Kitamuro, T., Takahashi, K., Ogawa, K., Udono-Fujimori, R., Takeda, K., Furuyama, K., Nakayama, M., Sun, J., Fujita, H., Hida, W., *et al.* (2003). Bach1 functions as a hypoxia-inducible repressor for the heme oxygenase-1 gene in human cells. J Biol Chem *278*, 9125-9133.
Kohar, I., Baca, M., Suarna, C., Stocker, R., and Southwell-Keely, P.T. (1995). Is alpha-tocopherol a reservoir for alpha-tocopheryl hydroquinone? Free Radic Biol Med *19*, 197-207.
Kojima, I., Tanaka, T., Inagi, R., Nishi, H., Aburatani, H., Kato, H., Miyata, T., Fujita, T., and Nangaku, M. (2009). Metallothionein is upregulated by hypoxia and stabilizes hypoxia-inducible factor in the kidney. Kidney Int *75*, 268-277.
Kong, S.M., Chan, B.K., Park, J.S., Hill, K.J., Aitken, J.B., Cottle, L., Farghaian, H., Cole, A.R., Lay, P.A., Sue, C.M., *et al.* (2014). Parkinson's disease-linked human PARK9/ATP13A2 maintains zinc homeostasis and promotes alpha-Synuclein externalization via exosomes. Hum Mol Genet *23*, 2816-2833.
Korichneva, I. (2006). Zinc dynamics in the myocardial redox signaling network. Antioxid Redox Signal *8*, 1707-1721.
Korthuis, R.J., Granger, D.N., Townsley, M.I., and Taylor, A.E. (1985). The role of oxygen-derived free radicals in ischemia-induced increases in canine skeletal muscle vascular permeability. Circ Res *57*, 599-609.
Korthuis, R.J., Gute, D.C., Blecha, F., and Ross, C.R. (1999). PR-39, a proline/arginine-rich antimicrobial peptide, prevents postischemic microvascular dysfunction. Am J Physiol *277*, H1007-1013.
Kown, M.H., Van der Steenhoven, T., Blankenberg, F.G., Hoyt, G., Berry, G.J., Tait, J.F., Strauss, H.W., and Robbins, R.C. (2000). Zinc-mediated reduction of apoptosis in cardiac allografts. Circulation *102*, III228-232.
Koyasu, S., Kobayashi, M., Goto, Y., Hiraoka, M., and Harada, H. (2018). Regulatory mechanisms of hypoxia-inducible factor 1 activity: Two decades of knowledge. Cancer Sci *109*, 560-571.
Krauss, S., Zhang, C.Y., and Lowell, B.B. (2005). The mitochondrial uncoupling-protein homologues. Nat Rev Mol Cell Biol *6*, 248-261.
Krezel, A., Hao, Q., and Maret, W. (2007). The zinc/thiolate redox biochemistry of metallothionein and the control of zinc ion fluctuations in cell signaling. Arch Biochem Biophys *463*, 188-200.
Krezel, A., and Maret, W. (2006). Zinc-buffering capacity of a eukaryotic cell at physiological pZn. J Biol Inorg Chem *11*, 1049-1062.

Krezel, A., and Maret, W. (2017). The Functions of Metamorphic Metallothioneins in Zinc and Copper Metabolism. Int J Mol Sci *18*.
Kumar, A., Dailey, L.A., Swedrowska, M., Siow, R., Mann, G.E., Vizcay-Barrena, G., Arno, M., Mudway, I.S., and Forbes, B. (2016). Quantifying the magnitude of the oxygen artefact inherent in culturing airway cells under atmospheric oxygen versus physiological levels. FEBS Lett *590*, 258-269.
Kuroo, M., Nagai, R., Tsuchimochi, H., Katoh, H., Yazaki, Y., Ohkubo, A., and Takaku, F. (1989). Developmentally Regulated Expression of Vascular Smooth-Muscle Myosin Heavy-Chain Isoforms. Journal of Biological Chemistry *264*, 18272-18275.
Kwok, S.C. (2013). Zinc Protoporphyrin Upregulates Heme Oxygenase-1 in PC-3 Cells via the Stress Response Pathway. Int J Cell Biol *2013*, 162094.
Lai, R.H., Miller, M.J., and Jeffery, E. (2010). Glucoraphanin hydrolysis by microbiota in the rat cecum results in sulforaphane absorption. Food & Function *1*, 161-166.
Lakkisto, P., Palojoki, E., Backlund, T., Saraste, A., Tikkanen, I., Voipio-Pulkki, L.M., and Pulkki, K. (2002). Expression of heme oxygenase-1 in response to myocardial infarction in rats. J Mol Cell Cardiol *34*, 1357-1365.
Landi, L., Fiorentini, D., Galli, M.C., SeguraAguilar, J., and Beyer, R.E. (1997). DT-diaphorase maintains the reduced state of ubiquinones in lipid vesicles thereby promoting their antioxidant function. Free Radical Bio Med *22*, 329-335.
Lassegue, B., San Martin, A., and Griendling, K.K. (2012). Biochemistry, physiology, and pathophysiology of NADPH oxidases in the cardiovascular system. Circ Res *110*, 1364-1390.
Lassegue, B., Sorescu, D., Szocs, K., Yin, Q., Akers, M., Zhang, Y., Grant, S.L., Lambeth, J.D., and Griendling, K.K. (2001). Novel gp91(phox) homologues in vascular smooth muscle cells : nox1 mediates angiotensin II-induced superoxide formation and redox-sensitive signaling pathways. Circ Res *88*, 888-894.
Laughlin, M.H., and Tomanek, R.J. (1987). Myocardial capillarity and maximal capillary diffusion capacity in exercise-trained dogs. J Appl Physiol (1985) *63*, 1481-1486.
Law, W., Kelland, E.E., Sharp, P., and Toms, N.J. (2003). Characterisation of zinc uptake into rat cultured cerebrocortical oligodendrocyte progenitor cells. Neuroscience Letters *352*, 113-116.
Lazarczyk, M., Pons, C., Mendoza, J.A., Cassonnet, P., Jacob, Y., and Favre, M. (2008). Regulation of cellular zinc balance as a potential mechanism of EVER-mediated protection against pathogenesis by cutaneous oncogenic human papillomaviruses. J Exp Med *205*, 35-42.
Lechler, P., Klein, S.M., Prantl, L., Englert, C., Renkawitz, T., and Grifka, J. (2011). Hypoxic downregulation of cellular proliferation and loss of phenotype stability in human osteoblasts is mediated by HIF-1alpha. Clin Hemorheol Microcirc *49*, 279-286.

Lee, M., Won, Y., Shin, Y., Kim, J.H., and Chun, J.S. (2016). Reciprocal activation of hypoxia-inducible factor (HIF)-2alpha and the zinc-ZIP8-MTF1 axis amplifies catabolic signaling in osteoarthritis. Osteoarthritis Cartilage *24*, 134-145.
Lehnert, M., Arteel, G.E., Smutney, O.M., Conzelmann, L.O., Zhong, Z., Thurman, R.G., and Lemasters, J.J. (2003). Dependence of liver injury after hemorrhage/resuscitation in mice on NADPH oxidase-derived superoxide. Shock *19*, 345-351.
Lei, C., Deng, J., Wang, B., Cheng, D., Yang, Q., Dong, H., and Xiong, L. (2011). Reactive oxygen species scavenger inhibits STAT3 activation after transient focal cerebral ischemia-reperfusion injury in rats. Anesth Analg *113*, 153-159.
Leonard, M.O., Kieran, N.E., Howell, K., Burne, M.J., Varadarajan, R., Dhakshinamoorthy, S., Porter, A.G., O'Farrelly, C., Rabb, H., and Taylor, C.T. (2006). Reoxygenation-specific activation of the antioxidant transcription factor Nrf2 mediates cytoprotective gene expression in ischemia-reperfusion injury. FASEB J *20*, 2624-2626.
Leoncini, E., Malaguti, M., Angeloni, C., Motori, E., Fabbri, D., and Hrelia, S. (2011). Cruciferous Vegetable Phytochemical Sulforaphane Affects Phase II Enzyme Expression and Activity in Rat Cardiomyocytes through Modulation of Akt Signaling Pathway. Journal of Food Science *76*, H175-H181.
Li, B., Cui, W.P., Tan, Y., Luo, P., Chen, Q., Zhang, C., Qu, W., Miao, L.N., and Cai, L. (2014). Zinc is essential for the transcription function of Nrf2 in human renal tubule cells in vitro and mouse kidney in vivo under the diabetic condition. Journal of Cellular and Molecular Medicine *18*, 895-906.
Li, C., and Jackson, R.M. (2002). Reactive species mechanisms of cellular hypoxia-reoxygenation injury. Am J Physiol Cell Physiol *282*, C227-241.
Li, D., Tian, H., Li, X., Mao, L., Zhao, X., Lin, J., Lin, S., Xu, C., Liu, Y., Guo, Y., *et al.* (2020a). Zinc promotes functional recovery after spinal cord injury by activating Nrf2/HO-1 defense pathway and inhibiting inflammation of NLRP3 in nerve cells. Life Sci *245*, 117351.
Li, D.Y., Tian, H., Li, X., Mao, L., Zhao, X.G., Lin, J.Q., Lin, S., Xu, C., Liu, Y.Y., Guo, Y., *et al.* (2020b). Zinc promotes functional recovery after spinal cord injury by activating Nrf2/HO-1 defense pathway and inhibiting inflammation of NLRP3 in nerve cells. Life Sciences *245*.
Li, F., Abuarab, N., and Sivaprasadarao, A. (2016). Reciprocal regulation of actin cytoskeleton remodelling and cell migration by Ca2+ and Zn2+: role of TRPM2 channels. J Cell Sci *129*, 2016-2029.
Li, J., Zhang, C., Xing, Y., Janicki, J.S., Yamamoto, M., Wang, X.L., Tang, D.Q., and Cui, T. (2011). Up-regulation of p27(kip1) contributes to Nrf2-mediated protection against angiotensin II-induced cardiac hypertrophy. Cardiovasc Res *90*, 315-324.
Li, Q., Li, B., Liu, C., Wang, L., Tang, J., and Hong, L. (2018). Protective role of Nrf2 against mechanical-stretch-induced apoptosis in mouse fibroblasts: a potential therapeutic

target of mechanical-trauma-induced stress urinary incontinence. Int Urogynecol J *29*, 1469-1477.
Li, Y.Y., Zhang, T., Li, X.Q., Zou, P., Schwartz, S.J., and Sun, D.X. (2013). Kinetics of sulforaphane in mice after consumption of sulforaphane-enriched broccoli sprout preparation. Molecular Nutrition & Food Research *57*, 2128-2136.
Liang, H., Yuan, Q.P., Dong, H.R., and Liu, Y.M. (2006). Determination of sulforaphane in broccoli and cabbage by high-performance liquid chromatography. J Food Compos Anal *19*, 473-476.
Liang, L.Y., Wang, M.M., Liu, M., Zhao, W., Wang, X., Shi, L., Zhu, M.J., Zhao, Y.L., Liu, L., Maurya, P., *et al.* (2020). Chronic toxicity of methamphetamine: Oxidative remodeling of pulmonary arteries. Toxicol In Vitro *62*, 104668.
Lien, C.F., Lee, W.S., Wang, I.C., Chen, T.I., Chen, T.L., and Yang, K.T. (2018). Intermittent hypoxia-generated ROS contributes to intracellular zinc regulation that limits ischemia/reperfusion injury in adult rat cardiomyocyte. Journal of Molecular and Cellular Cardiology *118*, 122-132.
Lin, A.A., and Miller, W.M. (1992). Modulation of Glutathione Level in Cho Cells - Effects of Oxygen Concentration and Prior Exposure to Hypoxia. Annals of the New York Academy of Sciences-Series *665*, 117-126.
Lin, C.L., Tseng, H.C., Chen, R.F., Chen, W.P., Su, M.J., Fang, K.M., and Wu, M.L. (2011a). Intracellular zinc release-activated ERK-dependent GSK-3 beta-p53 and Noxa-Mcl-1 signaling are both involved in cardiac ischemic-reperfusion injury. Cell Death and Differentiation *18*, 1651-1663.
Lin, C.L., Tseng, H.C., Chen, R.F., Chen, W.P., Su, M.J., Fang, K.M., and Wu, M.L. (2011b). Intracellular zinc release-activated ERK-dependent GSK-3beta-p53 and Noxa-Mcl-1 signaling are both involved in cardiac ischemic-reperfusion injury. Cell Death Differ *18*, 1651-1663.
Liou, C.S., Sirk, S.J., Diaz, C.A.C., Klein, A.P., Fischer, C.R., Higginbottom, S.K., Erez, A., Donia, M.S., Sonnenburg, J.L., and Sattely, E.S. (2020). A Metabolic Pathway for Activation of Dietary Glucosinolates by a Human Gut Symbiont. Cell *180*, 717-+.
Little, P.J., Bhattacharya, R., Moreyra, A.E., and Korichneva, I.L. (2010). Zinc and cardiovascular disease. Nutrition *26*, 1050-1057.
Liu, K., Fang, C., Shen, Y., Liu, Z., Zhang, M., Ma, B., and Pang, X. (2017). Hypoxia-inducible factor 1a induces phenotype switch of human aortic vascular smooth muscle cell through PI3K/AKT/AEG-1 signaling. Oncotarget *8*, 33343-33352.
Lu, S.C. (1999). Regulation of hepatic glutathione synthesis: current concepts and controversies. FASEB J *13*, 1169-1183.
Lu, S.C. (2009). Regulation of glutathione synthesis. Molecular Aspects of Medicine *30*, 42-59.

Lu, S.C. (2013). Glutathione synthesis. Biochim Biophys Acta *1830*, 3143-3153.
Lysiak, J.J., Zheng, S., Woodson, R., and Turner, T.T. (2007). Caspase-9-dependent pathway to murine germ cell apoptosis: mediation by oxidative stress, BAX, and caspase 2. Cell Tissue Res *328*, 411-419.
Ma, Q. (2013). Role of nrf2 in oxidative stress and toxicity. Annu Rev Pharmacol Toxicol *53*, 401-426.
Madi, H.A., Riches, K., Warburton, P., O'Regan, D.J., Turner, N.A., and Porter, K.E. (2009). Inherent differences in morphology, proliferation, and migration in saphenous vein smooth muscle cells cultured from nondiabetic and Type 2 diabetic patients. Am J Physiol Cell Physiol *297*, C1307-1317.
Maines, M.D. (1988). Heme Oxygenase - Function, Multiplicity, Regulatory Mechanisms, and Clinical-Applications. Faseb Journal *2*, 2557-2568.
Makarov, P.R., Wiswedel, I., Augustin, W., and Schild, L. (2002). Hypoxia/reoxygenation-induced damage to mitochondrial activity is determined by glutathione threshold in astroglia-rich cell cultures. Brain Research *933*, 91-97.
Malairaman, U., Dandapani, K., and Katyal, A. (2014). Effect of Ca2EDTA on zinc mediated inflammation and neuronal apoptosis in hippocampus of an in vivo mouse model of hypobaric hypoxia. PLoS One *9*, e110253.
Maltese, G., Psefteli, P.M., Rizzo, B., Srivastava, S., Gnudi, L., Mann, G.E., and Siow, R.C. (2017). The anti-ageing hormone klotho induces Nrf2-mediated antioxidant defences in human aortic smooth muscle cells. J Cell Mol Med *21*, 621-627.
Mammadova-Bach, E., and Braun, A. (2019). Zinc Homeostasis in Platelet-Related Diseases. Int J Mol Sci *20*.
Mansfield, K.D., Simon, M.C., and Keith, B. (2004). Hypoxic reduction in cellular glutathione levels requires mitochondrial reactive oxygen species. J Appl Physiol (1985) *97*, 1358-1366.
Maret, W. (2003). Cellular zinc and redox states converge in the metallothionein/thionein pair. Journal of Nutrition *133*, 1460s-1462s.
Maret, W. (2006). Zinc coordination environments in proteins as redox sensors and signal transducers. Antioxid Redox Signal *8*, 1419-1441.
Maret, W. (2011). Metals on the move: zinc ions in cellular regulation and in the coordination dynamics of zinc proteins. Biometals *24*, 411-418.
Maret, W. (2017a). Zinc in Cellular Regulation: The Nature and Significance of "Zinc Signals". International Journal of Molecular Sciences *18*.
Maret, W. (2017b). Zinc in Cellular Regulation: The Nature and Significance of "Zinc Signals". Int J Mol Sci *18*.
Maret, W. (2018). Metallomics: The Science of Biometals and Biometalloids. Adv Exp Med Biol *1055*, 1-20.

Maret, W. (2019). The redox biology of redox-inert zinc ions. Free Radic Biol Med *134*, 311-326.
Mari, M., Morales, A., Colell, A., Garcia-Ruiz, C., Kaplowitz, N., and Fernandez-Checa, J.C. (2013). Mitochondrial glutathione: Features, regulation and role in disease. Bba-Gen Subjects *1830*, 3317-3328.
Marreiro, D.D., Cruz, K.J.C., Morais, J.B.S., Beserra, J.B., Severo, J.S., and de Oliveira, A.R.S. (2017). Zinc and Oxidative Stress: Current Mechanisms. Antioxidants-Basel *6*.
Mates, J.M., Segura, J.A., Alonso, F.J., and Marquez, J. (2008). Intracellular redox status and oxidative stress: implications for cell proliferation, apoptosis, and carcinogenesis. Archives of Toxicology *82*, 273-299.
Maxwell, S.R., and Lip, G.Y. (1997). Reperfusion injury: a review of the pathophysiology, clinical manifestations and therapeutic options. Int J Cardiol *58*, 95-117.
McCord, J.M. (1985). Oxygen-derived free radicals in postischemic tissue injury. N Engl J Med *312*, 159-163.
McCoubrey, W.K., Huang, T.J., and Maines, M.D. (1997). Isolation and characterization of a cDNA from the rat brain that encodes hemoprotein heme oxygenase-3. European Journal of Biochemistry *247*, 725-732.
McMahon, M., Lamont, D.J., Beattie, K.A., and Hayes, J.D. (2010). Keap1 perceives stress via three sensors for the endogenous signaling molecules nitric oxide, zinc, and alkenals. Proc Natl Acad Sci U S A *107*, 18838-18843.
McMahon, M., Swift, S.R., and Hayes, J.D. (2018). Zinc-binding triggers a conformational-switch in the cullin-3 substrate adaptor protein KEAP1 that controls transcription factor NRF2. Toxicol Appl Pharmacol *360*, 45-57.
McNulty, P.H., King, N., Scott, S., Hartman, G., McCann, J., Kozak, M., Chambers, C.E., Demers, L.M., and Sinoway, L.I. (2005). Effects of supplemental oxygen administration on coronary blood flow in patients undergoing cardiac catheterization. Am J Physiol Heart Circ Physiol *288*, H1057-1062.
Meacham, K.A., Cortes, M.P., Wiggins, E.M., Maass, A., Latorre, M., Ralle, M., and Burkhead, J.L. (2018). Altered zinc balance in the Atp7b(-/-) mouse reveals a mechanism of copper toxicity in Wilson disease. Metallomics *10*, 1595-1606.
Medvedeva, Y.V., Lin, B., Shuttleworth, C.W., and Weiss, J.H. (2009). Intracellular Zn2+ accumulation contributes to synaptic failure, mitochondrial depolarization, and cell death in an acute slice oxygen-glucose deprivation model of ischemia. J Neurosci *29*, 1105-1114.
Meister, A. (1974). Glutathione, metabolism and function via the gamma-glutamyl cycle. Life Sci *15*, 177-190.
Meister, A. (1993). Biosynthesis and Functions of Glutathione. Proceedings of the First European Workshop on Glutathione, 2-10.
Meister, A. (1995). Glutathione biosynthesis and its inhibition. Methods Enzymol *252*, 26-30.

Meister, A., and Anderson, M.E. (1983). Glutathione. Annu Rev Biochem *52*, 711-760.
Meng, L., and Yu, B. (2011). Oxygen- and glucose-deprived culture promotes cell proliferation and invasion of vascular smooth muscle cells. International Journal of Molecular Medicine *28*, 777-783.
Messer, H.H., Murray, E.J., and Goebel, N.K. (1982). Removal of trace metals from culture media and sera for in vitro deficiency studies. J Nutr *112*, 652-657.
Meyrick, B., and Reid, L. (1978). The effect of continued hypoxia on rat pulmonary arterial circulation. An ultrastructural study. Lab Invest *38*, 188-200.
Michaelsen, J.T., Dehnert, S., Giustarini, D., Beckmann, B., and Tsikas, D. (2009). HPLC analysis of human erythrocytic glutathione forms using OPA and N-acetyl-cysteine ethyl ester: evidence for nitrite-induced GSH oxidation to GSSG. J Chromatogr B Analyt Technol Biomed Life Sci *877*, 3405-3417.
Mittal, M., Kumar, K., Anghore, D., and Rawal, R.K. (2017). ICP-MS: Analytical Method for Identification and Detection of Elemental Impurities. Curr Drug Discov Technol *14*, 106-120.
Miyai, T., Hojyo, S., Ikawa, T., Kawamura, M., Irie, T., Ogura, H., Hijikata, A., Bin, B.H., Yasuda, T., Kitamura, H., *et al.* (2014). Zinc transporter SLC39A10/ZIP10 facilitates antiapoptotic signaling during early B-cell development. Proc Natl Acad Sci U S A *111*, 11780-11785.
Moens, A.L., Champion, H.C., Claeys, M.J., Tavazzi, B., Kaminski, P.M., Wolin, M.S., Borgonjon, D.J., Van Nassauw, L., Haile, A., Zviman, M., *et al.* (2008). High-dose folic acid pretreatment blunts cardiac dysfunction during ischemia coupled to maintenance of high-energy phosphates and reduces postreperfusion injury. Circulation *117*, 1810-1819.
Moi, P., Chan, K., Asunis, I., Cao, A., and Kan, Y.W. (1994). Isolation of Nf-E2-Related Factor-2 (Nrf2), a Nf-E2-Like Basic Leucine-Zipper Transcriptional Activator That Binds to the Tandem Nf-E2/Ap1 Repeat of the Beta-Globin Locus-Control Region. P Natl Acad Sci USA *91*, 9926-9930.
Moncada, S., and Higgs, A. (1993). The L-arginine-nitric oxide pathway. N Engl J Med *329*, 2002-2012.
Moncada, S., Palmer, R.M., and Higgs, E.A. (1991). Nitric oxide: physiology, pathophysiology, and pharmacology. Pharmacol Rev *43*, 109-142.
Mori, Y., Takahashi, N., Polat, O.K., Kurokawa, T., Takeda, N., and Inoue, M. (2016). Redox-sensitive transient receptor potential channels in oxygen sensing and adaptation. Pflugers Arch *468*, 85-97.
Mosmann, T. (1983). Rapid colorimetric assay for cellular growth and survival: application to proliferation and cytotoxicity assays. J Immunol Methods *65*, 55-63.
Murakami, H., Kim, S.J., and Downey, H.F. (1989). Persistent right coronary flow reserve at low perfusion pressure. Am J Physiol *256*, H1176-1184.

Murakami, M., and Hirano, T. (2008). Intracellular zinc homeostasis and zinc signaling. Cancer Sci *99*, 1515-1522.
Murphy, B.J., Kimura, T., Sato, B.G., Shi, Y., and Andrews, G.K. (2008). Metallothionein induction by hypoxia involves cooperative interactions between metal-responsive transcription factor-1 and hypoxia-inducible transcription factor-1alpha. Mol Cancer Res *6*, 483-490.
Murphy, B.J., Sato, B.G., Dalton, T.P., and Laderoute, K.R. (2005). The metal-responsive transcription factor-1 contributes to HIF-1 activation during hypoxic stress. Biochem Biophys Res Commun *337*, 860-867.
Murphy, C.L., and Polak, J.M. (2004). Control of human articular chondrocyte differentiation by reduced oxygen tension. J Cell Physiol *199*, 451-459.
Muthuraman, A., Ramesh, M., and Chauhan, A. (2011). Mitochondrial dependent apoptosis: ameliorative effect of flunarizine on ischemia-reperfusion of celiac artery-induced gastric lesions in the rat. Dig Dis Sci *56*, 2244-2251.
Nagel, T., Resnick, N., Dewey, C.F., Jr., and Gimbrone, M.A., Jr. (1999). Vascular endothelial cells respond to spatial gradients in fluid shear stress by enhanced activation of transcription factors. Arterioscler Thromb Vasc Biol *19*, 1825-1834.
Nakagiri, A., Sunamoto, M., and Murakami, M. (2007). NADPH oxidase is involved in ischaemia/reperfusion-induced damage in rat gastric mucosa via ROS production--role of NADPH oxidase in rat stomachs. Inflammopharmacology *15*, 278-281.
Nakayama, M., Takahashi, K., Kitamuro, T., Yasumoto, K., Katayose, D., Shirato, K., Fujii-Kuriyama, Y., and Shibahara, S. (2000). Repression of heme oxygenase-1 by hypoxia in vascular endothelial cells. Biochem Bioph Res Co *271*, 665-671.
Nedd, S., Redler, R.L., Proctor, E.A., Dokholyan, N.V., and Alexandrova, A.N. (2014). Cu,Zn-superoxide dismutase without Zn is folded but catalytically inactive. J Mol Biol *426*, 4112-4124.
Neuville, P., Geinoz, A., Benzonana, G., Redard, M., Gabbiani, F., Ropraz, P., and Gabbiani, G. (1997). Cellular retinol-binding protein-1 is expressed by distinct subsets of rat arterial smooth muscle cells in vitro and in vivo. American Journal of Pathology *150*, 509-521.
Newby, D., Marks, L., and Lyall, F. (2005). Dissolved oxygen concentration in culture medium: assumptions and pitfalls. Placenta *26*, 353-357.
Nishino, T. (1994). The conversion of xanthine dehydrogenase to xanthine oxidase and the role of the enzyme in reperfusion injury. J Biochem *116*, 1-6.
Nishito, Y., and Kambe, T. (2019). Zinc transporter 1 (ZNT1) expression on the cell surface is elaborately controlled by cellular zinc levels. Journal of Biological Chemistry *294*, 15686-15697.
Niu, G., Sapoznik, E., and Soker, S. (2014). Bioengineered blood vessels. Expert Opin Biol Ther *14*, 403-410.

Nowbar, A.N., Gitto, M., Howard, J.P., Francis, D.P., and Al-Lamee, R. (2019). Mortality From Ischemic Heart Disease Analysis of Data From the World Health Organization and Coronary Artery Disease Risk Factors From NCD Risk Factor Collaboration. Circ-Cardiovasc Qual *12*.

Numata, T., Ogawa, N., Takahashi, N., and Mori, Y. (2013). TRP channels as sensors of oxygen availability. Pflugers Arch *465*, 1075-1085.

O'Reilly, K.E., Rojo, F., She, Q.B., Solit, D., Mills, G.B., Smith, D., Lane, H., Hofmann, F., Hicklin, D.J., Ludwig, D.L., *et al.* (2006). mTOR inhibition induces upstream receptor tyrosine kinase signaling and activates Akt. Cancer Res *66*, 1500-1508.

Ogawa, K., Sun, J., Taketani, S., Nakajima, O., Nishitani, C., Sassa, S., Hayashi, N., Yamamoto, M., Shibahara, S., Fujita, H., *et al.* (2001). Heme mediates derepression of Maf recognition element through direct binding to transcription repressor Bach1. EMBO J *20*, 2835-2843.

Ogo, O.A., Tyson, J., Cockell, S.J., Howard, A., Valentine, R.A., and Ford, D. (2015). The zinc finger protein ZNF658 regulates the transcription of genes involved in zinc homeostasis and affects ribosome biogenesis through the zinc transcriptional regulatory element. Mol Cell Biol *35*, 977-987.

Ohtsuji, M., Katsuoka, F., Kobayashi, A., Aburatani, H., Hayes, J.D., and Yamamoto, M. (2008). Nrf1 and Nrf2 play distinct roles in activation of antioxidant response element-dependent genes. J Biol Chem *283*, 33554-33562.

Okunade, O., Niranjan, K., Ghawi, S.K., Kuhnle, G., and Methven, L. (2018). Supplementation of the Diet by Exogenous Myrosinase via Mustard Seeds to Increase the Bioavailability of Sulforaphane in Healthy Human Subjects after the Consumption of Cooked Broccoli. Molecular Nutrition & Food Research *62*.

Omata, Y., Salvador, G.A., Supasai, S., Keenan, A.H., and Oteiza, P.I. (2013). Decreased Zinc Availability Affects Glutathione Metabolism in Neuronal Cells and in the Developing Brain. Toxicological Sciences *133*, 90-100.

Osol, G. (1995). Mechanotransduction by vascular smooth muscle. J Vasc Res *32*, 275-292.

Oster, O., Dahm, M., and Oelert, H. (1993). Element concentrations (selenium, copper, zinc, iron, magnesium, potassium, phosphorous) in heart tissue of patients with coronary heart disease correlated with physiological parameters of the heart. Eur Heart J *14*, 770-774.

Oteiza, P.I. (2012). Zinc and the modulation of redox homeostasis. Free Radic Biol Med *53*, 1748-1759.

Otterbein, L.E., and Choi, A.M.K. (2000). Heme oxygenase: colors of defense against cellular stress. Am J Physiol-Lung C *279*, L1029-L1037.

Owens, G.K. (1995). Regulation of differentiation of vascular smooth muscle cells. Physiol Rev *75*, 487-517.

Owens, G.K., Kumar, M.S., and Wamhoff, B.R. (2004). Molecular regulation of vascular smooth muscle cell differentiation in development and disease. Physiol Rev *84*, 767-801.
Pacher, P., Beckman, J.S., and Liaudet, L. (2007). Nitric oxide and peroxynitrite in health and disease. Physiol Rev *87*, 315-424.
Paller, M.S., Hoidal, J.R., and Ferris, T.F. (1984). Oxygen free radicals in ischemic acute renal failure in the rat. J Clin Invest *74*, 1156-1164.
Palmer, R.M., Ashton, D.S., and Moncada, S. (1988). Vascular endothelial cells synthesize nitric oxide from L-arginine. Nature *333*, 664-666.
Palmiter, R.D. (1987). Molecular biology of metallothionein gene expression. Experientia Suppl *52*, 63-80.
Palmiter, R.D., Findley, S.D., Whitmore, T.E., and Durnam, D.M. (1992). MT-III, a brain-specific member of the metallothionein gene family. Proc Natl Acad Sci U S A *89*, 6333-6337.
Pan, R., and Liu, K.J. (2016). ZNT-1 Expression Reduction Enhances Free Zinc Accumulation in Astrocytes After Ischemic Stroke. Acta Neurochir Suppl *121*, 257-261.
Panusatid, C., Thangsiriskul, N., and Peerapittayamongkol, C. (2022). Methods for mitochondrial health assessment by High Content Imaging System. MethodsX *9*, 101685.
Papaiahgari, S., Yerrapureddy, A., Hassoun, P.M., Garcia, J.G., Birukov, K.G., and Reddy, S.P. (2007). EGFR-activated signaling and actin remodeling regulate cyclic stretch-induced NRF2-ARE activation. Am J Respir Cell Mol Biol *36*, 304-312.
Paradies, G., Petrosillo, G., Pistolese, M., Di Venosa, N., Federici, A., and Ruggiero, F.M. (2004). Decrease in mitochondrial complex I activity in ischemic/reperfused rat heart: involvement of reactive oxygen species and cardiolipin. Circ Res *94*, 53-59.
Parat, M.O., Richard, M.J., Beani, J.C., and Favier, A. (1997). Involvement of zinc in intracellular oxidant/antioxidant balance. Biol Trace Elem Res *60*, 187-204.
Parker, P.E., Bashour, F.A., Downey, H.F., Kechejian, S.J., and Williams, A.G. (1975). Coronary hemodynamics during reperfusion following acute coronary ligation in dogs. Am Heart J *90*, 593-599.
Parks, D.A., and Granger, D.N. (1986). Xanthine oxidase: biochemistry, distribution and physiology. Acta Physiol Scand Suppl *548*, 87-99.
Parrinello, S., Samper, E., Krtolica, A., Goldstein, J., Melov, S., and Campisi, J. (2003). Oxygen sensitivity severely limits the replicative lifespan of murine fibroblasts. Nat Cell Biol *5*, 741-747.
Patrushev, N., Seidel-Rogol, B., and Salazar, G. (2012). Angiotensin II requires zinc and downregulation of the zinc transporters ZnT3 and ZnT10 to induce senescence of vascular smooth muscle cells. PLoS One *7*, e33211.
Patt, A., Harken, A.H., Burton, L.K., Rodell, T.C., Piermattei, D., Schorr, W.J., Parker, N.B., Berger, E.M., Horesh, I.R., Terada, L.S., *et al.* (1988). Xanthine oxidase-derived hydrogen

peroxide contributes to ischemia reperfusion-induced edema in gerbil brains. J Clin Invest *81*, 1556-1562.
Pennington, S.M., Klutho, P.R., Xie, L., Broadhurst, K., Koval, O.M., McCormick, M.L., Spitz, D.R., and Grumbach, I.M. (2018). Defective protein repair under methionine sulfoxide A deletion drives autophagy and ARE-dependent gene transcription. Redox Biol *16*, 401-413.
Perkins, K.A., Pershad, S., Chen, Q., McGraw, S., Adams, J.S., Zambrano, C., Krass, S., Emrich, J., Bell, B., Iyamu, M., *et al.* (2012). The effects of modulating eNOS activity and coupling in ischemia/reperfusion (I/R). Naunyn Schmiedebergs Arch Pharmacol *385*, 27-38.
Perry, M.A., Wadhwa, S., Parks, D.A., Pickard, W., and Granger, D.N. (1986). Role of oxygen radicals in ischemia-induced lesions in the cat stomach. Gastroenterology *90*, 362-367.
Piantadosi, C.A., Carraway, M.S., Babiker, A., and Suliman, H.B. (2008). Heme oxygenase-1 regulates cardiac mitochondrial biogenesis via Nrf2-mediated transcriptional control of nuclear respiratory factor-1. Circ Res *103*, 1232-1240.
Piantadosi, C.A., and Zhang, J. (1996). Mitochondrial generation of reactive oxygen species after brain ischemia in the rat. Stroke *27*, 327-331; discussion 332.
Piao, C.S., Gao, S., Lee, G.H., Kim, D.S., Park, B.H., Chae, S.W., Chae, H.J., and Kim, S.H. (2010a). Sulforaphane protects ischemic injury of hearts through antioxidant pathway and mitochondrial K-ATP channels. Pharmacological Research *61*, 342-348.
Piao, C.S., Gao, S., Lee, G.H., Kim, D.S., Park, B.H., Chae, S.W., Chae, H.J., and Kim, S.H. (2010b). Sulforaphane protects ischemic injury of hearts through antioxidant pathway and mitochondrial K(ATP) channels. Pharmacol Res *61*, 342-348.
Pirkmajer, S., and Chibalin, A.V. (2011). Serum starvation: caveat emptor. Am J Physiol Cell Physiol *301*, C272-279.
Plum, L.M., Rink, L., and Haase, H. (2010a). The essential toxin: impact of zinc on human health. Int J Environ Res Public Health *7*, 1342-1365.
Plum, L.M., Rink, L., and Haase, H. (2010b). The Essential Toxin: Impact of Zinc on Human Health. Int J Env Res Pub He *7*, 1342-1365.
Pober, J.S., Min, W., and Bradley, J.R. (2009). Mechanisms of endothelial dysfunction, injury, and death. Annu Rev Pathol *4*, 71-95.
Portal, L., Martin, V., Assaly, R., d'Anglemont de Tassigny, A., Michineau, S., Berdeaux, A., Ghaleb, B., and Pons, S. (2013). A model of hypoxia-reoxygenation on isolated adult mouse cardiomyocytes: characterization, comparison with ischemia-reperfusion, and application to the cardioprotective effect of regular treadmill exercise. J Cardiovasc Pharmacol Ther *18*, 367-375.
Powell, C.S., and Jackson, R.M. (2003). Mitochondrial complex I, aconitase, and succinate dehydrogenase during hypoxia-reoxygenation: modulation of enzyme activities by MnSOD. Am J Physiol Lung Cell Mol Physiol *285*, L189-198.

Powell, S.R. (2000). The antioxidant properties of zinc. J Nutr *130*, 1447S-1454S.
Prasad, A.S., and Bao, B. (2019). Molecular Mechanisms of Zinc as a Pro-Antioxidant Mediator: Clinical Therapeutic Implications. Antioxidants-Basel *8*.
Proudfoot, D., and Shanahan, C. (2012). Human vascular smooth muscle cell culture. Methods Mol Biol *806*, 251-263.
Qayumi, A.K., Janusz, M.T., Dorovini-Zis, K., Lyster, D.M., Jamieson, W.R., Poostizadeh, A., Feeley, E.J., and Nikbakht-Sangari, M. (1994). Additive effect of allopurinol and deferoxamine in the prevention of spinal cord injury caused by aortic crossclamping. J Thorac Cardiovasc Surg *107*, 1203-1209.
Qin, Z., Zhu, K., Xue, J., Cao, P., Xu, L., Xu, Z., Liang, K., Zhu, J., and Jia, R. (2019). Zinc-induced protective effect for testicular ischemia-reperfusion injury by promoting antioxidation via microRNA-101-3p/Nrf2 pathway. Aging (Albany NY) *11*, 9295-9309.
Quaife, C.J., Findley, S.D., Erickson, J.C., Froelick, G.J., Kelly, E.J., Zambrowicz, B.P., and Palmiter, R.D. (1994). Induction of a new metallothionein isoform (MT-IV) occurs during differentiation of stratified squamous epithelia. Biochemistry *33*, 7250-7259.
Rachmat, F.D., Rachmat, J., Sastroasmoro, S., and Wanandi, S.I. (2013). Effect of allopurinol on oxidative stress and hypoxic adaptation response during surgical correction of tetralogy of fallot. Acta Med Indones *45*, 94-100.
Rahil-Khazen, R., Bolann, B.J., Myking, A., and Ulvik, R.J. (2002). Multi-element analysis of trace element levels in human autopsy tissues by using inductively coupled atomic emission spectrometry technique (ICP-AES). J Trace Elem Med Bio *16*, 15-25.
Rahman, K. (2007). Studies on free radicals, antioxidants, and co-factors. Clinical Interventions in Aging *2*, 219-236.
Rajagopalan, S., Rane, A., Chinta, S.J., and Andersen, J.K. (2016). Regulation of ATP13A2 via PHD2-HIF1alpha Signaling Is Critical for Cellular Iron Homeostasis: Implications for Parkinson's Disease. J Neurosci *36*, 1086-1095.
Rajpurohit, R., Koch, C.J., Tao, Z.L., Teixeira, C.M., and Shapiro, I.M. (1996). Adaptation of chondrocytes to low oxygen tension: Relationship between hypoxia and cellular metabolism. Journal of Cellular Physiology *168*, 424-432.
Rangasamy, T., Guo, J., Mitzner, W.A., Roman, J., Singh, A., Fryer, A.D., Yamamoto, M., Kensler, T.W., Tuder, R.M., Georas, S.N., *et al.* (2005). Disruption of Nrf2 enhances susceptibility to severe airway inflammation and asthma in mice. J Exp Med *202*, 47-59.
Rashidi, N., Tafazzoli-Shadpour, M., Haghighipour, N., and Khani, M.M. (2018). Morphology and contractile gene expression of adipose-derived mesenchymal stem cells in response to short-term cyclic uniaxial strain and TGF-beta1. Biomed Tech (Berl) *63*, 317-326.
Ratcliffe, P.J. (2007). HIF-1 and HIF-2: working alone or together in hypoxia? Journal of Clinical Investigation *117*, 862-865.

Ratcliffe, P.J., O'Rourke, J.F., Maxwell, P.H., and Pugh, C.W. (1998). Oxygen sensing, hypoxia-inducible factor-1 and the regulation of mammalian gene expression. Journal of Experimental Biology *201*, 1153-1162.
Ray, J.B., Arab, S., Deng, Y., Liu, P., Penn, L., Courtman, D.W., and Ward, M.E. (2008). Oxygen regulation of arterial smooth muscle cell proliferation and survival. Am J Physiol-Heart C *294*, H839-H852.
Reffelmann, T., Hale, S.L., Dow, J.S., and Kloner, R.A. (2003). No-reflow phenomenon persists long-term after ischemia/reperfusion in the rat and predicts infarct expansion. Circulation *108*, 2911-2917.
Rensen, S.S., Doevendans, P.A., and van Eys, G.J. (2007). Regulation and characteristics of vascular smooth muscle cell phenotypic diversity. Neth Heart J *15*, 100-108.
Reusch, P., Wagdy, H., Reusch, R., Wilson, E., and Ives, H.E. (1996). Mechanical strain increases smooth muscle and decreases nonmuscle myosin expression in rat vascular smooth muscle cells. Circ Res *79*, 1046-1053.
Rieger, J.M., Shah, A.R., and Gidday, J.M. (2002). Ischemia-reperfusion injury of retinal endothelium by cyclooxygenase- and xanthine oxidase-derived superoxide. Exp Eye Res *74*, 493-501.
Risbano, M.G., and Gladwin, M.T. (2013). Therapeutics targeting of dysregulated redox equilibrium and endothelial dysfunction. Handb Exp Pharmacol *218*, 315-349.
Robledinos-Anton, N., Fernandez-Gines, R., Manda, G., and Cuadrado, A. (2019). Activators and Inhibitors of NRF2: A Review of Their Potential for Clinical Development. Oxid Med Cell Longev *2019*, 9372182.
Rodriguez, L.V., Alfonso, Z., Zhang, R., Leung, J., Wu, B., and Ignarro, L.J. (2006). Clonogenic multipotent stem cells in human adipose tissue differentiate into functional smooth muscle cells. Proc Natl Acad Sci U S A *103*, 12167-12172.
Roseborough, G., Gao, D., Chen, L., Trush, M.A., Zhou, S., Williams, G.M., and Wei, C. (2006). The mitochondrial K-ATP channel opener, diazoxide, prevents ischemia-reperfusion injury in the rabbit spinal cord. Am J Pathol *168*, 1443-1451.
Ross, D., Kepa, J.K., Winski, S.L., Beall, H.D., Anwar, A., and Siegel, D. (2000). NAD(P)H : quinone oxidoreductase 1 (NQO1): chemoprotection, bioactivation, gene regulation and genetic polymorphisms. Chem-Biol Interact *129*, 77-97.
Ross, D., and Siegel, D. (2004). NAD(P)H : Quinone oxidoreductase 1 (NQO1, DT-diaphorase), functions and pharmacogenctics. Quinones and Quinone Enzymes, Pt B *382*, 115-144.
Rousar, T., Kucera, O., Lotkova, H., and Cervinkova, Z. (2012). Assessment of reduced glutathione: comparison of an optimized fluorometric assay with enzymatic recycling method. Anal Biochem *423*, 236-240.

Rovner, A.S., Murphy, R.A., and Owens, G.K. (1986). Expression of smooth muscle and nonmuscle myosin heavy chains in cultured vascular smooth muscle cells. J Biol Chem *261*, 14740-14745.
Ruhee, R.T., and Suzuki, K. (2020). The Integrative Role of Sulforaphane in Preventing Inflammation, Oxidative Stress and Fatigue: A Review of a Potential Protective Phytochemical. Antioxidants-Basel *9*.
Ruiz, E., Siow, R.C., Bartlett, S.R., Jenner, A.M., Sato, H., Bannai, S., and Mann, G.E. (2003). Vitamin C inhibits diethylmaleate-induced L-cystine transport in human vascular smooth muscle cells. Free Radic Biol Med *34*, 103-110.
Ruttkay-Nedecky, B., Nejdl, L., Gumulec, J., Zitka, O., Masarik, M., Eckschlager, T., Stiborova, M., Adam, V., and Kizek, R. (2013). The role of metallothionein in oxidative stress. Int J Mol Sci *14*, 6044-6066.
Salazar, G., Huang, J., Feresin, R.G., Zhao, Y., and Griendling, K.K. (2017). Zinc regulates Nox1 expression through a NF-kappa B and mitochondrial ROS dependent mechanism to induce senescence of vascular smooth muscle cells. Free Radical Bio Med *108*, 225-235.
Salceda, S., and Caro, J. (1997). Hypoxia-inducible factor 1alpha (HIF-1alpha) protein is rapidly degraded by the ubiquitin-proteasome system under normoxic conditions. Its stabilization by hypoxia depends on redox-induced changes. J Biol Chem *272*, 22642-22647.
Sanchez, V.B., Ali, S., Escobar, A., and Cuajungco, M.P. (2019). Transmembrane 163 (TMEM163) protein effluxes zinc. Arch Biochem Biophys *677*, 108166.
Santini, M.P., Forte, E., Harvey, R.P., and Kovacic, J.C. (2016). Developmental origin and lineage plasticity of endogenous cardiac stem cells. Development *143*, 1242-1258.
Sarbassov, D.D., Guertin, D.A., Ali, S.M., and Sabatini, D.M. (2005). Phosphorylation and regulation of Akt/PKB by the rictor-mTOR complex. Science *307*, 1098-1101.
Satoh, T., McKercher, S.R., and Lipton, S.A. (2013). Nrf2/ARE-mediated antioxidant actions of pro-electrophilic drugs. Free Radic Biol Med *65*, 645-657.
Schwarz, M., Lossow, K., Kopp, J.F., Schwerdtle, T., and Kipp, A.P. (2019). Crosstalk of Nrf2 with the Trace Elements Selenium, Iron, Zinc, and Copper. Nutrients *11*.
Segal, S.S. (1994). Cell-to-cell communication coordinates blood flow control. Hypertension *23*, 1113-1120.
Seki, T., Naruse, M., Naruse, K., Yoshimoto, T., Tanabe, A., Imaki, T., Hagiwara, H., Hirose, S., and Demura, H. (1997). Interrelation between nitric oxide synthase and heme oxygenase in rat endothelial cells. Eur J Pharmacol *331*, 87-91.
Semenza, G.L. (2001). HIF-1 and mechanisms of hypoxia sensing. Curr Opin Cell Biol *13*, 167-171.
Semenza, G.L. (2014). Hypoxia-Inducible Factor 1 and Cardiovascular Disease. Annual Review of Physiology, Vol 76 *76*, 39-56.

Sener, T.E., Yuksel, M., Ozyilmaz-Yay, N., Ercan, F., Akbal, C., Simsek, F., and Sener, G. (2015). Apocynin attenuates testicular ischemia-reperfusion injury in rats. J Pediatr Surg *50*, 1382-1387.
Seymour, E.M., Bennink, M.R., and Bolling, S.F. (2013). Diet-relevant phytochemical intake affects the cardiac AhR and nrf2 transcriptome and reduces heart failure in hypertensive rats. J Nutr Biochem *24*, 1580-1586.
Sgarbi, G., Gorini, G., Costanzini, A., Barbato, S., Solaini, G., and Baracca, A. (2017). Hypoxia decreases ROS level in human fibroblasts. Int J Biochem Cell Biol *88*, 133-144.
Shakibi, J.G., Nazarian, I., and Moezzi, B. (1982). Myocardial metal content in patients who expired from cyanotic congenital heart disease and acute rheumatic heart disease. Jpn Heart J *23*, 717-723.
Shen, B.B., Mei, M., Pu, Y.M., Zhang, H.H., Liu, H., Tang, M.Z., Pan, Q.G., He, Y., Wu, X.F., and Zhao, H.W. (2019a). Necrostatin-1 Attenuates Renal Ischemia and Reperfusion Injury via Meditation of HIF-1 alpha/mir-26a/TRPC6/PARP1 Signaling. Mol Ther-Nucl Acids *17*, 701-713.
Shen, H., Eguchi, K., Kono, N., Fujiu, K., Matsumoto, S., Shibata, M., Oishi-Tanaka, Y., Komuro, I., Arai, H., Nagai, R., *et al.* (2013). Saturated fatty acid palmitate aggravates neointima formation by promoting smooth muscle phenotypic modulation. Arterioscler Thromb Vasc Biol *33*, 2596-2607.
Shen, Y., Liu, X., Shi, J., and Wu, X. (2019b). Involvement of Nrf2 in myocardial ischemia and reperfusion injury. Int J Biol Macromol *125*, 496-502.
Shibahara, S., Han, F., Li, B., and Takeda, K. (2007). Hypoxia and heme oxygenases: Oxygen sensing and regulation of expression. Antioxid Redox Sign *9*, 2209-2225.
Shin, J.M., Lee, K.M., Lee, H.J., Yun, J.H., and Nho, C.W. (2019). Physalin A regulates the Nrf2 pathway through ERK and p38 for induction of detoxifying enzymes. Bmc Complem Altern M *19*.
Shiratsuki, S., Hara, T., Munakata, Y., Shirasuna, K., Kuwayama, T., and Iwata, H. (2016). Low oxygen level increases proliferation and metabolic changes in bovine granulosa cells. Mol Cell Endocrinol *437*, 75-85.
Siegel, D., Gustafson, D.L., Dehn, D.L., Han, J.Y., Boonchoong, P., Berliner, L.J., and Ross, D. (2004). NAD(P)H : quinone oxidoreductase 1: Role as a superoxide scavenger. Molecular Pharmacology *65*, 1238-1247.
Sies, H., Belousov, V.V., Chandel, N.S., Davies, M.J., Jones, D.P., Mann, G.E., Murphy, M.P., Yamamoto, M., and Winterbourn, C. (2022). Defining roles of specific reactive oxygen species (ROS) in cell biology and physiology. Nat Rev Mol Cell Biol *23*, 499-515.
Sies, H., and Jones, D.P. (2020). Reactive oxygen species (ROS) as pleiotropic physiological signalling agents. Nat Rev Mol Cell Bio *21*, 363-383.

Silva-Gomes, S., Santos, A.G., Caldas, C., Silva, C.M., Neves, J.V., Lopes, J., Carneiro, F., Rodrigues, P.N., and Duarte, T.L. (2014). Transcription factor NRF2 protects mice against dietary iron- induced liver injury by preventing hepatocytic cell death. Journal of Hepatology *60*, 354-361.

Silva-Palacios, A., Ostolga-Chavarria, M., Sanchez-Garibay, C., Rojas-Morales, P., Galvan-Arzate, S., Buelna-Chontal, M., Pavon, N., Pedraza-Chaverri, J., Konigsberg, M., and Zazueta, C. (2019). Sulforaphane protects from myocardial ischemia-reperfusion damage through the balanced activation of Nrf2/AhR. Free Radic Biol Med *143*, 331-340.

Sindreu, C., Palmiter, R.D., and Storm, D.R. (2011). Zinc transporter ZnT-3 regulates presynaptic Erk1/2 signaling and hippocampus-dependent memory. P Natl Acad Sci USA *108*, 3366-3370.

Sinha-Hikim, I., Shen, R., Paul Lee, W.N., Crum, A., Vaziri, N.D., and Norris, K.C. (2010). Effects of a novel cystine-based glutathione precursor on oxidative stress in vascular smooth muscle cells. Am J Physiol Cell Physiol *299*, C638-642.

Siow, R.C., Sato, H., Leake, D.S., Pearson, J.D., Bannai, S., and Mann, G.E. (1998). Vitamin C protects human arterial smooth muscle cells against atherogenic lipoproteins: effects of antioxidant vitamins C and E on oxidized LDL-induced adaptive increases in cystine transport and glutathione. Arterioscler Thromb Vasc Biol *18*, 1662-1670.

Sirbu, A., Palamarciuc, O., Babak, M.V., Lim, J.M., Ohui, K., Enyedy, E.A., Shova, S., Darvasiova, D., Rapta, P., Ang, W.H., *et al.* (2017). Copper(II) thiosemicarbazone complexes induce marked ROS accumulation and promote nrf2-mediated antioxidant response in highly resistant breast cancer cells. Dalton T *46*, 3833-3847.

Smith, M.J., Yang, F., Griffiths, A., Morrell, A., Chapple, S.J., Siow, R.C.M., Stewart, T., Maret, W., and Mann, G.E. (2023). Redox and metal profiles in human coronary endothelial and smooth muscle cells under hyperoxia, physiological normoxia and hypoxia: Effects of NRF2 signaling on intracellular zinc. Redox Biol *62*, 102712.

Smith, P.K., Krohn, R.I., Hermanson, G.T., Mallia, A.K., Gartner, F.H., Provenzano, M.D., Fujimoto, E.K., Goeke, N.M., Olson, B.J., and Klenk, D.C. (1985). Measurement of Protein Using Bicinchoninic Acid. Analytical Biochemistry *150*, 76-85.

Solini, A., Zamboni, P., Passaro, A., Fellin, R., and Ferrannini, E. (2006). Acute vascular events and electrolytes variations in elderly patients. Hormone and Metabolic Research *38*, 197-202.

Song, M.O., Mattie, M.D., Lee, C.H., and Freedman, J.H. (2014). The role of Nrf1 and Nrf2 in the regulation of copper-responsive transcription. Experimental Cell Research *322*, 39-50.

Srinivas, V., Zhang, L.P., Zhu, X.H., and Caro, J. (1999). Characterization of an oxygen/redox-dependent degradation domain of hypoxia-inducible factor alpha (HIF-alpha) proteins. Biochem Biophys Res Commun *260*, 557-561.

Srivastava, S., Blower, P.J., Aubdool, A.A., Hider, R.C., Mann, G.E., and Siow, R.C. (2016). Cardioprotective effects of Cu((II))ATSM in human vascular smooth muscle cells and cardiomyocytes mediated by Nrf2 and DJ-1. Sci Rep *6*, 7.
Stewart, T.J. (2019). Across the spectrum: integrating multidimensional metal analytics for in situ metallomic imaging. Metallomics *11*, 29-49.
Su, B., Mitra, S., Gregg, H., Flavahan, S., Chotani, M.A., Clark, K.R., Goldschmidt-Clermont, P.J., and Flavahan, N.A. (2001). Redox regulation of vascular smooth muscle cell differentiation. Circulation Research *89*, 39-46.
Sun, Z., Huang, Z.P., and Zhang, D.D. (2009). Phosphorylation of Nrf2 at Multiple Sites by MAP Kinases Has a Limited Contribution in Modulating the Nrf2-Dependent Antioxidant Response. Plos One *4*.
Sussulini, A., Becker, J.S., and Becker, J.S. (2017). Laser ablation ICP-MS: Application in biomedical research. Mass Spectrom Rev *36*, 47-57.
Suzuki, T., Muramatsu, A., Saito, R., Iso, T., Shibata, T., Kuwata, K., Kawaguchi, S.I., Iwawaki, T., Adachi, S., Suda, H., *et al.* (2019). Molecular Mechanism of Cellular Oxidative Stress Sensing by Keap1. Cell Rep *28*, 746-758 e744.
Suzuki, T., and Yamamoto, M. (2015). Molecular basis of the Keap1-Nrf2 system. Free Radic Biol Med *88*, 93-100.
Takagishi, T., Hara, T., and Fukada, T. (2017). Recent Advances in the Role of SLC39A/ZIP Zinc Transporters In Vivo. International Journal of Molecular Sciences *18*.
Tao, J., Barnett, J.V., Watanabe, M., and Ramirez-Bergeron, D. (2018). Hypoxia Supports Epicardial Cell Differentiation in Vascular Smooth Muscle Cells through the Activation of the TGFbeta Pathway. J Cardiovasc Dev Dis *5*.
Tarbell, J.M. (2010). Shear stress and the endothelial transport barrier. Cardiovasc Res *87*, 320-330.
Tebay, L.E., Robertson, H., Durant, S.T., Vitale, S.R., Penning, T.M., Dinkova-Kostova, A.T., and Hayes, J.D. (2015). Mechanisms of activation of the transcription factor Nrf2 by redox stressors, nutrient cues, and energy status and the pathways through which it attenuates degenerative disease. Free Radic Biol Med *88*, 108-146.
Tejero, J., Shiva, S., and Gladwin, M.T. (2019). Sources of Vascular Nitric Oxide and Reactive Oxygen Species and Their Regulation. Physiol Rev *99*, 311-379.
Tenhunen, R., Marver, H.S., and Schmid, R. (1968). Enzymatic Conversion of Heme to Bilirubin by Microsomal Heme Oxygenase. P Natl Acad Sci USA *61*, 748-&.
Terada, L.S., Dormish, J.J., Shanley, P.F., Leff, J.A., Anderson, B.O., and Repine, J.E. (1992). Circulating xanthine oxidase mediates lung neutrophil sequestration after intestinal ischemia-reperfusion. Am J Physiol *263*, L394-401.

Thyberg, J., Hedin, U., Sjolund, M., Palmberg, L., and Bottger, B.A. (1990). Regulation of differentiated properties and proliferation of arterial smooth muscle cells. Arteriosclerosis *10*, 966-990.
Toedebusch, R., Belenchia, A., and Pulakat, L. (2018). Cell-Specific Protective Signaling Induced by the Novel AT2R-Agonist NP-6A4 on Human Endothelial and Smooth Muscle Cells. Front Pharmacol *9*, 928.
Tonelli, C., Chio, I.I.C., and Tuveson, D.A. (2018). Transcriptional Regulation by Nrf2. Antioxid Redox Signal *29*, 1727-1745.
Tousoulis, D., Antoniades, C., and Stefanadis, C. (2005). Evaluating endothelial function in humans: a guide to invasive and non-invasive techniques. Heart *91*, 553-558.
Tousoulis, D., and Davies, G. (1998). Acetylcholine and endothelial function. Circulation *98*, 1588-1589.
Toyokuni, S. (1999). Reactive oxygen species-induced molecular damage and its application in pathology. Pathol Int *49*, 91-102.
Tran, H.B., Jakobczak, R., Abdo, A., Asare, P., Reynolds, P., Beltrame, J., Hodge, S., and Zalewski, P. (2022). Immunolocalization of zinc transporters and metallothioneins reveals links to microvascular morphology and functions. Histochemistry and Cell Biology *158*, 485-496.
Tran, T.P., Tu, H., Liu, J., Muelleman, R.L., and Li, Y.L. (2012). Mitochondria-derived superoxide links to tourniquet-induced apoptosis in mouse skeletal muscle. PLoS One *7*, e43410.
Trepiana, J., Meijide, S., Navarro, R., Hernandez, M.L., Ruiz-Sanz, J.I., and Ruiz-Larrea, M.B. (2017). Influence of oxygen partial pressure on the characteristics of human hepatocarcinoma cells. Redox Biology *12*, 103-113.
Triggle, C.R., Samuel, S.M., Ravishankar, S., Marei, I., Arunachalam, G., and Ding, H. (2012). The endothelium: influencing vascular smooth muscle in many ways. Can J Physiol Pharmacol *90*, 713-738.
Tsuda, M., Imaizumi, K., Katayama, T., Kitagawa, K., Wanaka, A., Tohyama, M., and Takagi, T. (1997). Expression of zinc transporter gene, ZnT-1, is induced after transient forebrain ischemia in the gerbil. J Neurosci *17*, 6678-6684.
Tsunemi, T., Hamada, K., and Krainc, D. (2014). ATP13A2/PARK9 regulates secretion of exosomes and alpha-synuclein. J Neurosci *34*, 15281-15287.
Tuncay, E., and Turan, B. (2016). Intracellular Zn2+ Increase in Cardiomyocytes Induces both Electrical and Mechanical Dysfunction in Heart via Endogenous Generation of Reactive Nitrogen Species. Biol Trace Elem Res *169*, 294-302.
Turer, A.T., and Hill, J.A. (2010). Pathogenesis of myocardial ischemia-reperfusion injury and rationale for therapy. Am J Cardiol *106*, 360-368.

Turker Sener, L., Albeniz, G., Dinc, B., and Albeniz, I. (2017). iCELLigence real-time cell analysis system for examining the cytotoxicity of drugs to cancer cell lines. Exp Ther Med *14*, 1866-1870.

Ungvari, Z., Bailey-Downs, L., Gautam, T., Jimenez, R., Losonczy, G., Zhang, C., Ballabh, P., Recchia, F.A., Wilkerson, D.C., Sonntag, W.E., *et al.* (2011). Adaptive induction of NF-E2-related factor-2-driven antioxidant genes in endothelial cells in response to hyperglycemia. Am J Physiol Heart Circ Physiol *300*, H1133-1140.

Utting, J.C., Robins, S.P., Brandao-Burch, A., Orriss, I.R., Behar, J., and Arnett, T.R. (2006). Hypoxia inhibits the growth, differentiation and bone-forming capacity of rat osteoblasts. Exp Cell Res *312*, 1693-1702.

Valko, M., Jomova, K., Rhodes, C.J., Kuca, K., and Musilek, K. (2016). Redox- and non-redox-metal-induced formation of free radicals and their role in human disease. Archives of Toxicology *90*, 1-37.

Valko, M., Morris, H., and Cronin, M.T.D. (2005). Metals, toxicity and oxidative stress. Current Medicinal Chemistry *12*, 1161-1208.

Vallee, B.L., and Falchuk, K.H. (1993). The biochemical basis of zinc physiology. Physiol Rev *73*, 79-118.

van Eys, G.J., Niessen, P.M., and Rensen, S.S. (2007). Smoothelin in vascular smooth muscle cells. Trends Cardiovas Med *17*, 26-30.

vanderLoop, F.T.L., Schaart, G., Timmer, E.D.J., Ramaekers, F.C.S., and vanEys, G.J.J.M. (1996). Smoothelin, a novel cytoskeletal protein specific for smooth muscle cells. Journal of Cell Biology *134*, 401-411.

Veber, M., Dolivo, D., Rolle, M., and Dominko, T. (2018). Pro-myogenic and low-oxygen culture increases expression of contractile smooth muscle markers in human fibroblasts. J Tissue Eng Regen M *12*, 572-582.

Veness-Meehan, K.A., Cheng, E.R., Mercier, C.E., Blixt, S.L., Johnston, C.J., Watkins, R.H., and Horowitz, S. (1991). Cell-specific alterations in expression of hyperoxia-induced mRNAs of lung. Am J Respir Cell Mol Biol *5*, 516-521.

Vickers, S., Schiller, H.J., Hildreth, J.E., and Bulkley, G.B. (1998). Immunoaffinity localization of the enzyme xanthine oxidase on the outside surface of the endothelial cell plasma membrane. Surgery *124*, 551-560.

Viswanath, K., Bodiga, S., Balogun, V., Zhang, A., and Bodiga, V.L. (2011). Cardioprotective effect of zinc requires ErbB2 and Akt during hypoxia/reoxygenation. Biometals *24*, 171-180.

Vomund, S., Schafer, A., Parnham, M.J., Brune, B., and von Knethen, A. (2017). Nrf2, the Master Regulator of Anti-Oxidative Responses. Int J Mol Sci *18*.

Vretzakis, G., Ferdi, E., Papaziogas, B., Dragoumanis, C., Pneumatikos, J., Tsangaris, I., Tsakiridis, K., and Konstantinou, F. (2004). Coronary sinus venoarterial CO2 difference in different hemodynamic states. Acta Anaesthesiol Belg *55*, 221-227.
Walder, C.E., Green, S.P., Darbonne, W.C., Mathias, J., Rae, J., Dinauer, M.C., Curnutte, J.T., and Thomas, G.R. (1997). Ischemic stroke injury is reduced in mice lacking a functional NADPH oxidase. Stroke *28*, 2252-2258.
Waller, B.F. (1989). The Eccentric Coronary Atherosclerotic Plaque - Morphologic Observations and Clinical Relevance. Clinical Cardiology *12*, 14-20.
Waller, B.F., Orr, C.M., Slack, J.D., Pinkerton, C.A., Van Tassel, J., and Peters, T. (1992). Anatomy, histology, and pathology of coronary arteries: a review relevant to new interventional and imaging techniques--Part I. Clin Cardiol *15*, 451-457.
Wallert, M., Ziegler, M., Wang, X., Maluenda, A., Xu, X., Yap, M.L., Witt, R., Giles, C., Kluge, S., Hortmann, M., *et al.* (2019). alpha-Tocopherol preserves cardiac function by reducing oxidative stress and inflammation in ischemia/reperfusion injury. Redox Biol *26*, 101292.
Wang, G., Jacquet, L., Karamariti, E., and Xu, Q. (2015). Origin and differentiation of vascular smooth muscle cells. J Physiol *593*, 3013-3030.
Wang, J., Wang, S., Wang, W., Chen, J., Zhang, Z., Zheng, Q., Liu, Q., and Cai, L. (2019). Protection against diabetic cardiomyopathy is achieved using a combination of sulforaphane and zinc in type 1 diabetic OVE26 mice. J Cell Mol Med *23*, 6319-6330.
Wang, W., Li, S., Wang, H., Li, B., Shao, L., Lai, Y., Horvath, G., Wang, Q., Yamamoto, M., Janicki, J.S., *et al.* (2014). Nrf2 enhances myocardial clearance of toxic ubiquitinated proteins. J Mol Cell Cardiol *72*, 305-315.
Wang, X.J., Hayes, J.D., Higgins, L.G., Wolf, C.R., and Dinkova-Kostova, A.T. (2010). Activation of the NRF2 signaling pathway by copper-mediated redox cycling of para- and ortho-hydroquinones. Chem Biol *17*, 75-85.
Wang, Z., Zhang, A., Meng, W., Wang, T., Li, D., Liu, Z., and Liu, H. (2018). Ozone protects the rat lung from ischemia-reperfusion injury by attenuating NLRP3-mediated inflammation, enhancing Nrf2 antioxidant activity and inhibiting apoptosis. Eur J Pharmacol *835*, 82-93.
Ward, J.P. (2008). Oxygen sensors in context. Biochim Biophys Acta *1777*, 1-14.
Warpsinski, G., Smith, M.J., Srivastava, S., Keeley, T.P., Siow, R.C.M., Fraser, P.A., and Mann, G.E. (2020). Nrf2-regulated redox signaling in brain endothelial cells adapted to physiological oxygen levels: Consequences for sulforaphane mediated protection against hypoxia-reoxygenation. Redox Biol *37*, 101708.
Wasa, M., Soh, H., Shimizu, Y., and Fukuzawa, M. (2005). Glutamine stimulates amino acid transport during ischemia reperfusion in human intestinal epithelial cells. Journal of Surgical Research *123*, 75-81.

Wastney, M.E., Aamodt, R.L., Rumble, W.F., and Henkin, R.I. (1986). Kinetic analysis of zinc metabolism and its regulation in normal humans. Am J Physiol *251*, R398-408.
Wheaton, W.W., and Chandel, N.S. (2011). Hypoxia. 2. Hypoxia regulates cellular metabolism. Am J Physiol Cell Physiol *300*, C385-393.
White, M., Rouleau, J.L., Ruddy, T.D., De Marco, T., Moher, D., and Chatterjee, K. (1991). Decreased coronary sinus oxygen content: a predictor of adverse prognosis in patients with severe congestive heart failure. J Am Coll Cardiol *18*, 1631-1637.
Wiafe, B., Adesida, A., Churchill, T., Adewuyi, E.E., Li, Z., and Metcalfe, P. (2017). Hypoxia-increased expression of genes involved in inflammation, dedifferentiation, pro-fibrosis, and extracellular matrix remodeling of human bladder smooth muscle cells. In Vitro Cell Dev Biol Anim *53*, 58-66.
Widlansky, M.E., Gokce, N., Keaney, J.F., Jr., and Vita, J.A. (2003). The clinical implications of endothelial dysfunction. J Am Coll Cardiol *42*, 1149-1160.
Wilschefski, S.C., and Baxter, M.R. (2019). Inductively Coupled Plasma Mass Spectrometry: Introduction to Analytical Aspects. Clin Biochem Rev *40*, 115-133.
Wind, S., Beuerlein, K., Armitage, M.E., Taye, A., Kumar, A.H., Janowitz, D., Neff, C., Shah, A.M., Wingler, K., and Schmidt, H.H. (2010). Oxidative stress and endothelial dysfunction in aortas of aged spontaneously hypertensive rats by NOX1/2 is reversed by NADPH oxidase inhibition. Hypertension *56*, 490-497.
Wohrley, J.D., Frid, M.G., Moiseeva, E.P., Orton, E.C., Belknap, J.K., and Stenmark, K.R. (1995). Hypoxia selectively induces proliferation in a specific subpopulation of smooth muscle cells in the bovine neonatal pulmonary arterial media. J Clin Invest *96*, 273-281.
Woodruff, T., Blake, D.R., Freeman, J., Andrews, F.J., Salt, P., and Lunec, J. (1986). Is chronic synovitis an example of reperfusion injury? Ann Rheum Dis *45*, 608-611.
Wu, G., and He, X. (2006). Threonine 41 in beta-catenin serves as a key phosphorylation relay residue in beta-catenin degradation. Biochemistry *45*, 5319-5323.
Wu, L., and Juurlink, B.H. (2001). The impaired glutathione system and its up-regulation by sulforaphane in vascular smooth muscle cells from spontaneously hypertensive rats. J Hypertens *19*, 1819-1825.
Wu, Y.F., Lv, C.Z., Zou, L.G., Sun, J., Song, X.J., Zhang, Y., and Mao, J.W. (2021). Approaches for enhancing the stability and formation of sulforaphane. Food Chemistry *345*.
Xu, B., Zhang, J., Strom, J., Lee, S., and Chen, Q.M. (2014a). Myocardial ischemic reperfusion induces de novo Nrf2 protein translation. Biochim Biophys Acta *1842*, 1638-1647.
Xu, L., He, S., Yin, P., Li, D., Mei, C., Yu, X., Shi, Y., Jiang, L., and Liu, F. (2016). Punicalagin induces Nrf2 translocation and HO-1 expression via PI3K/Akt, protecting rat intestinal epithelial cells from oxidative stress. Int J Hyperthermia *32*, 465-473.

Xu, Z.L., Kim, S., and Huh, J. (2014b). Zinc plays a critical role in the cardioprotective effect of postconditioning by enhancing the activation of the RISK pathway in rat hearts. Journal of Molecular and Cellular Cardiology *66*, 12-17.
Xu, Z.L., and Zhou, J. (2013). Zinc and myocardial ischemia/reperfusion injury. Biometals *26*, 863-878.
Xue, J., Wang, S., Wu, J.C., Hannafon, B.N., and Ding, W.Q. (2013). Zinc at Sub-Cytotoxic Concentrations Induces Heme Oxygenase-1 Expression in Human Cancer Cells. Cellular Physiology and Biochemistry *32*, 100-110.
Xue, M.Z., Qian, Q.W., Adaikalakoteswari, A., Rabbani, N., Babaei-Jadidi, R., and Thornalley, P.J. (2008). Activation of NF-E2-related factor-2 reverses biochemical dysfunction of endothelial cells induced by hyperglycemia linked to vascular disease. Diabetes *57*, 2809-2817.
Yamamoto, M., Kensler, T.W., and Motohashi, H. (2018). The KEAP1-NRF2 System: a Thiol-Based Sensor-Effector Apparatus for Maintaining Redox Homeostasis. Physiol Rev *98*, 1169-1203.
Yamamoto, T., Suzuki, T., Kobayashi, A., Wakabayashi, J., Maher, J., Motohashi, H., and Yamamoto, M. (2008). Physiological significance of reactive cysteine residues of Keap1 in determining Nrf2 activity. Mol Cell Biol *28*, 2758-2770.
Yamasaki, S., Sakata-Sogawa, K., Hasegawa, A., Suzuki, T., Kabu, K., Sato, E., Kurosaki, T., Yamashita, S., Tokunaga, M., Nishida, K., *et al.* (2007). Zinc is a novel intracellular second messenger. J Cell Biol *177*, 637-645.
Yamashita, S., Miyagi, C., Fukada, T., Kagara, N., Che, Y.S., and Hirano, T. (2004). Zinc transporter LIVI controls epithelial-mesenchymal transition in zebrafish gastrula organizer. Nature *429*, 298-302.
Yang, M.M., Dart, C., Kamishima, T., and Quayle, J.M. (2020). Hypoxia and metabolic inhibitors alter the intracellular ATP:ADP ratio and membrane potential in human coronary artery smooth muscle cells. Peerj *8*.
Yang, W., Li, C., Ward, D.M., Kaplan, J., and Mansour, S.L. (2000). Defective organellar membrane protein trafficking in Ap3b1-deficient cells. J Cell Sci *113 (Pt 22)*, 4077-4086.
Ye, B., Maret, W., and Vallee, B.L. (2001). Zinc metallothionein imported into liver mitochondria modulates respiration. P Natl Acad Sci USA *98*, 2317-2322.
Ye, C.Y., Lian, G.L., Wang, T.J., Chen, A., Chen, W.X., Gong, J., Luo, L., Wang, H.J., and Xie, L.D. (2022). The zinc transporter ZIP12 regulates monocrotaline-induced proliferation and migration of pulmonary arterial smooth muscle cells via the AKT/ERK signaling pathways. Bmc Pulmonary Medicine *22*.
Yin, X.J., de Carvalho, L.P., Chan, M.Y., and Li, S.F.Y. (2017). Integrated metabolomics and metallomics analyses in acute coronary syndrome patients. Metallomics *9*, 734-743.

Yokota, H., Narayanan, S.P., Zhang, W., Liu, H., Rojas, M., Xu, Z., Lemtalsi, T., Nagaoka, T., Yoshida, A., Brooks, S.E., *et al.* (2011). Neuroprotection from retinal ischemia/reperfusion injury by NOX2 NADPH oxidase deletion. Invest Ophthalmol Vis Sci *52*, 8123-8131.

Yokoyama, Y., Beckman, J.S., Beckman, T.K., Wheat, J.K., Cash, T.G., Freeman, B.A., and Parks, D.A. (1990). Circulating xanthine oxidase: potential mediator of ischemic injury. Am J Physiol *258*, G564-570.

Yoo, Y.C., Lee, S.K., Yang, J.Y., In, S.W., Kima, K.W., Chung, K.H., Chung, M.G., and Choung, S.Y. (2002). Organ distribution of heavy metals in autopsy material from normal Korean. J Health Sci *48*, 186-194.

Yoshida, T., Kaestner, K.H., and Owens, G.K. (2008). Conditional deletion of Kruppel-like factor 4 delays downregulation of smooth muscle cell differentiation markers but accelerates neointimal formation following vascular injury. Circ Res *102*, 1548-1557.

Yu, L., Li, Q., Yu, B., Yang, Y., Jin, Z., Duan, W., Zhao, G., Zhai, M., Liu, L., Yi, D., *et al.* (2016). Berberine Attenuates Myocardial Ischemia/Reperfusion Injury by Reducing Oxidative Stress and Inflammation Response: Role of Silent Information Regulator 1. Oxid Med Cell Longev *2016*, 1689602.

Yu, X., and Kensler, T. (2005). Nrf2 as a target for cancer chemoprevention. Mutat Res-Fund Mol M *591*, 93-102.

Zago, M.P., and Oteiza, P.I. (2001). The antioxidant properties of zinc: Interactions with iron and antioxidants. Free Radical Bio Med *31*, 266-274.

Zakkar, M., Van der Heiden, K., Luong, L.A., Chaudhury, H., Cuhlmann, S., Hamdulay, S.S., Krams, R., Edirisinghe, I., Rahman, I., Carlsen, H., *et al.* (2009a). Activation of Nrf2 in Endothelial Cells Protects Arteries From Exhibiting a Proinflammatory State. Arterioscl Throm Vas *29*, 1851-U1353.

Zakkar, M., Van der Heiden, K., Luong le, A., Chaudhury, H., Cuhlmann, S., Hamdulay, S.S., Krams, R., Edirisinghe, I., Rahman, I., Carlsen, H., *et al.* (2009b). Activation of Nrf2 in endothelial cells protects arteries from exhibiting a proinflammatory state. Arterioscler Thromb Vasc Biol *29*, 1851-1857.

Zhan, K.Y., Yu, P.L., Liu, C.H., Luo, J.H., and Yang, W. (2016). Detrimental or beneficial: the role of TRPM2 in ischemia/reperfusion injury. Acta Pharmacol Sin *37*, 4-12.

Zhang, D.D., and Hannink, M. (2003). Distinct cysteine residues in Keap1 are required for Keap1-dependent ubiquitination of Nrf2 and for stabilization of Nrf2 by chemopreventive agents and oxidative stress. Mol Cell Biol *23*, 8137-8151.

Zhang, G., Sheng, M., Wang, J., Teng, T., Sun, Y., Yang, Q., and Xu, Z. (2018). Zinc improves mitochondrial respiratory function and prevents mitochondrial ROS generation at reperfusion by phosphorylating STAT3 at Ser(727). J Mol Cell Cardiol *118*, 169-182.

Zhang, H., Yang, N., He, H., Chai, J., Cheng, X., Zhao, H., Zhou, D., Teng, T., Kong, X., Yang, Q., *et al.* (2021). The zinc transporter ZIP7 (Slc39a7) controls myocardial reperfusion injury by regulating mitophagy. Basic Res Cardiol *116*, 54.
Zhang, X.L., Shu, X.O., Xiang, Y.B., Yang, G., Li, H.L., Gao, J., Cai, H., Gao, Y.T., and Zheng, W. (2011). Cruciferous vegetable consumption is associated with a reduced risk of total and cardiovascular disease mortality. American Journal of Clinical Nutrition *94*, 240-246.
Zhang, Z.G., Wang, S.D., Zhou, S.S., Yan, X.Q., Wang, Y.G., Mellen, N., Kong, M.Y., Gu, J.L., Tan, Y., Zheng, Y., *et al.* (2014). Sulforaphane prevents the development of cardiomyopathy in type 2 diabetic mice probably by reversing oxidative stress-induced inhibition of LKB1/AMPK pathway. Journal of Molecular and Cellular Cardiology *77*, 42-52.
Zhao, F., Sellgren, K., and Ma, T. (2009). Low-oxygen pretreatment enhances endothelial cell growth and retention under shear stress. Tissue Eng Part C Methods *15*, 135-146.
Zhao, J.F., Bertoglio, B.A., Gee, K.R., and Kay, A.R. (2008). The zinc indicator FluoZin-3 is not perturbed significantly by physiological levels of calcium or magnesium. Cell Calcium *44*, 422-426.
Zhao, L., Oliver, E., Maratou, K., Atanur, S.S., Dubois, O.D., Cotroneo, E., Chen, C.N., Wang, L., Arce, C., Chabosseau, P.L., *et al.* (2015). The zinc transporter ZIP12 regulates the pulmonary vascular response to chronic hypoxia. Nature *524*, 356-360.
Zhdanov, A.V., Dmitriev, R.I., Hynes, J., and Papkovsky, D.B. (2014). Kinetic analysis of local oxygenation and respiratory responses of mammalian cells using intracellular oxygen-sensitive probes and time-resolved fluorometry. Methods Enzymol *542*, 183-207.
Zhu, H., Cao, Z., Zhang, L., Trush, M.A., and Li, Y. (2007). Glutathione and glutathione-linked enzymes in normal human aortic smooth muscle cells: chemical inducibility and protection against reactive oxygen and nitrogen species-induced injury. Mol Cell Biochem *301*, 47-59.
Zhu, H., Jia, Z., Zhang, L., Yamamoto, M., Misra, H.P., Trush, M.A., and Li, Y. (2008). Antioxidants and phase 2 enzymes in macrophages: regulation by Nrf2 signaling and protection against oxidative and electrophilic stress. Exp Biol Med (Maywood) *233*, 463-474.
Zielonka, J., and Kalyanaraman, B. (2018). Small-molecule luminescent probes for the detection of cellular oxidizing and nitrating species. Free Radic Biol Med *128*, 3-22.
Zielonka, J., Lambeth, J.D., and Kalyanaraman, B. (2013). On the use of L-012, a luminol-based chemiluminescent probe, for detecting superoxide and identifying inhibitors of NADPH oxidase: a reevaluation. Free Radical Bio Med *65*, 1310-1314.
Zimna, A., and Kurpisz, M. (2015). Hypoxia-Inducible Factor-1 in Physiological and Pathophysiological Angiogenesis: Applications and Therapies. Biomed Res Int *2015*, 549412.

Zitka, O., Skalickova, S., Gumulec, J., Masarik, M., Adam, V., Hubalek, J., Trnkova, L., Kruseova, J., Eckschlager, T., and Kizek, R. (2012). Redox status expressed as GSH:GSSG ratio as a marker for oxidative stress in paediatric tumour patients. Oncology Letters *4*, 1247-1253.

Zorov, D.B., Juhaszova, M., and Sollott, S.J. (2014). Mitochondrial reactive oxygen species (ROS) and ROS-induced ROS release. Physiol Rev *94*, 909-950.

Zweier, J.L., Broderick, R., Kuppusamy, P., Thompsongorman, S., and Lutty, G.A. (1994). Determination of the Mechanism of Free-Radical Generation in Human Aortic Endothelial-Cells Exposed to Anoxia and Reoxygenation. Journal of Biological Chemistry *269*, 24156-24162.